AD NUMBER
AD862594
LIMITATION CHANGES
TO: **Approved for public release; distribution is unlimited.**
FROM: **Distribution authorized to U.S. Gov't. agencies and their contractors; Administrative/Operational Use; SEP 1969. Other requests shall be referred to Army Aviation Materiel Labs., Fort Eustis, VA.**
AUTHORITY
USAAMMRDL ltr 18 Jun 1971

AD

USAAVLABS TECHNICAL REPORT 69-1

ANALYTICAL STUDY OF HELICOPTER GUST RESPONSE AT HIGH FORWARD SPEEDS

By

K. W. Harvey
B. L. Blankenship
J. M. Drees

September 1969

U. S. ARMY AVIATION MATERIEL LABORATORIES
FORT EUSTIS, VIRGINIA

CONTRACT DA 44-177-AMC-308(T)
BELL HELICOPTER COMPANY
FORT WORTH, TEXAS

250

Disclaimers

The findings in this report are not to be construed as an official Department of the Army position unless so designated by other authorized documents.

When Government drawings, specifications, or other data are used for any purpose other than in connection with a definitely related Government procurement operation, the United States Government thereby incurs no responsibility nor any obligation whatsoever; and the fact that the Government may have formulated, furnished, or in any way supplied the said drawings, specifications, or other data is not to be regarded by implication or otherwise as in any manner licensing the holder or any other person or corporation, or conveying any rights or permission, to manufacture, use, or sell any patented invention that may in any way be related thereto.

Trade names cited in this report do not consitute an official endorsement or approval of the use of such commercial hardware or software.

Disposition Instructions

Destroy this report when no longer needed. Do not return it to the originator.

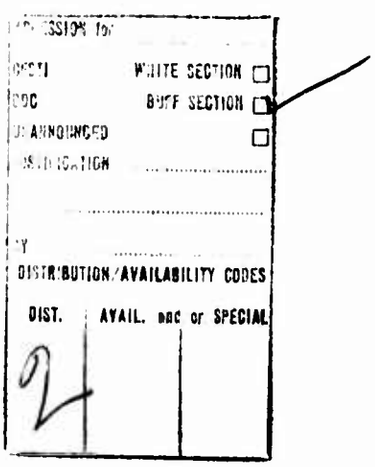

DEPARTMENT OF THE ARMY
HEADQUARTERS US ARMY AVIATION MATERIEL LABORATORIES
FORT EUSTIS, VIRGINIA 23604

The present military design specification for helicopter gust loads, MIL-S-8698(ASG), relegates helicopter design practice to that of a specialized fixed-wing case offering no gust load alleviation at rotor disc loadings of six pounds per square foot and above. Although very conservative, this criterion poses no design restrictions for the low-speed flight regime because other maneuver load factors are more critical.

Recent advancements in rotorcraft forward speed capability together with higher disc loadings have increased the importance of gust design criteria. Thus, the program was initiated to analytically determine the gust response of helicopter rotor/fuselage systems for both loaded and unloaded rotors at high forward speeds. A computer program for determining the response of a helicopter free to pitch, roll, yaw, and translate vertically while penetrating a gust environment was developed. This program, universally applicable to single-, tandem-, and tilt-rotor configurations, was used to run case studies for investigating such parameters as rotor hub restraint, disc loading, rotor thrust coefficient-solidity ratio, advancing tip Mach number, forward speed, and gust profile on gust response. The intent was to digest these findings and to make recommendations to improve and expand military specifications for helicopter gust load design.

The decision to develop a single computer program universally applicable to a myriad of VTOL configurations did impose limitations on computer storage and running time. These limitations precluded a more rigorous approach to the analysis, particularly a more realistic rotor wake representation, provision for more than four rotor blades, and the inclusion of torsional flexibility with full aeroelastic coupling.

Among the major conclusions of this study are:

1. The use of a rotor-mass ratio to determine gust alleviation by analogy with fixed-wing practice is unsatisfactory.

2. Rotor thrust coefficient-solidity ratio is among the most influential parameters on gust alleviation.

3. Consideration of the aircraft to be penetrating the gust environment at a finite speed has such a profound influence on gust alleviation that for a sine-squared gust profile, the effect of nonsteady aerodynamics is insignificant.

The conclusion that unsteady aerodynamics is a second-order influence is supported by an independent effort, "Dynamic Response of a Helicopter to a Gust", sponsored by the U. S. Naval Air Systems Command under Contract NOa(s) 53-318c, wherein individual rotor blades of 2-, 3-, and 4-bladed rotors are considered to penetrate a gust gradient.

Task 1F162204A14608
Contract DA 44-177-AMC-308(T)
USAAVLABS Technical Report 69-1
September 1969

ANALYTICAL STUDY OF HELICOPTER GUST RESPONSE AT HIGH FORWARD SPEEDS

BHC Report 299-099-106

By

K. W. Harvey
B. L. Blankenship
J. M. Drees

Prepared by

Bell Helicopter Company
Fort Worth, Texas

for

U. S. ARMY AVIATION MATERIEL LABORATORIES
FORT EUSTIS, VIRGINIA

SUMMARY

An analytical study of helicopter gust response at high forward speeds is presented. A digital computer program describes the rigid-body aircraft motions in space and gives an aeroelastic representation of two rotors. The rotors can be positioned to form main-and-tail, tandem, or side-by-side configurations. Many types of rotors (articulated, semirigid, and rigid) can be evaluated. Compounding with auxiliary propulsion, using wings to unload the rotor, and converting from lifting to prop-rotor conditions can be simulated. Starting with specified trimmed flight, any feasible maneuver can be performed while subjecting the aircraft to gusts or other external influences.

For this study, a number of refinements which specifically pertain to gust response were included in the program. The most important of these appears to be the consideration of gradual gust penetration. Effects of nonsteady aerodynamics are also included in a simplified form.

The study results cover a wide range of forward speeds and rotor and blade loadings for many current VTOL configurations. Variations were made to study the effects of gust shape, rotor type, and advancing-blade-tip Mach number on response to gusts. In a group of compound single-rotor helicopter configurations, variation in wing lift allowed a study of the effect on response of rotor unloading by the wing. Dynamic effects from rotor blade flexural motions were also considered. Several cases with special devices for reducing gust response of the rotor were computed. The effect of Lock number was determined by comparison of several cases where all other principal parameters were held constant. Three hundred and three cases were evaluated in the study. A simple empirical expression, based on 50-ft/sec sine-squared gust cases, was developed that will adequately predict the rotor gust-load ratio, $\Delta T/T_{hover}$, for a wide range of helicopter and compound designs:

$$\frac{\Delta T}{T_{hover}} = \frac{0.057}{\left(C_T/\sigma\right)_{hover}} + 0.85\,\frac{L_W}{T_{hover}} - C \qquad (1)$$

A principal finding is that the present MIL-S-8698 (ASG) requirements are not adequate and are too severe for modern high-speed helicopters. Recommendations for an improved design specification and future investigation are included in this report.

FOREWORD

An analytical investigation of gust responses of helicopters at high forward speeds was conducted at the Bell Helicopter Company (BHC) under U. S. Army Contract DA 44-177-AMC-308(T) (Task 1F162204A14608) from June 24, 1965 to April 26, 1967. The program was sponsored by the U. S. Army Aviation Materiel Laboratories (USAAVLABS), Fort Eustis, Virginia. Mr. J. H. McGarvey was the technical representative for USAAVLABS.

Technical information concerning articulated rotors was provided by Kaman Aircraft Company. In addition to the authors of this report, principal Bell Helicopter Company personnel associated with the project were Messrs. B. Bird, G. Brooks, and G. Weber.

BLANK PAGE

TABLE OF CONTENTS

TABLE OF CONTENTS - Continued

ILLUSTRATIONS

ILLUSTRATIONS - Continued

ILLUSTRATIONS - Continued

ILLUSTRATIONS - Continued

ILLUSTRATIONS - Continued

ILLUSTRATIONS - Continued

TABLES

TABLES - Continued

LIST OF SYMBOLS

A	vector of allowable errors in trim solution
Δa_x	change in forward acceleration (g)
Δa_z	change in vertical acceleration (g)
a_1	rotor flapping coefficient, fore-and-aft component (rad)
B	coefficients in rotor blade bending-moment analysis
b	number of blades for rotor
C	constant
[C]	structural damping matrix
C_L	lift coefficient for blade segment
C_T	rotor thrust coefficient
CF	centrifugal force (lb)
c	rotor blade chord (in.)
cg	center of gravity
D	rotor diameter (ft); aerodynamic drag force (lb)
DL	rotor disc loading: weight/rotor area (lb/sq ft)
d	distance from the origin to the point considered (ft)
E	error vector for one trim iteration
$\overline{E}$	vector of error magnitudes for a trim iteration
EI	section bending stiffness (lb-in.^{2})
e	flapping hinge offset (ft)
F	aerodynamic force (lb)
$\overline{F}$	net applied force vector in general equation of motion
F_H	internal horizontal force at flapping hinge (lb)

LIST OF SYMBOLS - Continued

F_v	internal vertical force at flapping hinge (lb)
$F_o(\psi)$	applied force in flapping equation (lb)
$\left[F_1\right]$, $\left[F_2\right]$, $\left[F_3\right]$	force matrices for stopped- or trailed-rotor analysis
$\vec{G}$	net applied moment vector in general equation of motion
g	acceleration due to gravity (ft/sec^2)
g_{HOR}	horizontal acceleration (g)
$g_o(\psi)$	coefficient of β in the flapping equation of motion
H_g	gust ramp length (ft)
$\vec{h}$	angular momentum vector (slug-ft^2/sec)
$h_o(\psi)$	coefficient of $d\beta/d\psi$ in rotor flapping equation
$I(D)$	product of Wagner function and Buettiker function
I_{TORS}	total torsional inertia of the drive system (lb-in.-sec^2)
I_x	mass moment of inertia about the x-axis (lb-in.-sec^2)
I_{xz}	product of inertia about the y-axis (lb-in.-sec^2)
I_y	mass moment of inertia about the y-axis (lb-in.-sec^2)
I_z	mass moment of inertia about the z-axis (lb-in.-sec^2)
$\vec{i}$	unit vector along x-axis of respective coordinate system
$\vec{j}$	unit vector along y-axis of respective coordinate system
K	spring constant for rotor hub (ft-lb/rad)

LIST OF SYMBOLS - Continued

K_g	gust-alleviation factor
$K_{g_{adj}}$	adjusted gust-alleviation factor for tandem configuration
K_{g_r}	gust-alleviation factor for a rotor
K_{g_w}	gust-alleviation factor for a wing
k, k'	variables in induced velocity equation
$[k]$	structural stiffness matrix
$\vec{k}$	unit vector along z-axis of respective coordinate system
L	applied moment about the x-axis (ft-lb); aerodynamic lift force (lb)
ΔL	change in wing lift (lb)
L_w	total wing lift (lb)
M	applied moment about the y-axis (ft-lb)
M_{B_i}	beamwise bending moment at ith station of blade (upper surface in compression) (in.-lb)
M_{C_i}	chordwise bending moment at ith station of blade (trailing edge in compression) (in.-lb)
M_{C_1}, M_{C_2}	cosine components of applied moment on rotors 1 and 2 for maneuver rotor equations (ft-lb)
M_{GUST}	blade bending moment due to a gust (in.-lb)
M_P	moment at center of rotor hub (ft-lb)
M_{S_1}, M_{S_2}	sine components of applied moment on rotors 1 and 2 for maneuver rotor equations (ft-lb)
M_{STEADY}	blade bending moment at trim (in.-lb)
M_t	advancing blade-tip Mach number
m	mass (lb-sec^2/ft)

LIST OF SYMBOLS - Continued

$[m]$	structural mass matrix
N	applied moment about the z-axis (ft-lb)
Δn	gust-load factor; change in normal acceleration (g)
$\vec{\Delta n}$	incremental rotation of coordinate system (rad)
Δn_r	change in normal acceleration due to rotor (g)
O	origin of moving coordinate system
$\overline{O}$	origin of fixed reference system
$\vec{o}$	vector from $\overline{O}$ to O
PCG	prop-rotor collective-pitch governor
P(x,y,z)	a point in the (x,y,z) system
p	roll rate in body coordinates (rad/sec)
Q	vertical shear at rotor hinge point (lb)
Q_R	torque required in drive system equation (ft-lb)
Q_S	torque supplied in drive system equation (ft-lb)
q	pitch rate in body coordinates (rad/sec)
R	radius of rotor (ft)
r	yaw rate in body coordinates (rad/sec)
r_1, r_2	coefficients in Wagner Function
S	area of rotor or wing (ft^2)
SHP	shaft horsepower (hp)
S_{B_i}	beamwise shear at ith blade station (lb)
S_{C_i}	chordwise shear at ith blade station (lb)
TRSWC	tail-rotor sidewash coefficient
$[T]$	coordinate transformation matrix

LIST OF SYMBOLS - Continued

ΔT	change in thrust (lb)
T_{hover}	rotor thrust in hover (lb)
U_P	wind velocity component perpendicular to blade-span axis and to U_T (ft/sec)
U_T	wind velocity component perpendicular to blade-span axis and to axis of no feathering (ft/sec)
V	forward velocity of rotorcraft (ft/sec)
V_c	velocity of origin of moving system (ft/sec)
V_g	vertical gust velocity (ft/sec)
V_i	induced velocity (ft/sec)
V_p	velocity of a point relative to fixed reference (ft/sec)
ΔV_P	dynamic out-of-plane velocity (ft/sec)
V_s	velocity of main-rotor swashplate (ft/sec)
ΔV_T	dynamic in-plane velocity (ft/sec)
V_x	intermediate velocity component (ft/sec)
W	weight (lb)
X	force applied in x-direction (lb)
$\{x\}$	structural displacement vector
x_B	body system x-coordinate
x_F	fixed system x-coordinate
x_{i_j}	state variables at jth blade station
x_P	x-position of any point on rotorcraft relative to fixed reference
Y	force applied in y-direction (lb)
y_B	body system y-coordinate
y_F	fixed system y-coordinate

Z	force applied in z-direction
z_B	body system z-coordinate
z_F	fixed system z-coordinate
Z_o	state vector in trim iteration procedure

GREEK LETTERS

α	angle of attack of the airfoil (rad)
α_c	angle of attack of the swashplate (rad)
$\Delta\alpha_r$	change in angle of attack on the rotor (rad)
β	rotor flapping angle (rad)
β_o	coning angle of the rotor (rad)
γ	Lock number
Δ	prefix indicating increment
δ_o, δ_1, δ_2	coefficients for nondivergent-drag equation (dimensionless, /deg, /deg^2)
δ_3	angle determining pitch-flap coupling (deg)
θ	rotor blade pitch angle (deg,rad)
$\Delta\theta/\Delta n$	blade pitch change rate due to bobweight (deg/g)
θ_D	dynamic pitch change (rad)
θ_{TW}	total blade twist (rad)
θ_o	geometric blade pitch at the root (rad)
λ	inflow ratio
$\bar{\lambda}$	average inflow ratio
μ	rotor advance ratio
μ_g	mass ratio
ρ	air density (slug/ft^3)

LIST OF SYMBOLS - Continued

$\vec{\rho}$	vector from cg to a point on the body
σ	rotor solidity
$\Phi(s)$	Wagner Function
ϕ_o	out-of-plane slope at blade root (rad)
χ	induced velocity angle correction for rear rotor of tandem configuration (rad)
ψ	azimuth angle (deg)
Ω_i	angular speed of ith rotor (rad/sec)
$\vec{\omega}$	angular speed of body (rad/sec)

OPERATORS

D	differentiation with respect to time in body reference
$\overline{D}$	differentiation with respect to time in fixed reference
$(\cdot)$	differentiation with respect to time
$(')$	differentiation with respect to azimuth angle

SUBSCRIPTS

B	body
c	moving reference origin
D	dynamic
F	fixed
g	gust
H	horizontal
R	rotor
S	swashplate
V	vertical
W	wing

CONFIGURATION TYPES

CSRH	compound single-rotor helicopter
PSRH	pure single-rotor helicopter
SSH	side-by-side helicopter
TRH	tandem-rotor helicopter

GUST TYPES

RFTP	rooftop-gust shape; function of space but not of time (implies gradual penetration by rotorcraft); gust velocity is vertical
RMPV	vertical ramp-gust shape (spatial function)
SEDV	sharp-edged vertical-gust shape (spatial function)
SSQH	sine-squared horizontal-gust shape (spatial function); V_g is directed aft
SSQL	sine-squared horizontal-gust shape (spatial function); V_g is lateral
SSQV	sine-squared vertical-gust shape (spatial function)
SUDH	sudden horizontal gust; gust velocity is the same at all points on the rotorcraft at any time (function of time but not of space--no penetration is implied); V_g is directed aft
SUDL	sudden lateral gust (time function only)
SUDV	sudden vertical gust (time function only)

ROTOR HUB TYPES

AR	articulated rotor
RR	rigid rotor
SR	semirigid or teetering rotor

LIST OF CASES

LIST OF CASES - Continued

LIST OF CASES - Continued

BLANK PAGE

INTRODUCTION

Rotary-wing aircraft experience milder reactions to gusts than do most fixed-wing aircraft. One of the earliest reports of this difference, a paper by Focke (1), presents qualitative reactions of two pilots on a dual flight, one in a helicopter with side-by-side rotors and the other in a fixed-wing airplane. A similar test was conducted later by NACA (2) with instrumentation to measure normal forces in the aircraft flying through turbulent air.

The relatively mild reaction of the rotary-wing aircraft is not substantiated by the simple theoretical expressions currently in use, particularly those that evolved from fixed-wing experience. Figure 1 shows an example of gust-load factors due to sharp-edged gusts, computed by NACA's Charts for Estimation of Longitudinal Stability Derivatives for a Helicopter Rotor in Forward Flight (3). This procedure neglects stall and compressibility effects and assumes instantaneous changes in rotor angle of attack, induced velocity, and blade flapping.

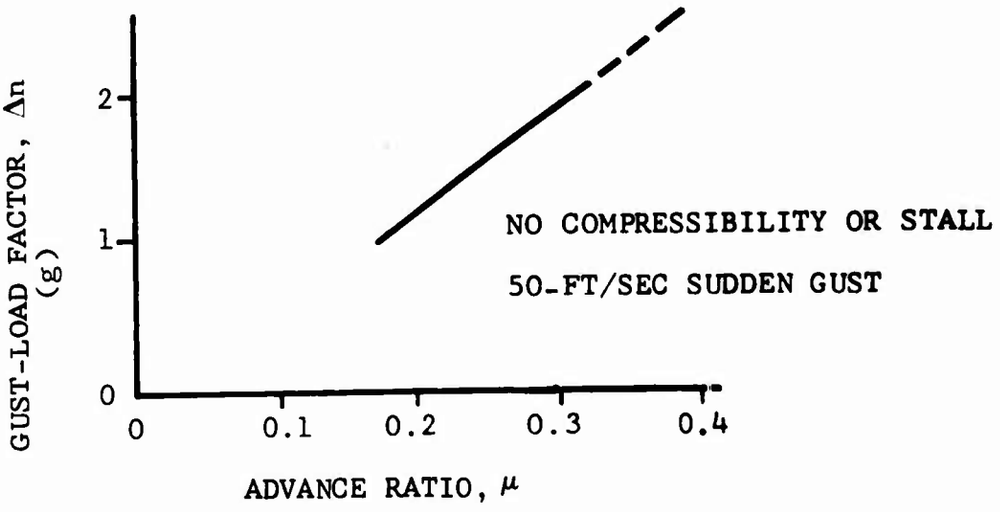

Figure 1. Gust-Load Factor Computed for the UH-1B Helicopter Using Linear Theory.

Current military design requirements (4) permit the use of an alleviation factor which is a function of rotor disc loading. However, this factor is unity for disc loadings greater than 6 pounds per square foot, as shown in Figure 2.

At high speeds and for disc loadings greater than 5 pounds per square foot, the computed gust-load factors are very high. When, in addition, maneuver loads are superimposed on gusts (as has occasionally been required in certain design studies), an

unrealistic design situation is created. The rapid development of compound aircraft and helicopters with higher forward speeds and disc loadings has made the current method of determining gust response prohibitively conservative.

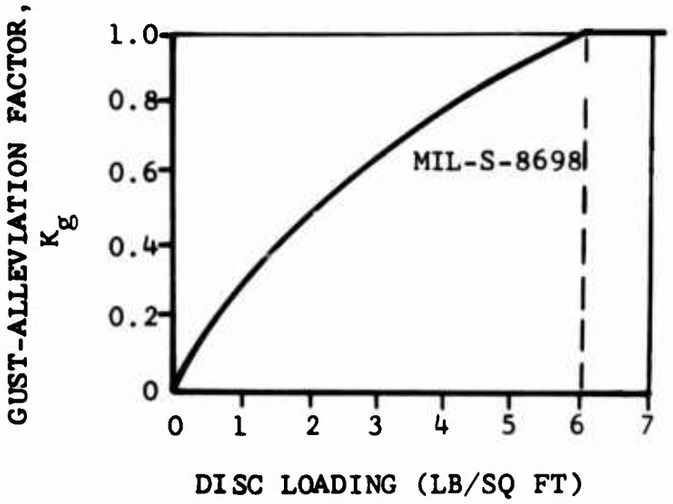

Figure 2. Gust-Alleviation Factor as Allowed by Military Specification.

On the other hand, recent studies indicate that the thrust capability of the rotor decreases with increasing advance ratio. The aerodynamic limit shown in Figure 3 is calculated by a digital method based on Gessow's development (5) and includes the effects of stall and compressibility. Also shown in Figure 3 is a practical limit based on flight test data (6). The practical limit is a result of oscillatory rotor loads and stall flutter effects, and is the controlling limit on rotor thrust capability at high advance ratios. This conclusion is supported by the findings of Ham and Young (7).

Unloading the rotor by adding a wing would give the rotor a greater margin to accept gusts. The advantage, however, is not as great as might be expected, because the rotor will usually assume the larger share of the lift increase resulting from gusts, as shown by tests with the AVLABS-Bell High-Performance Helicopter (6). The military design specification would allow a gust-alleviation factor that is unrealistically low for an unloaded rotor, illustrating again that a revision of the requirements is necessary.

The desirability of a detailed study to bring the treatment of gust effects on rotary-wing aircraft up to par with that of fixed-wing technology was pointed out in 1965 (8). Sine-

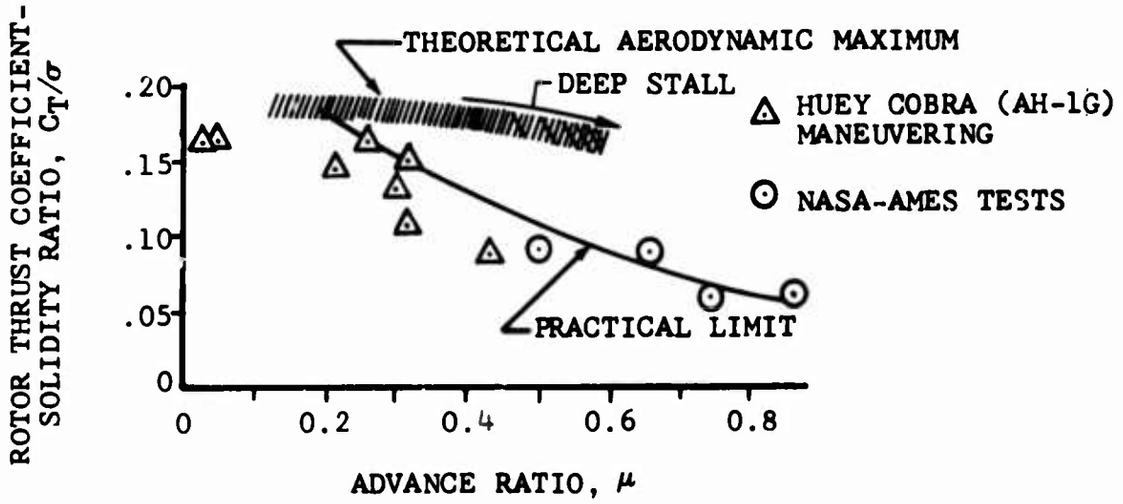

Figure 3. Rotor Limits as a Function of Advance Ratio.

squared gust shapes were considered instead of sharp-edged gusts, and a mass ratio replaced disc loading in the determination of the gust-alleviation factor. Figure 4 shows the result of that study. It indicates a considerable reduction of the gust-alleviation factor from the present requirements. The scope of that study, however, was insufficient to define new requirements for all contemporary types of rotary-wing aircraft. Furthermore, gradual penetration into the gust, nonsteady aerodynamics, and aeroelastic feedback were not considered.

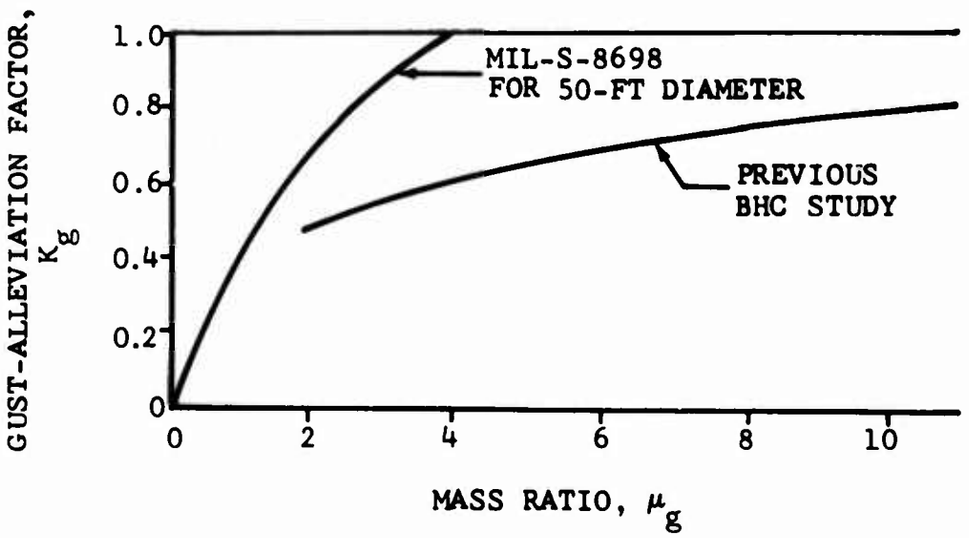

Figure 4. Results of a Previous Gust Study in Comparison With MIL Requirements.

These factors are considered and evaluated in this study. Recommendations for improved design criteria and future studies are presented herein.

Also included in this report are the basic mathematical equations and a discussion of the computational procedures used. A description of the analysis is presented in Program C81-11 Rotorcraft Flight Simulation (9), which was prepared in support of this study. Reference 9 is available at no charge upon request from Bell Helicopter Company, PO Box 482, Fort Worth, Texas 76101.

A magnetic tape library program providing data storage and retrieval of the time histories of 124 variables each for 94 maneuvers has been prepared. This program permits the examination of maneuver variables, some of which are not presented in this report, without recourse to computer reruns of the cases studied. This magnetic tape library program will be made available on a loan basis from the US Army Aviation Materiel Laboratories to investigators intent upon further studying the subject reported herein.

CONCLUSIONS

The universal maneuver computing program developed for this contract permits study of the gust response of a wide variety of VTOL aircraft configurations and rotor systems. Gust shape and intensity were varied, as were forward speed, disc loading, rotor thrust coefficient-solidity ratio, and advancing-tip Mach number. In all, 303 cases were investigated, from which the following principal conclusions are drawn:

1. The gust-alleviation factors, K_g, computed in this study indicate that the requirements of MIL-S-8698 (ASG) do not adequately provide for the conditions of modern helicopters, and are in need of revision. The use of a rotor mass ratio, μ_g, to determine K_g by analogy with the fixed-wing approach, as suggested in Reference 8, also does not give satisfactory results.

2. The most important result of the study, from a design and requirements point of view, is the finding that for all the helicopters and compounds investigated the rotor gust-load ratio, $\Delta T/T_{hover}$, can be expressed by a simple empirical expression as a function of the rotor thrust coefficient-solidity ratio in hover, C_T/σ, and the wing lift ratio, L_W/T_{hover}, prior to the gust:

$$\frac{\Delta T}{T_{hover}} = \frac{0.057}{\left(C_T/\sigma\right)_{hover}} + 0.85\,\frac{L_W}{T_{hover}} - C \qquad (1)$$

This method gives reasonable accuracy with appropriate conservatism with $C \approx 0.2$ for semirigid (teetering) rotors and about 0.1 for rigid and articulated rotors.

For a compound helicopter the wing gust load may be determined separately, using conventional fixed-wing methods. An alleviation of the wing gust load, owing to the interaction with the rotor, was identified and found to be related to the rotor thrust coefficient, C_T/σ. It is believed that this approach, after further refinement, presents a convenient basis for design rules and gust requirements.

3. The relative effects of various parameters on gust response can be summarized as follows:

   - Disc loading: Little influence
   - Rotor thrust coefficient-solidity ratio, C_T/σ: Major effect (see equation (1))

- Compounding: Considerable effect at high values of C_T/σ due to lift sharing with a wing
- Rotor type: Some effect, depends on dynamics
- Number of blades: Little effect
- Number of rotors: Increased effect for tandem configuration
- Forward velocity and advancing-tip Mach number: Little influence
- Lock number: Slight reduction of gust load with increased Lock number
- Pitch-flap coupling: Little effect
- Pitch-cone coupling: Appreciable effect
- Bobweight in collective system: Appreciable effect
- RPM effects: Not investigated
- Rotor-blade planform taper: Not investigated
- Rotor-blade cg-ac offset: Not investigated

4. Gradual gust penetration, nonsteady rotor aerodynamics and aeroelastic feedback proved to be the most influential factors for sharp-edged vertical gusts. For sine-squared gust shapes, the effects of gradual gust penetration appear to be most prominent. After various gust shapes were investigated (sharp-edged, sine-squared, ramp, rooftop, horizontal), a sine-squared gust with a maximum velocity of 50 feet per second and a ramp length of 90 feet was selected as the best representation for the detailed analysis.

5. Gust effects on tilt-rotor configurations, during conversion and in the high-speed airplane mode, were evaluated. Gust loads on the stopped-rotor and trailed-rotor configurations were investigated in a separate analysis. Flapping stability at high advance ratios in relation to gust disturbances was studied briefly. Although no general conclusions are formulated in regard to these various subjects, important information is presented in this report for specific design conditions.

RECOMMENDATIONS

1. A broad range of configurations and parameters was investigated using a sophisticated mathematical model developed as a part of the study. This approach produced gross answers to questions of gust response for a wide variety of rotary-wing VTOL aircraft. This broad approach, however, would not permit detailed studies of key parameters without undue expansion of the scope of the work. Yet it is of interest to make small incremental changes in a number of specific parameters (Lock number, ratio of wing lift to rotor lift, gross weight, etc.). Therefore, further studies, supplementing the present results, are recommended.

2. New gust requirements, differing from those of MIL-S-8698 (ASG), and applicable to all pure and compound helicopters, should be formulated. These requirements should relate the maximum rotor gust load directly to the hovering thrust coefficient-solidity ratio, C_T/σ, and to the ratio of wing lift to hovering thrust prior to the gust. Conservative values of the maximum wing gust load can be calculated conventionally, and possibly adjusted by using a rotor-interference factor.

3. Considerable nose-up pitching was computed for the tandem cases with aft cg. For the forward cg case, the configuration is stable and the gust response agrees with the thrust change formula of the preceding section. The stability characteristics of the chosen design examples are uncertain. A more thorough investigation, with emphasis on the parameters relating to pitch stability, is desirable.

4. Future analytical studies should include statistical methods for considering the effects of random gusts.

5. The conclusions of this study should be verified experimentally, particularly for the range of configurations and parameters of current production rotorcraft.

APPROACH AND SCOPE OF THE PROGRAM

Adequate treatment of the helicopter gust-response problem requires a degree of mathematical refinement which was impractical for engineering studies before the advent of large, high-speed computers. Although restraint is still necessary to keep computer time and storage requirements within reason, a considerable advancement of the state of the art is now possible. The development of a computing procedure to handle the detailed gust-response analysis was a principal part of the work done for this investigation.

One of the major goals of this study was to consider the effects of gradually penetrating a gust shape, as opposed to all points on the rotorcraft sensing a given gust velocity at the same time. To denote the cases where gradual penetration was used, reference will be made to a specific gust shape, such as sharp-edged, sine-squared, or ramp. For cases where gradual penetration was not used (i.e., instantaneous immersion of the entire aircraft), the disturbance will be referred to as a sudden gust.

The aim of the study was to establish a practical method for determining gust-response design requirements for rotorcraft. A procedure involving two steps was originally planned: first, the calculation of response to a sudden gust using a minimum of analytical refinement; second, the use of a factor to account for effects not included therein. The simplified analysis would replace the response formulas given in References 10 or 11, and the factor would be similar in application to the gust-alleviation factor discussed in Reference 11. In general, the gust response for each combination of physical parameters and flight conditions was computed both with and without the added, detailed refinements. A gust-alleviation factor due to the refinements was determined for each combination by a comparison of the results. Although this approach was followed throughout the study, an overall review led to the derivation of a rule for rotorcraft gust response which can be used without any preliminary analysis or additional factors.

Since the formulas developed for the calculation of fixed-wing gust response usually assume a sudden immersion in a gust, some comparisons with existing theory can be made for sudden-gust responses calculated with the simplified analysis.

Figure 1 (page 1) shows that the calculated load factor increases rapidly with forward speed when the method of Reference 3 is used. These results are obtained by assuming an instantaneous angle-of-attack change of

$$\Delta\alpha_r = \tan^{-1}\frac{V_g}{V} \qquad (2)$$

It is assumed that $\Delta\alpha_r$ is applied suddenly and simultaneously over the entire rotor disc, and that induced velocity and blade flapping adjust instantaneously. Additionally, no effects of stall and compressibility are taken into account. It is obvious that each of these assumptions implies unrealistic situations. Removing the assumptions may have an important bearing on the results, but it will also quickly increase the computational complexities.

The theories of linear aerodynamics are entirely inadequate at the high forward speeds of interest to this study. Therefore, it is assumed that methods such as those developed by NACA (5) can be used to account for stall and compressibility effects as a part of the short-method baseline. The effect of this modification on the calculated gust-load factor for the case of sudden immersion in a gust is shown in Figure 5.

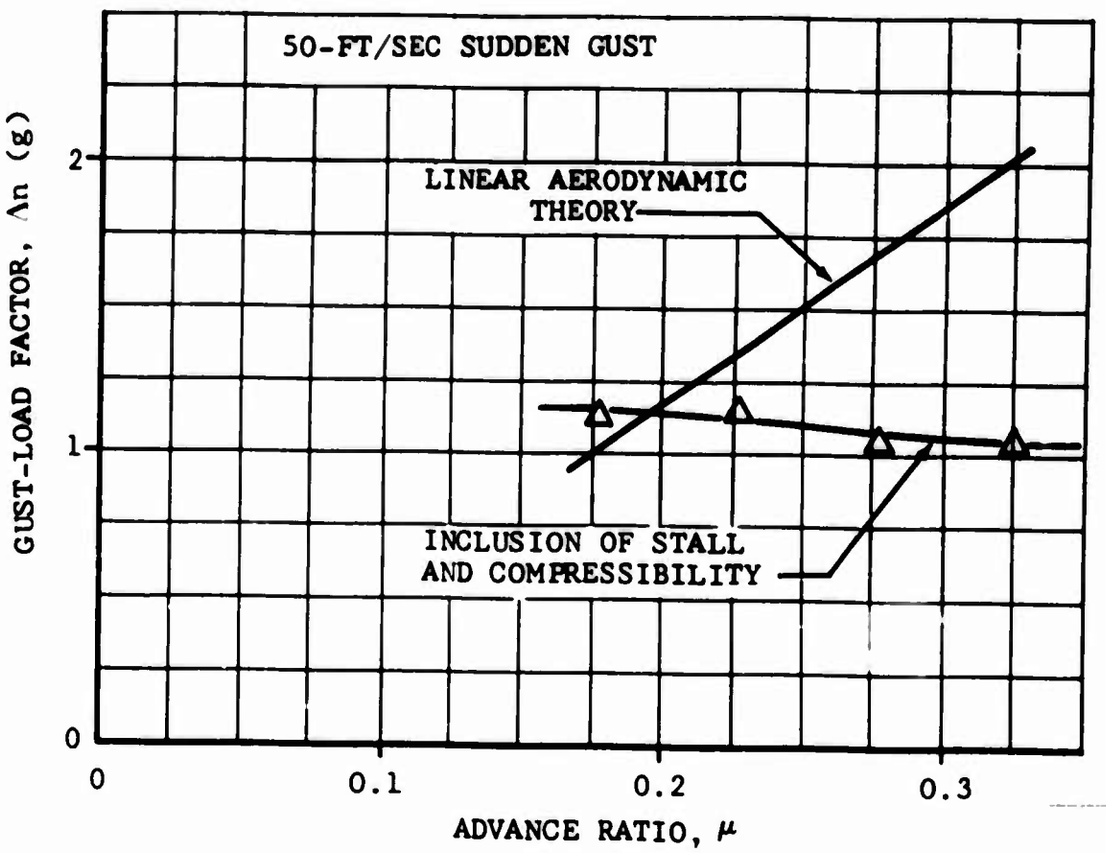

Figure 5. Gust-Load Factor for the UH-1B, Showing Importance of Using Improved Aerodynamic Methods Over Linear Theory.

For the simplified method, sudden immersion of the entire rotorcraft in a gust and steady-state aerodynamics are assumed. However, stall and compressibility effects on the rotor blades are included.

The possibility of using a stability derivative technique for gust response was considered. The equations and coefficient definitions given in Reference 12, Section 14, constitute an analytical basis for this method. Gust-response characteristics calculated from stability-derivative equations would not reflect effects of stall and compressibility. Only small perturbations about the trim point can be allowed because of the variations in stability-derivative values. At best, this technique would be more limited than the simplified method previously described. Early in the course of this study it was decided that the stability-derivative method would not be used.

The detailed analysis of gust response includes:

- gradual penetration,
- nonsteady aerodynamics,
- aeroelastic feedback, and
- a realistic gust-velocity function.

The gradual penetration effect is obtained by assuming that the gust velocity is a function of location along the zero heading axis. As the rotorcraft moves along this axis, gust-velocity values at different locations on the fuselage or rotors will not necessarily be the same at a given time. Pitching motion of the fuselage and rotor blade flapping are emphasized by simulating the rotorcraft penetrating a gust as a function of time. Gradual penetration is considered to be more realistic than the sudden immersion assumption.

The simplest way of handling aerodynamic variations is to assume that the situation under consideration can change from one steady-state condition to another instantaneously. Nonsteady (transient or time variant) aerodynamic effects were treated in an elementary way by Lucassen and Drees (13). The principal nonsteady aerodynamic effect on gust response included in this analysis is the behavior of lift following a change in blade (or other aerodynamic surface) angle of attack.

The effect of gust shapes was first treated in Reference 8. The most refined approach to date is probably that of Segel (14), but limitations on computer storage and run time precluded the use of that method. Instead, a simplified approach is used. By a gust-velocity function is meant a mathematical equation or table such that, given the position x_p of any point on the rotorcraft, the gust velocity at that point can be obtained. It should be noted that, in general, x_p is a function of time.

Figure 6 shows the individual effects, computed with the present program, of gradual penetration, nonsteady aerodynamics, and realistic gust-velocity functions. An appreciable variation is registered in each case.

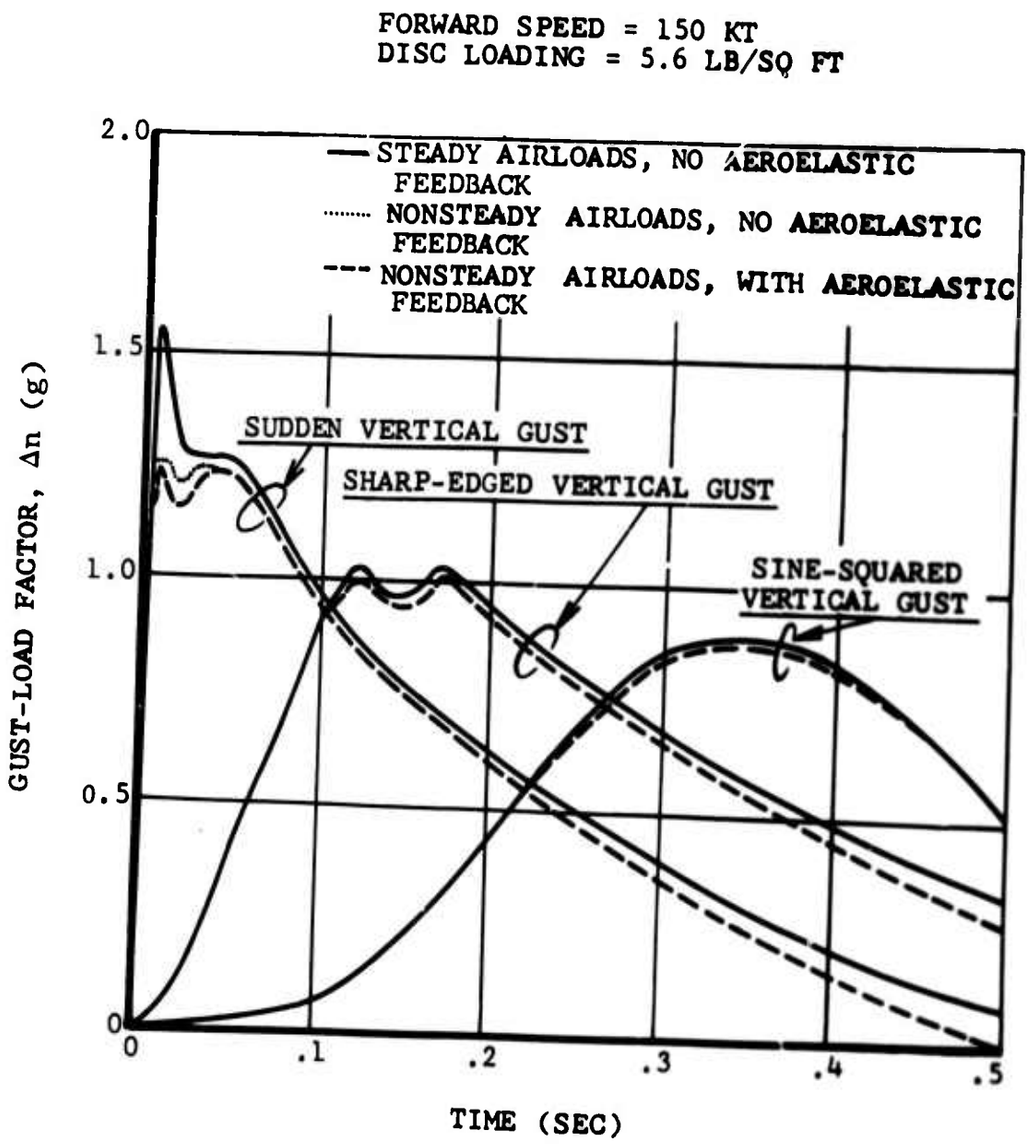

Figure 6. Effects of Gradual Penetration, Nonsteady Aerodynamics, Aeroelastic Feedback, and Gust Shape.

A summary of these effects is presented in Figure 7. It is shown that the nonsteady aerodynamics have a large influence if applied in the case of a sudden immersion. The effect of gradual penetration is more pronounced. The combination of nonsteady aerodynamics and gradual penetration shows that the nonsteady aerodynamics have become an insignificant influence. Adding the effect of a sine-squared gust produces another significant effect.

One more major item was investigated in connection with gust response: the inclusion of aerolastic feedback in the rotor aerodynamics. This was done by computing the velocities and pitch variations associated with blade elastic deformations and adding these to the components used for rigid blade aerodynamic analysis. This refinement has increased considerably the computer program complexity and running time, and the preparatory work required to arrive at feasible rotor systems that would not show undesirable resonances. Figures 6 and 7 show that aeroelastic feedback has a second-order effect on the gust-load factor. Another example of the effect of aeroelastic feedback is given in Figure 8. It is seen that the maximum rotor thrust is little affected, but that larger variations are found for the rotor blade-oscillatory bending moments.

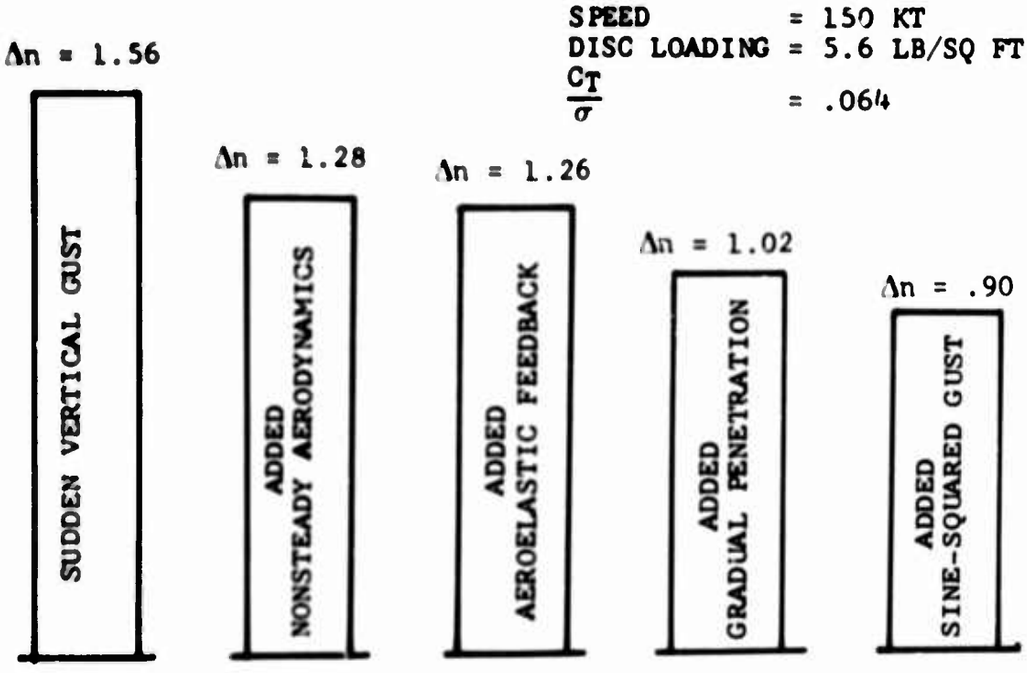

Figure 7. Bar Graph Illustrating the Relative Importance of the Most Influential Effects in the Detailed Analysis of Gust Response.

Legend: 1. Gradual Penetration, Without Aeroelastic Feedback
2. Gradual Penetration, With Aeroelastic Feedback

100 KT
324 RPM
6600 LB G.W.

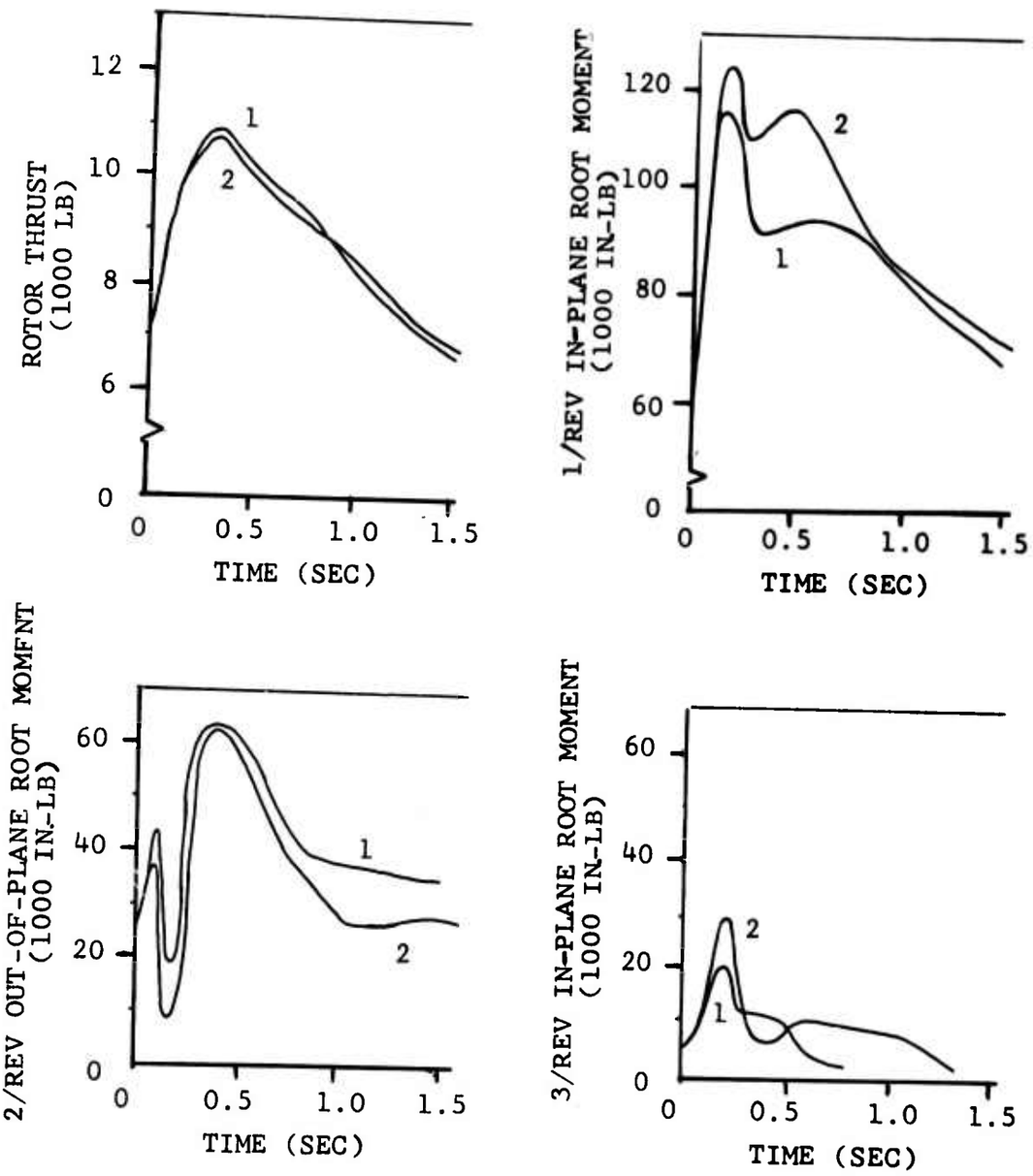

Figure 8. Calculated Time Histories of UH-1B Rotor Loads for 30-Ft/Sec Sharp-Edged Gust.

DEFINITION OF GUST-ALLEVIATION FACTOR

A main objective of this study was to determine for each configuration and condition the ratio of the maximum gust load due to a sine-squared gust to the maximum gust load due to a sudden gust. In this reference the maximum gust load due to a sudden gust was computed using the assumptions of the simplified analysis. The maximum gust load due to the sine-squared gust was computed using various combinations of effects from the detailed analysis.

A value of this ratio, called the gust-alleviation factor, would be given for a particular case by

$$K_g = \frac{\Delta n_{\text{sine-squared}}}{\Delta n_{\text{sudden}}} \tag{3}$$

Since K_g may be dependent on one or more aspects of the configuration or condition, gust-factor functions, or variations of K_g with case parameters, will be discussed in a later section.

The gust-factor calculation using a sine-squared gust was considered in Reference 8, but gradual penetration and nonsteady aerodynamics were not considered. It was proposed in Reference 8 that K_g might be a function of a mass ratio (see Figure 4, page 3),

$$\mu_{g_{\text{rotor}}} = \frac{4W/S}{\rho \pi R g} \tag{4}$$

by analogy with fixed-wing practice, where the factor

$$\mu_{g_{\text{fixed-wing}}} = \frac{2W/S}{m \rho c g} \tag{5}$$

is used.

As a result of the study, it became apparent that the mass-ratio approach to determining a gust factor K_g does not lead to satisfactory results. Attempts were therefore made in the final analysis to seek a new way to arrive at useful rules for design requirements.

SCOPE OF THE GUST STUDY

The scope of the gust study is summarized as follows:

- Development of the mathematical tools necessary to handle the problem.

- Subjection of a wide variety of rotary-wing configurations to sudden and sine-squared gusts, both vertical and horizontal, while varying forward speed, disc loading, blade thrust coefficients, Lock number, etc. Table I and Appendix II summarize the cases considered, together with principal rotor and wing parameters, trim values, gust description, and response results. Rectangular planform rotor blades with linear twist and zero cg-ac offset were used in all cases.

- Development of design rules which may be used for future requirements.

TABLE I. SUMMARY OF CASES

Configuration	Variable	Rotor	No. of Cases	Case Number
Pure Single-Rotor Helicopter	Mach Number	Semirigid	16	1 - 16
	Disc Loading and Thrust Coefficient	Semirigid	18	17 - 32 217 - 218
		Articulated and Rigid	4	219 - 222
	Gust Profile	Semirigid	2	33 - 34
	Gust Direction	Semirigid	4	35 - 38
	Rotor Type	Articulated and Rigid	32	39 - 70
Compound Single-Rotor Helicopter	Mach Number	Semirigid	40	71 - 110
	Disc Loading and Thrust Coefficient	Semirigid	28	111 - 134 223 - 226
		Articulated and Rigid	8	227 - 234
	Rotor Type	Articulated and Rigid	44	135 - 166 169 - 178 181 - 182
Pure Tandem Helicopter	Gust Profile	Articulated	10	183 - 190 272, 274

TABLE I - Continued

Configuration	Variable	Rotor	No. of Cases	Case Number
Trailing Rotor	Forward Speed		4	191 - 194
Stopped Rotor	Forward Speed		4	195 - 198
Tilt Rotor	Helicopter Mode		2	199 - 200
	Transition Mode		4	201 - 204
	Airplane Mode		10	205 - 214
Special Cases	Gust-Alleviation Devices		7	235 - 237 247 - 249 269
	Gust Strength		3	238 - 240
	Low Speed		4	243 - 246
	Effects of Nonsteady Aero, Gradual Penetration and Aeroelastic Feedback		13	250 - 262
	Horizontal Side Gust		2	263 - 264
	Hub Spring		5	265 - 268 270
	Blade Torsional Restraint		3	275 - 277
	Lock Number		36	278 - 313
			303	

DEVELOPMENT OF MATHEMATICAL MODEL

GENERAL DISCUSSION

The principal mathematical tool used to compute the responses of VTOL aircraft to gusts is a further development of a previously available BHC computing program. References 8, 15, and 16 describe the early program, with its applications to a wide variety of problems, such as performance, stability and control, maneuvers, determination of structural loads in rotor blades, autorotational landings, and the effects of gusts on rotary-wing aircraft. The principal improvements in the mathematical representation of the aircraft that have been made during the course of this study are:

- Adding roll and lateral degrees of freedom, to complete the freedom of the rigid-body fuselage in space.
- Adding a second complete rotor system representation which can be oriented to act as a tail rotor, the aft rotor of a tandem helicopter, or the left rotor of a side-by-side rotorcraft configuration.
- Including aeroelastic feedback capability in the rotor-load calculations.
- Enlarging the boundary conditions to permit the evaluation of rigid, semirigid, and articulated rotors with two, three, or four blades.
- Refining the aerodynamic theory for rotors and fixed surfaces to include the effects of nonsteady aerodynamics.
- Refining the gust representation by including the effect of gradual immersion of the aircraft: first the front of the rotor, then the fuselage, and finally the elevator and tail rotor (in the case of a single-rotor helicopter).
- Adding planform taper to the rotor representation.

The various configurations that can be handled with this program are summarized in Table II. The most important built-in options are listed in Table III. Figure 9 presents the major building blocks of the program. A flow chart of the program is shown in Figure 10.

TABLE II. POSSIBLE CONFIGURATION VARIATION	
1.	Single-rotor helicopter with tail rotor
2.	Counterrotating tandem-rotor helicopter
3.	Counterrotating side-by-side-rotor helicopter
4.	Propeller airplane (1 or 2 propellers)
5.	Jet airplane (1 or 2 jets)
6.	Winged helicopter (any type)
7.	Helicopter with 1 or 2 auxiliary propulsion units (props or jets)
8.	Full compound helicopter (with wings and auxiliary propulsion)
9.	Prop-rotor convertiplane
10.	Tilt-wing convertiplane
11.	Rigid, semirigid, or articulated rotors
12.	2, 3, or 4 blades on each rotor
13.	Interconnect control couplings of swashplate with differential wing angle and elevator control. Rudder control through rotor control and/or fin lift control
14.	Control features such as δ_3, bobweights, etc.
15.	Engine, rotor, and/or propeller governors

Most of the configuration variations are made possible by generalizations in the analysis. For example, for each rotor the location of the mast base or pivot point in three dimensions must be specified by input data. The mast length and inclination are also inputs. Thus the first three configurations can be included in one procedure. Provisions for differences in aerodynamic interference effects for these three types of rotorcraft are also controlled by input data.

Another technique used to change configurations is deletion logic. Having made provisions for two rotors, two propellers, two jet propulsion units, and wings, Configurations 4 through 8 of Table II can be constructed by deleting those items not required. The computer program contains conditional branches

TABLE III. AVAILABLE OPTIONS OF PROGRAM DETAIL
1a. Trim section only, providing performances, control position, stability derivatives
1b. Trim section and oscillatory rotor loads
2a. Basic maneuver section, not including rotor loads, aeroelastic feedback, or nonsteady aerodynamics. Permits study of aircraft reactions to displacements of pilot's controls and/or response to gusts and other external influences. Output includes aircraft position in space, rotor flapping, torque, rpm, etc.
2b. Add computation of rotor loads
2c. Add aeroelastic feedback
2d. Add nonsteady aerodynamics
3. Documentation includes option to preserve data on library tapes

so that particular sections of the calculations can be skipped and quantities dependent on the skipped sections remain unchanged. For example, if no propellers are wanted, the propeller input data group is set to zero. Preceding entry into the subroutine for propeller analysis, the computer checks propeller data and reacts to the zero inputs by skipping that subroutine altogether. Propeller thrust and horsepower required remain at initialized values of zero and hence do not change the net forces and moments computed.

Other effects are generalized by branching to alternate procedures as required by the controlling input data. Rotor types and number of blades are examples. The convertiplane types (9 and 10 of Table II) are essentially different from the side-by-side-rotor helicopter only in rotor parameters and in capability of change in attitude of the rotor masts, either with or without accompanying change in wing incidence. These change capabilities are included in the data for the time-variant section.

The many features of the analysis and computer program pointed out in Tables II and III and Figure 8 are obtained by these techniques. The program, as Table III and Figure 9 indicate, has two major sections: (a) trim section and (b) maneuver section.

In the trim section the aircraft is brought to a stabilized trim, which becomes the initial condition for the maneuver

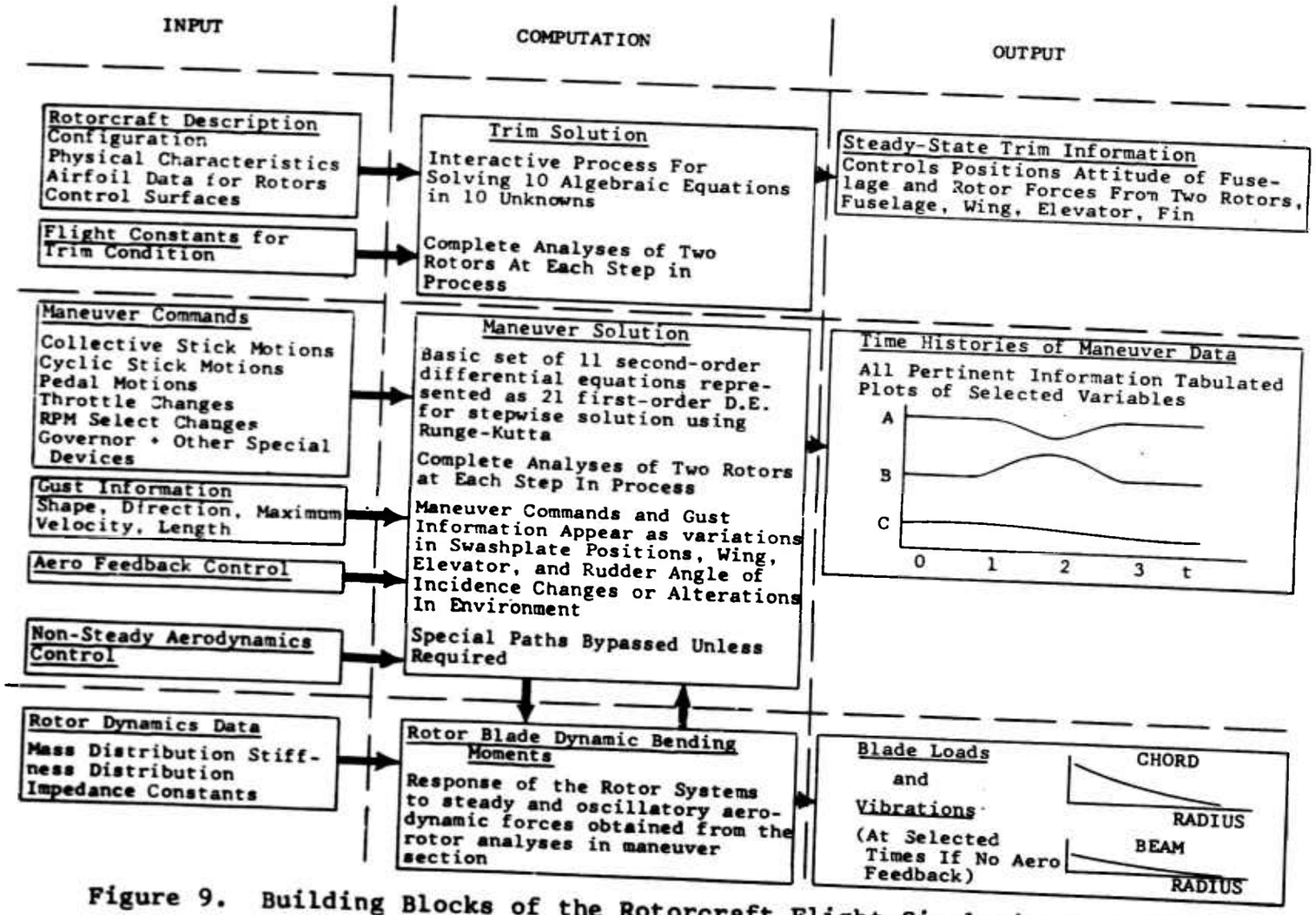

Figure 9. Building Blocks of the Rotorcraft Flight-Simulation Program.

section. Any realistic stabilized-flight condition can be specified by forward velocity, rate of climb, rpm, gross weight, etc. In the maneuver section the aircraft is subjected to a variation in conditions, which for this study was an external disturbance due to a gust.

The operation of the program takes considerable skill, because the representation of the aircraft has become so detailed that it approaches the complexity of the actual rotorcraft. Specifically, for high forward speeds, a wrong elevator setting or a blade resonance owing to improper rotor dynamics will prevent the proper operation of the program. Furthermore, the many nonlinearities, such as those caused by rotor blade stall, may preclude finding a trim solution if the initial approximations require large iteration steps.

The running time of the program depends on the detailing options requested by the user. Approximate running times for an IBM 360 Model 65 computer, assuming that the trim condition is found within a reasonable number of iterations, are given in Table IV.

A condensed discussion of some of the topics and the organization of the program is given in this report. A detailed mathematical description of the program is given in Reference 9.

The effects of gusts on stopped and trailing rotors have been treated separately because the aerodynamic and dynamic analyses of the maneuver program are not believed to be applicable to the peculiar conditions that prevail for stopped rotor blades. The analytical approach is briefly described in a later section of this report. More detailed information is given in Reference 17.

TABLE IV. COMPUTING TIMES

Time to trim	2 min
100-time-points maneuver without rotor loads	4 min (includes trim)
100-time-points maneuver with rotor loads, no feedback	5.5 min (includes trim)
100-time-points maneuver with rotor loads and feedback	9 min (includes trim)
Inclusion of nonsteady airloads	adds 2.5 min to above maneuver
Requesting loads on two rotors instead of one	adds 4 min

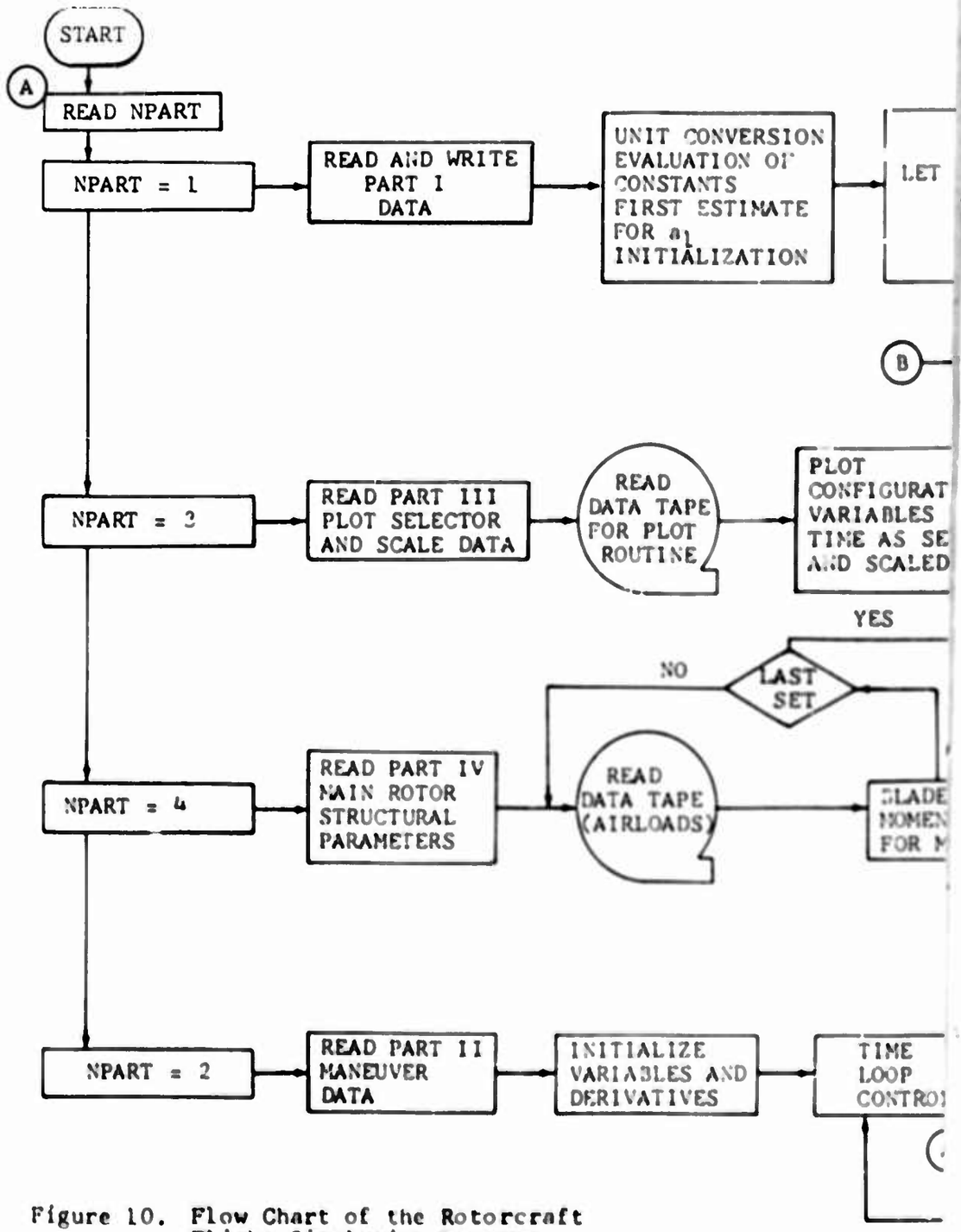

Figure 10. Flow Chart of the Rotorcraft Flight-Simulation Program.

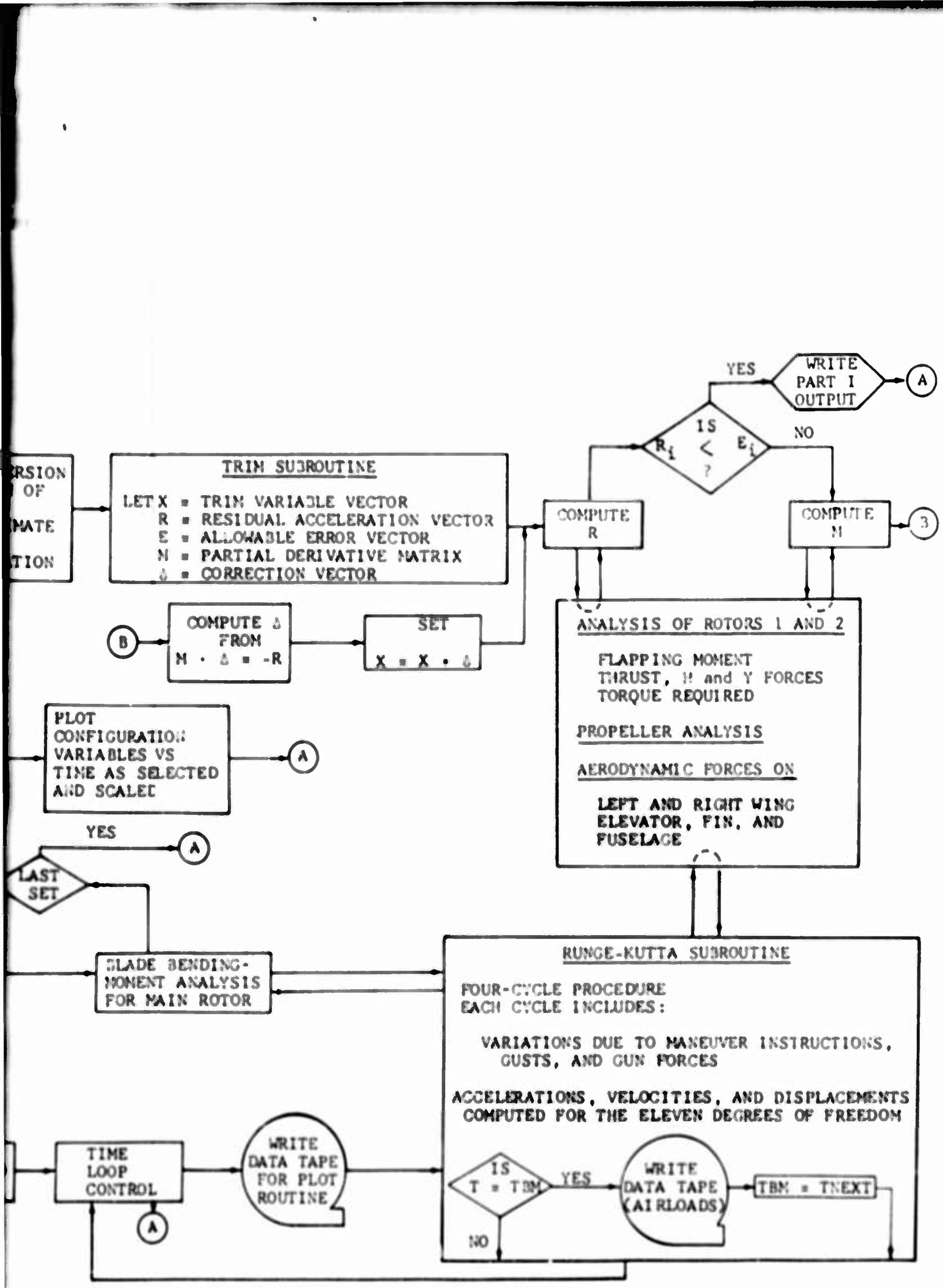
RSION OF NATE TION
TRIM SUBROUTINE
LET X = TRIM VARIABLE VECTOR
R = RESIDUAL ACCELERATION VECTOR
E = ALLOWABLE ERROR VECTOR
N = PARTIAL DERIVATIVE MATRIX
Δ = CORRECTION VECTOR
B
COMPUTE Δ FROM N · Δ = -R
SET X = X + Δ
COMPUTE R
IS R_i < E_i ?
YES
WRITE PART I OUTPUT
A
NO
COMPUTE N
3
ANALYSIS OF ROTORS 1 AND 2
FLAPPING MOMENT
THRUST, X and Y FORCES
TORQUE REQUIRED
PROPELLER ANALYSIS
AERODYNAMIC FORCES ON
LEFT AND RIGHT WING
ELEVATOR, FIN, AND
FUSELAGE
PLOT CONFIGURATION VARIABLES VS TIME AS SELECTED AND SCALED
A
YES
A
LAST SET
BLADE BENDING-MOMENT ANALYSIS FOR MAIN ROTOR
RUNGE-KUTTA SUBROUTINE
FOUR-CYCLE PROCEDURE
EACH CYCLE INCLUDES:
VARIATIONS DUE TO MANEUVER INSTRUCTIONS, GUSTS, AND GUN FORCES
ACCELERATIONS, VELOCITIES, AND DISPLACEMENTS COMPUTED FOR THE ELEVEN DEGREES OF FREEDOM
TIME LOOP CONTROL
A
WRITE DATA TAPE FOR PLOT ROUTINE
IS T = TBM
YES
WRITE DATA TAPE (AIRLOADS)
TBM = TNEXT
NO

MANEUVER COMPUTING PROGRAM

Rigid motions of the rotorcraft can be fully described by the usual six body equilibrium equations, plus two flapping equations for each rotor and a drive-system rotation equation. The fuselage equations are written in body-axis reference as given by Etkin (12), to avoid variation in inertia parameters. The rotor equations are in tip-path-plane reference, and the drive-system rotation is referred to main (forward or right) rotor rpm for convenience. The 11 basic equations state that for each degree of freedom the time derivative of momentum is equal to the sum of the relevant forces or moments.

For a trim solution, the momentum derivatives are zero and the equations are algebraic in the following control and attitude variables: the body Euler angles relative to a fixed reference system (three), rotor-flapping components relative to the swashplate (four), fore-and-aft and lateral cyclic stick position (two), collective-stick position (one), and pedal position (one). For maneuver considerations the conditions may be viewed as a set of second-order differential equations in displacements relative to the fixed reference. However, since velocity components in fuselage reference are important output items, a set of 21 first-order differential equations is used to simulate the rotorcraft's flight. The basic variables in this system are instantaneous linear and angular velocities of the body (six), instantaneous pitch and roll velocities of the rotors (four), the linear and angular displacements of the body relative to the fixed reference system (six), rotor attitude components relative to the swashplate axes (four), and the angular velocity of the drive system (one). Transformations of velocities from body to fixed reference and from tip-path-plane to swashplate reference are necessary as intermediate steps in the computational process.

The aerodynamic forces and moments acting on the rotorcraft are dependent on attitude and control-position displacements and velocities and variations in wind velocity. Generally, the aerodynamic forces are computed in one reference and are transformed to another for summing. For this reason, and because of the relationships among the mast, swashplate, and tip-path-plane, many transformations are necessary. Special subroutines were developed to handle passage from one to another of the following reference systems: fixed (one), body (one), flight path (one), mast (two), swashplate (two), tip-path-plane body (two), tip-path-plane wind (two), swashplate body (two), swashplate wind (two), and wind direction system at top of mast (two). These reference systems are shown schematically in Figure 11. The tip-path-plane-body reference system has its x-axis in the body xz-plane. The tip-path-plane-wind axis system has its x-axis in a plane normal to the tip-path plane and containing the wind vector.

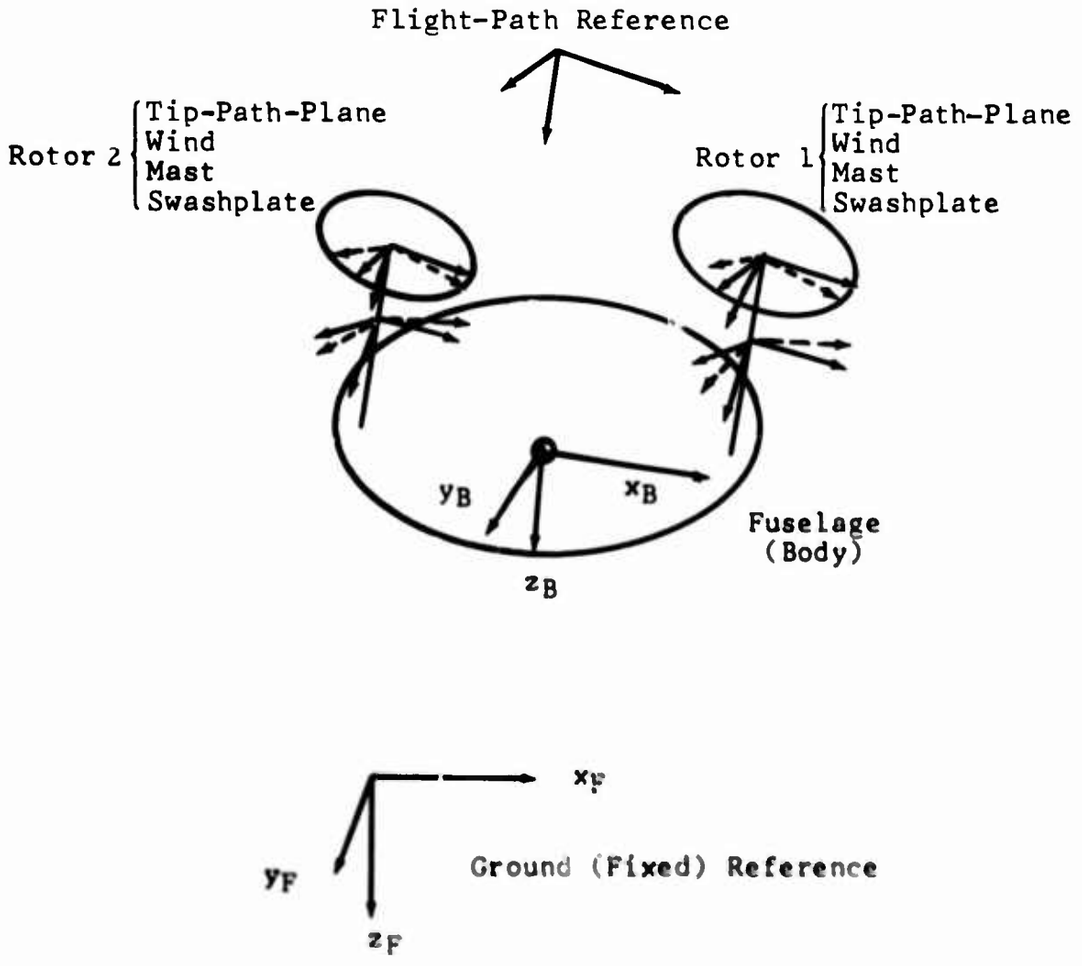

Figure 11. Schematic of Reference Systems.

Basic Equations of Motion

The equations of motion of a free body relative to a set of axes fixed to the body are derived in Reference 12 from the momentum-equilibrium expressions. The development is given in a more general form in Craig's dissertation on classical dynamics (Reference 18, Chapter XII). Using $\bar{D}$ and D to indicate differentiation with respect to time in the fixed and body reference systems respectively, the momentum equations may be derived as follows.

Consider a fixed coordinate system with origin $\bar{O}$ and a moving coordinate system (body reference system) with origin O; x, y, z axes; and unit vectors $\vec{i}$, $\vec{j}$, $\vec{k}$. Let $\vec{o}$ be the radius vector from $\bar{O}$ to O and $\vec{\rho}$ the radius vector from O to a point P(x,y,z). The radius vector from $\bar{O}$ to P can then be written as $(\vec{o} + \vec{\rho})$. Let $\vec{\omega}$ be the rotational vector of the body coordinate system relative to the fixed system. Then

$$\bar{D}(\vec{o}+\vec{\rho}) = \bar{D}(\vec{o}) + \bar{D}(\vec{\rho}) = \bar{D}(\vec{o}) + D(\vec{\rho}) + \vec{\omega}\times\vec{\rho}$$

Let $\vec{v}_c$ be the velocity of O relative to $\bar{O}$, and $\vec{v}_p$ the velocity of P relative to $\bar{O}$, and note that $D(\vec{\rho}) = 0$. Then

$$\vec{v}_P = \vec{v}_c + \vec{\omega}\times\vec{\rho}$$

and the angular momentum of the body is

$$\vec{h} = \int_V [\vec{\rho}\times\vec{v}_c + \vec{\omega}\times\vec{\rho}]\, dm$$

With $\vec{F}$ and $\vec{G}$ representing the net applied force and moment respectively, the momentum equations can be expressed as follows:

$$\begin{aligned} \vec{F} &= \bar{D}\left(m\vec{v}_c\right) = D\left(m\vec{v}_c\right) + m\vec{\omega}\times\vec{v}_c \\ \vec{G} &= \bar{D}(\vec{h}) = D(\vec{h}) + \vec{\omega}\times\vec{h} \end{aligned} \qquad (6)$$

If $\vec{v}_c$, $\vec{\omega}$, and $\vec{\rho}$ are expressed in terms of body reference components as

$$\vec{v}_c = U\vec{i} + V\vec{j} + W\vec{k}$$

$$\vec{\omega} = p\vec{i} + q\vec{j} + r\vec{k}$$

$$\vec{\rho} = x\vec{i} + y\vec{j} + z\vec{k}$$

the equations 4.4.3 and 4.4.4 of Reference 12 may be written directly from equation (6). The cross products of inertia involving lateral coordinates have been dropped due to the assumed symmetry of the body about an xz-plane. This reduces the components of $\vec{h}$ as follows:

$$\vec{h} \cdot \vec{i} = I_x p - I_{xz} r$$

$$\vec{h} \cdot \vec{j} = I_y q$$

$$\vec{h} \cdot \vec{k} = -I_{xz} p + I_z r$$

All other terms are retained.

In this analysis the center of gravity, the gross weight, and mass moments and products of inertia are assumed to include pylon and rotor blade weights. Variation in mast tilt is considered by computing a new cg location and new values of the inertia quantities. Rates of change in mass moments and products of inertia, which would appear in the components of $D(\vec{h})$, are not taken into account.

The drive-system rotation equation allows evaluation of $\dot{\Omega}$ and Ω. The rotor angular velocities Ω_1 and Ω_2 are computed by applying the appropriate gear ratios to Ω. The rotor flapping equations are represented as the components of

$$I_i \left(\ddot{\beta}_i + \Omega_i^2 \beta_i\right) = M_i, \qquad i = 1, 2$$

where M_i and β_i are, respectively, applied moment and flapping angle viewed as harmonic series based on Ω_i, and the index i identifies the particular rotor.

The Euler-angle derivatives are introduced in Reference 12 by noting that an infinitesimal rotation Δn in time Δt can be written

$$\vec{\Delta n} = \vec{i}_3 \Delta\phi + \vec{j}_2 \Delta\theta + \vec{k}_1 \Delta\psi$$

where the subscripts indicate the axis system from which each component is obtained (Reference 12, Figure 4.2).

Then

$$\vec{\Delta n} = \lim_{\Delta t \to 0} \frac{\vec{\Delta n}}{\Delta t} = \vec{i}_3 \dot{\phi} + \vec{j}_2 \dot{\theta} + \vec{k}_1 \dot{\psi}$$

Since

$$\vec{\omega} = p\vec{i} + q\vec{j} + r\vec{k}$$

$$[p, q, r] = [\vec{i} \cdot \vec{\omega}, \vec{j} \cdot \vec{\omega}, \vec{k} \cdot \vec{\omega}]$$

or

$$[p,\ q,\ r] = [\dot{\phi},\ \dot{\theta}\ ,\dot{\psi}\ ] \begin{bmatrix} \vec{i}\cdot\vec{i}_3 & \vec{j}\cdot\vec{i}_3 & \vec{k}\cdot\vec{i}_3 \\ \vec{i}\cdot\vec{j}_2 & \vec{j}\cdot\vec{j}_2 & \vec{k}\cdot\vec{j}_2 \\ \vec{i}\cdot\vec{k}_1 & \vec{j}\cdot\vec{k}_1 & \vec{k}\cdot\vec{k}_1 \end{bmatrix}$$

The unit vector dot products are, by rows, the direction cosines for the Euler-angle velocity vectors relative to the body-axis system. Thus,

$$[p,\ q,\ r] = [\dot{\phi},\ \dot{\theta}\ ,\dot{\psi}] \begin{bmatrix} 1 & 0 & 0 \\ 0 & \cos\phi & -\sin\phi \\ -\sin\theta & \cos\theta\ \sin\phi & \cos\theta\ \cos\phi \end{bmatrix} \quad (7)$$

These equations may be solved for $\dot{\phi}$, $\dot{\theta}$,$\dot{\psi}$, as given by equation 4.5.4 of Reference 12.

These relationships provide a means of determining the change in orientation of the body when p, q, and r are known. The rotor Euler-angle expressions are similarly derived except that $\dot{\psi}_i$ is assumed to be zero. The angular velocity r_i, while not zero under this assumption, is small relative to Ω_i and is not included. Equations for $\dot{\phi}_i$ and $\dot{\theta}_i$ can be read from Equation 7.

The Euler angular velocity expressions govern the orientation of the fuselage and rotors. The velocities in body reference (U, V, W) must be transformed into fixed reference components ($\dot{x}$, $\dot{y}$, $\dot{z}$) to obtain distance traveled relative to the fixed system and heading and climb angles. The transformation matrix is given below for quick reference:

$$[T] = \begin{bmatrix} \cos\psi\cos\theta & \cos\psi\sin\theta\sin\phi - \sin\psi\cos\phi & \cos\psi\sin\theta\cos\phi + \sin\psi\sin\phi \\ \sin\psi\cos\theta & \sin\psi\sin\theta\sin\phi + \cos\psi\cos\phi & \sin\psi\sin\theta\cos\phi - \cos\psi\sin\phi \\ -\sin\theta & \cos\theta\sin\phi & \cos\theta\cos\phi \end{bmatrix} \quad (8)$$

The full set of equations of motion, including the orientation equations, is presented in component form in Table V. Expressions for the applied forces and moments, X, Y, Z, L, M, N, Q, M_{C_1}, M_{S_1}, M_{C_2}, M_{S_2}, are developed in detail in Reference 9.

TABLE V. EQUATIONS OF MOTION

$$X = m(\dot{U} + qW - rV)$$

$$Y = m(\dot{V} + rU - pW)$$

$$Z = m(\dot{W} + pV - qU)$$

$$L = I_x\dot{p} - I_{xz}\dot{r} + qr(I_z - I_y) - I_{xz}pq$$

$$M = I_y\dot{q} + rp(I_x - I_z) + I_{xz}(p^2 - r^2)$$

$$N = I_z\dot{r} - I_{xz}\dot{p} + pq(I_y - I_x) + I_{xz}qr$$

$$Q_S = I_{TORS}\dot{\Omega} + Q_R$$

$$M_{C_1} = -I_{b_1}(\dot{q}_1 + 2\Omega_1 p_1)$$

$$M_{S_1} = -I_{b_1}(\dot{p}_1 - 2\Omega_1 q_1)$$

$$M_{C_2} = -I_{b_2}(\dot{q}_2 + 2\Omega_2 p_2)$$

$$M_{S_2} = -I_{b_2}(\dot{p}_2 - 2\Omega_2 q_2)$$

$$\dot{\theta} = q\cos\phi - r\sin\phi$$

$$\dot{\phi} = p + q\sin\phi\tan\theta + r\cos\phi\tan\theta$$

$$\dot{\psi} = (q\sin\phi + r\cos\phi)/\cos\theta$$

$$\dot{\theta}_1 = q_1/\cos\theta_1$$

$$\dot{\phi}_1 = p_1$$

$$\dot{\theta}_2 = q_2/\cos\theta_2$$

$$\dot{\phi}_2 = p_2$$

$$[\dot{x}, \dot{y}, \dot{z}] = [U, V, W][T]$$

Aerodynamic Forces and Moments

Rotors, Propellers, Auxiliary Propulsion

The rotor aerodynamic performance and airloads analysis is similar to that described by Blankenship and Harvey (15), but a number of minor improvements such as planform taper have been added (9). Both rotors are treated in the same manner and in the same subroutine. The aeroelastic-feedback mechanism appears as velocity terms added to both inflow and tangential velocities, and an added term for blade-pitch variation in the local angle-of-attack expression. These added quantities are computed in the rotor blade bending-moment section. The dynamic pitch change, $\Delta\theta_D$, dynamic out-of-plane velocity, ΔV_P, and in-plane velocity, ΔV_T, are used in the rotor equations thus:

$$\theta = \theta_o + \frac{r}{R}\theta_{TW} - \tan\delta_3\left(\beta-\beta_o\right) + \Delta\theta_D$$

$$U_P = \left(\lambda\cos\beta - r\frac{\dot{\beta}}{\Omega R} - \mu\sin\beta\cos\psi\right)\Omega R - W_{Gust} + \Delta V_P$$

$$U_T = \left(\frac{r}{R} + \mu\sin\psi\right)\Omega R - U_{Gust}\sin\psi - V_{Gust}\cos\psi + \Delta V_T$$

$$\phi = \tan^{-1}\left(U_P/U_T\right)$$

$$\alpha = \theta + \phi$$

The velocity at the swashplate for the main rotor of a pure single-rotor helicopter is given by

$$\vec{V}_S = \vec{V}_c + \vec{\omega} \times \vec{\rho}_S$$

The expression for local inflow ratio is

$$\lambda = \bar{\lambda} + \frac{V_x}{\Omega R}\left[1 - (1 + k\cos\psi)\,\frac{4}{3}\,\frac{r}{R}\right]$$

where

$$\bar{\lambda} = \left(\left|V_S\right|\sin\alpha_c - v_i\right)/\Omega R$$

$$v_x = (1 + kk')v_i$$

$$\mu = \left|V_S\right|\cos\alpha_c/\Omega R$$

The angle of attack of the swashplate, α_c, is obtained from the components of $\vec{V}_S$.

k is a function of advance ratio discussed in Reference 19. k' is a function of ψ and r derived empirically to reproduce local induced-flow variations due to tip-vortex effects and is discussed in Reference 16. The following approximations are used:

$$k = \begin{cases} 11.25\mu, & \mu \le .1067 \\ 1.36 - 1.5\mu, & .1067 < \mu \le .5733 \\ .5, & .5733 < \mu \end{cases}$$

$$k' = 10 \sin[6(\psi - 45°)] \sqrt{-\frac{1}{2}\left|\vec{V}_S\right|^2 + \frac{1}{2}\sqrt{\left|\vec{V}_S\right|^4 + 4v_i^2}}$$

for $\frac{r}{R} \ge .8$ and $45° \le \psi < 165°$ or $225° \le \psi < 315°$

Outside these limits k' = 0.

Preparation for analyzing Rotor 2 is essentially the same as for Rotor 1. If Rotor 2 is a tail rotor, the sidewash effect is brought in as a modifier on the V-component (body reference) of the hub velocity.

$$\vec{V}_{S_2} \cdot \vec{j}_B = \vec{V}_c \cdot \vec{j}_B(1 - \text{TRSWC}) + \left[\vec{j}_B \vec{\omega} \vec{\rho}_{S_2}\right]$$

where TRSWC is input data to account for the sidewash effect on the tail rotor. Also, the swashplate plane is rotated 90° about the x_B-axis.

If Rotor 2 is the rear rotor in a tandem configuration, the air may be disturbed. The equations used are

$$\chi = \tan^{-1}\left[\left(\left|\vec{V}_{S_2}\right| \sin\alpha_{c_1} - v_{i_1}\right) \Big/ \left|\vec{V}_{S_2}\right| \cos\alpha_{c_1}\right] 57.3$$

$$\Delta v_{i_2} = v_{i_1}\left(1.04 - .005\,\chi + .000298\,\chi^2\right)$$

If Rotor 2 is the left rotor in a side-by-side configuration, no unusual treatment is used. In all cases Rotor 2 is assumed to rotate counter to Rotor 1, so that various sign shifts must be made.

The program can be used for performance studies, but it should be noted that the airfoil data are approximated by suitable nonlinear functions of angle of attack and Mach

number, as shown in Figure 12. The rotor analysis is quasi-steady-state based on the tip-path plane, rather

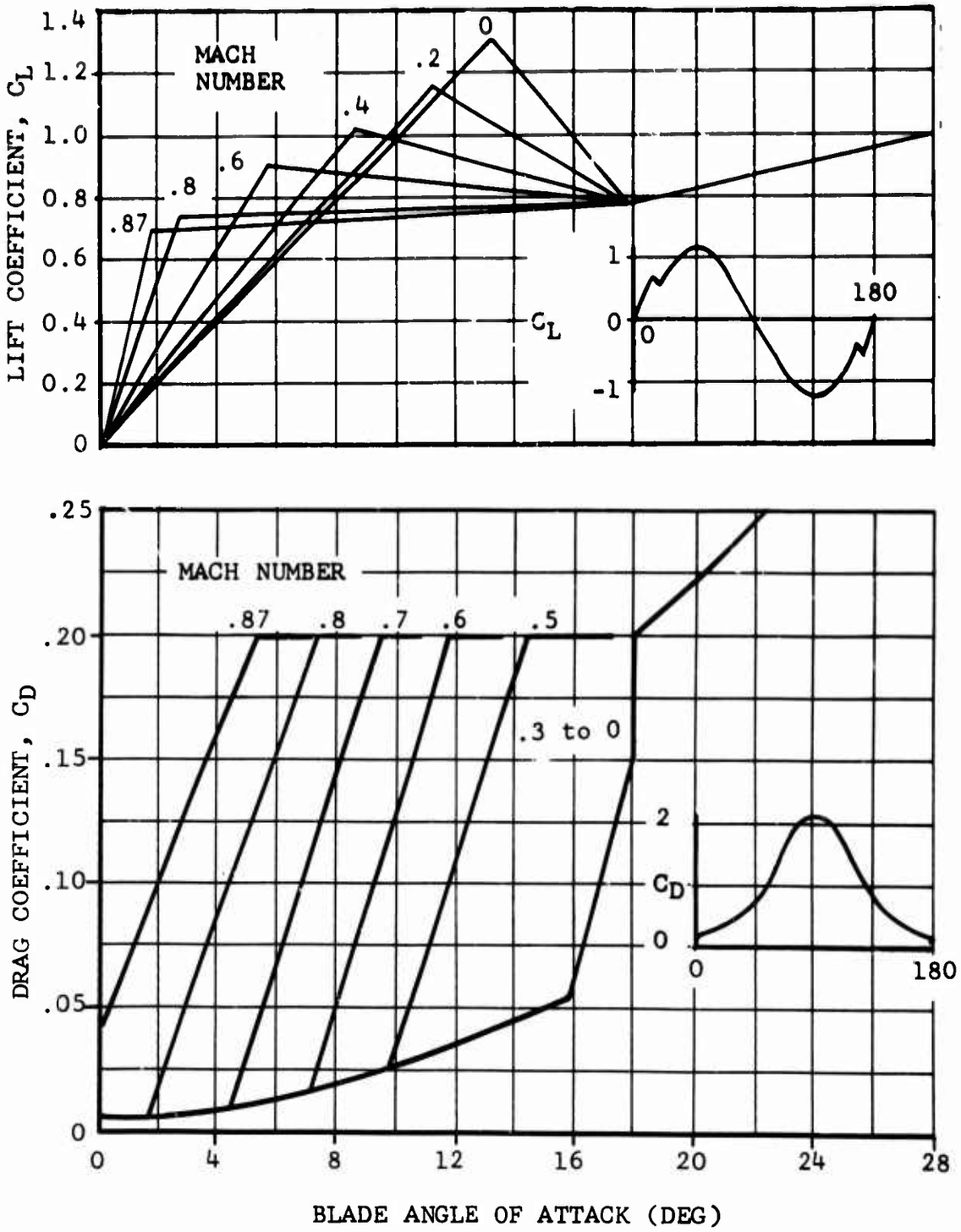

Figure 12. Example of Airfoil Characteristics as Described by Aerodynamic Functions.

than a time-variant step-by-step process for each blade. Harmonic components of aerodynamic-shear distributions through four per rev are computed and supplied to the rotor dynamics analysis section. The rotor aerodynamic analysis sections of the program consume a large portion of the total time required to run a case. When aeroelastic feedback is included, the time used for each pass through the rotor analysis is more than doubled.

A simplified analysis of a propeller for auxiliary propulsion was developed for a special design concept and remains in the program. One propeller can be selected and located at the center of the rotorcraft, or two propellers can be placed a specified distance on either side of the center. Either thrust or collective pitch can be required. Provision is made for nonlinear twist and for tapered planform. This feature is separate from the converted rotor option. Auxiliary jet-thrust simulation is included as specified forces acting through certain points and directed forward at a given angle to the centerline of the aircraft.

Rotor Blade Bending-Moment Analysis

The rotor blade bending-moment program is a tabular method similar to the Myklestad procedure (20). The analysis is based on the assumption that the displacement, slope, shear, and moment at any point on a beam are linear functions of the corresponding four root or base values of these state variables. It is further assumed that the forcing functions and state variables can be treated as consisting of uncoupled harmonic components based on rotor rpm. This assumption allows the single-blade representation, because the conditions at the hub depend on the harmonic component as well as the hub type and number of blades. A set of eight linear equations can then be written for a particular harmonic. These relate the state variables at a point on the beam with index j to the state variables at the root. Formally, for the ith variable at the jth point on the beam,

$$x_{ij} = B_{ijo} + \sum_{R=1}^{8} B_{ijR} x_{oR}, \quad i = 1, 8 \qquad (9)$$

Recursive expressions for determining the coefficients appearing in the above equations are applied to a segmented representation of the rotor blade. These coefficients are functions of the dynamic parameters of the beam and of the harmonic components.

At least four of the eight root boundary values are known for the given harmonic, hub type, and number of blades.

Since the tip shears and moments are zero, the equations for these four quantities are solved for the remaining four unknown root conditions. For example, consider a two-bladed, semirigid rotor, first harmonic component. The known root conditions are:

- out-of-plane deflection and moment equal to zero
- in-plane deflection and slope equal to zero.

Then the four equations to solve are

$$\left.\begin{aligned}
S_{B_{Tip}} &= B_{3_{Tip,0}} + B_{3_{Tip,2}}\phi_0 + B_{3_{Tip,3}}S_{B_0} \\
&\quad + B_{3_{Tip,7}}S_{C_0} + B_{3_{Tip,8}}M_{C_0} = 0 \\
M_{B_{Tip}} &= B_{4_{Tip,0}} + B_{4_{Tip,2}}\phi_0 + B_{4_{Tip,3}}S_{B_0} \\
&\quad + B_{4_{Tip,7}}S_{C_0} + B_{4_{Tip,8}}M_{C_0} = 0 \\
S_{C_{Tip}} &= B_{7_{Tip,0}} + B_{7_{Tip,2}}\phi_0 + B_{7_{Tip,3}}S_{B_0} \\
&\quad + B_{7_{Tip,7}}S_{C_0} + B_{7_{Tip,8}}M_{C_0} = 0 \\
M_{C_{Tip}} &= B_{8_{Tip,0}} + B_{8_{Tip,2}}\phi_0 + B_{8_{Tip,3}}S_{B_0} \\
&\quad + B_{8_{Tip,7}}S_{C_0} + B_{8_{Tip,8}}M_{C_0} = 0
\end{aligned}\right\} \quad (10)$$

These equations are solved for the out-of-plane root slope, ϕ_0, and shear, S_{B_0}, and in-plane root shear, S_{C_0}, and moment, M_{C_0}. Since all quantities in the state equations are now determined, the displacement, etc., along the beam can be computed from the equations (9) for each harmonic. Net values over the rotor disc are obtained by superposition.

Equations showing the effects of the centrifugal force field and the blade-pitch angle, including linear twist, are detailed in Reference 15. The pitch-change values are based on torsional moments arising from aerodynamic pitching moments on the blade segment, and the cross product, F x d, where F is the aerodynamic force vector and d is the deflection of a segment. These moments are assumed to act against a control linkage represented by a spring, while the blade is assumed to be rigid in torsion. The velocities arising

from blade response are computed from the deflection harmonics and are superposed.

The pitch changes and velocities at each of 20 blade segments, and at up to 12 azimuth locations, are used in the subsequent rotor aerodynamic analysis. Since this dynamic consideration is not used in the trim section, a modified trim attitude may be expected. Rather than introduce still another loop in the steady-flight solution program, the dynamic contributions are fed back gradually within the time-variant section.

Certain limitations are inherent in the representations. The number of blades, type of hub, and harmonic component under consideration combine to determine the root conditions. Hence, each contingency must be accounted for in the program. At present, the program can handle steady through fourth-harmonic components for the following rotor types:

- articulated
- semirigid
- semirigid with hub restraint
- rigid

Each of these rotor types can have two, three, or four blades. In practical applications, the two-bladed rotor is not combined with a rigid hub.

The feedback feature of the program can be suppressed if it is not needed for a particular job. The rotor's dynamic response can be computed at specified times without feedback if desired. If either of the provisions for computing rotor oscillatory loads is to be used, the rotor must be designed dynamically to avoid resonances, since the dynamic response is calculated on an undamped basis.

Wings, Control Surfaces, and Fuselage

Wing forces are derived from wing-geometry parameters, and flight-path and ship-motion vectors. A left wing and a right wing are represented because the angle of attack is not necessarily the same on both sides. Finite aspect ratio is taken into account (21), and realistic lift-and-drag-coefficient functions include stall and Mach number effects (22). Ailerons are simulated by allowing variation of wing incidence with stick motions.

The horizontal stabilizer-elevator and fin-rudder are simulated similarly to the wing-aileron. The fuselage has angle-of-attack-dependent lift, drag, and pitching-moment characteristics, and yaw-dependent side-force, drag, and yawing-moment characteristics.

Special Aerodynamic Considerations

Allowances in the program for unusual airflow are made in several ways. As has already been indicated, induced velocity on the rotors, including first-order effects of nonuniform inflow due to the wake-vortex system, is taken into account. Furthermore, some part of the main-rotor induced velocity is felt by the wing in the case of composite craft. The elevator is affected by rotor downwash and wing wake, and the fin is affected by the tail-rotor induced velocity. The airstream may be bent by the fuselage so that the fin's angle of attack is influenced (sidewash effect). In tandem-rotor configurations, the aft rotor may be flying into a flow that has been disturbed by the forward rotor. These variations have been simulated in the aerodynamic equations.

Nonsteady aerodynamic considerations have also been included in the program (23). They are discussed on page 41.

The aerodynamic representation includes the capability for gradual penetration of a gust. The change in rotor thrust, resulting from local angle-of-attack changes due to the presence of gust velocities over a segment of the rotor disc, is constrained to a gradual variation. The whole rotorcraft gradually enters the gust. Hence at a given time, a gust velocity dependent on the gust shape and the component location applies at all points on the aircraft in a plane normal to the flight path; wing and elevator also penetrate the gust gradually. The lift-buildup functions appear to give good results. When more concise theoretical developments are available, new functions can replace the present ones without difficulty.

Engine-Governor-Torsional System

The drive system includes the engine, two rotors, propellers if any, and two types of governors. An engine-governor simulation matches the total torque required to the engine output in normal operation. Power recovery after a full or partial throttle chop is simulated by a parabolic function that includes engine lag time. Power available is increased to its maximum, held until required rpm is attained, then set as for normal operation. A change in rpm results if torque required exceeds the range from zero to maximum available. In addition, a prop-rotor collective-pitch governor (PCG) controls rpm by changing rotor collective pitch during changes in throttle setting (effectively, horsepower supplied). This servomechanism is represented as having a dead band to reduce hunting, and an acceleration capability to a maximum pitch-change rate. This allows a throttle variation (represented by horsepower-supplied change rate) while maintaining, within limits, a specified rpm. Variations in main-rotor rpm and torque required produce reactions in body-motion degrees of freedom as well as in the rotor's performance.

Control System

The control system, as represented, consists of pilot-control capabilities and servomechanisms. The pilot controls are collective and cyclic sticks, pedals, throttle, mast-tilt actuator, rpm selector, and engine-governor selector. These controls are linked to the swashplate, control surfaces, and other affected mechanisms, and the displacement ratios are specified (where appropriate) by input data. In the trim section, the stick and pedal positions are the primary values to be found. In the maneuver section, each of these controls can be moved at specified rates (or switched on) during selected time intervals.

Several automatic mechanisms that affect the controls are represented. Pitch stabilizing is induced by a transfer function sensitive to pitch displacement from trim, pitch velocity and acceleration. This function produces changes in cyclic and collective pitch, subject to a lag factor. Yaw stability is handled similarly.

RPM is maintained either by a standard governor which varies the power supplied, or by the PCG which varies rotor collective pitch. These mechanisms are more fully described above in the Engine-Governor-Torsional System. If one or two propellers are used for auxiliary propulsion, an automatic control that varies the propeller's collective pitch with forward speed is available. Provision is made for a pilot-input override.

A flat-tracker mechanism may be activated to hold the trim values of either rotor-to-mast flap angles or specified flap angles within a stated tolerance by varying cyclic pitch. Collective-pitch-bobweight coupling can be switched on or off at data-specified times. Pitch-flap and pitch-cone coupling are controlled by configuration parameters. They are not subject to change during maneuvers.

Solution Procedures for Trim and Maneuvers

For a given description of the rotorcraft and its steady-state flight conditions, the trim parameters listed earlier must be found from the set of algebraic equations obtained by equating the first 11 equations in Table V, page 30, to zero. By assuming that the required horsepower is available, the drive-system rotation equation can be omitted, since rpm is input. With 10 equations and 11 unknowns, a value may be assigned to one of the unknowns. In the current version of the program, the fuselage yaw angle is assigned. There remains a set of 10 nonlinear algebraic equations in 10 unknowns.

It is impractical to attempt to write these equations in explicit form since, among other complications, the entire rotor analysis is involved. However, an iterative procedure which depends on the evaluation of functions can be employed

for solution. The procedure begins with the substitution of an initial-approximation vector, Z_o, in the force and moment sum functions and computation of their values. If Z_o is the exact solution, all the functions will be zero and the equations are satisfied. Otherwise, the function values are a vector, E, and Z_o must be changed so that the magnitudes of the components of E are reduced. The total differential of a function is the sum of the products of the partial derivative of the function with respect to each independent variable, and the differential of that variable. The set of net changes desired in the functions is -E, the negative of the error vector. Let Δ be the vector representing the set of independent-variable differentials, and M the matrix of function partial derivatives. It now appears that $M \cdot \Delta = -E$ represents a set of linear equations, that values of Δ can be computed, and that $Z_o + \Delta$ will be the correct-answer vector. This is not altogether true, however, because the partial derivatives are not constant, but are evaluated numerically about the point specified by Z_o. It may be possible, though, to converge to good results by replacing Z_o with a new approximation, $Z_o + \Delta$, and substituting again in the functions. Let $\overline{E}$ be the vector whose components have the magnitudes of the elements of E, and A, an allowable-error vector. If $\overline{E}$-A has no positive components, the solution is satisfactory. If not, the elements of M are reevaluated and the process is repeated. After satisfactory results are obtained, stick and pedal positions are checked against stop and range data, and required horsepower is checked against available horsepower. If all of the conditions are met, the program proceeds to the maneuver section. The numerical solution method described above is suggested in many texts. If we consider a function of many variables expanded in a Taylor's series in the neighborhood of a point, the equations in the first-order partial derivatives, as used in the program, result when all higher-order terms of the series are ignored. However, since many of the equations are strongly nonlinear (especially in the case of high advance ratios), considerable difficulty may be experienced in applying this technique. This is a problem that is often encountered in the numerical analysis of large nonlinear systems (24).

Considerable effort has been expended in the course of this study in searching for improvements to the method used for calculating trim solutions. Inclusion of second-order partial derivatives has been tried, but without marked improvement in capability. Work is continuing in two directions to expedite solutions: (1) limited analyses (i.e., linear theory) using empirical data to provide better initial approximations; and (2) more precise mathematical analysis.

Stability derivatives about the trim point are computed numerically using the same program technique as for the other partial derivatives. The calculation of these velocity-based rates can be selected if required by the user of the program.

Maneuvers are activated by input data which result in time-dependent changes in control positions or aerodynamic environment. Certain automatic-control devices can also be turned on or off at specific times. Response to these changes is derived from stepwise solution of the differential equations, with the trim values being used as initial conditions. Thus the stability and control characteristics of the configuration can be ascertained. Almost any maneuver that a given type of rotorcraft is capable of executing may be simulated.

A Runge-Kutta procedure (25) is used to solve the differential equations. The process is characterized as four-pass, noniterative, and noncorrective. It is noncorrective because the initial values for the second time step are the final values computed in the first time step, and no further influence due to previous values is included. Computer time becomes a problem in this section because each cycle involves complete analysis of two rotors. Predictor-corrector methods of solution (26,27) are being considered as a means for improving this part of the program.

The process is somewhat complicated by the transformations of the reference axes that are involved. The first group of equations, in fuselage-reference accelerations, is integrated to yield fuselage-reference velocities. The instantaneous angular velocities are transformed to Euler-angle velocities, which are used to compute new Euler angles. The instantaneous linear velocities are transformed to fixed-reference, and these quantities are used to compute linear displacement. The rotor equations are handled similarly. Two objectives are realized:

Equations are retained in straightforward, simple form, including constant mass moments of inertia; and

Fuselage-reference velocities, which are needed for stability and control studies, are computed as a necessary part of the procedure.

Input and Output

The input data required for this computer program are fully discussed by Blankenship and Bird (9). An effort was made to keep the number of inputs to a minimum, and to express them in conventional units. The parameters are organized into logical categories in the input format. In addition to quantifying data, identification and program control data are included.

The computer data output is fully annotated and, except for conditional output, is self-explanatory. When undesirable or unusual numerical situations occur in the computing process, output messages stating the nature of the problem are provided. In addition to digital information, plots of most of the

variables can be obtained automatically, controlled by the data specifying the variable and the range.

A program capability for retaining maneuver data on tape for retrieval and plotting when required is also available. Subsidiary programs may be used to set up a permanent library of case results. The principal input and output features are illustrated in Figure 9.

WING NONSTEADY AERODYNAMICS

Nonsteady aerodynamics for a fixed wing are treated by the methods developed by Küssner and Wagner (28,29). The Wagner function represents the lift buildup due to a sudden change in angle of attack, and is given by the equation

$$\Phi(s) = C_o + C_1 e^{r_1 s} + C_2 e^{r_2 s} \qquad (11)$$

where s is the distance traveled in semichords, and C_o, C_1, C_2, r_1, and r_2 are constants which must be selected to reflect the wing aspect ratio. Following a sudden change in angle of attack, a "starting" vortex is generated that partially suppresses the sudden increase in wing lift. The "starting" vortex remains stationary in space, thereby losing its influence on the moving wing. Depending upon wing aspect ratio, the initial lift increment for the Wagner function is approximately one-half of the final lift increment, as shown in Figure 13.

The Küssner function represents the lift buildup for a wing gradually penetrating a gust, where the lift builds up from zero (no initial increment). For the general case of a shaped gust profile the wing simultaneously experiences a change in gust velocity and a change in angle of attack due to aircraft pitch response. It is necessary, therefore, to combine the Wagner and Küssner functions into a single analytical expression. An approximation of the Küssner function is obtained by multiplying the Wagner function by the average gust velocity at four points along the wing chord (leading edge, 0.25c, 0.50c, and 0.75c). For a sharp-edged gust, the approximation results in a series of steps as the control points successively enter the gust. Figure 13 also shows the Küssner function and the approximation used for this study.

ROTOR NONSTEADY AERODYNAMICS

For a rotor, Drees and Lucassen (8,13) report that a noticeable reduction of the lift increase due to a sudden gust is to be expected if nonsteady aerodynamics are considered. Since Drees and Lucassen assumed the rotor to act as a fixed circular wing,

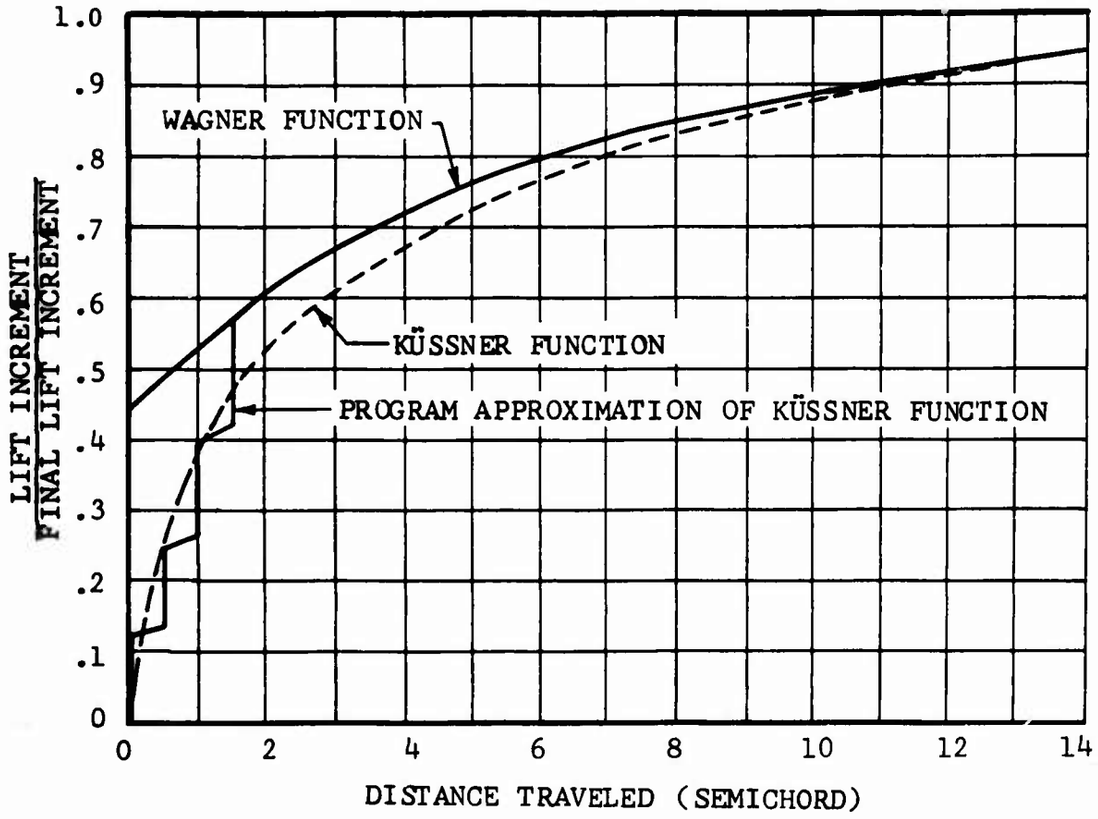

Figure 13. Wagner Function, Küssner Function, and Approximation of Küssner Function.

their results show only the qualitative influence of nonsteady aerodynamics on the gust response of a rotor.

Recent analytical methods (14,30,31), which use detailed representations of the free vortices shed from the rotor blades, produce the lift functions needed for this study. Limitations on storage and computing time, however, precluded the use of such methods in the present analysis. Following the concepts used by Wagner and Küssner in the fixed wing analyses, a more suitable solution was developed during the course of this study by Buettiker and Weber (32,23). The two major components of the rotor wake are considered separately:

1. The far wake consists of the helical pattern of vortices that is shed from the rotor tips after a change in rotor lift.

2. The near wake consists of vortices that are shed along the trailing edge of a blade due to changes in the local blade angle of attack.

Consider, briefly, a rotor with an infinite number of blades but with the usual values of solidity and rotational speed. Each local airfoil section travels a distance of many chord lengths in a negligible amount of time because the chord length is nominally zero. Therefore, there is no delay in the lift buildup on the local airfoil due to local changes in gust velocity or angle of attack. Furthermore, the local effects of vortices shed from the trailing edge of preceding adjacent blades are cancelled by the effects of vortices shed from the trailing edges of following adjacent blades. The tip vortices (far wake) remain as the only contributor to nonsteady aerodynamic effects for a rotor with an infinite number of blades.

For a finite number of blades, the far wake effects are unchanged. An additional consideration is that a finite time is required for the lift to change at a local airfoil section. The delay in lift buildup is comparable to the fixed-wind nonsteady aerodynamic effect, except that the distances traveled must be expressed in terms of rotor diameters instead of wing semichords. The near-wake effect (reflecting a finite number of blades with finite chord length) is superposed with the far-wake effect to represent nonsteady aerodynamics for a rotor.

Far Wake Effect

Buettiker's analysis assumes that, due to appropriate control inputs, a sudden change in rotor lift is distributed uniformly over the rotor disc and that the rotor does not flap. The induced flow is calculated versus time at four sampling points on the disc (0.75R, 4 azimuth positions). Typical results are shown in Figure 14. Note that the maximum local induced velocity is reached first at the forward part of the rotor (180° azimuth position) and somewhat later for the aft part of the rotor (0° azimuth position). These calculations include only the net circulation of the wake increment as it develops. The average induced velocity gradually increases and reaches its final value shortly after the new tip-vortex sheet from the forward part of the rotor passes beneath the aft part of the rotor. A flow pattern then is established with the highest induced velocity near the aft section of the rotor. Since the change in the induced velocity is zero at the time of the sudden lift change, the subsequent wake development results in a decay of the initial lift increment to a smaller steady-state value. The solid line of Figure 15 presents an example of the far-wake lift function as calculated for a rotor with a solidity of 0.07 at an advance ratio of 0.5. Note that the initial lift is about 8 percent higher than the final lift.

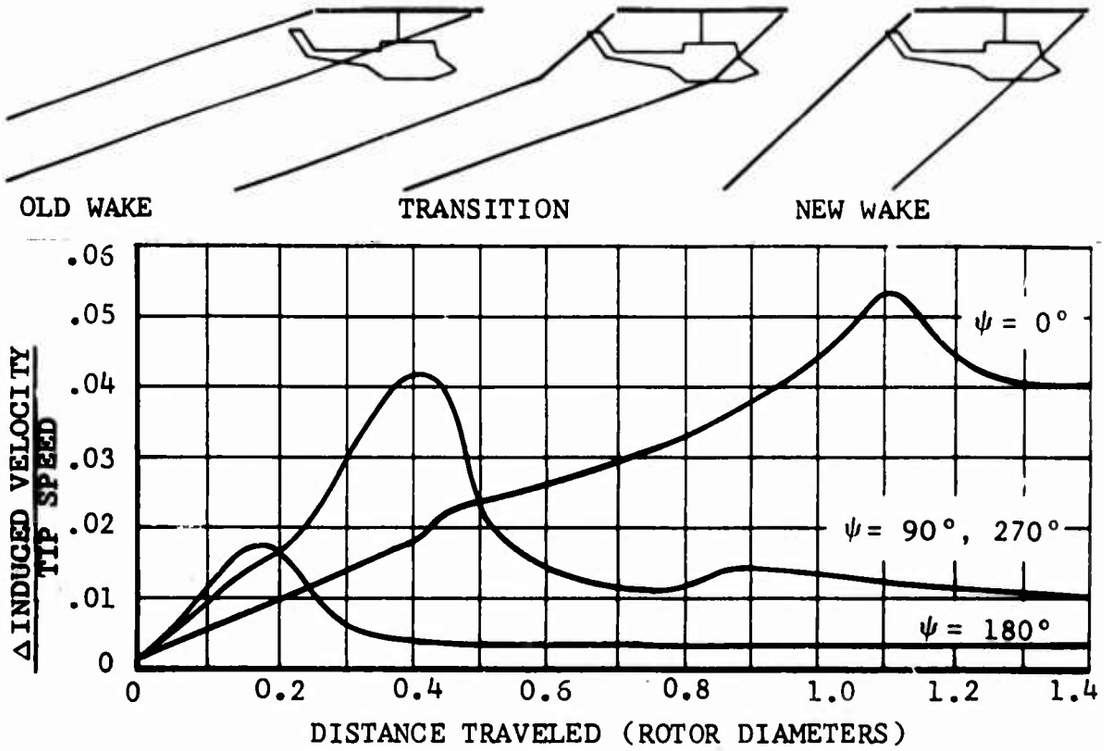

Figure 14. Induced Velocity at 0.75R after a Sudden Lift Change.

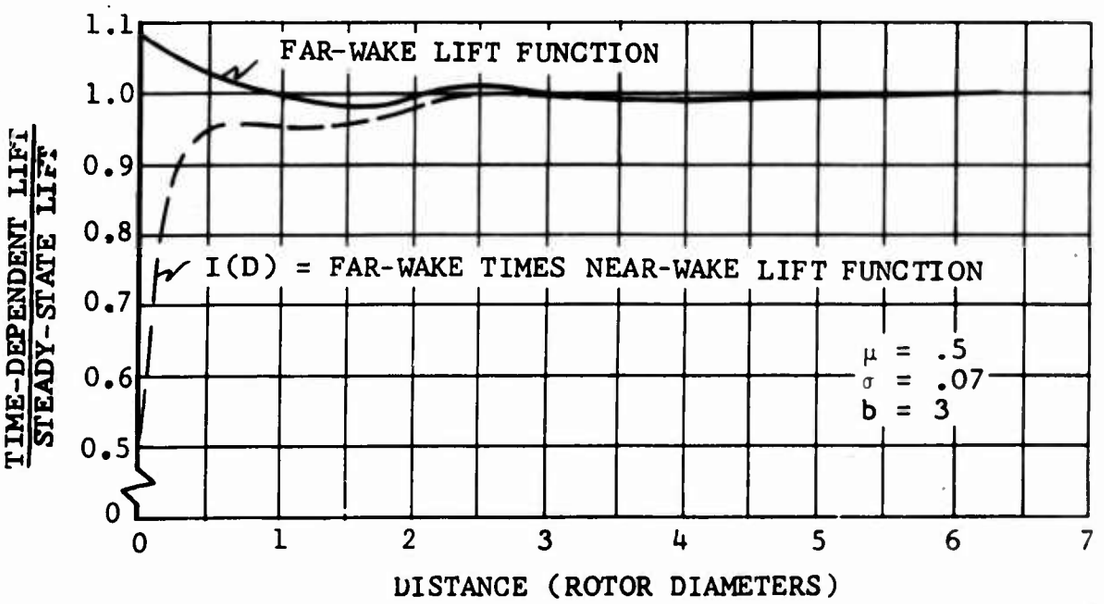

Figure 15. Lift Buildup Due to Wake.

Near-Wake Effect

The lift on a rotor with a small number of blades cannot build up instantaneously. By analogy with fixed-wing theory, vortices are shed along the trailing edge of the rotor blade as the lift changes, causing a time-variant induced flow that reduces the lift increment on the local airfoil section. This phenomenon is identical to the fixed-wing effect that is represented by the Wagner function. In the analysis, the far-wake effect and the near-wake effect are superposed by multiplying the far-wake lift function by the Wagner function.

Far-wake lift functions were calculated for 25 combinations of solidity and advance ratio for both a 3-bladed rotor and a 36-bladed rotor (to approximate an infinite number of blades). Solidity was varied from 0.05 to 0.09 in steps of 0.01; advance ratio was varied from 0.1 to 0.5 in steps of 0.1. A large change in either solidity or advance ratio shows no appreciable effect on the total nonsteady-aerodynamic lift function for a rotor (23). For each set of 25 parameter combinations, an average lift function was established that should be valid for the entire range of solidities and advance ratios that were used in the computer case studies. The lift function for a 36-bladed rotor exceeds 0.9 after the rotor travels about 0.15 diameter; the lift function for a 3-bladed rotor exceeds 0.9 after the rotor travels 0.32 diameter. The lift function for the combined far-wake and near-wake effects is synthesized by a sixth-order polynominal:

$$I(D) = + 0.5 + C_1 D + C_2 D^2 + C_3 D^3 + C_4 D^4 + C_5 D^5 + C_6 D^6$$

where D is the distance, in rotor diameters, traveled after the disturbance. The resulting lift function (shown by the dotted line of Figure 15) has an initial lift change that is equal to one-half of the final lift change, and reaches 90 percent of the final value within a distance traveled of about 0.25 diameter. Note that this analysis is not valid for hovering or low forward speeds.

In relation to the lift function for a 3-bladed rotor, the synthesized function yields conservative results for thrust increase and slightly understates the relative importance of rotor nonsteady aerodynamics, but the evaluation of the computer case results showed that this effect was among the least significant of those studied. Although considerations of stall, compressibility, and reverse flow were excluded by the selection of sampling points (at 0.75R and 4 equally-spaced azimuth positions) for the above development, valid first-order quantitative effects should be obtained for rotors with any finite number of blades.

Immediately after an angle-of-attack change, there is a greater induced velocity than during the steady state, and the vortices move very slowly away from the rotor plane. A lift overshoot should be expected. References 33 and 34 tend to confirm this expectation. Measurements reported in Reference 14, however, show little overshoot of the average lift. Figure 16 shows a comparison of the lift function used in this study with results from Reference 14. (Note that Reference 14 includes a gradual pitch increase which tends to reduce the initial slope of the lift curve.)

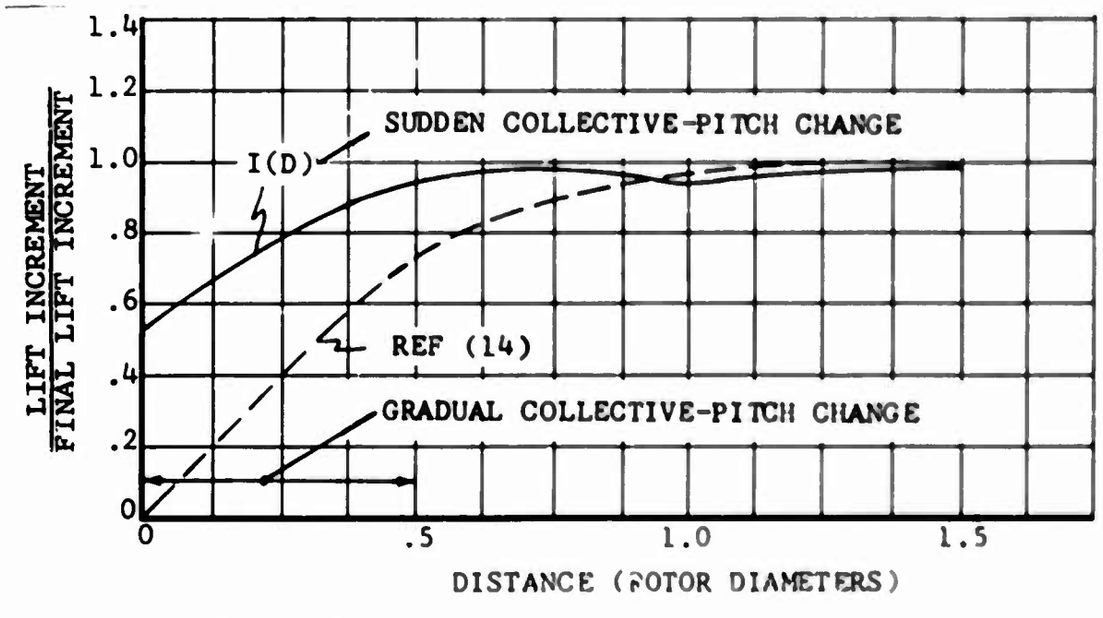

Figure 16. Correlation of Lift Buildup.

The method for evaluating the time-dependent lift buildup uses the Duhamel Integral (35), in which the lift functions $\Phi(s)$ for the wing and I(D) for the rotor assume the roles of the indicial admittances of the systems. Since the maneuver program computes the steady-state wing lift and rotor thrust due to a gust or angle-of-attack change, the lift and thrust are used as inputs for the time-dependent lift computation. This procedure has the advantage that the nonsteady lift functions for both the rotor and the wing are treated in the same manner by a simple mathematical procedure. The storage requirements in the computer are minimized, and the time required is acceptable: a maximum of 50 seconds is required for 100 time steps, using the lift function I(D). The computation of this information from the wake itself would take more than 15 minutes.

In retrospect, it is believed that a more desirable approach might be to keep the far-wake and near-wake effects separate (see Figure 15), to relate the near-wake effects to the lift functions of each local blade element, and to relate the far-wake effect to the rotor thrust. The advantage would result from effectively including the nonsteady lift functions in the calculation of steady-state flight conditions. The computational involvements would be far less than with a full-wake representation. This approach is suggested as a future modification of the program.

GUST MODEL

The mathematical representation of gust velocities, horizontal or vertical, is accomplished with time-variant air-velocity functions. These gust-shape functions are represented in the maneuver section as follows:

Sharp-edged

$$V_g = \begin{cases} 0, & d<d_1 \\ c, & d\geq d_1 \end{cases}$$

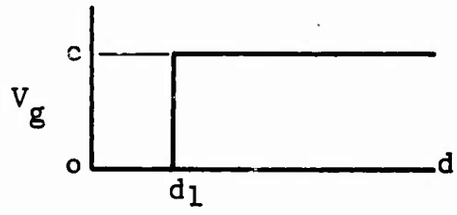

Ramp

$$V_g = \begin{cases} 0, & d<d_1 \\ b(d-d_1), & d_1\leq d<d_1+H_g \\ bH_g, & d\geq d_1+H_g \end{cases}$$

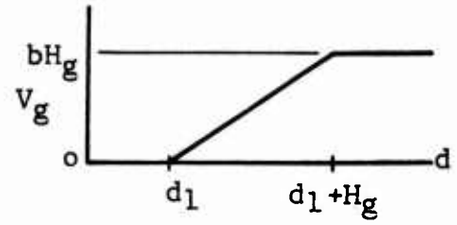

Sine-squared

$$V_g = \begin{cases} 0, & d<d_1 \\ a \sin^2 \pi\left(\dfrac{d-d_1}{2H_g}\right), & d_1\leq d<d_1+2H_g \\ 0, & d\geq d_1+2H_g \end{cases}$$

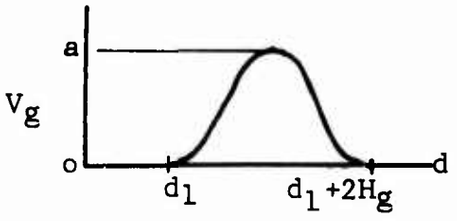

where d = distance from the origin to the point considered

d_1 = distance from the origin to the gust

H_g = ramp length or distance over which the gust velocity increases

a,b,c = constants controlling the gust amplitudes

The duration and maximum velocity reached, as well as the shape, are determined by input data.

The introduction of the gradual penetration into the program involves careful "bookkeeping" to establish the exact gust velocity on each part of the aircraft at any given time. The locations of rotor hubs, wing, elevator, and fin are already inputs to the program for calculating force and moment balance. The output format includes a presentation of the instantaneous-gust velocities over the rotor disc. Figure 17 shows examples of such an output for a sine-squared gust with a ramp length of 90 feet on a helicopter traveling at a speed of 200 knots.

The important question - which gust model to use - is discussed at some length in Reference 8. In that study, the sine-squared gust shape is introduced in parallel with the techniques developed for fixed-wing aircraft (11, 36). The problem is that the ramp length of the gust for fixed-wing aircraft is expressed in terms of the chord length (ramp length = 12.5 chords). Obviously, this measure cannot be used for a rotor. It is therefore concluded in Reference 8 that the gust function must be related to the circumstances actually found in the atmosphere (which are, of course, independent of the chord length of a particular aircraft).

References 10 and 37 present information on gust envelopes, determined indirectly by flying fixed-wing airplanes through gusts. Using the analyses developed for fixed-wing airplanes, a region determined by the maximum gust velocity and ramp length was found to contain almost all the test data. Figure 18 shows that the gust velocity (V_g) in this envelope reaches a maximum of about 50 feet per second at a ramp length (H_g) of 90 feet. Although a roof-top gust model was used, very little change is expected when a sine-squared gust shape is substituted, as is shown later (page 57).

Figure 18 indicates that very high gust velocities will not be present in the atmosphere without a considerable ramp length. Understandably, then, high-velocity gusts will build up more gradually than sharp-edged gusts, and the gust loads will be relatively lower.

The sine-squared gust shape was chosen as the most realistic model for this study. A later section of this report shows the establishment of critical values for the gust velocity (V_g) and ramp length (H_g) to produce the maximum load factor. The sine-squared gust is invariably used in conjunction with the gradual penetration and the nonsteady aerodynamic lift functions. The result is compared with the sudden gust case, in which the entire aircraft is instantaneously submerged in the gust with a velocity (V_g), without the benefits of gradual penetration and nonsteady aerodynamic effects.

For horizontal gusts, which are assumed to hit the aircraft from the front or the side, similar assumptions are made.

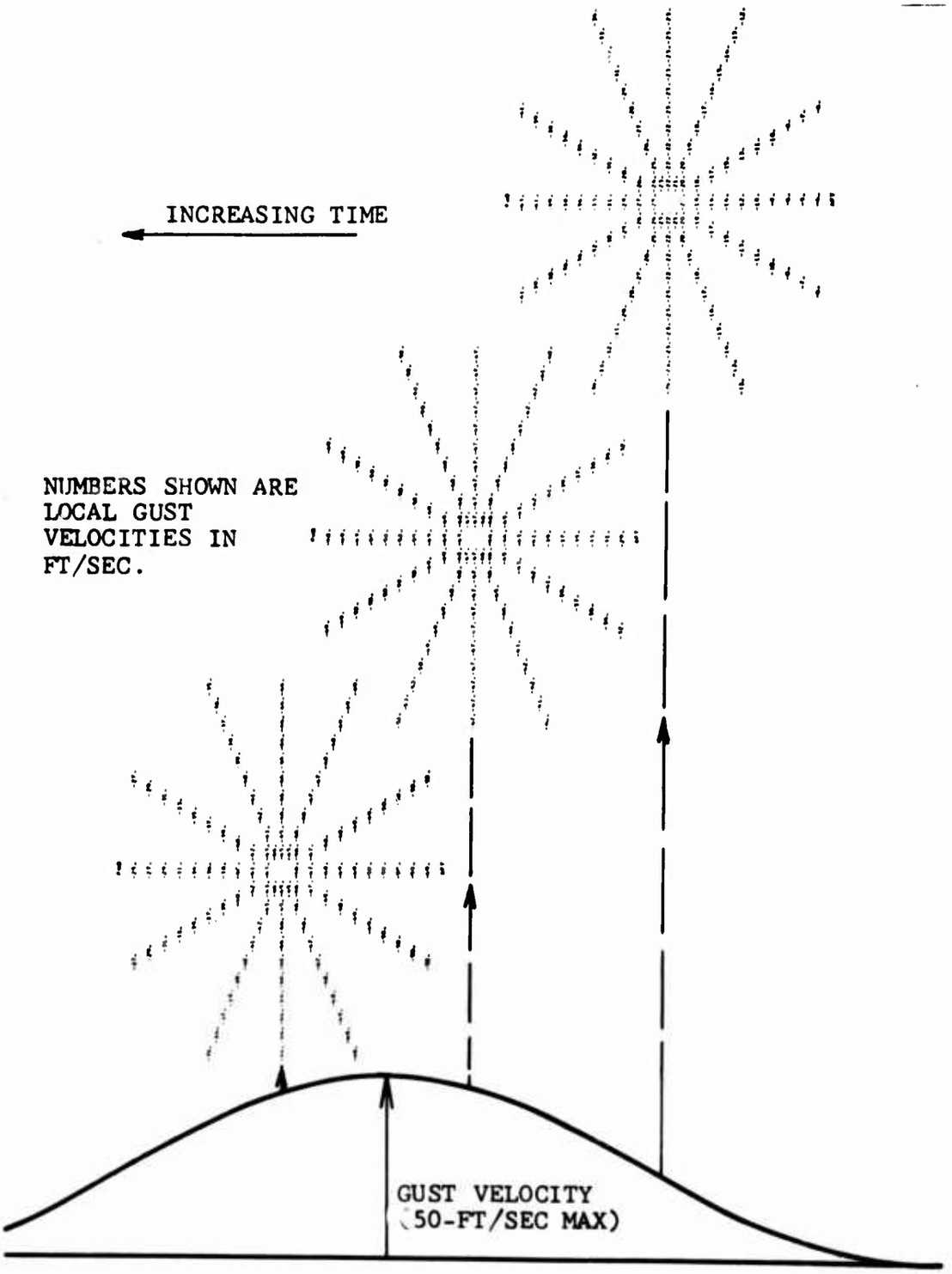

Figure 17. Gradual Gust Penetration (Automatic Computer Output).

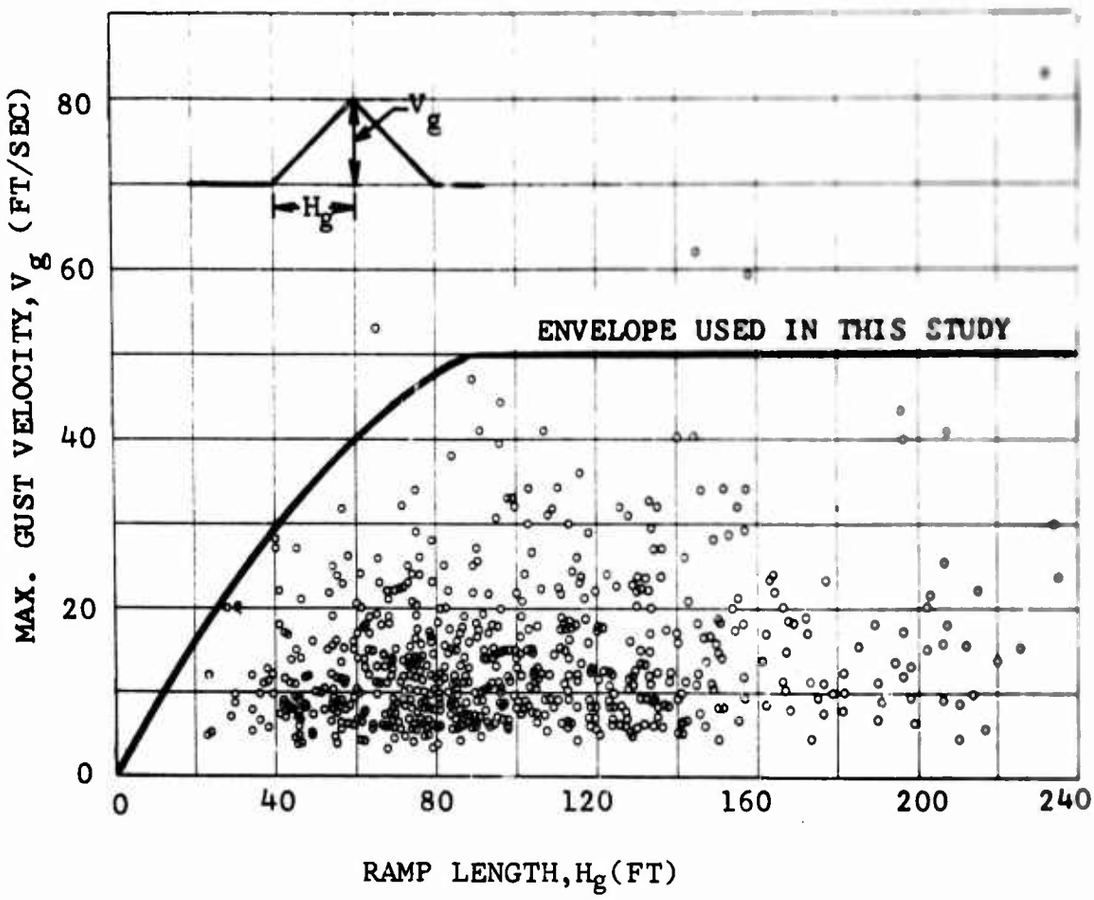

Figure 18. Envelope of Gust Based on Flight Tests With Fixed-Wing Aircraft.

STOPPED- AND TRAILED-ROTOR ANALYSIS

The response analysis for the stopped rotor and for the trailed rotor encountering a gust is presented in detail by Weber (17). Two gusts were used: a sine-squared gust with a 90-foot ramp length and a sudden gust, both with 50 feet per second maximum velocity.

Schematics of the stopped rotor and the trailed rotor are shown in Figures 19 and 20, respectively. The stopped rotor has two flexible blades cantilevered on a flexible mast. The mast is cantilevered at its base. The trailed rotor is shown in cruise condition with its three blades folded aft from the wing tip.

A computer program with provision for thirty-six degrees of freedom was written specifically for this analysis. The

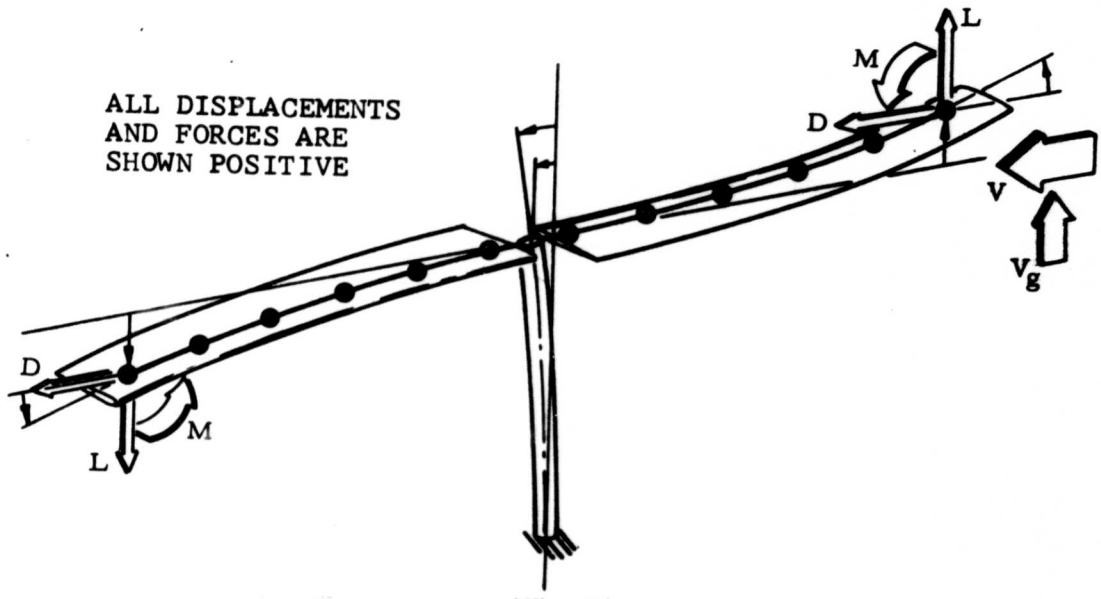

Figure 19. Schematic of Stopped Rotor.

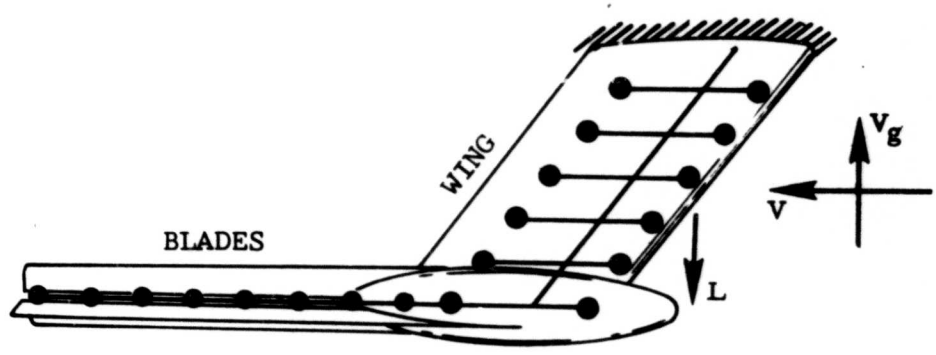

Figure 20. Trailed-Rotor Dynamic Representation and Sign Convention, Perspective View.

program forms the dynamic and aerodynamic matrices from the input data (17). The time-dependent solution to the equations is found by use of the Runge-Kutta technique. The basic equation for both cases is

$$[m]\{\ddot{x}\} + [c]\{\dot{x}\} + [k]\{x\} = \left[F_1\right]\{\ddot{x}\} + \left[F_2\right]\{\dot{x}\} + \left[F_3\right]\{x\} \quad (12)$$

The damping matrix [c] is considered to be diagonal, and the aerodynamic mass matrix $[F_1]$ is considered to be a second-order effect and consequently is neglected. The general equation can now be written:

$$[m]\{\ddot{x}\} + [c]\{\dot{x}\} + [k]\{x\} = \left[F_2\right]\{\dot{x}\} + \left[F_3\right]\{x\} \quad (13)$$

Because of the problem of generated input data, two methods of problem setup are used. The dynamics of the stopped rotor are set up so that the two blades and the mast are treated as three cantilevered systems. This allows easy generation of the stiffness matrices for each section. The boundary conditions are then applied, and the structure is assembled as a rigid rotor with a flexible mast; thus the coordinate system is such that all coupling terms between segments are included in the mass and aerodynamic matrices and are excluded from the stiffness matrix. For this problem, six mast segments and twelve blade segments (six per blade) are used with two degrees of freedom (displacement and slope) per segment. See Figure 19.

The dynamics portion of the trailed-rotor analysis uses a generalized coordinate system with the coupling between degrees of freedom being represented in the full stiffness matrix. The wing is represented by a series of masses arranged as "dumbbells" along the wing's elastic axis and parallel to the airflow (see Figure 20), with two control points per segment. The control points for the rotor blade are on the elastic axis. Only displacements of the control points are considered, with wing torsion represented as differential displacement of the control points. This method necessitates a mass matrix with coupling between bending and torsion for each segment but with no coupling between segments.

The aerodynamics are expressed as functions of displacements and displacement velocities. For the stopped rotor, the lift generated by blade flapping is the exciting force for the blades. The $dC_L/d\alpha$ for the first forward-blade segment is assumed to be 2π, while all other segments have a $dC_L/d\alpha$ of $2\pi/10$. This distribution approximates the lift distribution on a very low-aspect-ratio wing. The hub moment and the drag produced by this lift are used to excite the mast. Drag of the mast is neglected. The trailed-rotor analysis uses steady-state aerodynamics with a constant lift-curve slope. A lift-

curve slope of 2π is used for the wing, and $2\pi/10$ is used for the trailing-blade portion of the system.

FLAPPING STABILITY AT HIGH ADVANCE RATIO

Although this study pertains primarily to gust effects on loads and load factors, it is known that rotor-flapping stability may also be affected by gust inputs. Drees and McGuigan (8) discuss the flapping instability for an unloaded rotor. Jenkins (22) points out that the azimuth of the blade at which the disturbance is applied is of importance. While a detailed investigation of this matter falls outside the scope of this study, a general discussion of the problem is in order.

A 3/4R analysis and rigid-body free flapping are assumed. In the resulting equation of motion,

$$F_o(\psi) = \beta'' + h_o(\psi)\beta' + g_o(\psi)\beta \qquad (14)$$

where

$$h_o(\psi) = \frac{9}{32}\gamma\left|\frac{3}{4} + \mu\sin\psi\right|$$

$$g_o(\psi) = 1 + \frac{3}{8}\gamma\left|\frac{3}{4} + \mu\sin\psi\right|\left[\mu\cos\psi + \tan\delta_3\left(\frac{3}{4} + \mu\sin\psi\right)\right]$$

$$F_o(\psi) = \frac{3}{8}\gamma(\theta + \phi)\left|\frac{3}{4} + \mu\sin\psi\right|\left(\frac{3}{4} + \mu\sin\psi\right)$$

$F_o(\psi)$, $h_o(\psi)$, and $g_o(\psi)$ include all the aerodynamic effects.

The absolute value of the relative velocity at the 3/4-radius blade element is used in order to correctly account for the reversed-flow area. The damping coefficient, $h_o(\psi)$, is zero or positive for all values of ψ, but the spring rate, $g_o(\psi)$, can become negative.

Figure 21 shows variation of the damping coefficient with blade azimuth position for a Lock number (γ) of 2 and for values of μ from 0 to 3. The figure also shows variation of the spring rate with ψ for $\gamma = 2$, $\mu = 2$, and two values of $\delta 3$, 0 and 30 degrees. The damping coefficient goes to zero at azimuth values in the neighborhood of $\psi = 200$ degrees and $\psi = 340$ degrees. A negative spring rate appears first in the region between $\psi = 100$ degrees and $\psi = 180$ degrees. A second region of negative spring rate may appear at very high advance ratios (for $\mu \gg 1$) near $\psi = 240$ degrees. The mechanism causing this negative spring rate can be understood by considering the blade in a forward-swept condition ($\psi = 135$ degrees). In a flapped-up condition, an aerodynamic up-force will appear,

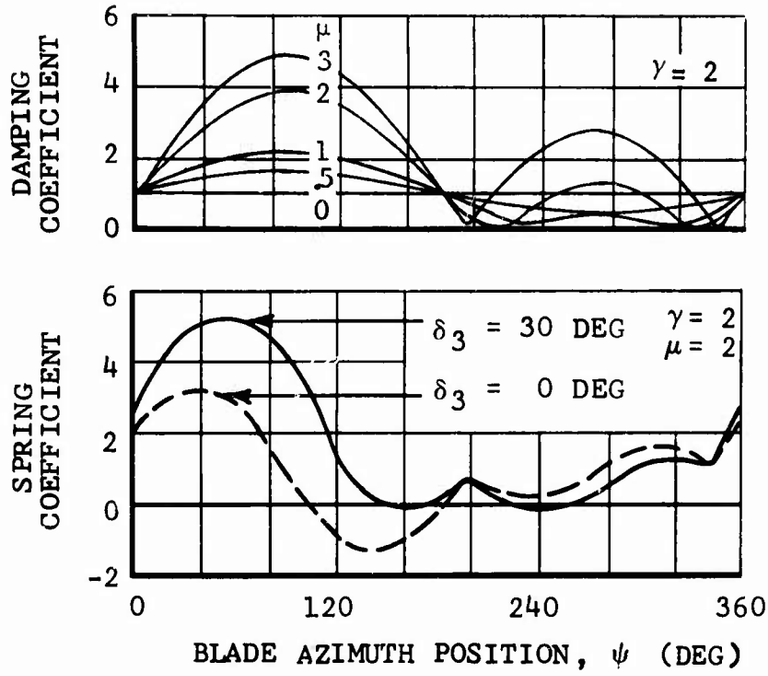

Figure 21. Blade-Flapping Stability Coefficients.

causing static divergence when it overcomes the restoring effect that centrifugal force imposes on flapping.

In Reference 22 it is shown that an initial disturbance at ψ = 90 degrees is more severe than one at ψ = 0 degrees. This is an understandable effect, as the disturbance initiated at zero degrees will be partially damped while the blade traverses the azimuth from zero to 90 degrees, before it enters the instability region between 100 and 180 degrees.

The simplified study has been expanded during the course of the contract to include investigation of the effects of gust velocity and rotor loading. The objective is to determine under what condition a 10-degree angle of attack will be reached by the blade element at 3/4 radius because of the combined effects of gust, rotor lift, and blade-flapping divergence in the region from ψ = 100 to 180 degrees. Simplifications are made by using average values for the functions $h_o(\psi)$ and $g_o(\psi)$. It is assumed that a sharp-edged gust is imposed on the blade just before it enters the region of unstable flapping spring rate $g_o(\psi)$. Figure 22 shows the result. Assuming that at 3/4 radius an angle of attack greater than 10 degrees would give rise to blade stall and high loads, high gust velocities (and the consequent increased blade loads) can be seen to decrease the

safe operating speed of the aircraft. Hence, high blade inertia (low Lock number, γ) is an advantageous feature.

This treatment of flapping stability is not sufficiently complete to predict the behavior of a specific rotor configuration. It should be expanded to include rigid and semirigid rotors, blade-bending flexibility, torsional degrees of freedom, hub restraint, etc. Nevertheless, it is believed that the general trends and first-order effects are valid. For the high-speed compound helicopter and stopped-rotor configurations in particular, flapping stability must be taken into account.

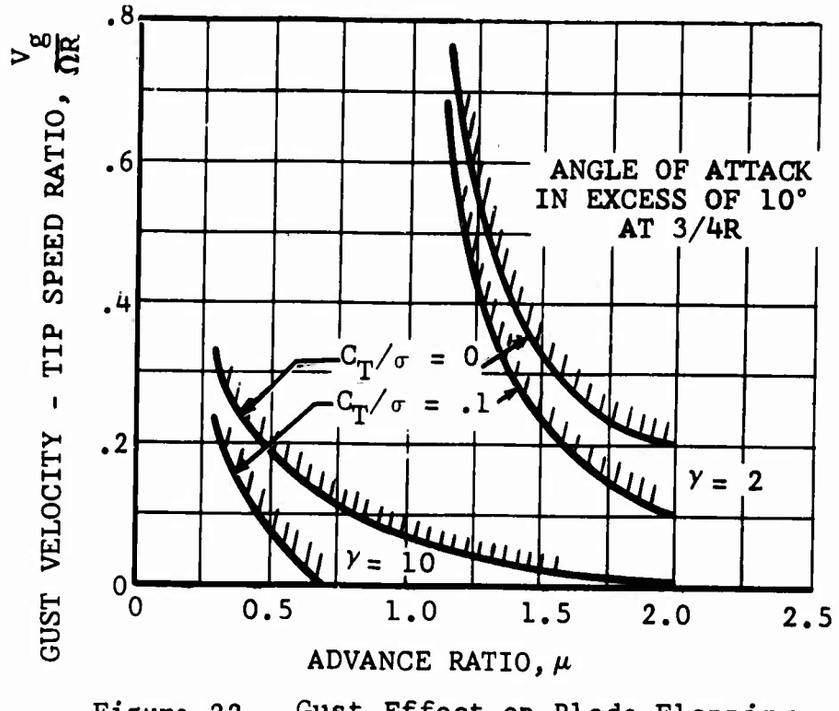

Figure 22. Gust Effect on Blade Flapping.

DISCUSSION OF RESULTS

GENERAL DISCUSSION

The cases investigated for this study are listed by categories in Table I (page 16) and summarized in more detail in Appendix II. Each individual sine-squared gust case resulted in a 385-page output of information concerning performance, stability and control characteristics, time history of the maneuver, and steady and oscillatory rotor loads. The output for sudden-gust cases is 56 pages per case. It was considered one of the objectives of this report to put order to the multitude of information in such a way that trends can be distinguished and conclusions can be drawn. Appendix III gives the principal results for 295 cases. The physical parameters of the rotors used for these cases are presented in Appendix IV. The stability derivatives for 9 cases are presented in Appendix V.

In this section of the report, the effects of the many combinations and variations are discussed after showing a sample output case and details of the parameter selection of aircraft and rotors used in this study.

Sample Case

A sample case is given in Appendix I. Only a selection of the 385 pages of computer output are given. Pages 137 and 138 (in Appendix I) show the input data as arranged in logical groups. Some principal quantities are indicated. The case is for a 8500-lb compound helicopter with a single, 2-bladed, semirigid rotor at 150-knot trim velocity. Aeroelastic feedback and nonsteady wing and rotor aerodynamics are included. Pitch-flap coupling (δ_3) is also included.

One cycle of the trim iteration-loop output is shown next (page 139). Forces and moments are listed and partial derivatives are presented for use in stability and control studies. The number of iterations to trim depends on many factors and can become excessive if the initial control position and values are not close to the final values, especially at high speed. (If no trim is achieved, messages will indicate the source of the problem.)

Next (page 140) are the output details for the trim condition. The forces on fuselage, rotors, wings, elevator, fin, and auxiliary propulsion are listed, as well as control positions, fuselage attitude, and performance information. The stability derivatives are shown on page 141.

At this point, the maneuver section becomes effective. Inputs defining details of the required disturbances or control motions

are listed on page 142. Computation of the maneuver then proceeds step by step.

Information is furnished concerning details of the fuselage and the rotor plane position in space, and the forces and moments applied to the rotorcraft. Output for one time point appears on page 143. Velocities due to blade vibrations, which are used as aeroelastic-feedback information, are listed on page 144. Blade control deflections are on the same page. The gust velocity versus azimuth is charted on page 145. A summary of the steady and oscillatory in-plane and out-of-plane rotor moments for 20 blade stations is given on page 146. All of the information is supplied for each time point. Automatically printed time histories conclude the data presentation (page 147).

Parameter Selection

The selected input parameters for the pure and compound single-rotor, tandem and side-by-side helicopters are listed in Table VI. The stopped-rotor parameters are given in Table XIX, and the trailed-rotor parameters are given in Table XX. The combinations cover the entire range of parameters specified in Table I (page 16) and Appendix II. Figure 23 summarizes the cases in terms of disc loading, blade loading, and configuration.

Mass and stiffness distributions of the rotor had to be selected such that no resonance condition would be encountered. Natural frequencies were computed for all rotors used in the study. Examples of the resulting automatically plotted frequency diagrams are given in Figure 24a, b, and c.

EFFECT OF GUST SHAPE

The effect of a sharp-edged gust versus a sine-squared gust was discussed in connection with Figure 6 (page 11). Other gust shapes are also possible. In Figure 25 a summary is given of response of a typical helicopter to

- sharp-edged gust (case 253)
- ramp gust (case 256 for H_g = 90 ft)
- rooftop gust (case 258)
- sine-squared gust (case 254)

In each of the four cases referred to above, aeroelastic feedback and gradual penetration were used. (Note that gradual penetration causes the aircraft to respond before the gust reaches the cg, where Δn is the load factor at the aircraft cg). It is seen that the ramp gust creates gust loads comparable to the rooftop and sine-squared gusts. The ramp gust, however, was not selected for use in the detailed analysis

calculations because of the wealth of data available for the rooftop and sine-squared gust shapes. Cases 33, 34, 255, and 256 are ramp-gust cases that have been run to compare with other gust-shape variations. The rooftop and sine-squared gusts give only slightly different maximum gust loads (.81 g for the rooftop gust versus .89 g for the sine-squared gust). For this reason the gust envelope presented in Figure 18, page 50, which pertains to a rooftop shape, is applied to the sine-squared gust shape. Ramp-length and maximum gust-velocity combinations selected from Figure 18 have been applied to the sample case cited on page 56 and presented in Appendix I. Time histories of gust-load factor are presented in Figure 26.

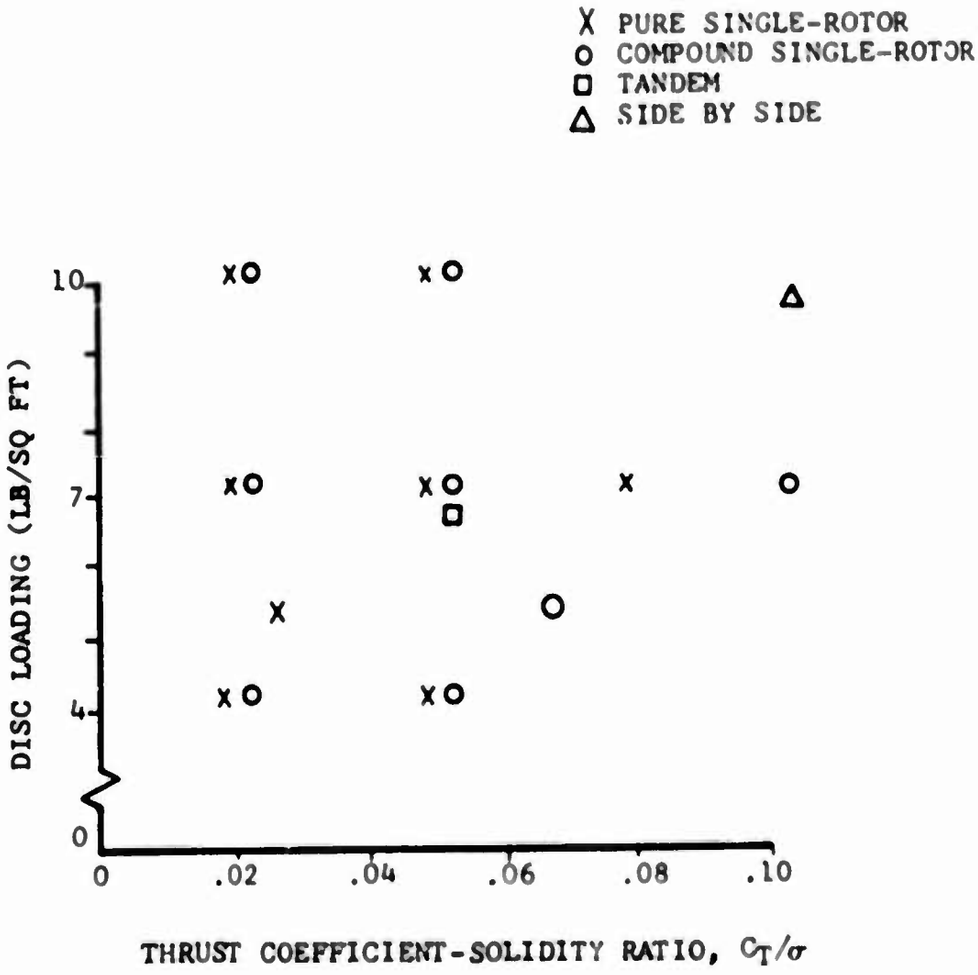

Figure 23. Summary of Case Parameters.

TABLE VI. INPUT DATA SELECTION					
	Pure Single Rotor	Com-pound No. 1	Com-pound No. 2	Tandem	Side by Side
FUSELAGE					
Gross Weight (lb)	15000	15000	8500	15000	23000
Location of Center of Gravity					
Station (in.)	250	250	193.85	320	320
Waterline (in.)	111	111	61.61	111	126
Butt Line (in.)	0	0	0	0	0
Roll Inertia (slug-ft^2)	7200	7200	2350	7200	119300
Pitch Inerita (slug-ft^2)	39000	39000	11716	39000	48200
Yaw Inertia (slug-ft^2)	36000	36000	10164	36000	140000
Product of Inertia I_{XZ} (slug-ft2)	3600	3600	-871	3600	0
Effective Drag Area at Zero Pitch (ft^2)	8.5	8.5	4.0	8.5	5.5
PYLON					
Weight (lb)	-	-	-	-	5000
Location of Center of Gravity at Zero Mast Tilt					
Station (in.)	-	-	-	-	320
Waterline (in.)	-	-	-	-	200
Drag Coefficient at Zero Tilt (ft2)	-	-	-	-	18.8
WING					
Area (ft^2)	-	225	27.8	-	330.5
Aspect Ratio	-	5	1000	-	7.44
Incidence (deg)	-	7.52	14.0	-	8.0
Collective-Stick Coupling (deg/in)	-	0	0	-	0
Lateral Cyclic-Stick Coupling (deg/in.)	-	.5	0	-	.438

TABLE VI.- Continued

	Pure Single Rotor	Compound No. 1	Compound No. 2	Tandem	Side by Side
WING (Cont'd)					
Location of Center of Pressure					
Station (in.)	-	250	192	-	310.5
Waterline (in.)	-	111	62	-	135.0
Butt Line (in.)	-	±100	±39	-	±144.0
Slope of Lift Curve (/deg)	-	.07	.0606	-	.07
Drag Coefficient at Zero Attack	-	.01	.01	-	.01
ROTOR 1					
Function	Main	Main	Main	Forward	Right
Number of Blades	4	4	2	4	3
Radius, Chord, RPM, etc.	(See Appendix II)				
Weight and Stiffness Distributions	(See Appendix IV)				
Twist (deg)	-10	-10	-10	-10	-29.06
Precone (deg)	2.5	2.5	2.75	2.5	1.75
Mast Length (ft)	7	7	0	7	6.17
Pitch-Cone Coupling Ratio	0	0	0	0	0
Pitch-Flap Coupling, δ_3 (deg)	20	20	0	20	20
Location of Shaft Pivot Point					
Station (in.)	250	250	200	40	320
Waterline (in.)	116	116	152.62	135	141
Butt Line (in.)	0	0	0	0	280.5
Slope of Lift Curve (/deg)	.100	.100	.107	.100	.100
Drag-Divergence Mach Number	.87	.82	.80	.87	.87

TABLE VI - Continued

	Pure Single Rotor	Compound No. 1	Compound No. 2	Tandem	Side by Side
ROTOR 1 (Cont'd)					
Coefficients for Nondivergent Drag Equation					
δ_0	.010	.010	.008	.010	.010
δ_1 (/deg)	-.00005	-.00005	0	-.00005	-.00005
δ_2 (/deg^2)	.00018	.00018	.00003	.00018	.00018
Gear Ratio	.01758	.01758	.0491	.01758	.02475
ROTOR 2					
Function	Tail	Tail	Tail	Aft	Left
Number of Blades	4	4	2	4	3
Radius, Chord, RPM, etc.	(See Appendix II)				
Weight and Stiffness Distributions	(See Appendix IV)				
Twist (deg)	0	0	0	-10	-29.06
Precone (deg)	0	0	1.5	2.5	1.75
Mast Length (ft)	2	2	0.0	9	6.17
Pitch-Cone Coupling Ratio	0	0	0	0	0
Pitch-Flap Coupling, δ_3 (deg)	35	35	45	20	30
Location of Shaft Pivot Point					
Station (in.)	700	602	520.7	510	320
Waterline (in.)	154	154	118.27	135	141
Butt Line (in.)	0	0	-14.85	0	280.5
Slope of Lift Curve (/deg)	.100	.100	.107	.100	.100
Drag-Divergence Mach Number	.87	.82	.80	.87	.87

TABLE VI - Continued

	Pure Single Rotor	Compound No. 1	Compound No. 2	Tandem	Side by Side
ROTOR 2 (Cont'd)					
Coefficients for Nondivergent Drag Equation					
δ_0	.010	.010	.010	.010	.010
δ_1 (/deg)	-.00005	-.00005	0	-.00005	-.00005
δ_2 (/deg)	.00018	.00018	.00003	.00018	.00018
Gear Ratio	.108	.120	.251	.01758	.02475
ELEVATOR					
Area (ft^2)	34	34	15.0	-	90
Aspect Ratio	2.5	2.5	1000	-	4.5
Incidence (deg)	-2.5	2	6.21	-	-2
Collective-Pitch Coupling (deg/in.)	0	0	0	-	0
F and A Cyclic-Stick Coupling (deg/in.)	0.5	1	.827	-	1.67
Mast-Tilt Coupling Factor	0	0	0	-	0
Location of Center of Pressure					
Station (in.)	502	602	398.5	-	635.3
Waterline (in.)	120	200	56		195
Slope of Lift Curve	.055	.058	.0524	-	.07
Drag Coefficient at Zero Attack	.010	.015	.008	-	.010
FIN					
Rudder Connection	No	Yes	No	No	Yes
Area (ft^2)	45	45	25	45	100
Aspect Ratio	2.5	2.5	1000	2.5	1.6
Incidence (deg)	10	1	4.5	0	0
Tail-Rotor Coupling Factor	0	2	0	-	0

TABLE VI - Continued

	Pure Single Rotor	Compound No. 1	Compound No. 2	Tandem	Side by Side
FIN (Cont'd)					
Location of Center of Pressure					
Station (in.)	700	602	501	520	609.6
Waterline (in.)	144	111	84	111	180.0
Butt Line (in.)	0	0	0	0	0
Slope of Lift Curve	.055	.055	.040	.055	.039
Drag Coefficient at Zero Attack	.01	.01	.008	.01	.01

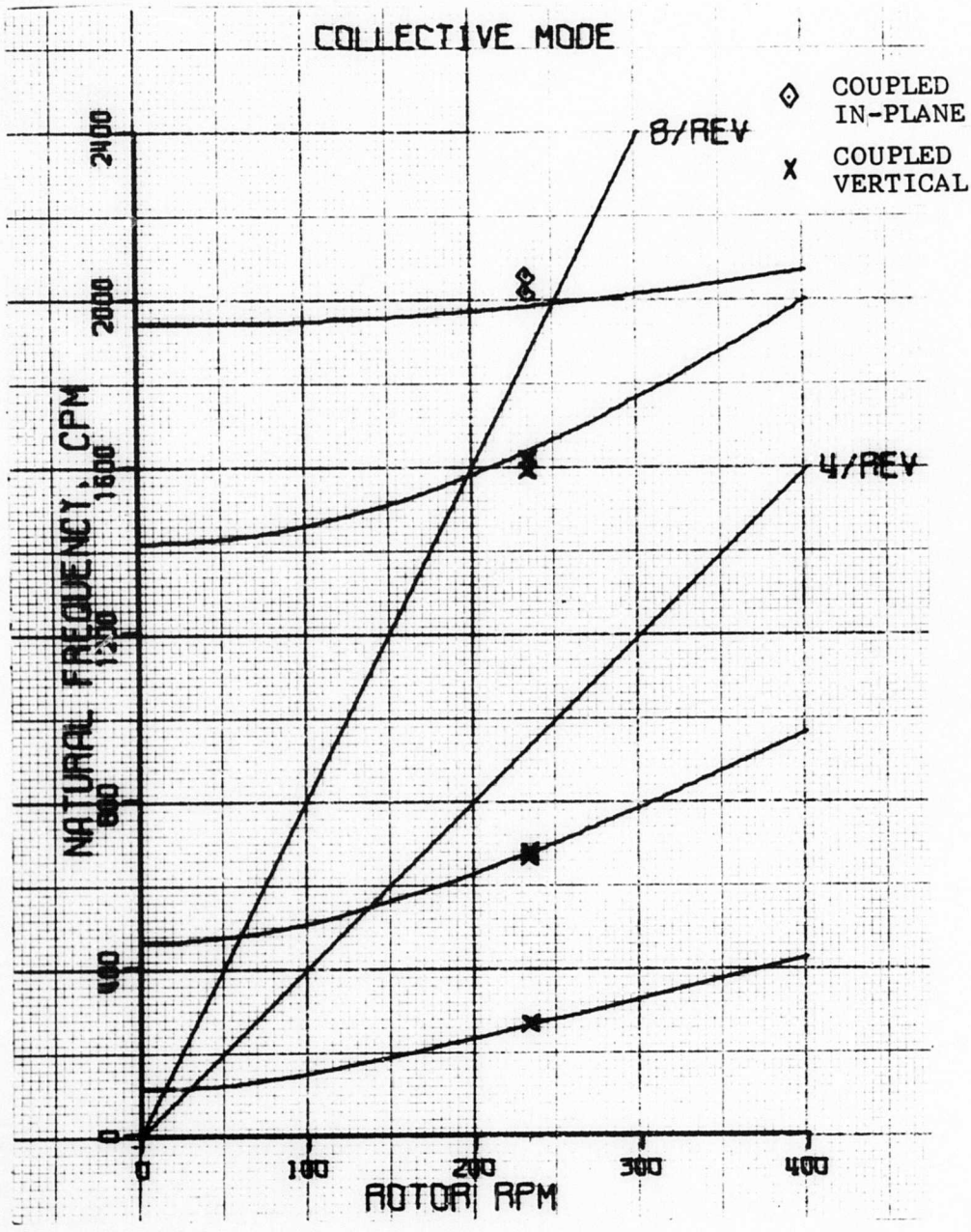

a. Collective Modes

Figure 24. Coupled Rotor Natural Frequencies (4-Bladed Rigid Rotor).

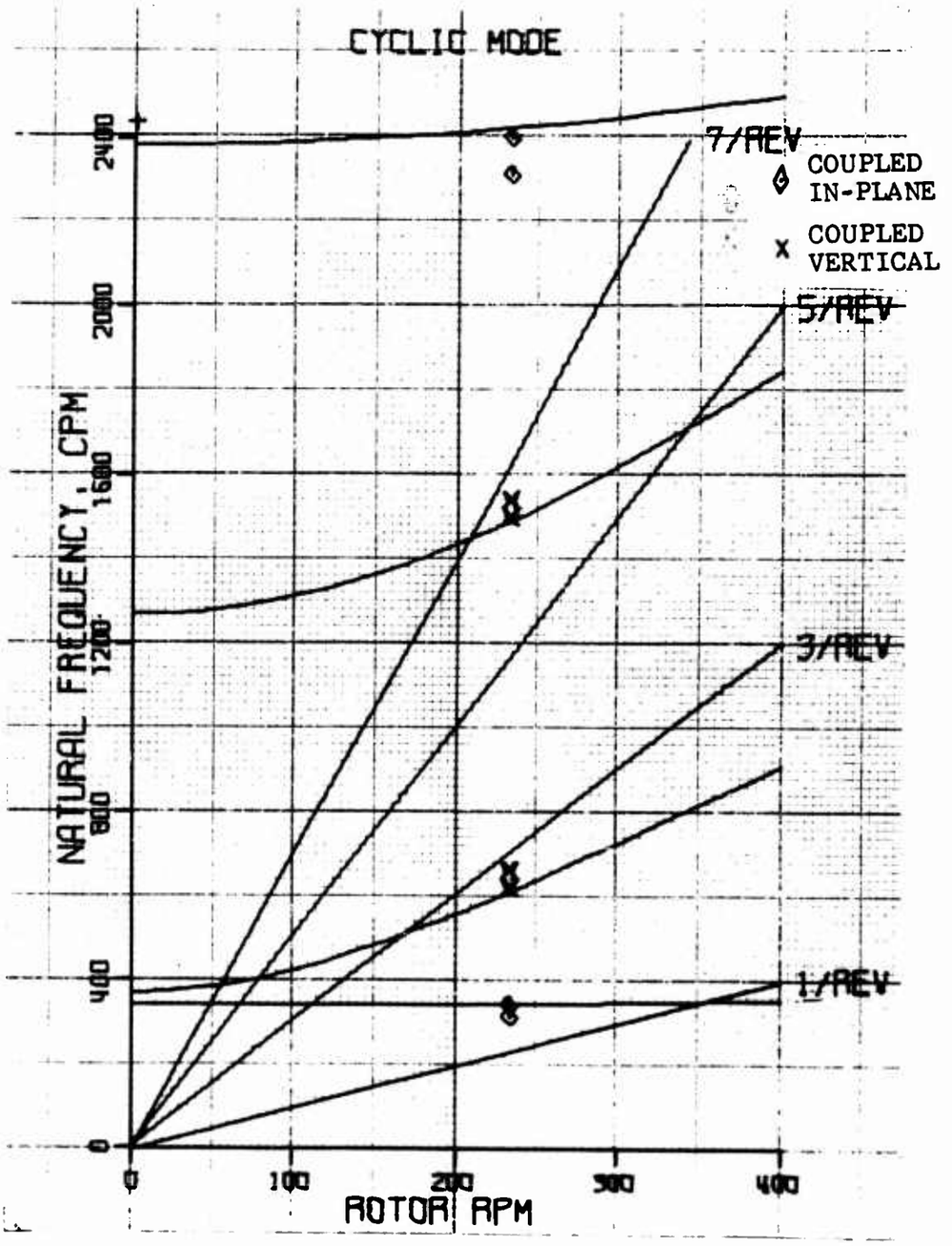

b. Cyclic Modes

Figure 24 - Continued.

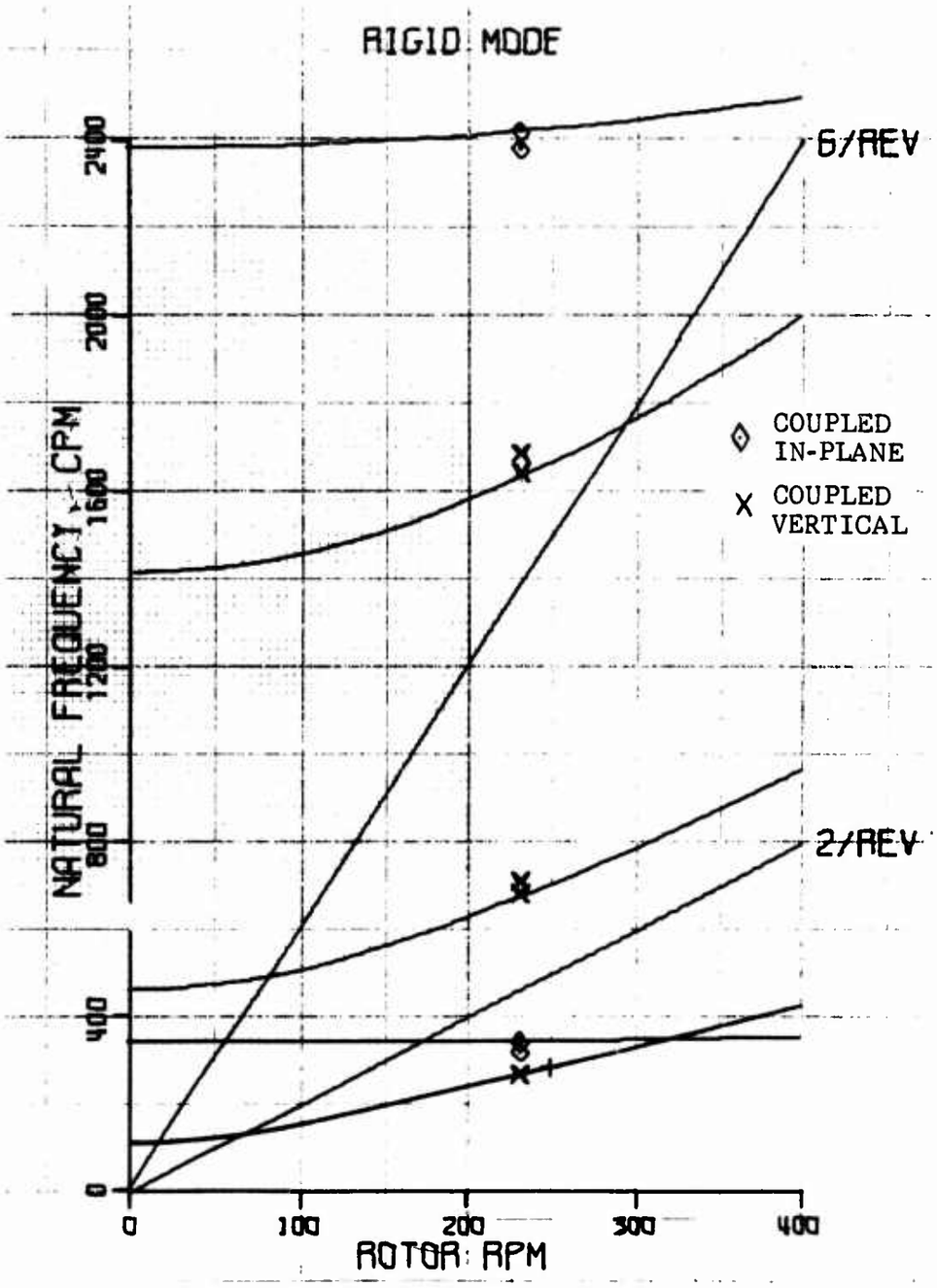

c. Rigid Modes

Figure 24 - Continued

COMPOUND SINGLE-ROTOR HELICOPTER
VELOCITY = 150 KT
GROSS WEIGHT = 8500 LB
DISC LOADING = 5.6 LB/SQ FT
C_T/σ = .064

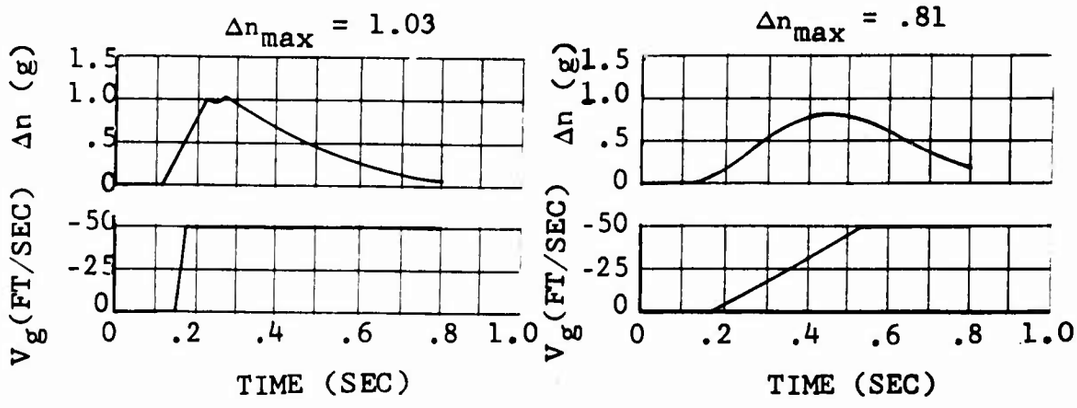

CASE 253 - SHARP-EDGED

CASE 256 - RAMP

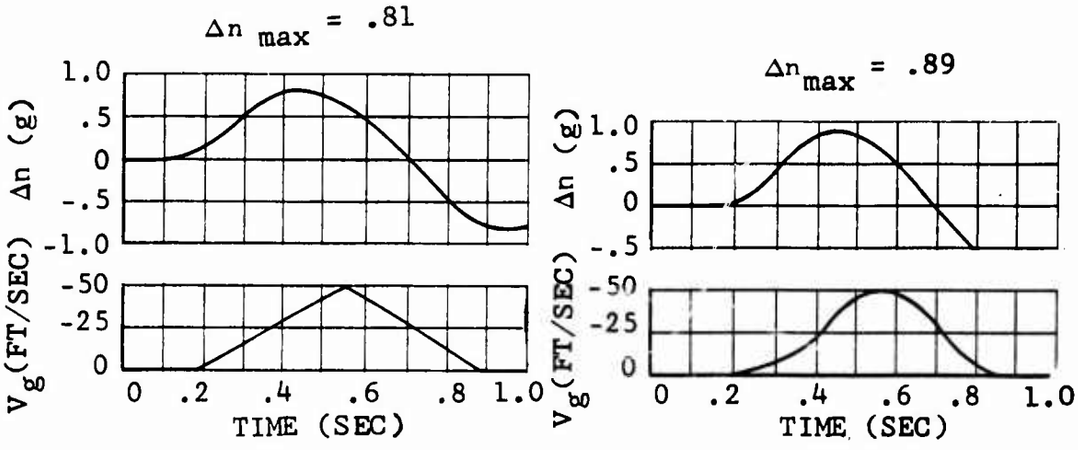

CASE 258 - ROOFTOP

CASE 254 - SINE-SQUARED

All cases include gradual penetration and nonsteady aerodynamics.
V_g is taken at the cg of the aircraft.

Figure 25. Effect of Gust Shape on the Gust-Load Factor.

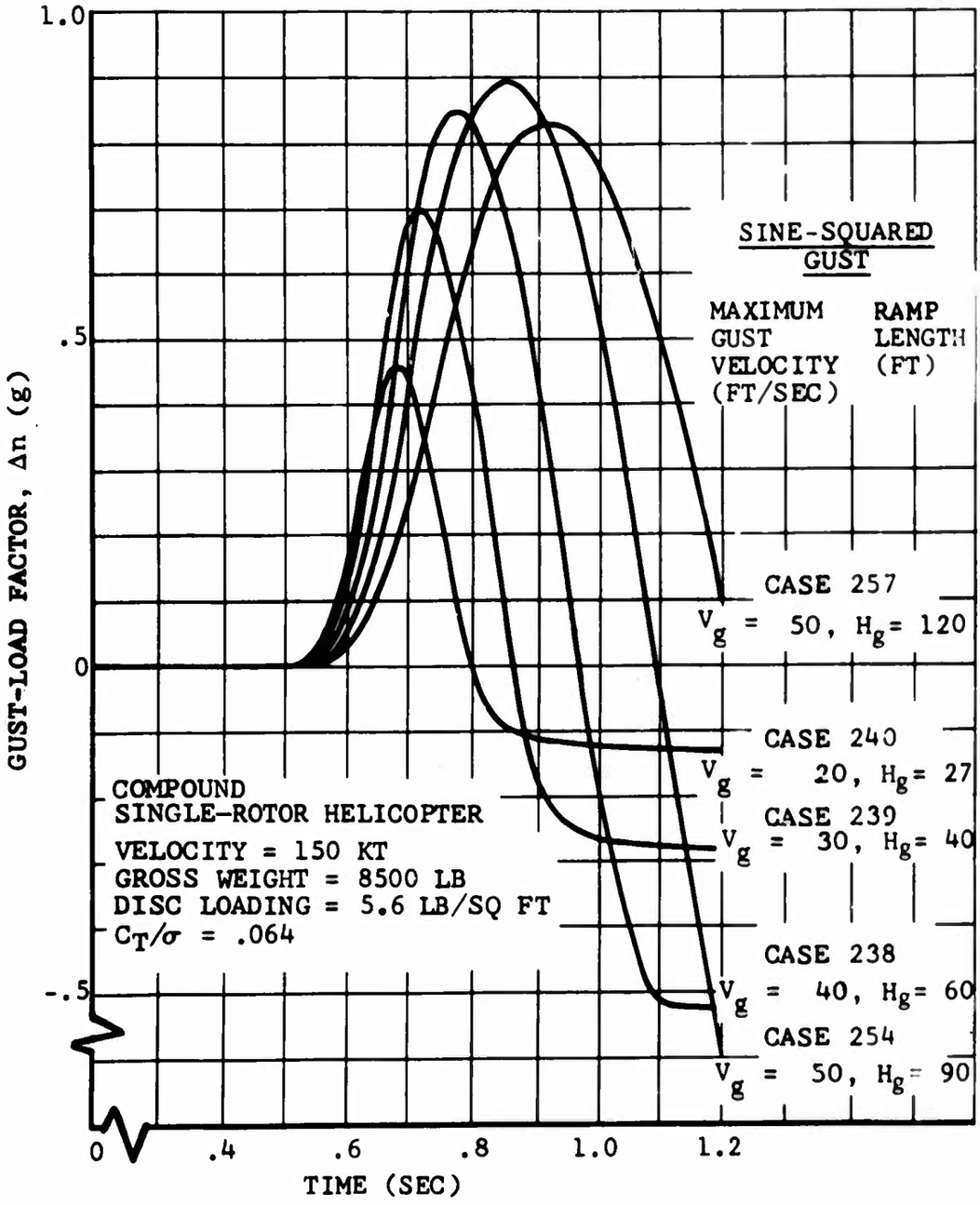

Figure 26. Effect of Ramp-Length and Gust-Velocity Combinations on the Gust-Load Factor.

In Figure 27 the effect of the Hg and V_g combinations (from Figure 18) on maximum gust load, blade flapping, fuselage pitching, and blade loads is shown. The maximum value of Δn occurs for the combination of H_g = 90 feet and V_g = 50 ft/sec. This combination is used throughout the remainder of this study although flapping and hub bending moments are more critical at longer ramp lengths.

EFFECT OF CONFIGURATION

Rotorcraft configurations represented in the gust-response case study are:

- pure single-rotor helicopter
- compound single-rotor helicopter
- pure tandem helicopter
- trailing rotor
- stopped rotor
- tilt rotor

About 85 percent of the cases were run on pure single-rotor helicopter and compound single-rotor helicopter configurations. The tilt-rotor cases include speed variations with mast tilt of 90 degrees, thus simulating aircraft flight conditions. Trailed-rotor and stopped-rotor cases were computed using methods as described previously.

The compound single-rotor helicopter cases generally produced higher values for the gust-alleviation factor, K_g, than did the pure single-rotor helicopter cases. Since the wing plays a principal role in the compound single-rotor helicopter configuration, factors were computed for the wing $\left(K_{g_w}\right)$ and for the rotor $\left(K_{g_r}\right)$ separately, thus:

$$K_{g_w} = \frac{\Delta L_{\text{sine-squared}}}{\Delta L_{\text{sudden}}}; \quad K_{g_r} = \frac{\Delta T_{\text{sine-squared}}}{\Delta T_{\text{sudden}}} \qquad (15,16)$$

The net value, K_g, for the compound single-rotor helicopter configuration, considering only wing and rotor effects, can be expressed as

$$K_g = \frac{\Delta L_{\text{sudden}} K_{g_w} + \Delta T_{\text{sudden}} K_{g_r}}{\Delta L_{\text{sudden}} + \Delta T_{\text{sudden}}} \qquad (17)$$

This value will differ slightly from the ratio $\Delta n_{\text{sine-squared}}/\Delta n_{\text{sudden}}$ since the fuselage, with control surfaces and tail rotor, has some effect. The advantage of separating rotor and wing gust-response ratios is to allow comparison with the other configurations.

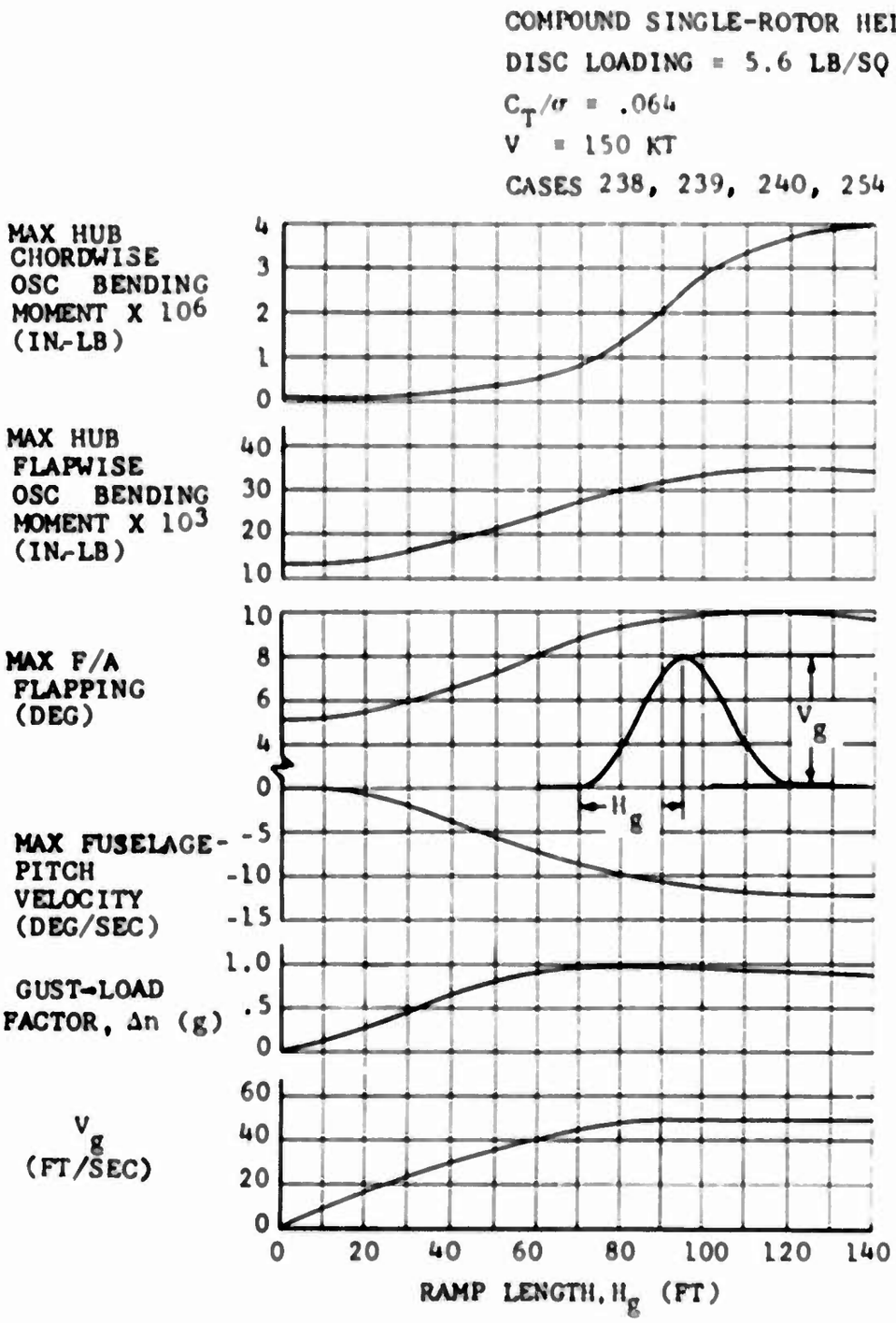

Figure 27. Effect of Combinations of H_g and V_g on a Compound High-Speed Helicopter for a Sine-Squared Gust

The compound single-rotor helicopter cases are characterized by the proportion of lift carried by the main rotor in steady flight. Although a broad range of auxiliary-thrust values was required to trim these cases, the gust-response characteristics were not materially affected. The average value of K_{g_r} for cases with thrust more than 1/3 the gross weight is .47, which compares closely with a mean K_g of .50 for pure single-rotor helicopter cases. Average K_{g_r} for compound single-rotor helicopters with unloaded rotor is .65. The histograms in Figures 28, 29, and 30 show the distribution of alleviation factors computed for these two configurations.

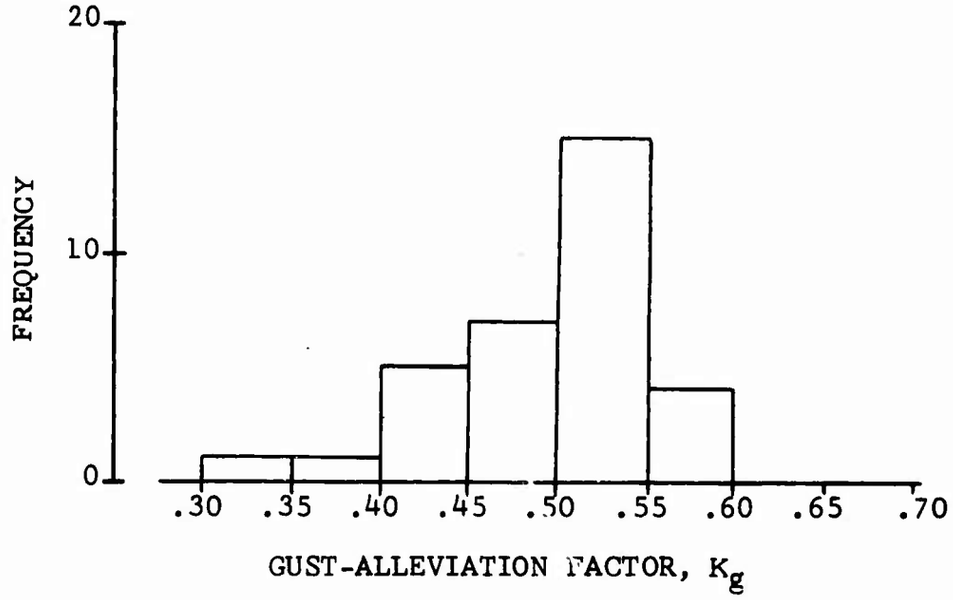

Figure 28. Histogram of Gust-Alleviation Factors for Pure Single-Rotor Configuration.

The compound single-rotor configuration cases may also be compared with the airplane configurations by considering K_{g_w} (Figure 30). For the compounds, K_{g_w} averaged .79, with about 50% of the cases having a value in the .80 to .85 interval. The average value of K_{g_w} for airplane cases is .83, thus establishing a strong relationship for all the wing-response evaluations.

Results of eight cases for the tandem configuration are summarized in Table VII. The sine-squared gust responses were adversely affected by choice of fuselage parameters determining pitch stability. Parameters selected for the tandem cases include low fuselage-pitching inertia, aft cg location, zero rotor overlap, and no elevator, all of which are conservative in regard to the sine-squared gust response. The results

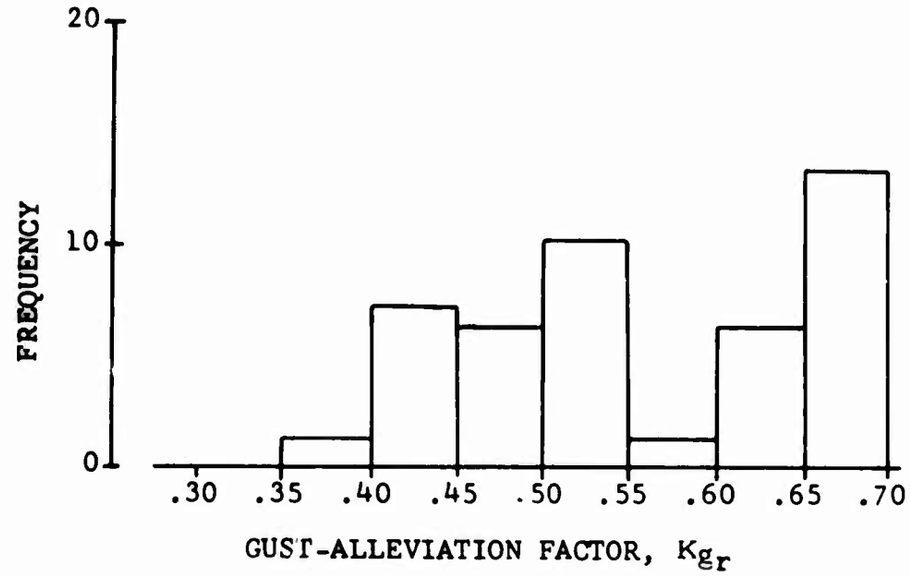

Figure 29. Histogram of Rotor Gust-Alleviation Factors for Compound Single-Rotor Configuration.

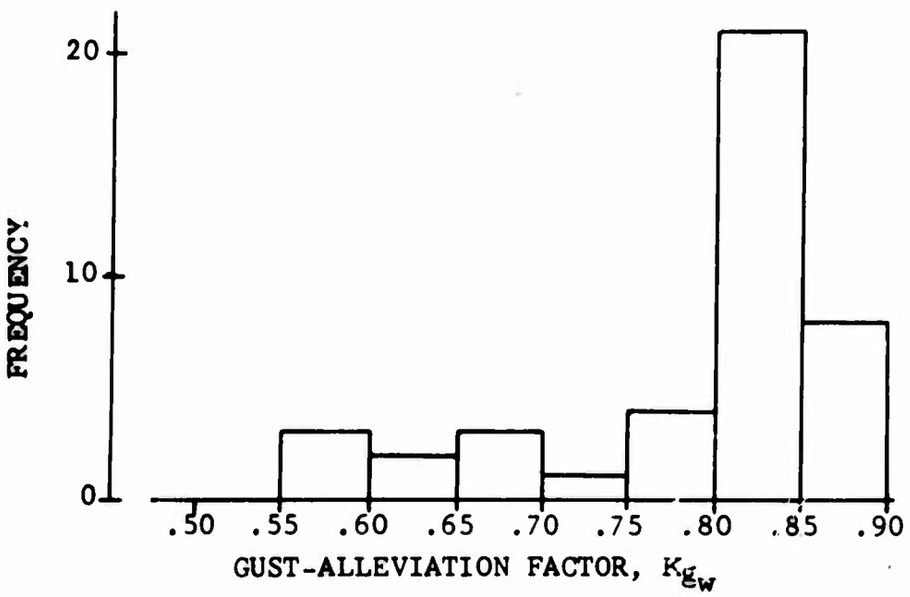

Figure 30. Histogram of Wing Gust-Alleviation Factor for Compound Configuration.

of this limited study suggest a need for further investigation to delineate the individual importance of these parameters.

Figure 31 is a time history of three variations of cg location. Pitch attitude, and aircraft normal acceleration are shown in relation to the gust disturbance. For the aft and neutral cg cases, the continued increase in g level after both rotors emerge from the gust is clearly a function of the severe pitch displacement and the high forward speed. A dashed line is also shown in Figure 31 as an approximation of the acceleration level attributable solely to pitch attitude. By removing this effect from the computed responses, adjusted gust-alleviation factors are obtained that agree with those for a single-rotor helicopter. The adjusted alleviation factors are included in Table VII below.

TABLE VII. PRINCIPAL RESULTS OF TANDEM-CONFIGURATION CASES

Case	Speed	DL	C_T/σ	Gust	Δn	K_g	$K_{g_{adj.}}$
183	200	7	.02	sudden	4.37	1.14	.57
184	200	7	.02	sine-squared	4.97		
185	200	7	.05	sudden	1.35	.77	.52
186	200	7	.05	sine-squared	1.04		
187	225	7	.02	sudden	4.09	1.12	.56
188	225	7	.02	sine-squared	4.56		
189	225	7	.05	sudden	1.22	.74	.58
190	225	7	.05	sine-squared	0.91		

A good measurement of the effects of a gust on a stopped rotor or a trailed rotor is the shear load at the root of the blade, shown as time histories in Figures 32 and 33 for airspeeds of 100, 200, 300, and 400 knots. The requirements of this study (Table I) specify only sine-squared gust encounters for these two configurations. To provide a common basis for evaluation of results, sudden-gust responses also have been computed and are presented herein without the assignment of additional case numbers. For identification purposes, the suffix "A" denotes sudden-gust response and "B" denotes sine-squared gust response.

In each case, the aircraft is considered to be flying faster than the transition speed and operating in the fixed-wing aircraft mode with the rotor(s) stopped and unloaded. For the trailed-rotor configuration, the three blades of each rotor are assumed to be folded aft as depicted in Figure 20 (page 51). For the stopped-rotor configuration (Figure 19), the analysis is restricted to a two-bladed rotor with the blades assumed to be completely stopped and locked at the forward and aft azimuth positions.

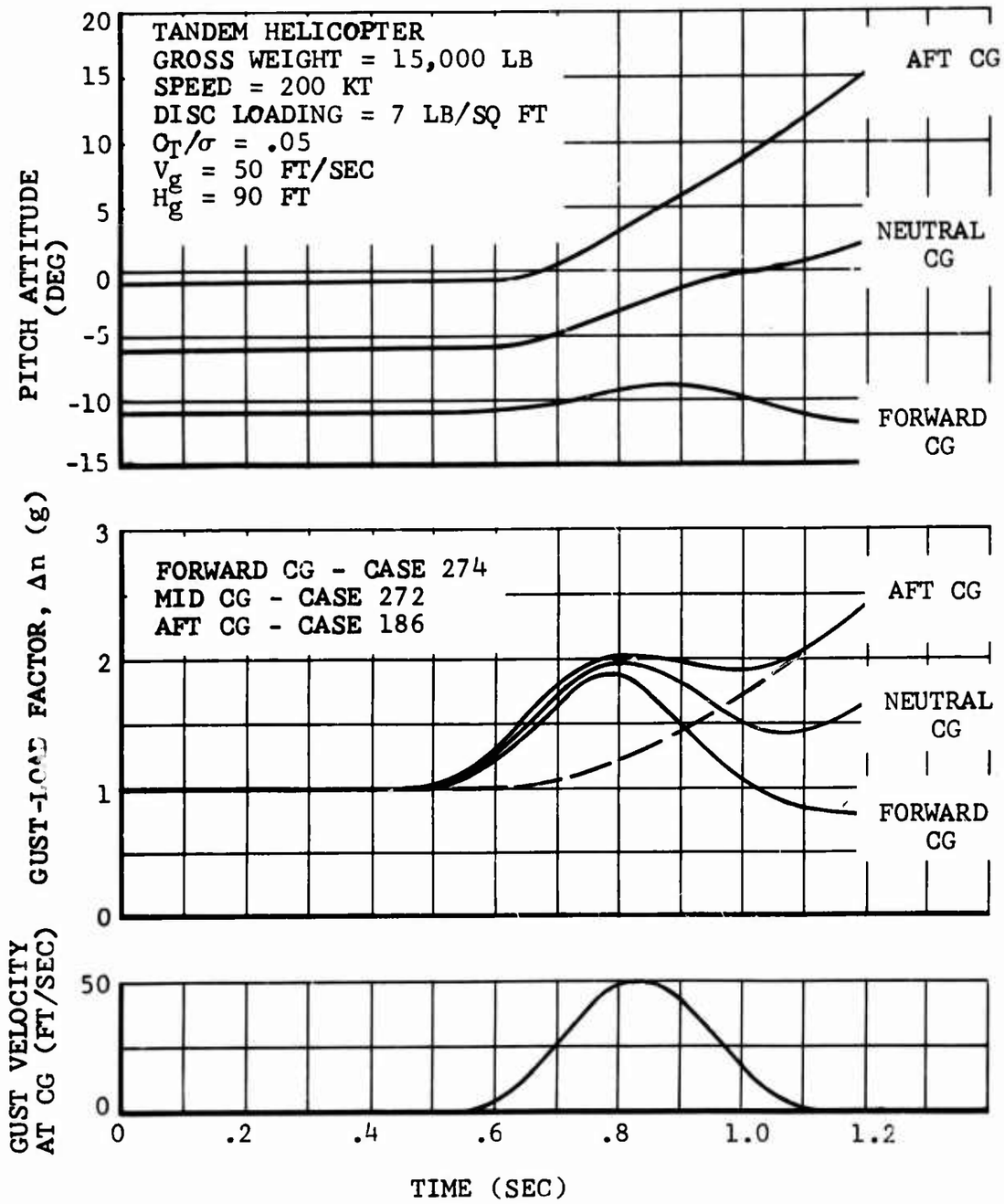

Figure 31. Time History of Tandem-Helicopter Response to 50-Ft/Sec Sine-Squared Gust.

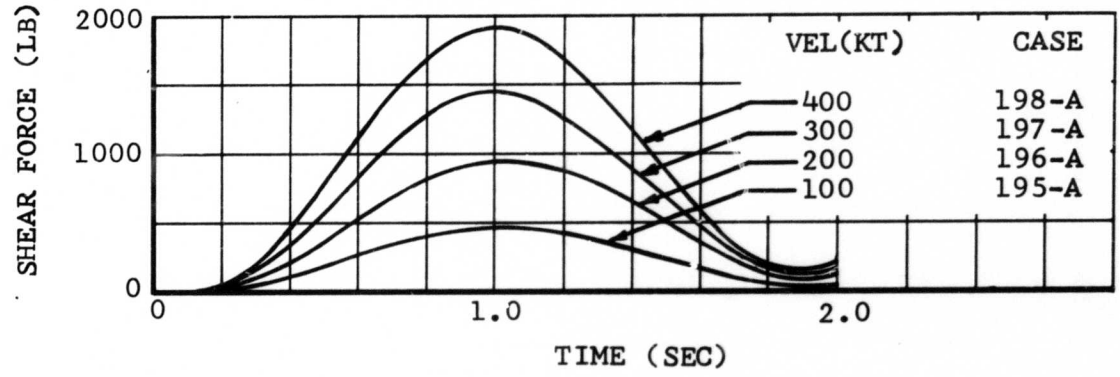

a. Sudden Vertical Gust

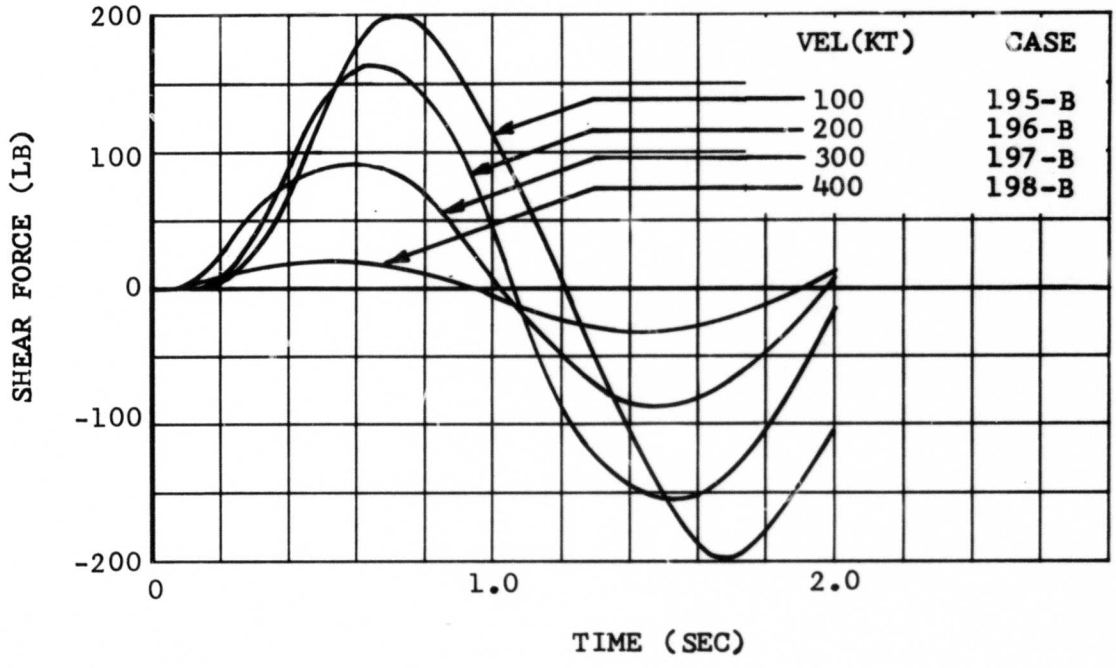

b. Sine-Squared Vertical Gust

Figure 32. Stopped-Rotor Shear at Forward Blade Root.

For a sudden gust, the root-shear loads of both configurations increase with increasing airspeed (Figures 32a and 33a). The response is essentially proportional to the product of the angle-of-attack change and the square of the forward speed. The angle-of-attack change, however, is inversely proportional to the forward speed. Except for pitching and heaving motions of the aircraft, then, the sudden-gust response of both configurations is directly proportional to the forward speed.

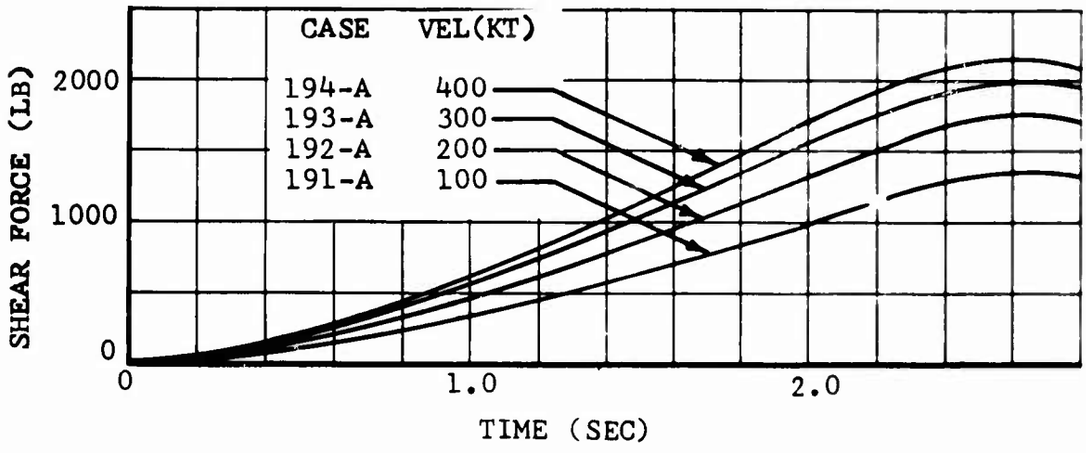

a. Sudden Vertical Gust

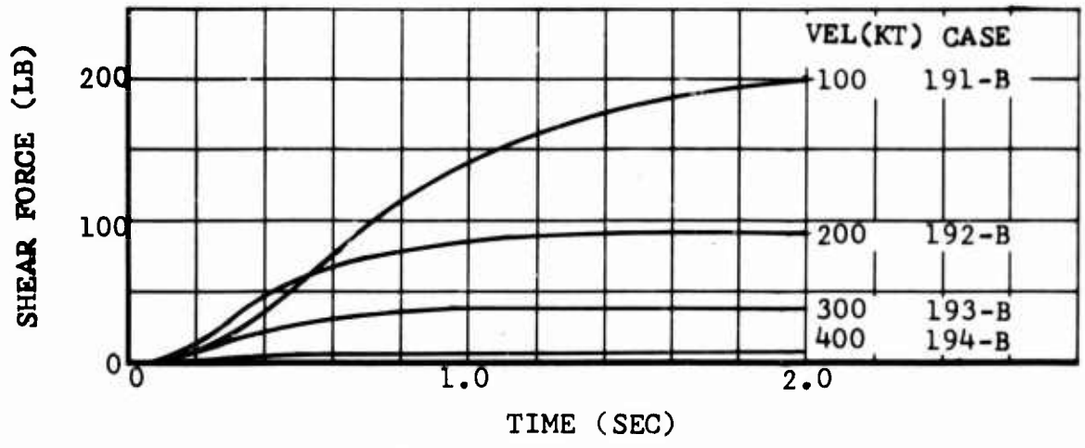

b. Sine-Squared Vertical Gust

Figure 33. Trailed-Rotor Shear at Wing Tip.

The period of the sudden-gust response is a function of the natural frequencies of the structural system and is independent of forward speed. In changing suddenly from one steady environment to another, the transient response builds up rapidily and oscillates while tending to decay to a steady value equal in magnitude to one-half of the first peak. This effect is illustrated in Figure 32a.

For a sine-squared gust, the root-shear loads of both configurations decrease with increasing airspeed (Figures 32b and 33b), because of the decreasing time that is required for the aircraft to pass through the gust field. At the lowest speed for which a response was computed (100 knots), the entire length of the sine-squared gust (180 feet) is traversed in only 1.07 seconds. The effective length of the gust and the equivalent traversal time are reduced by the shape of the gust; the first peak of

the stopped-rotor response for 100 knots occurs after about 0.7 second. Elapsed time to the first peak decreases with increasing forward speed. After the first response peak has been reached, the response period is controlled by the natural frequencies and pitching characteristics of the aircraft, as indicated in Figure 32b.

The difference in character of the gust-response time histories for the stopped- and trailed-rotor configurations is attributable to the wing-torsion effect for the latter. In a typical transient for this type of structure, wing bending and wing torsion respond at unequal periods. In comparison with Figure 32b (stopped-rotor), Figure 33b shows a relatively flatter first-peak response due to wing-torsion lagging wing-bending.

By dividing the shear load due to a sine-squared gust by the shear due to a sudden gust, a shear ratio can be obtained for each case. This shear ratio bears some similarity to K_g as calculated for the conventional helicopter cases. Figure 34 shows a comparison of the shear ratios based on maximum response for both a stopped rotor and a trailed rotor. The figure shows a marked decrease in the shear ratio as velocity increases.

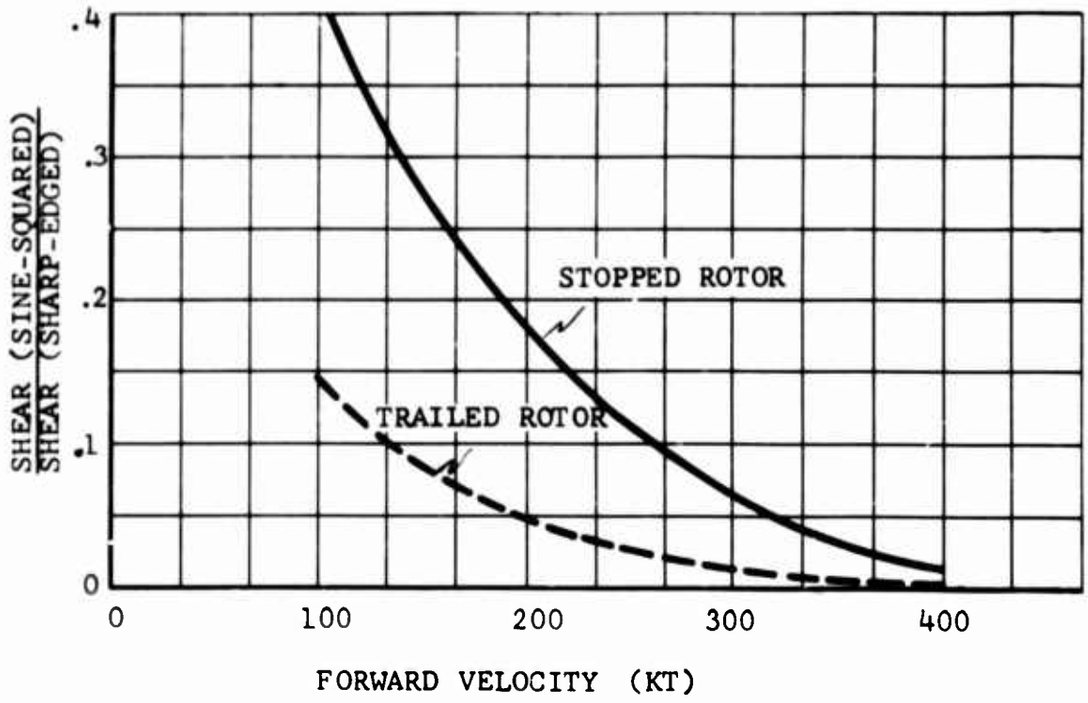

Figure 34. Gust Response for Stopped and Trailed Rotors, Cases 191-198.

The gust response of a tilt-rotor composite-type aircraft has been investigated in considerable detail. In the airplane mode, the gust response of this configuration is generally similar to that of a fixed-wing airplane, with the wing-lift increase proportional to the forward speed. An additional consideration is the vertical-force increment from the rotor.

Figure 35 shows gust-load factors versus velocity for both sudden and sine-squared gusts. Over the range from 200 to 300 knots, the gust-load factors vary linearly with speed and the gust-alleviation factor is almost constant at 0.83. For the parameters used in this study, a flapping instability was computed for the sine-squared gust case at 400 knots. Since the basic problem of prop-rotor stability is affected by many design considerations (wing stiffness, pylon mounting, control system, stabilizing devices, etc.) that are not represented in the analysis, this subject was not pursued further in this study. It is appropriate to note that no implications are made by these results as to either forward speed limitations or attainable design ranges for the tilt-rotor configuration.

Figure 35 also indicates the effect of wing stall at speeds below 200 knots. Figure 36 shows an example of the aircraft's behavior due to a 50-ft/sec sine-squared gust at a speed of 150 knots. The effect of wing stall is quite obvious. The gust-

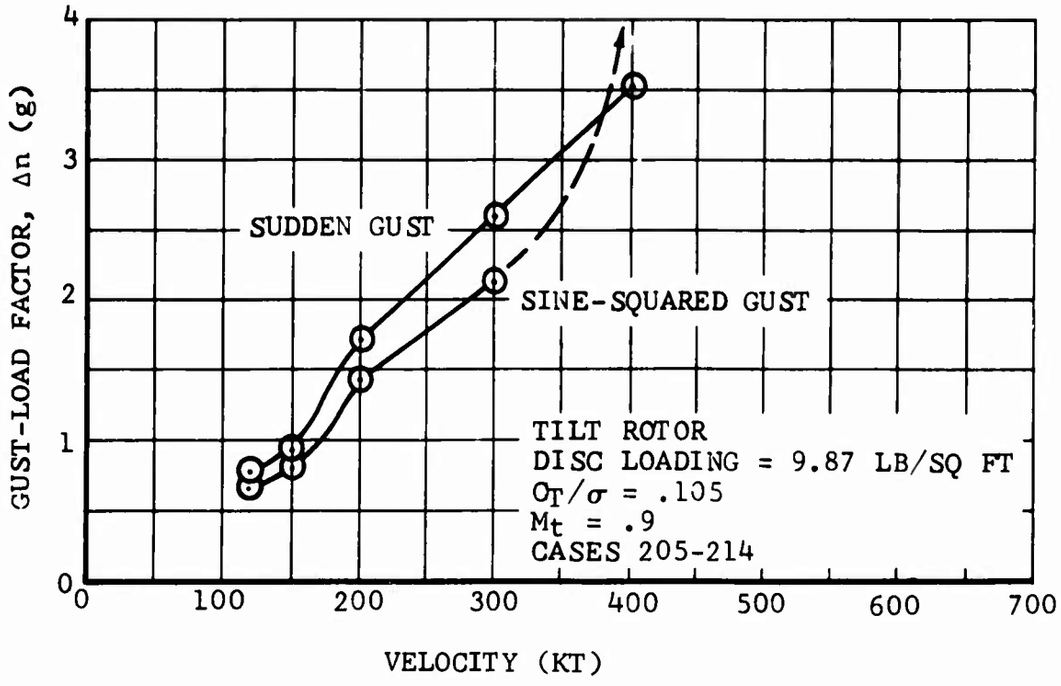

Figure 35. Acceleration Due to Gusts Versus Velocity, Tilt-Rotor Configuration in Airplane Mode.

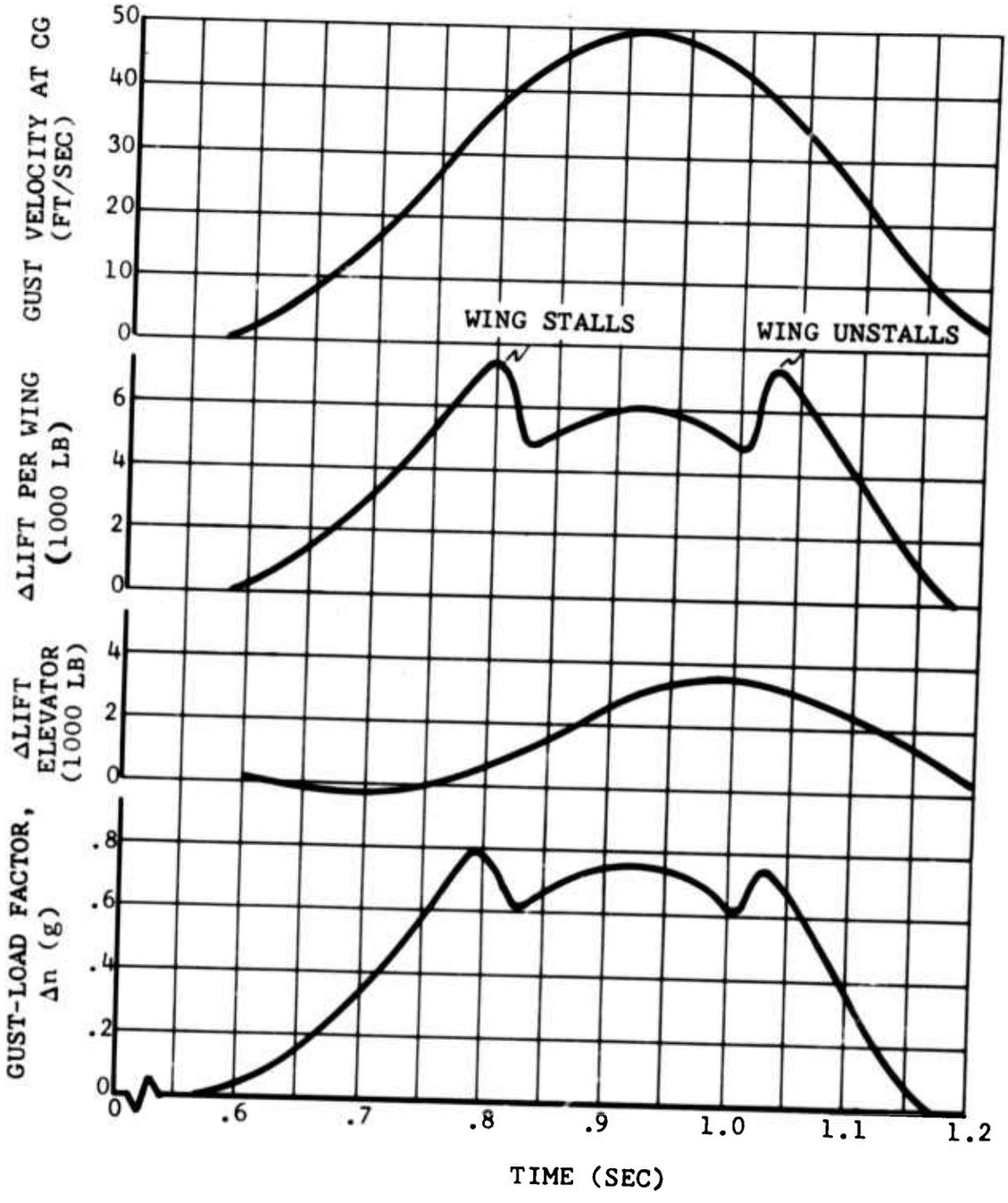

Figure 36. Vertical Sine-Squared Gust, Tilt-Rotor Airplane Configuration, 150 Knots, Case 208.

alleviation factor (0.81 at 120 knots) is not significantly affected by the occurrence of wing stall.

In the helicopter-mode, the tilt-rotor configuration responds to gust encounters in a manner typical of the compound configuration.

Figure 37 shows a time history of one of the cases where the aircraft is subjected to a 50-ft/sec sine-squared vertical gust during a pylon conversion process. The pylon moves from a partial conversion angle of 25 degrees toward the airplane position at a rate of 15 degrees per second. It can be seen that the gust produces both vertical and horizontal accelerations due to the increase in rotor thrust. The wing, of course, adds mainly to the vertical accelerations. Longitudinal blade flapping is increased by about 2 degrees. A number of similar cases were investigated; the vertical and the forward accelerations (body reference) due to a 50-ft/sec sine-squared gust during the conversion are given in Table VIII.

TABLE VIII. PRINCIPAL RESULTS OF TILT-ROTOR CASES

(Sine-Squared Gust)

Case	Speed (kt)	Conversion Angle (deg)		Body-Reference Acceleration (g)	
		At Start of Gust	At Peak of Gust	Δa_z (Vertical)	Δa_x (Forward)
201	120	30	38	.89	.42
202	120	60	68	.55	.36
203	150	30	36	1.37	.50
204	150	60	67	1.02	.57

In addition to the study requirements (Table I), Figure 38 presents the effect of a 50-ft/sec horizontal sine-squared gust on a tilt-rotor aircraft (in airplane mode) at 350 knots. The variation in rotor thrust and horizontal acceleration is shown along with the gust-velocity curve. The slightly negative (aft) acceleration during steady-state flight is due to the pitch attitude of the fuselage in the gravity field. The maximum change in forward acceleration (body reference) is about -.38 g for this case.

EFFECT OF ROTOR TYPE

In this study, rotors are characterized by the hub arrangement as articulated, semirigid, or rigid. The analysis was first

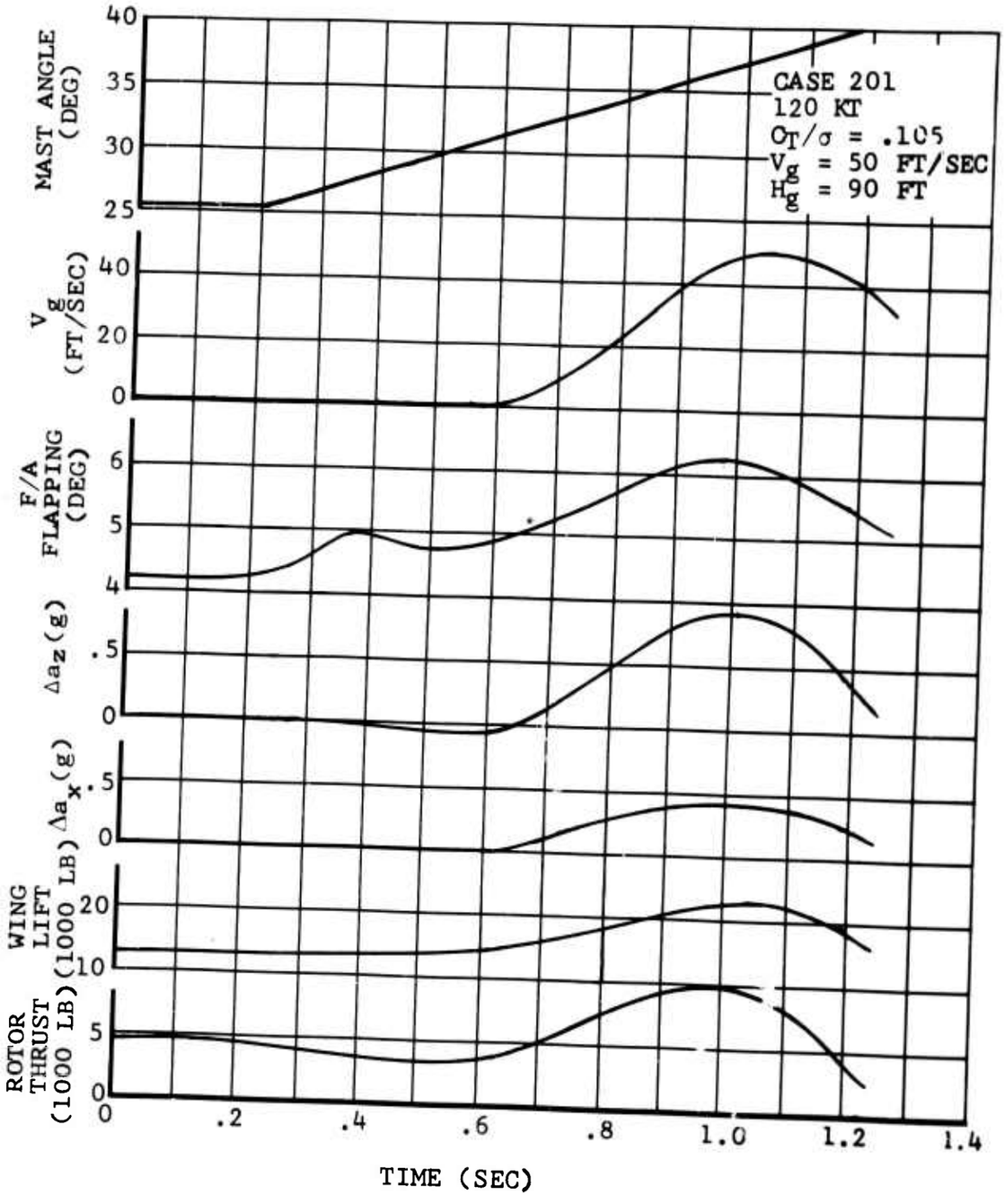

Figure 37. Sine-Squared Gust During Conversion of Side-by-Side Helicopter.

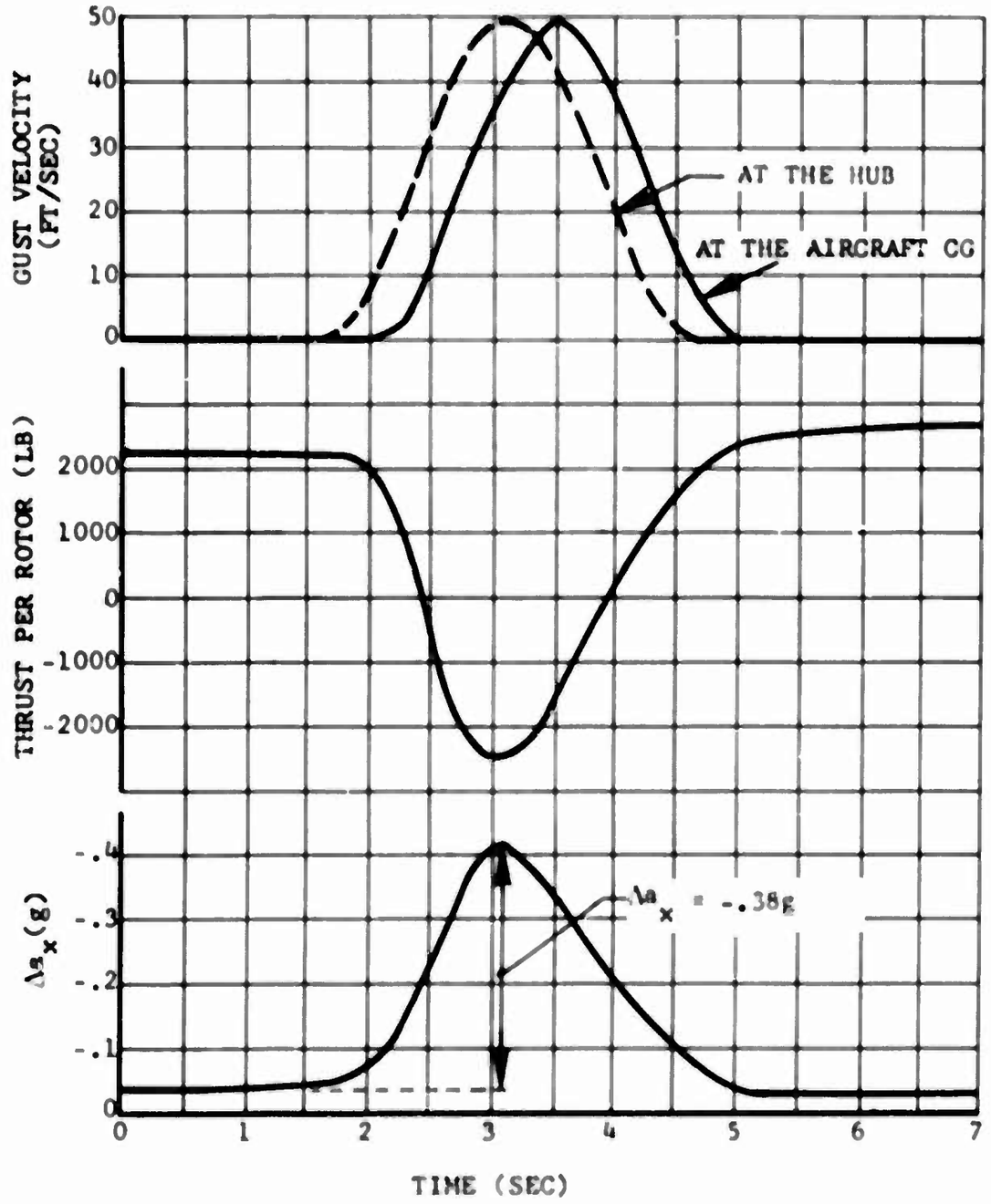

Figure 38. Horizontal Sine-Squared Gust, Tilt-Rotor Airplane Configuration, 350 Knots.

set up for a rotor with flapping hinge at the hub centerline and no chordwise articulation. This is called the semirigid rotor.

A rotor with no articulation still has some effective flapping as a result of elastic bending. This arrangement is referred to as a rigid rotor and is simulated by adding a spring restraint between the blade and the mast in the semirigid representation. A sketch of the resulting general configuration is shown in Figure 39a. The semirigid rotor is then a special case (spring constant, K, equal to zero).

The rotor with offset flapping hinges is called an articulated rotor (Figure 39b). This rotor type was related to the no-offset type by considering the moment transmitted to the top of the mast in either case.

The rotor types simulated with flapping spring, K, have a moment, $K\beta$, about the hub. In the case of the articulated rotor, the moment about the hub is the product of the vertical component of shear at the hinge point, Q, and the hinge-offset distance, e. If CF is the centrifugal force at the hinge, the vertical component of shear is approximately equal to $(CF)\sin\beta\cos\beta$ or, for small flapping angles, $(CF)\beta$. By choosing K so that $K = e(CF)$ per unit angle, the rigid rotor and articulated rotor can be compared. The articulated-rotor and rigid-rotor flapping responses to the sudden gust are, therefore, nearly identical, as computed in the program. The dynamic treatment in the bending-moment analysis is different, and variations in flapping appear in the sine-squared cases run with aerodynamic feedback.

The most extensive set of cases available for comparison is the group of 200-knot, .9 advancing blade-tip Mach number cases that were computed for five or more combinations of disc loading and blade loading for each of the three rotor types. Both pure and compound single-rotor helicopter configurations were included. Results of these cases are listed in Table IX.

The 20 semirigid, 24 articulated, and 24 rigid-rotor cases at 200 knots have the same average value of K_g, 0.50. The range for articulated and rigid rotors is .42-.56, while the compound single-rotor helicopter cases for semirigid rotors spread the range for that type to .40-.67. Corresponding cases (i.e., those having the same disc loading and C_T/σ) for articulated and rigid rotors generally have a K_g of near the same value.

Time histories for tip-path-plane-attitude variation during a sine-squared gust are shown in Figure 40a. The three rotor types shown are for a disc loading of 7.0 and C_T/σ of .05. Forward speed is 200 knots and advancing blade-tip Mach number is .90. As the rotor penetrates the gust, it produces positive

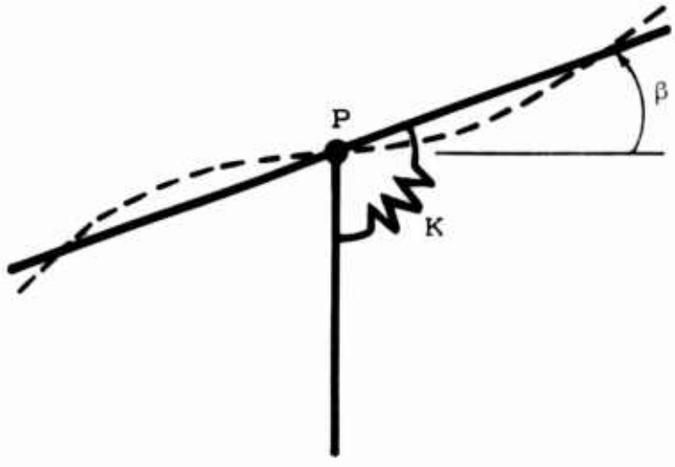

(a) Rigid Rotor

$M_p = K\beta$

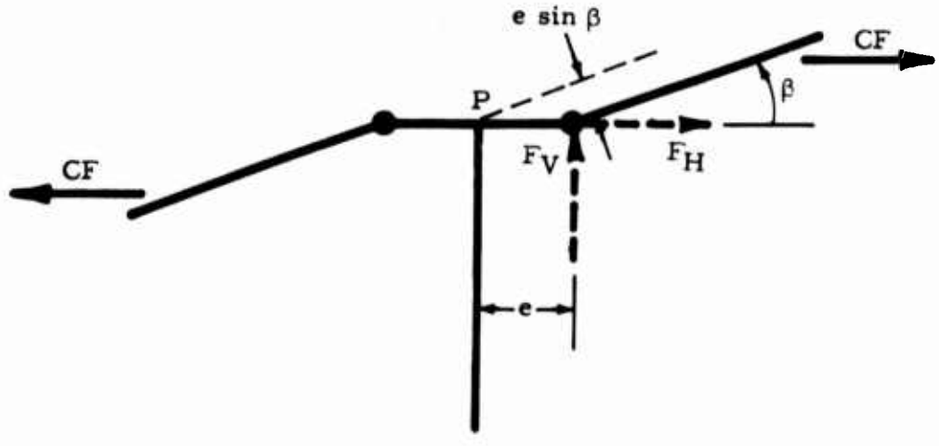

(b) Articulated Rotor

$M_p = e \text{ SIN } \beta \cdot CF \text{ COS } \beta \approx (e \cdot CF)\beta$

Figure 39. Schematic of Rotor Types.

flapping velocities in each case. The resulting displacements reach maximum value at about .85 second, or .35 second after the rotor encounters the gust. The articulated rotor has flapped more than a degree farther than the rigid rotor by this time.

The change in fuselage-pitch attitude with time (Figure 40b) and the change in flapping with respect to the swashplate (Figure 40c) indicate the interconnections affecting rotor response. As would be expected, flapping excursion for the semirigid is greater than for the other two hub types. The rigid case shows marked damping of the flapping oscillation. The lower value of K_g for the rigid, .44, as compared with .52 for the articulated, is attributed to blade-dynamics effects. The semirigid case has a K_g of .53.

TABLE IX. GUST-RESPONSE RESULTS FOR VARIOUS HUB TYPES - 200 KNOTS, .9 ADVANCING BLADE-TIP MACH NUMBER

Case	Conf	Hub Type	Disc Loading	C_T/σ	Δn_r SUDV	Δn_r SSQV	K_{g_r}	Max. Flap Vel.*
39-40	PSRH	AR	4.	.02	5.22	2.65	.521	15.6
17-18	PSRH	SR	4.	.02	5.19	2.39	.471	12.3
51-52	PSRH	RR	4.	.02	5.22	2.81	.551	16.2
135-136	CSRH	AR	4.	.02	5.63	2.81	.499	13.9
111-112	CSRH	SR	4.	.02	5.62	2.57	.457	12.2
147-148	CSRH	RR	4.	.02	5.63	2.89	.513	14.2
41-42	PSRH	AR	4.	.05	1.90	1.07	.565	28.3
21-22	PSRH	SR	4.	.05	1.91	1.03	.547	25.4
53-54	PSRH	RR	4.	.05	1.90	1.02	.537	25.9
137-138	CSRH	AR	4.	.05	1.86	1.02	.548	24.4
117-118	CSRH	SR	4.	.05	1.95	1.03	.528	15.2
149-150	CSRH	RR	4.	.05	1.98	1.04	.525	19.9
43-44	PSRH	AR	7.	.02	5.30	2.56	.492	14.9
55-56	PSRH	RR	7.	.02	5.30	2.55	.491	14.3
139-140	CSRH	AR	7.	.02	5.95	2.58	.434	12.5
151-152	CSRH	RR	7.	.02	5.95	2.64	.444	12.5

*For the sine-squared (even-numbered) cases.

TABLE IX - Continued

Case	Conf	Hub Type	Disc Loading	C_T/σ	Δn_r SUDV	Δn_r SSQV	K_{g_r}	Max. Flap Vel.*
45-46	PSRH	AR	7.	.05	1.84	.96	.522	26.7
9-10	PSRH	SR	7.	.05	1.87	.97	.516	26.3
57-58	PSRH	RR	7.	.05	1.84	.81	.440	19.8
141-142	CSRH	AR	7.	.05	1.70	.90	.529	25.4
91-92	CSRH	SR	7.	.05	2.22	1.46	.660	16.8
153-154	CSRH	RR	7.	.05	1.70	.90	.529	25.4
25-26	PSRH	SR	10.	.02	5.32	2.33	.438	12.0
47-48	PSRH	AR	10.	.02	5.31	2.21	.425	12.6
59-60	PSRH	RR	10.	.02	5.31	2.32	.447	13.1
123-124	CSRH	SR	10.	.02	5.48	2.19	.399	10.7
143-144	CSRH	AR	10.	.02	5.42	2.29	.423	12.1
155-156	CSRH	RR	10.	.02	5.42	2.34	.432	12.1
29-30	PSRH	SR	10.	.05	1.79	.94	.525	27.1
49-50	PSRH	AR	10.	.05	1.77	.88	.497	25.9
61-62	PSRH	RR	10.	.05	1.77	.91	.514	26.8
129-130	CSRH	SR	10.	.05	1.89	1.03	.545	18.7
145-146	CSRH	AR	10.	.05	1.78	.93	.522	12.1
157-158	CSRH	RR	10.	.05	1.78	.95	.534	22.4

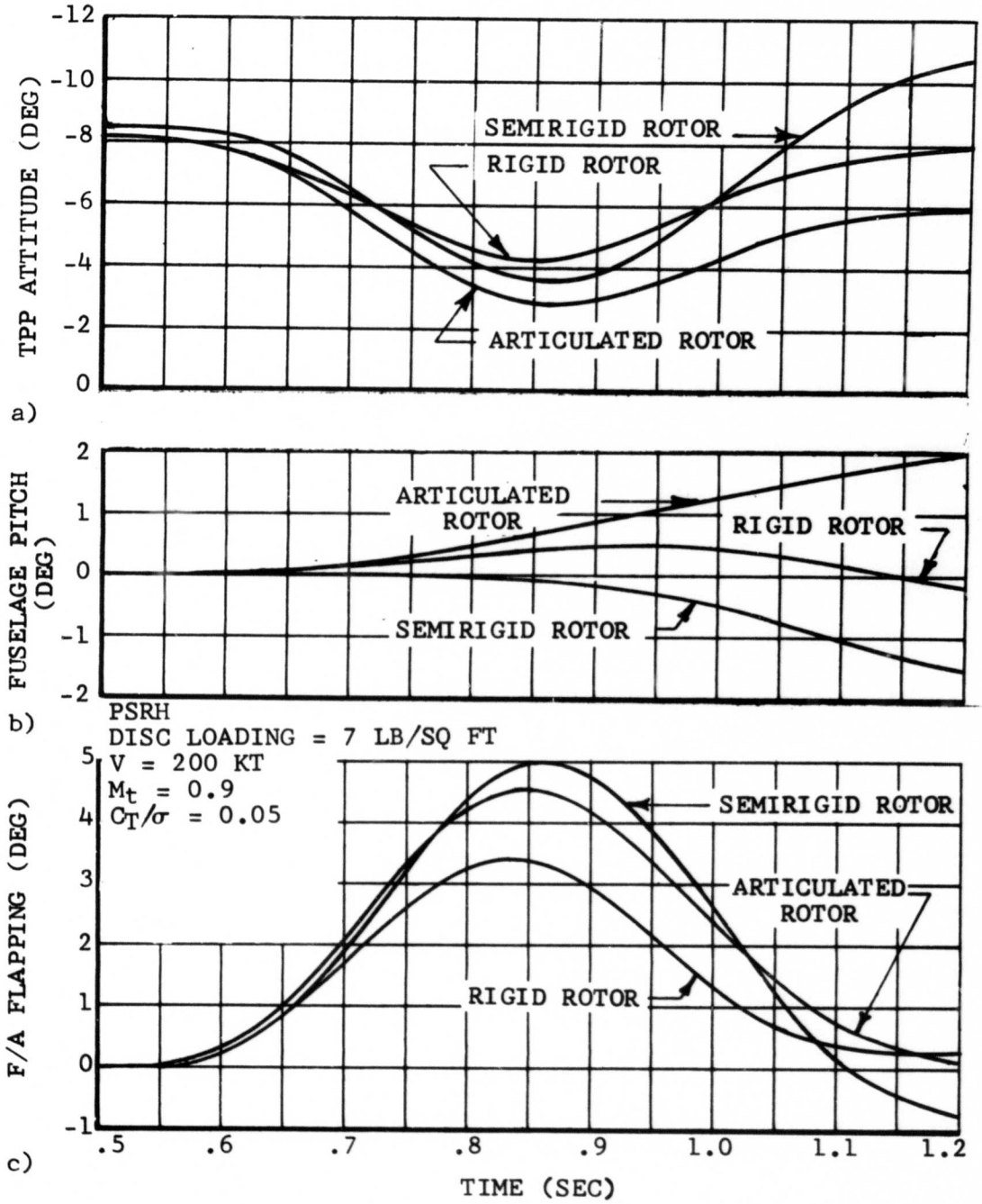

Semirigid - Case 10
Articulated - Case 46
Rigid - Case 58

Figure 40. Gust Response for Three Hub Types.

To obtain insight in the effect of hub rigidity (or hub spring) four additional cases have been run on a four-bladed rigid rotor where the hub stiffness is varied as an independent variable. The results are shown in Table X. It is found that increasing the hub stiffness increases both the gust-load factor Δn and the gust factor K_g.

TABLE X. RESULTS FOR VARIED HUB STIFFNESS ON A RIGID ROTOR

Hub-Spring Stiffness (Lb-In/Deg)	Vel (Kt)	Gust Type	Δn (g)	K_g
1260	120	Sine-squared	1.95	.756
		Sudden	3.58	
3675	120	Sine-squared	2.21	.855
		Sudden	3.58	

EFFECT OF DISC LOADING

Disc loadings of 4, 7, and 10 lb/sq ft were used for a variety of pure single-rotor helicopter and compound single-rotor helicopter cases. The tandem configuration has a disc loading of 7 lb/sq ft; the tilt-rotor configuration, near 10 lb/sq ft. The pure single-rotor helicopter cases are more suitable for showing effects of disc loading since the compound single-rotor helicopter cases are strongly influenced by rotor-to-wing-loading ratios. In addition to the 68 cases at 200 knots used in the discussion of effects of hub type (See Table IX), four cases at 175 knots and six cases at 225 knots are available for comparison.

Values of K_g for four-bladed, semirigid rotor helicopters at forward speeds of 175 to 225 knots and advancing blade-tip Mach numbers of .85 and .90 are shown in Figure 41. These cases were run with disc loadings of 4, 7, and 10 lb/sq ft. A slight downward trend of K_g is evident as the disc loading is increased. However, the low values of K_g for the combination of a rotor thrust coefficient-solidity ratio of .02 and a disc loading of 10 lb/sq ft are not considered to be significant because the rotor geometric parameters are not within reasonable limits. Variation of K_g with C_T/σ seems to be more pronounced than with either disc loading or forward velocity. Acceleration increments for the same cases are given in Figure 42. The slight variation with disc loading shown in this figure is overshadowed by the differences due to rotor thrust coefficient-solidity ratio.

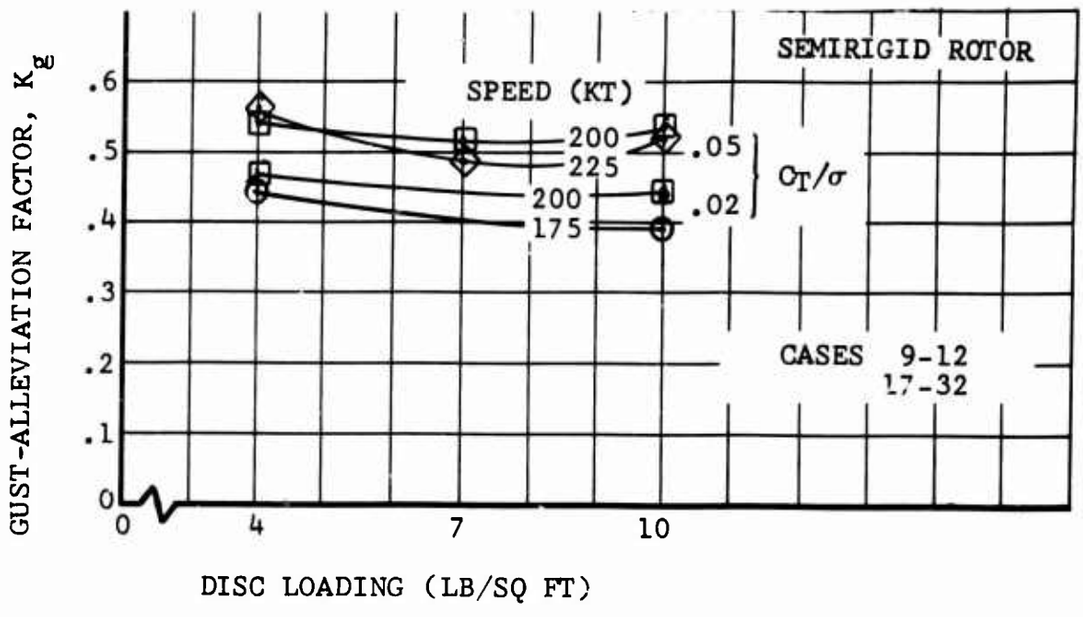

Figure 41. Effects of Disc Loading on Gust-Alleviation Factor.

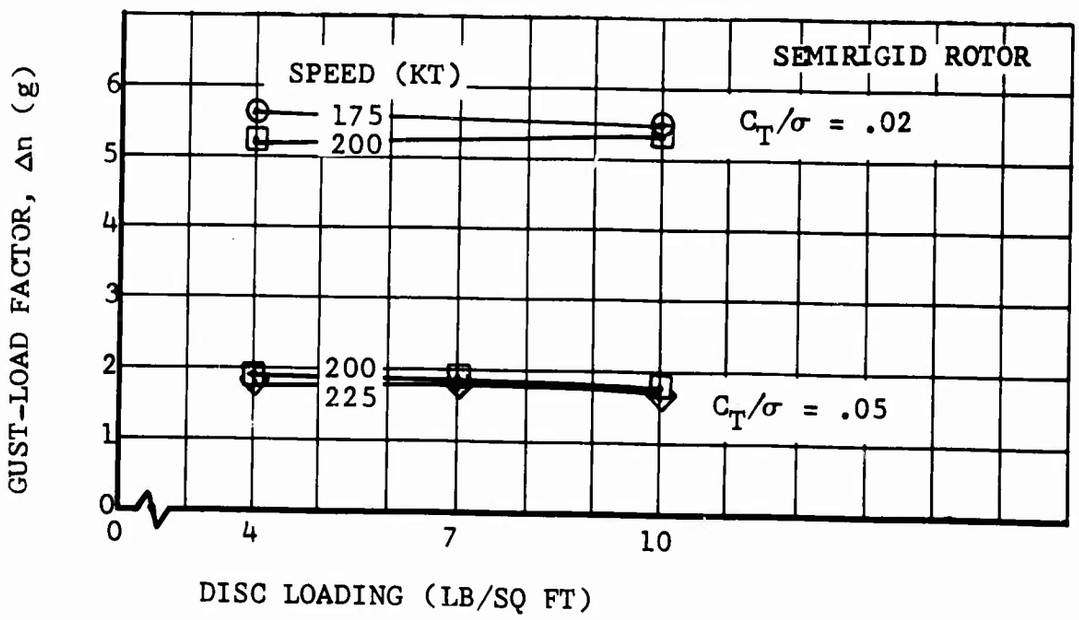

Figure 42. Effects of Disc Loading on Sudden-Gust Response.

Results from compound single-rotor helicopter cases are somewhat more scattered than for the pure single-rotor helicopter. Considering only the 200-knot cases, average values of K_g for the different disc loadings range from .40 to .51 for C_T/σ = .02 and from .53 to .67 for C_T/σ = .05. The Δn values for sudden-gust cases vary from 6.5 to 7.0 for the lower rotor thrust coefficient-solidity ratio and from 2.9 to 3.3 for the higher. Changes in vertical acceleration due to change in rotor thrust only range from 5.4 to 5.9 for low rotor C_T/σ and from 1.8 to 2.2 for high C_T/σ. No particular trend with disc loading can be deduced from these data.

EFFECT OF ROTOR THRUST COEFFICIENT-SOLIDITY RATIO, C_T/σ

The variation in the rotor thrust coefficient-solidity ratio, C_T/σ, which is a measure of the blade-lift coefficient, C_l, produces the most pronounced change in Δn results, as seen in Table IX. Figure 42 also shows a consistently large shift in Δn for sudden gusts in going from low thrust coefficients (C_T/σ = .02) to high coefficients (.05).

A remarkable correspondence of Δn levels due to sine-squared gusts at the same values of C_T/σ is revealed in Table IX. Since the acceleration change values shown in the table are based on rotor-thrust change only, the compound single-rotor helicopter may be included with the pure helicopter. At the lower value of C_T/σ, the range for Δn is from 2.2 to 2.9; while for C_T/σ = .05, the range is from 0.8 to 1.1. Thus, there is in excess of 1.0g lower response to sine-squared gusts for the C_T/σ = .05 cases in comparison with the C_T/σ = .02 cases.

A limited number of cases were computed at C_T/σ = .08. Figure 43 shows Δn for sine-squared and for sudden gusts as functions of C_T/σ. The reduction in normal acceleration response with increasing blade-lift coefficient is evident. Average values of Δn (sine-squared gust) for the .02 and .05 cases at 200 knots are used in Figure 43.

Increasing rotor-blade flapping velocity with rotor thrust coefficient-solidity ratio is evidenced by the results. Average values from Table IX are plotted in Figure 44. The values of C_T/σ = .08 are also shown.

EFFECT OF ADVANCING BLADE-TIP MACH NUMBER

Advancing blade-tip Mach number variations from .80 to .95 are used in a series of cases with disc loading of 7.0 lb/sq ft and C_T/σ = .05. These cases cover a forward-speed range from 200 to 350 knots, encompassing both pure and compound single-rotor helicopter configurations with four-bladed semirigid rotors.

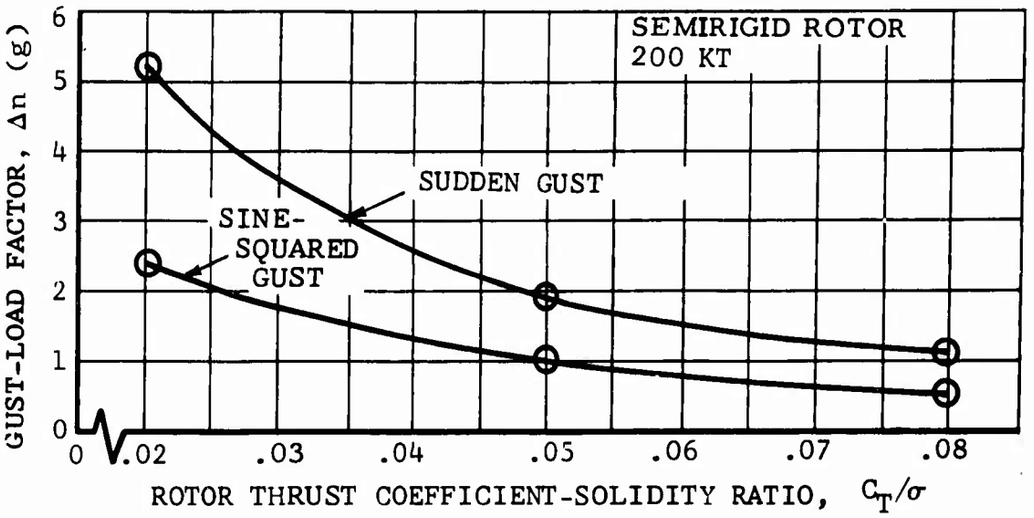

Figure 43. Effect of C_T/σ on Rotor Gust-Load Factor for Sudden and Sine-Squared Gusts.

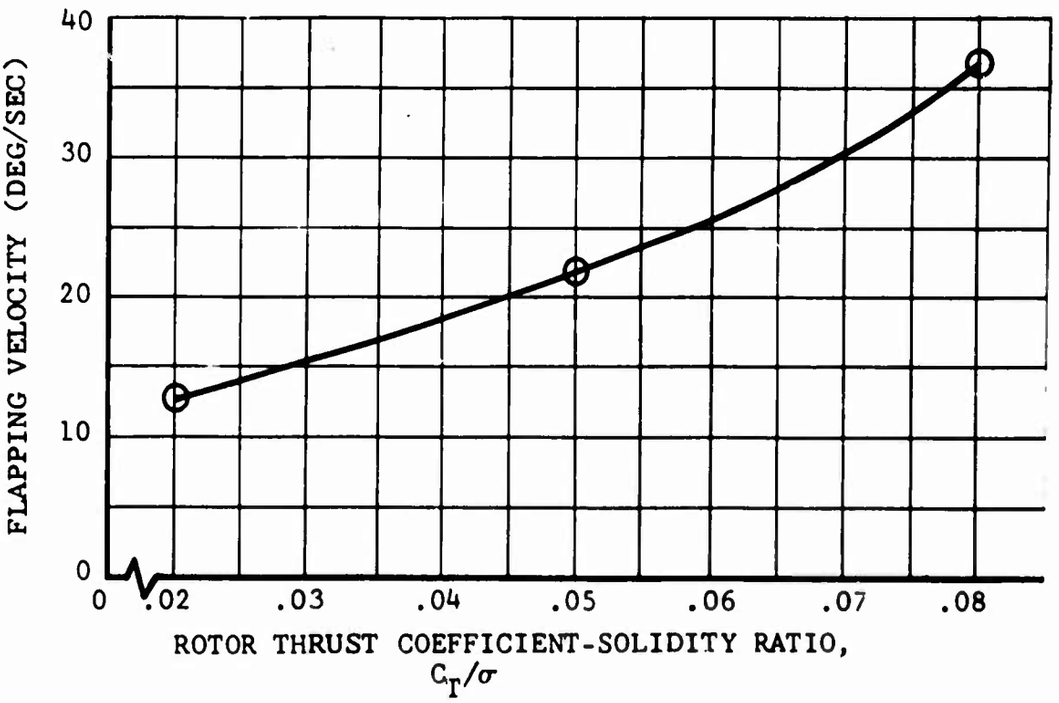

Figure 44. Effect of C_T/σ on Maximum Rotor-Flapping Velocity Due to Sine-Squared Gusts, Semi-rigid Rotor.

For the pure single-rotor helicopter, sine-squared gust runs, Δn holds almost constant at about .97 for 200 knots and .92 for 225 knots through advancing blade-tip Mach number of .90. At M_t = .95 there is a slight decrease in Δn values for both velocities. Corresponding to this situation, the K_g curves (Figure 45) turn sharply up at the high M_t end. This effect is associated with the input parameter for determination of drag divergence. In the calculations for this study, drag divergence begins at M_t = .87 for low angles of attack. A substantial portion of the outboard blade section is subject to significant compressibility effects at M_t = .95, resulting in an upturn in the gust-alleviation factor. This compressibility effect is further illustrated by plotting horsepower required vs M_t, as given in Figure 46 for a series of 200- and 225-knot cases.

Flapping velocities shown in Figure 47 for the pure single-rotor configuration sine-squared gust cases also indicate an increase in response with advancing blade-tip Mach number. The Lock number for all of these cases is γ = 8.3.

The situation for the compound-helicopter gust cases is again masked to some extent by other variables. Variations for Δn for sine-squared vertical gust cases are shown in Figure 48 for five velocities. Median values of .83 for K_{g_w} and .65 for K_{g_r} resulted from calculations.

EFFECT OF FORWARD SPEED

As has been previously indicated, values of alleviation factors do not change radically with forward speed. However, the principal features of response, vertical acceleration and rotor flapping, show an upward trend with increasing forward velocity. The compound configuration offers an interesting example since the rotor- and wing-lift increases must both be considered. The Δn values for the entire aircraft, including fuselage, elevator, and tail-rotor response are also of interest. The most extensive velocity sweep was made for the compound cases with disc loading of 7.0 lb/sq ft and C_T/σ = .05. Δn for the entire helicopter and for the rotor and wing is plotted in Figure 49. Note that the rotor response falls off slightly above 300 knots. This is due to increasing stall since the advance ratio is becoming very large. The wing-lift increase due to encountering the gust is proportional to the forward speed. Rotor-flapping velocity versus forward velocity for 20 compound single-rotor helicopter cases is given in Figure 50, and fuselage-pitching velocity versus velocity, in Figure 51. Fuselage-pitching velocity reduces with forward speed since the dynamic pressure at the elevator tends to act against a change in pitch orientation.

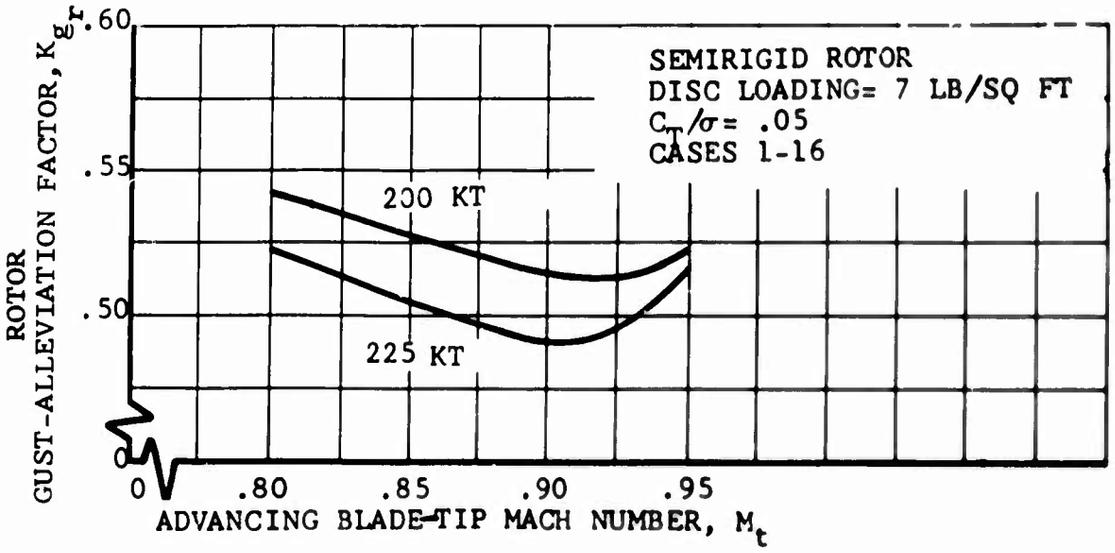

Figure 45. Rotor Gust-Alleviation Factor Versus Advancing Blade-Tip Mach Number for a Pure Single-Rotor Helicopter.

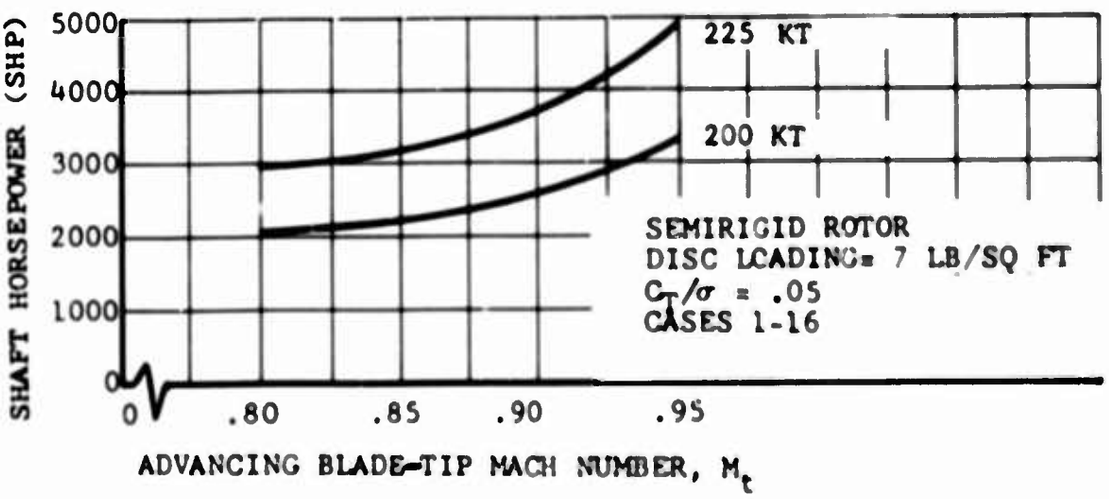

Figure 46. Required Shaft Horsepower Versus Advancing Blade-Tip Mach Number for a Pure Single-Rotor Helicopter.

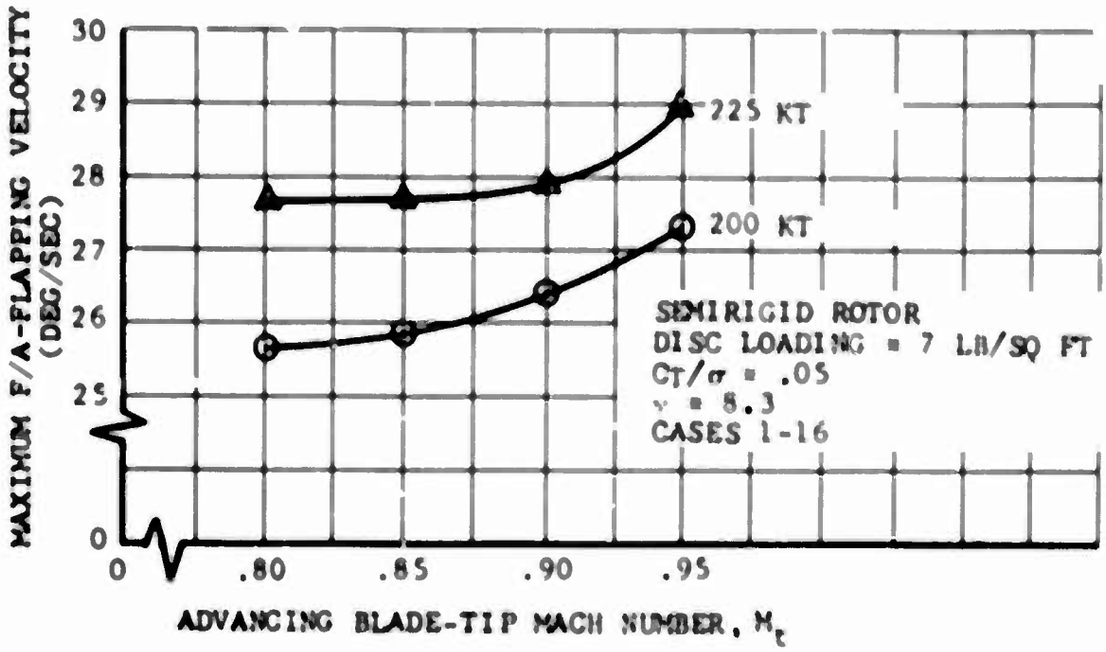

Figure 47. Flapping Velocity Versus Advancing Blade-Tip Mach Number for a Pure Single-Rotor Helicopter.

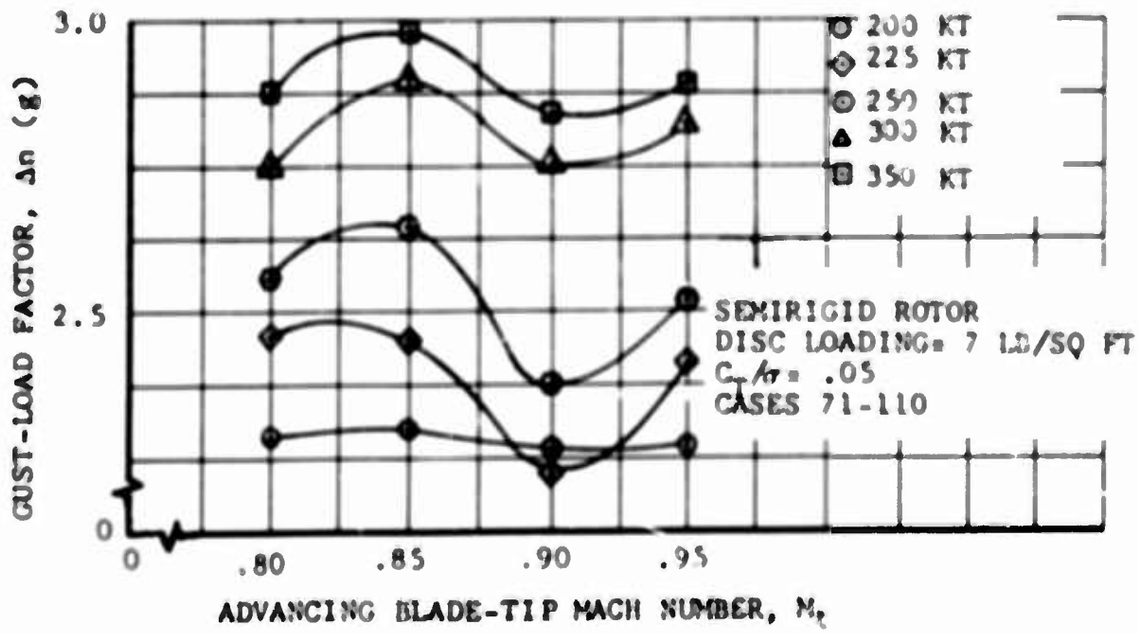

Figure 48. Gust-Load Factor Versus Advancing Blade-Tip Mach Number for a Compound Helicopter.

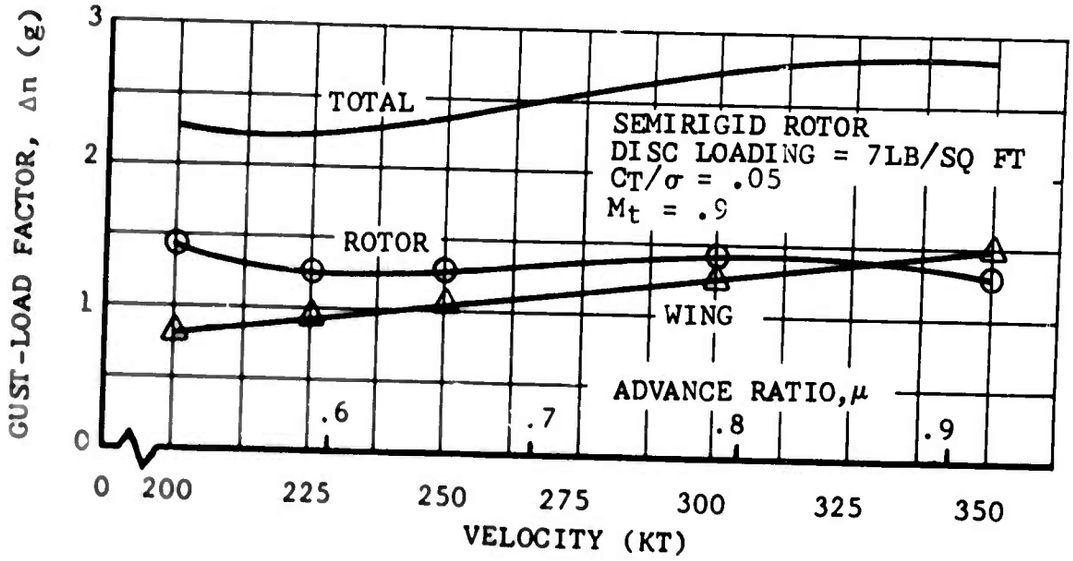

Figure 49. Acceleration Due to Sine-Squared Gust Versus Velocity for a Compound Single-Rotor Helicopter, Cases 91-110.

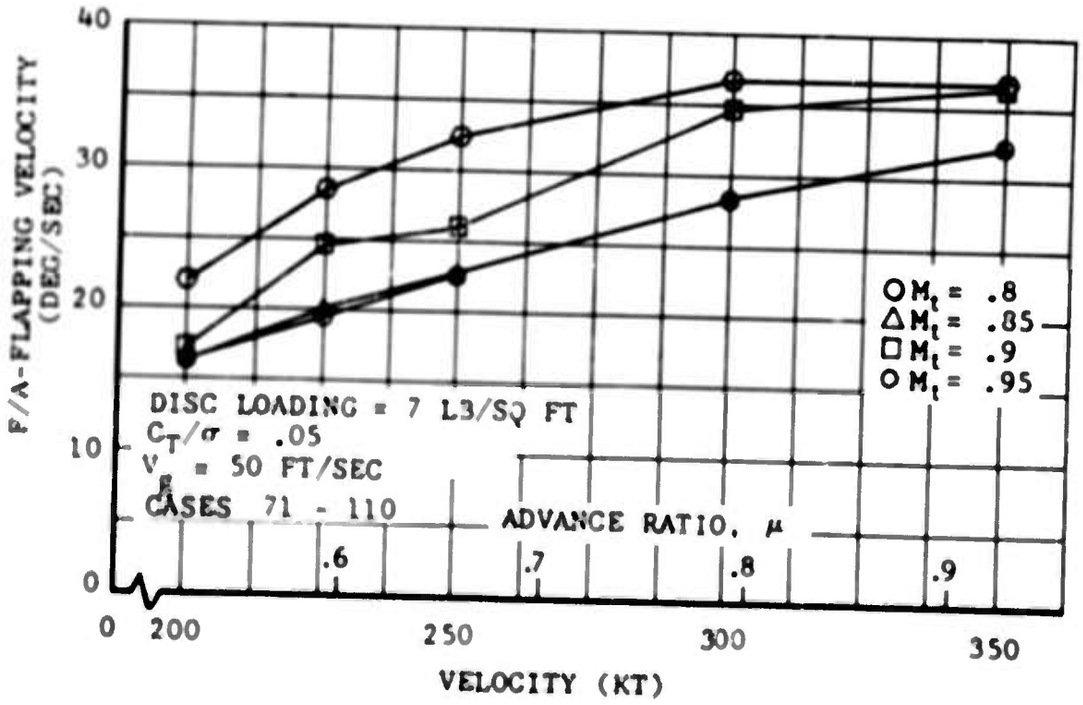

Figure 50. Flapping Velocity Versus Forward Speed for Sine-Squared Gust Cases, Compound Single-Rotor Helicopter.

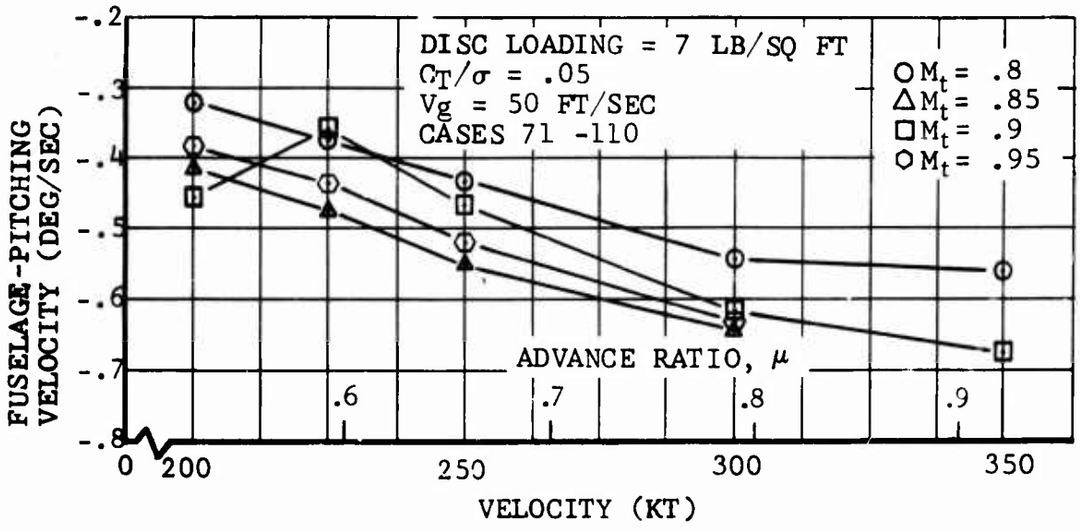

Figure 51. Fuselage-Pitching Velocity Versus Forward Speed for Sudden-Gust Cases, Compound Single-Rotor Helicopter.

EFFECT OF LOCK NUMBER, γ

The influence of Lock number on the gust response for three values of advance ratio has been evaluated for the articulated-, semirigid-, and rigid-rotor systems. A 50-ft/sec maximum-velocity gust was used in each of the 27 sine-squared gust cases. The simplified method, with a sudden gust, was used to compute responses for comparison with the detailed method calculations. Only one Lock-number value was used for the sudden-gust calculations because there is not time for this variation to affect the maximum Δn calculated. All of the cases in this group (cases 278 through 313) are four-bladed, pure single-rotor helicopter configurations with a disc loading of 7.0 lb/sq ft, C_T/σ of 0.05, and advancing blade-tip Mach number of .9. Advance ratios of .39, .45, and .50 were selected for the calculations. Lock-number values of 8.31, 5.56 and 4.43, used in these cases, were obtained by varying blade-tip weight.

The normal acceleration change due to gust loading, Δn, is listed in Table XI for each of the 36 cases. No significant variation with rotor configuration or with advance ratio was observed. There is, however, a definite indication of increasing Δn with increasing blade inertia.

For the articulated and semirigid rotors, the gust-alleviation factor varies with Lock number from .56 for γ = 8.31 to .66

for γ = 4.43 at μ = .45. The cases for μ = .39 and μ = .50 have only slightly different values of K_g at corresponding Lock numbers.

Time histories of the flapping, normal-acceleration increment, and flapping velocity are presented in Figures 52 through 57 for the different advance ratios for the articulated- and the semirigid-rotor types. The response curves for each of three Lock numbers of the sine-squared gust cases are shown on the same graph for a particular advance ratio and rotor type. The general character of the response is not changed over the range of Lock-number variation considered. The response curves for the rigid-rotor cases were practically the same as for the corresponding articulated-rotor cases. All of the configurations show the highest blade-flapping displacement and flapping velocity and the lowest Δn for the high Lock number (8.31). As Lock number is reduced, the maximum flapping velocity decreases and Δn increases.

The higher flapping velocities reduce the relative velocity normal to the tip-path plane as the gust passes across the forward section of the rotor disc. Lower rotor-thrust values are thus computed for the high Lock-number cases. These results emphasize that the effect of flapping velocity must be included in any analysis of gust response for helicopters.

TABLE XI. PRINCIPAL RESULTS OF LOCK-NUMBER VARIATION

Advance Ratio	Forward Speed	Lock Number	Articulated Rotor		Semirigid Rotor		Rigid Rotor	
μ	(kt)	γ	$\Delta n(g)$	K_g	$\Delta n(g)$	K_g	$\Delta n(g)$	K_g
.39	150	*8.31	1.78	-	1.75	-	1.78	-
.39	150	8.31	1.03	.58	1.02	.58	1.03	.58
.39	150	5.56	1.11	.62	1.10	.63	1.11	.62
.39	150	4.43	1.17	.66	1.16	.66	1.17	.66
.45	175	*8.31	1.81	-	1.83	-	1.81	-
.45	175	8.31	1.02	.56	1.02	.56	1.03	.57
.45	175	5.56	1.12	.62	1.11	.61	1.12	.62
.45	175	4.43	1.19	.66	1.19	.65	1.19	.66
.50	200	*8.31	1.83	-	1.85	-	1.83	-
.50	200	8.31	1.00	.55	0.99	.54	1.00	.55
.50	200	5.56	1.11	.61	1.11	.60	1.11	.61
.50	200	4.43	1.19	.65	1.18	.64	1.19	.65

*Indicates sudden-gust cases.

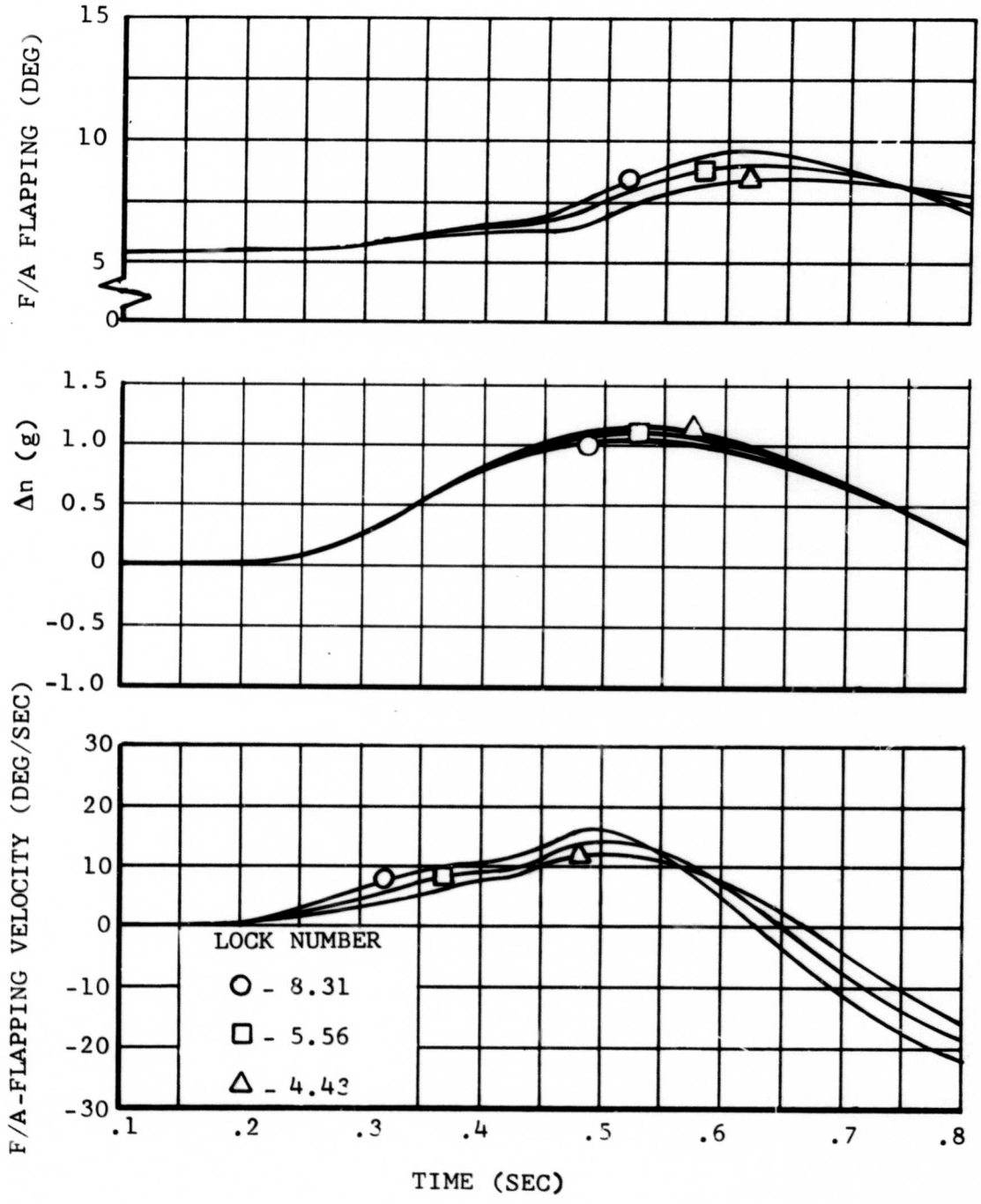

Figure 52. Effect of Lock Number on Response of Articulated Rotor to Sine-Squared Gust at 150 Knots.

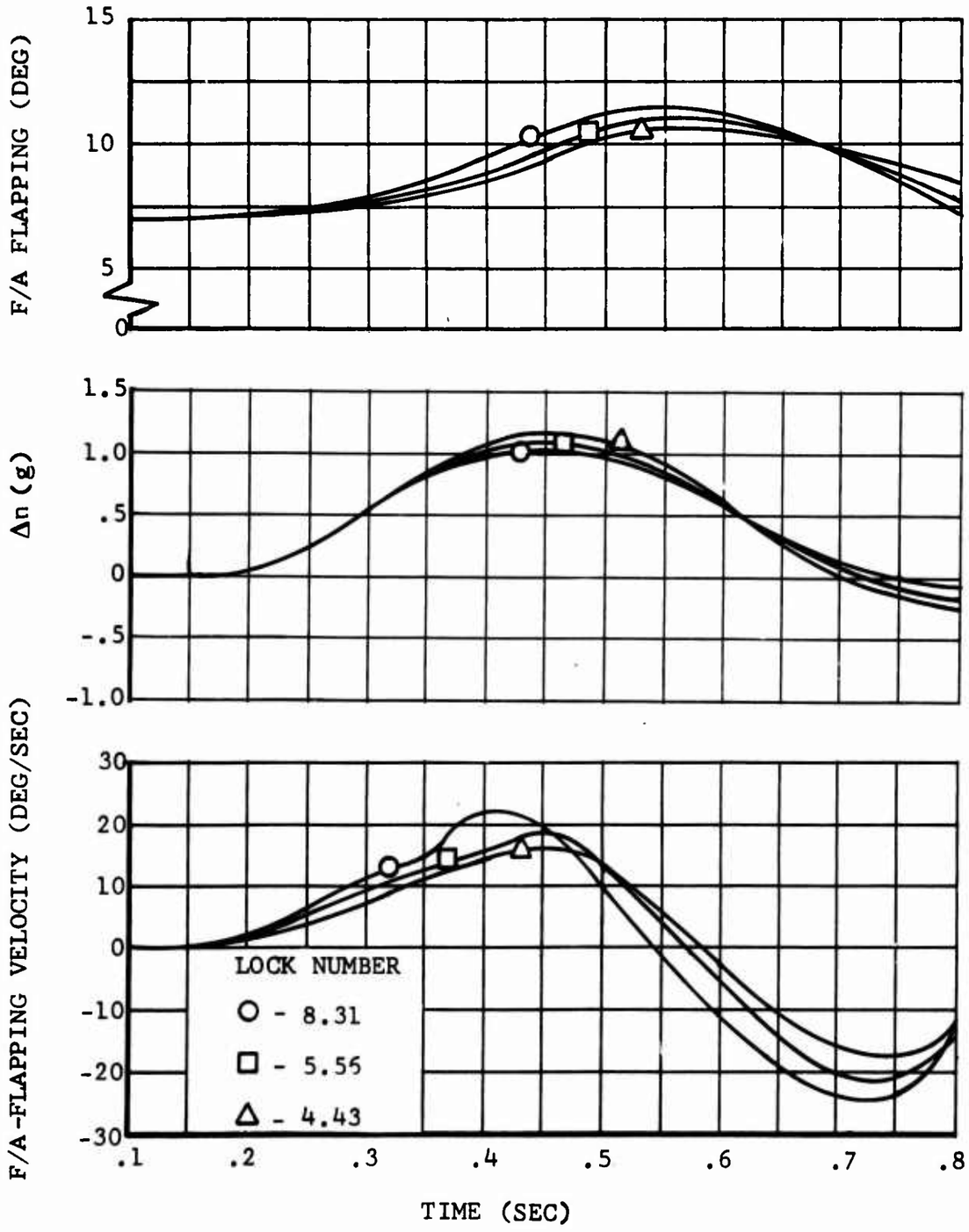

Figure 53. Effect of Lock Number on Response of Articulated Rotor to Sine-Squared Gust at 175 Knots.

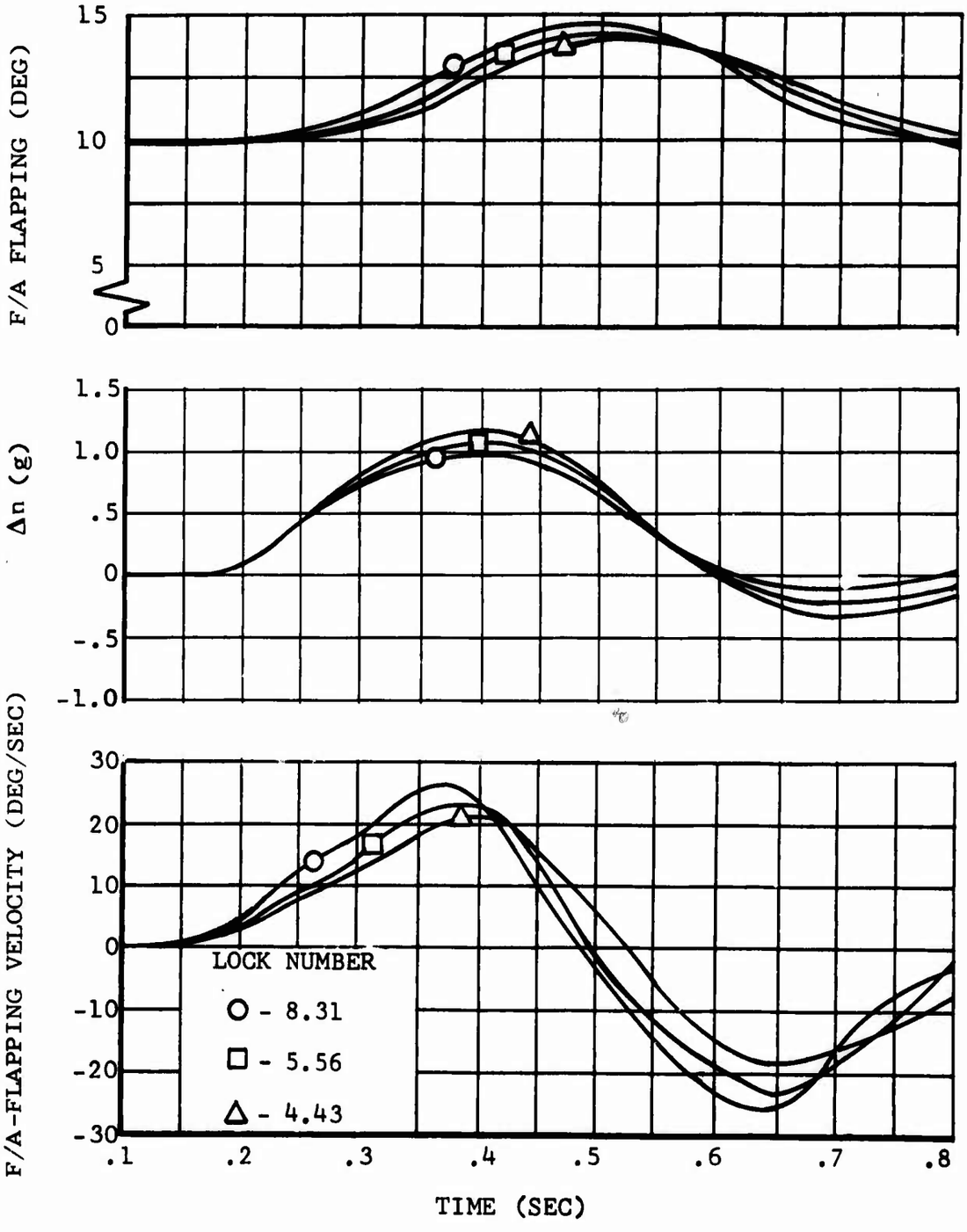

Figure 54. Effect of Lock Number on Response of Articulated Rotor to Sine-Squared Gust at 200 Knots.

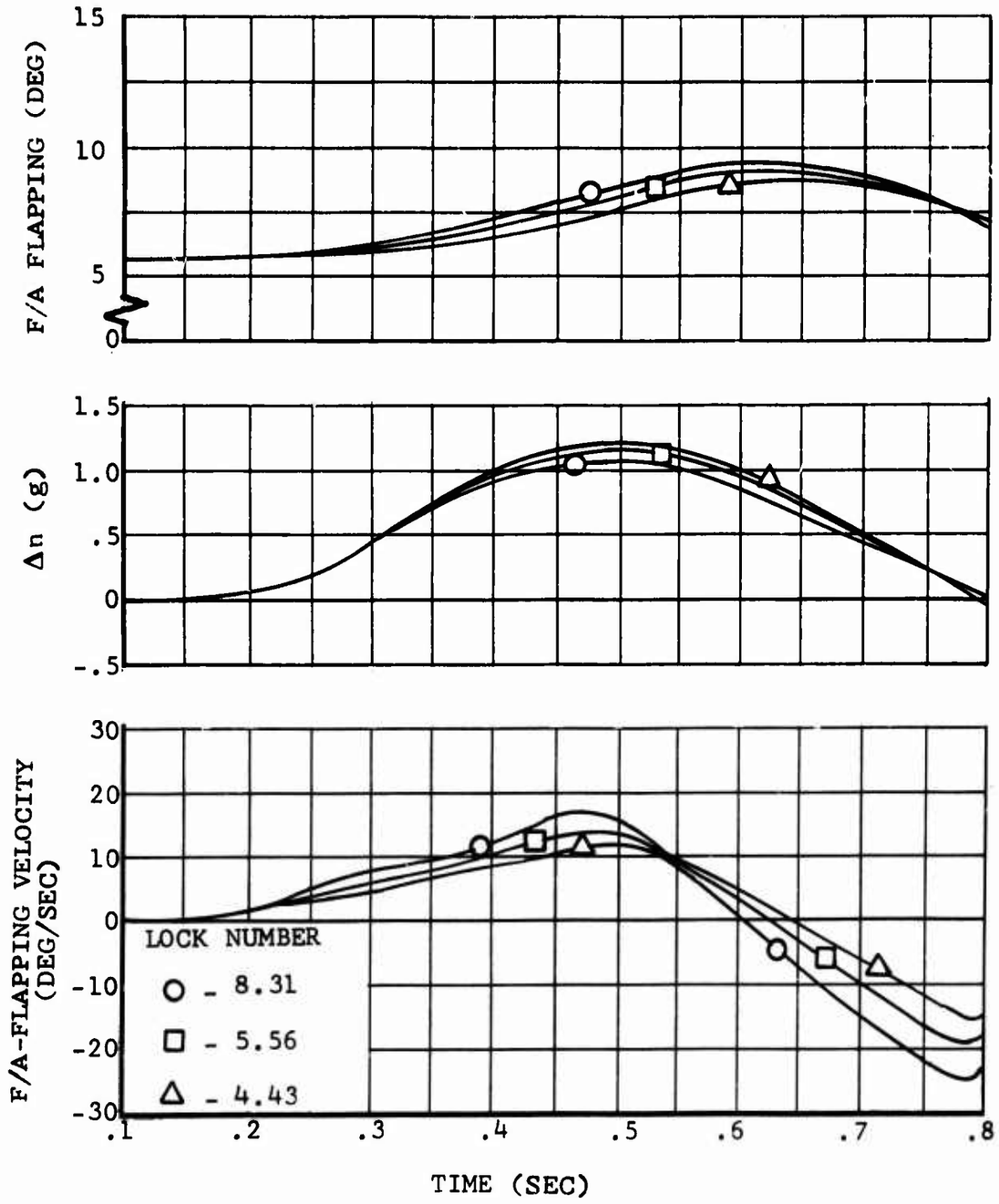

Figure 55. Effect of Lock Number on Response of Semirigid Rotor to Sine-Squared Gust at 150 Knots.

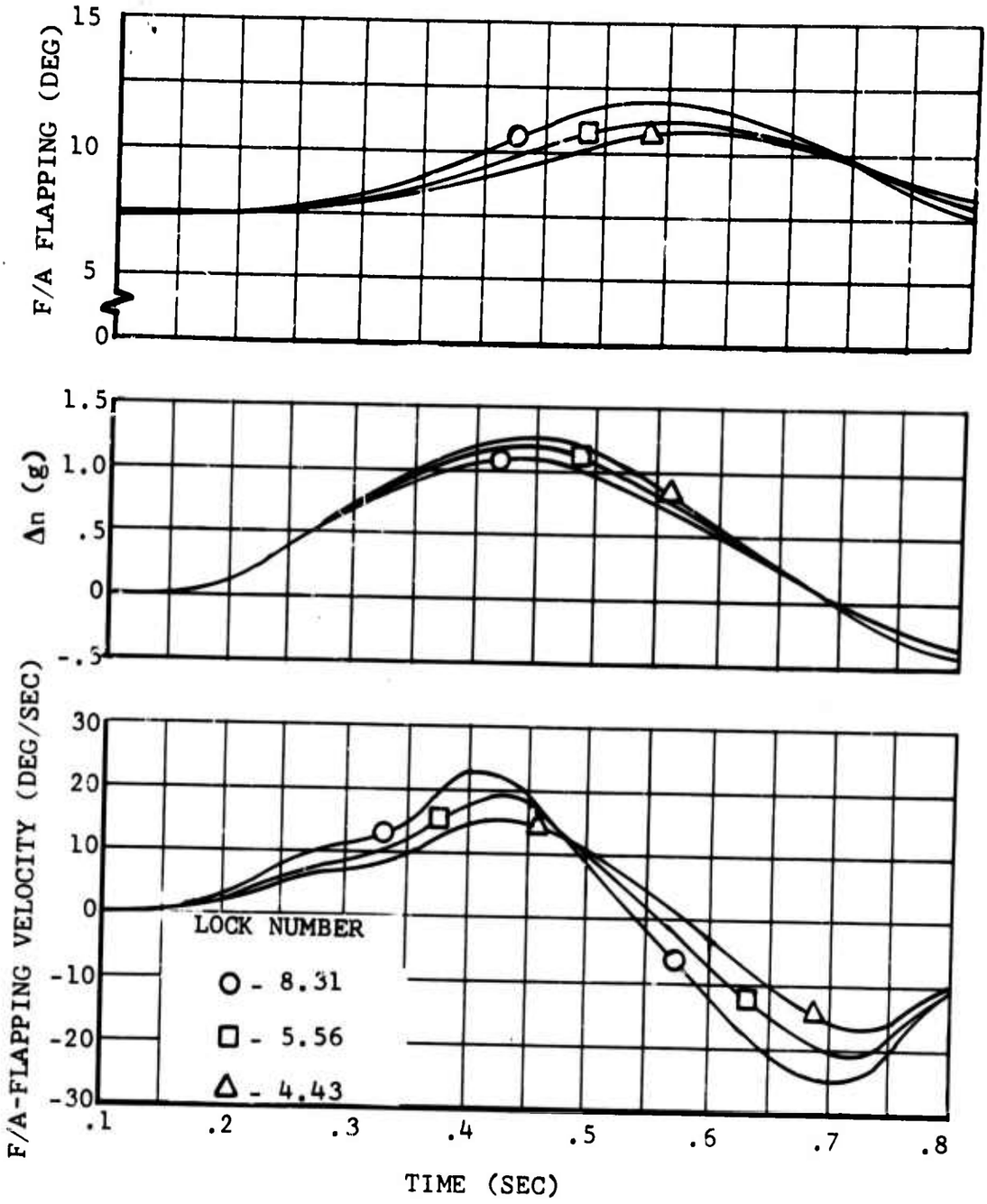

Figure 56. Effect of Lock Number on Response of Semirigid Rotor to Sine-Squared Gust at 175 Knots.

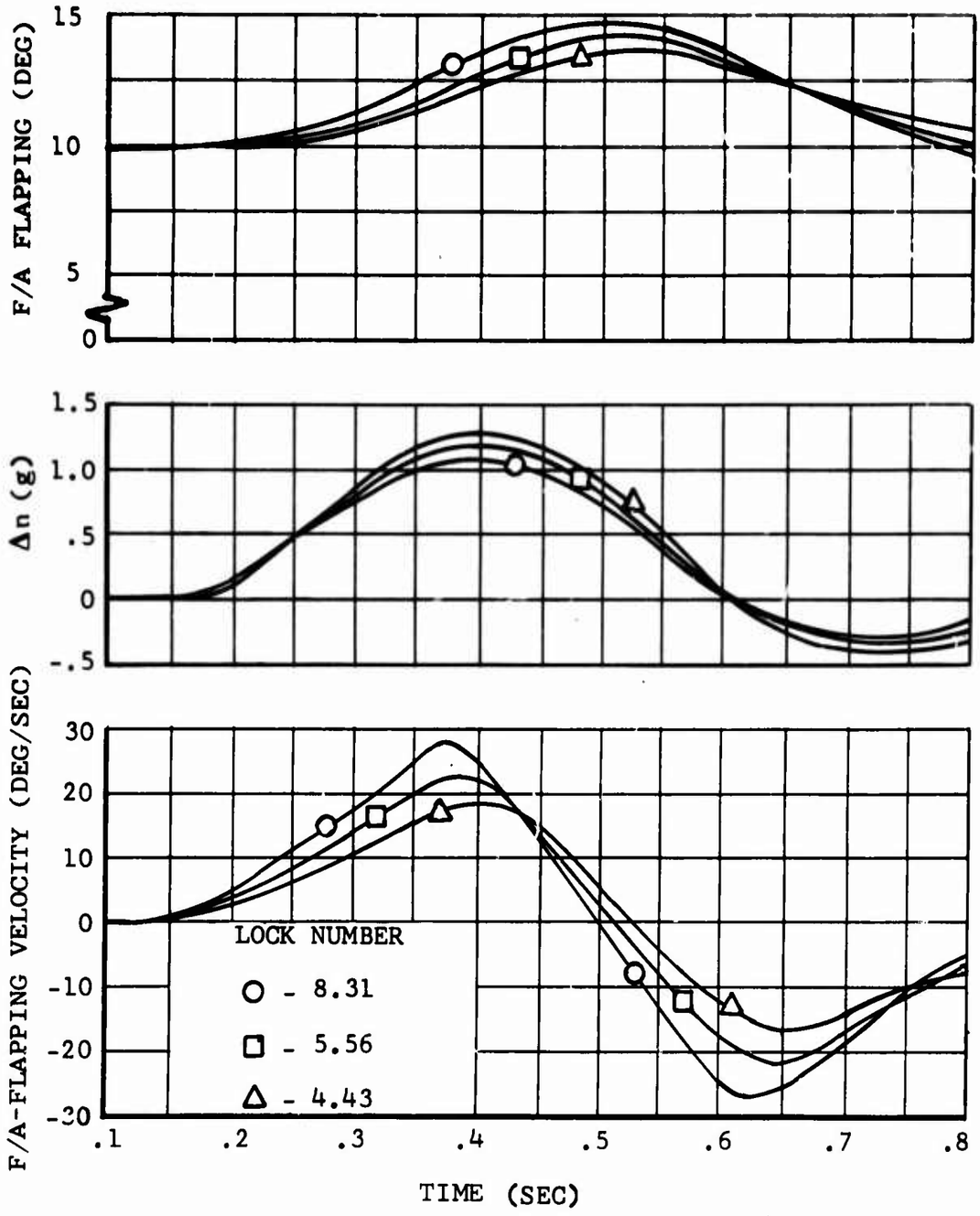

Figure 57. Effect of Lock Number on Response of Semirigid Rotor to Sine-Squared Gust at 200 Knots.

EFFECT OF ROTOR UNLOADING BY THE WING

The set of compound single-rotor helicopter cases (cases 71-134) was trimmed for a considerable range of rotor-thrust to wing-lift ratios. This variation, achieved while holding rotor rpm constant, had a significant effect on computed values of K_g, as was mentioned in the section on configuration effects. The lift-change ratios at maximum acceleration due to gusts as they vary with velocity are shown in Figure 58 for disc loading of 7 and C_t/σ of .05. As would be expected, the rotor thrust predominates at the lower speeds and the wing lift at the higher speeds. Further, it is seen that the ratio is higher for sudden gusts than for sine-squared gusts. This points up the generality of the lower value of alleviation factors for rotors than for wings, since for

$$\left(\frac{\Delta T}{\Delta L}\right)_{\text{sine-squared}} < \left(\frac{\Delta T}{\Delta L}\right)_{\text{sudden}}$$

$$\frac{\Delta T_{\text{sine-squared}}}{\Delta T_{\text{sudden}}} < \frac{\Delta L_{\text{sine-squared}}}{\Delta L_{\text{sudden}}}$$

The rotor-thrust-change ratio is equal to K_{g_r}, the alleviation factor for the rotor; and the wing-lift-change ratio is equal to K_{g_w}, the alleviation factor for the wing. Therefore,

$$K_{g_r} < K_{g_w} \tag{18}$$

The shaded bands in Figure 58 contain the load-share ratios at maximum loading for the majority of the compound-configuration cases considered. An analysis of the results calculated for 54 cases shows that the wing-lift change due to a gust versus velocity is very nearly linear for each of the gust shapes used. On the other hand, the rotor-lift increment is almost constant over the speed range. The rotor-thrust change due to a vertical sudden gust of 50 ft/sec averaged about 33,000 lb, while for the sine-squared gust of 50-ft/sec maximum amplitude, the average thrust change was 21,000 lb. The almost-constant rotor-thrust increment computed over the velocity range from 200 knots to 350 knots is consistent with the results shown in Figure 5, page 9. Thus the relative contribution of the rotor to gust response decreases as velocity increases.

EFFECT OF GUST-ALLEVIATING DEVICES

Three gust-alleviating devices were investigated:

- Pitch-cone coupling
- Pitch-flap coupling
- Bobweight in collective-pitch system

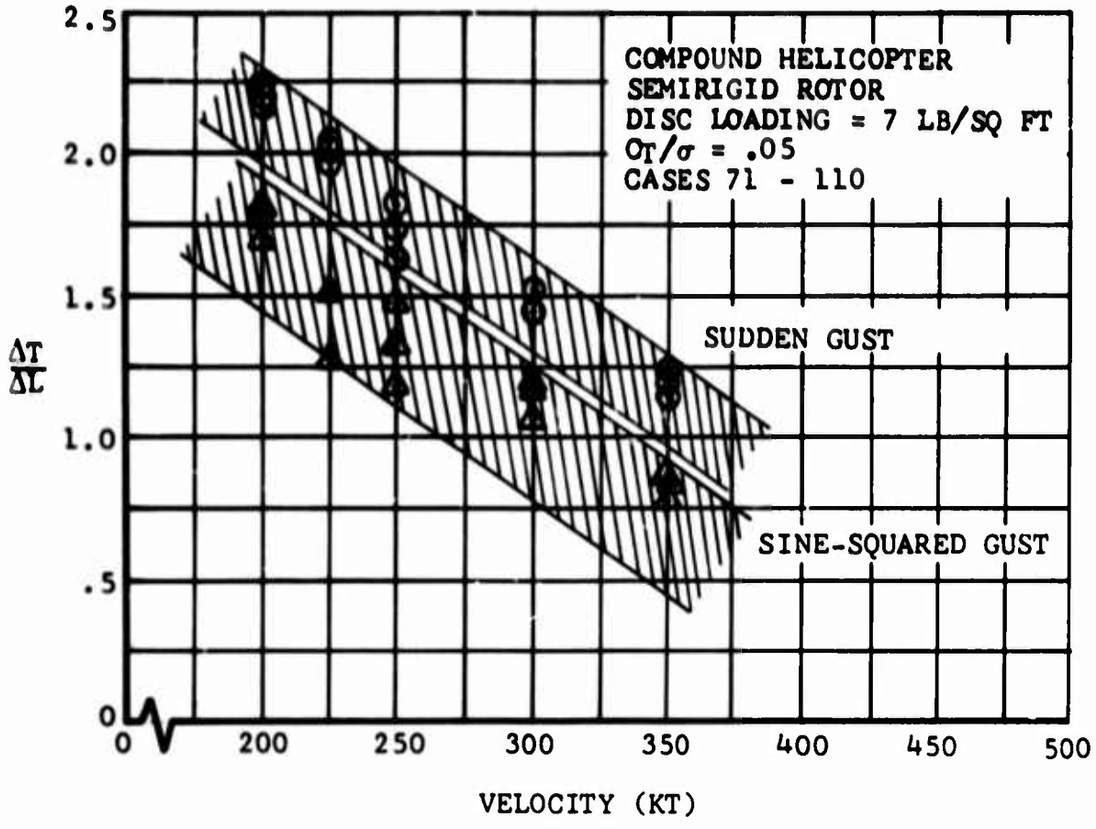

Figure 58. Ratio of Change in Rotor Thrust, ΔT, to Change in Wing Lift, ΔL, Due to Gusts Versus Forward Velocity.

Pitch-cone coupling is present in the rotor system when the steady-state component of the rotor-blade flapping angle produces simultaneously a change in blade pitch. Pitch-flap coupling results in a change in blade pitch proportional to the one-per-rev component of the blade-flapping angle.

The effect of pitch-cone coupling on the sharp-edged gust response of a compound helicopter with a two-bladed semi-rigid rotor is illustrated in Figure 59. These gust-response time histories include the effects of penetration, nonsteady aerodynamics, and aeroelastic feedback. The difference indicated in Figure 59 is due to a pitch-cone coupling ratio of -1 (for case 269), whereby a one-degree increase in rotor coning causes a one-degree reduction in the collective pitch setting at the rotor. A sketch is included in the figure to indicate one possible geometric configuration of the rotor that will produce this coupling. Note that, because the pitch-horn points are on the flapping axis at the rotor centerline, rotor flapping does not introduce additional control coupling.

Figure 60 shows the effect of pitch-cone coupling on the sine-squared gust response of a pure helicopter with a four-bladed semirigid rotor. The range of coupling values for these cases is from -.5 to +.5, with the former value causing a 15% reduction in the gust-load factor.

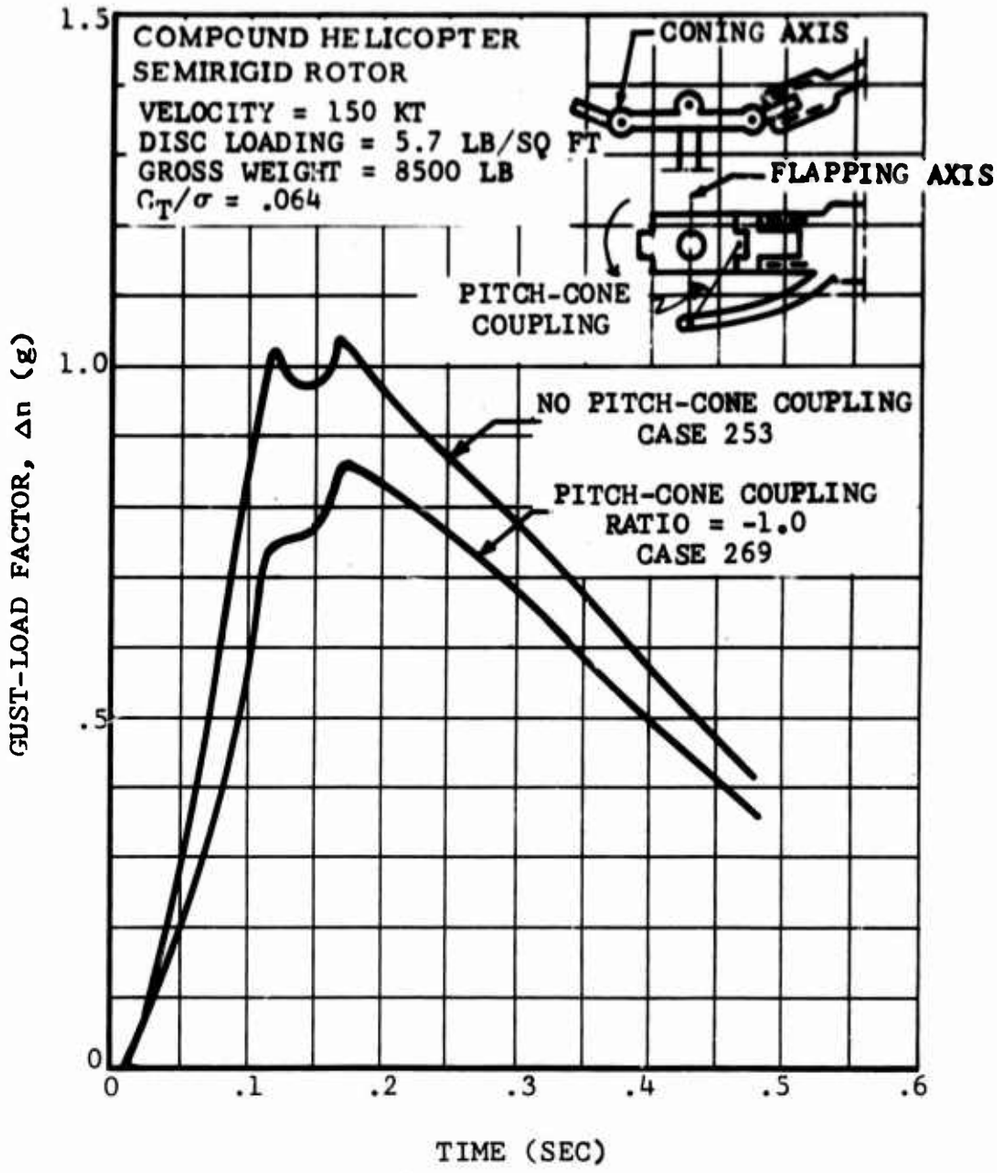

Figure 59. Effect of Pitch-Cone Coupling on Sharp-Edged Gust Response With Penetration, Nonsteady Airloads, and Aeroelastic Feedback.

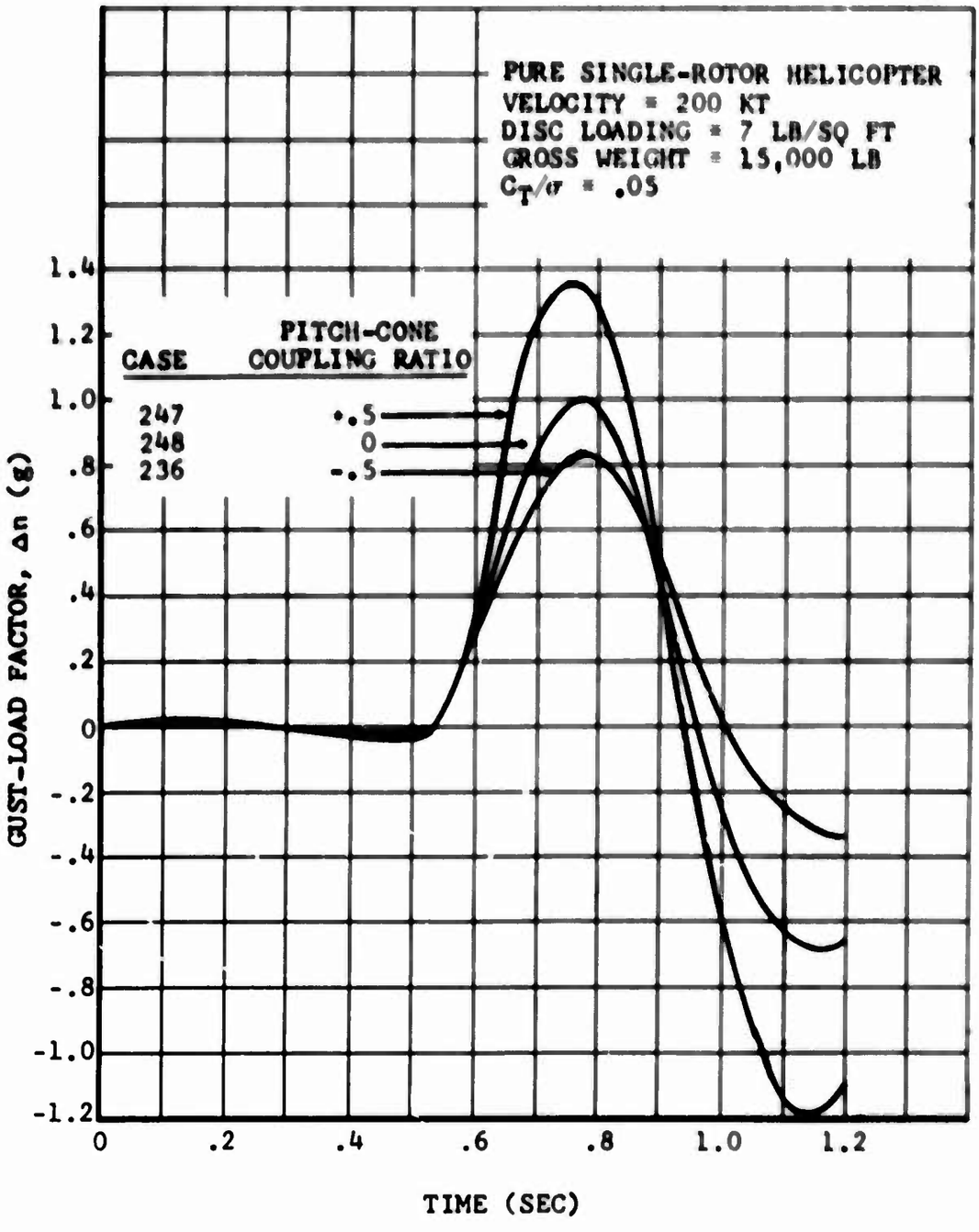

Figure 60. Effect of Pitch-Cone Coupling on Sine-Squared Gust Response.

The effect of pitch-flap coupling (δ_3) is shown in Figure 61 for a pure helicopter with a four-bladed semirigid rotor. The effect of 30 degrees of pitch-flap coupling on the maximum gust-load factor is very small. However, a considerable damping effect is indicated by the reduced overshoot. Figure 61 includes a sketch of one possible configuration with δ_3. In this arrangement, coning occurs about the offset hinges and causes no control coupling.

Combinations of pitch-cone coupling and pitch-flap coupling are possible in many ways. In articulated systems, the coupling ratios usually are equal because both coning and flapping occur about the offset axis of each blade. In rigid and semirigid rotors, the spanwise distribution of structural flexibility is an important consideration because bending of the structure has effects similar to those of a hinge.

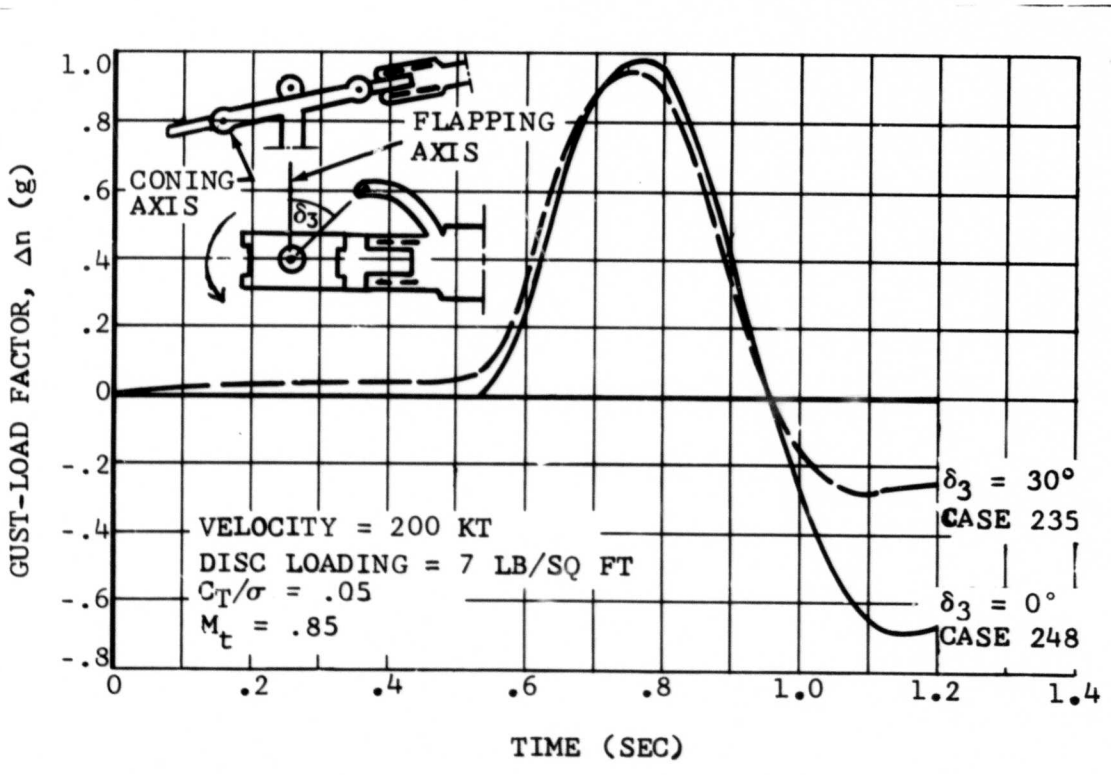

Figure 61. Gust Alleviation Due to Pitch-Flap Coupling (δ_3) for a Pure Single-Rotor Helicopter.

Pitch-flap coupling can have a pronounced influence on flapping stability, particularly at high advance ratios. Gust response at advance ratios greater than 1.0 depends primarily on flapping stability. Coupling between blade flapping and pitch can have a stabilizing effect. Figure 62 is a plot of the spring coefficient, $g_0(\psi)$ for $\delta_3 = 0$ and for $\delta_3 = 30^o$, from equation (14), page 53. This illustrates the local spring-rate variation for a high-μ case. The large region of instability starting in the second quadrant is considerably reduced by pitch-cone coupling. However, a secondary destabilizing trend develops in the third quadrant with increasing δ_3. Arrows in the negative spring-coefficient areas point in the direction of change in stability with increasing pitch-cone coupling. A closer investigation of this subject is in order for future studies.

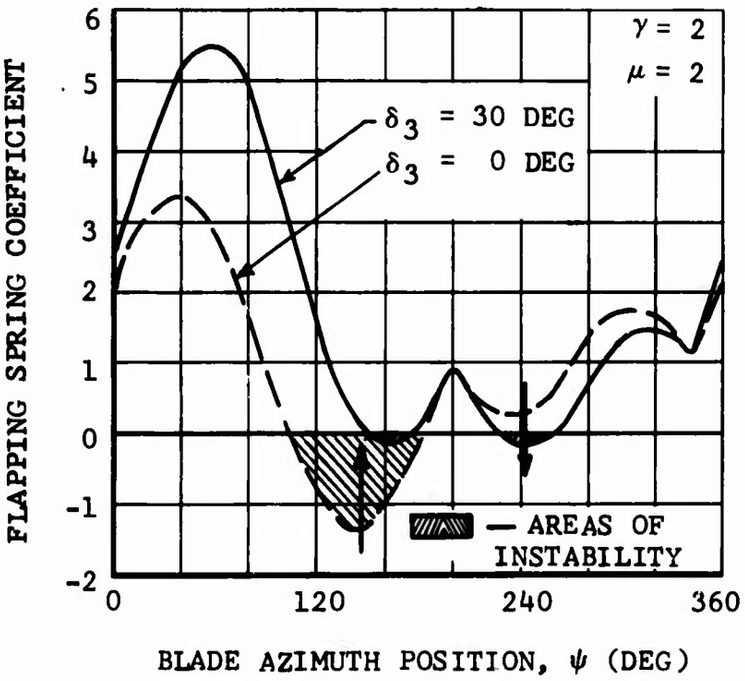

Figure 62. Effect of Pitch-Flap Coupling (δ_3) on Flapping Stability for a Pure Single-Rotor Helicopter.

A third possibility for reducing gust sensitivity is the use of a bobweight in the collective control system. This concept was discussed by Drees and McGuigan (8). In Figure 63 the effect of a mechanism which reduces the collective pitch one degree per g is shown. This bobweight rate reduces the response to the sine-squared gust by about 15%. Of course, this rate can be increased, and damping can be added to prevent instability which might otherwise occur.

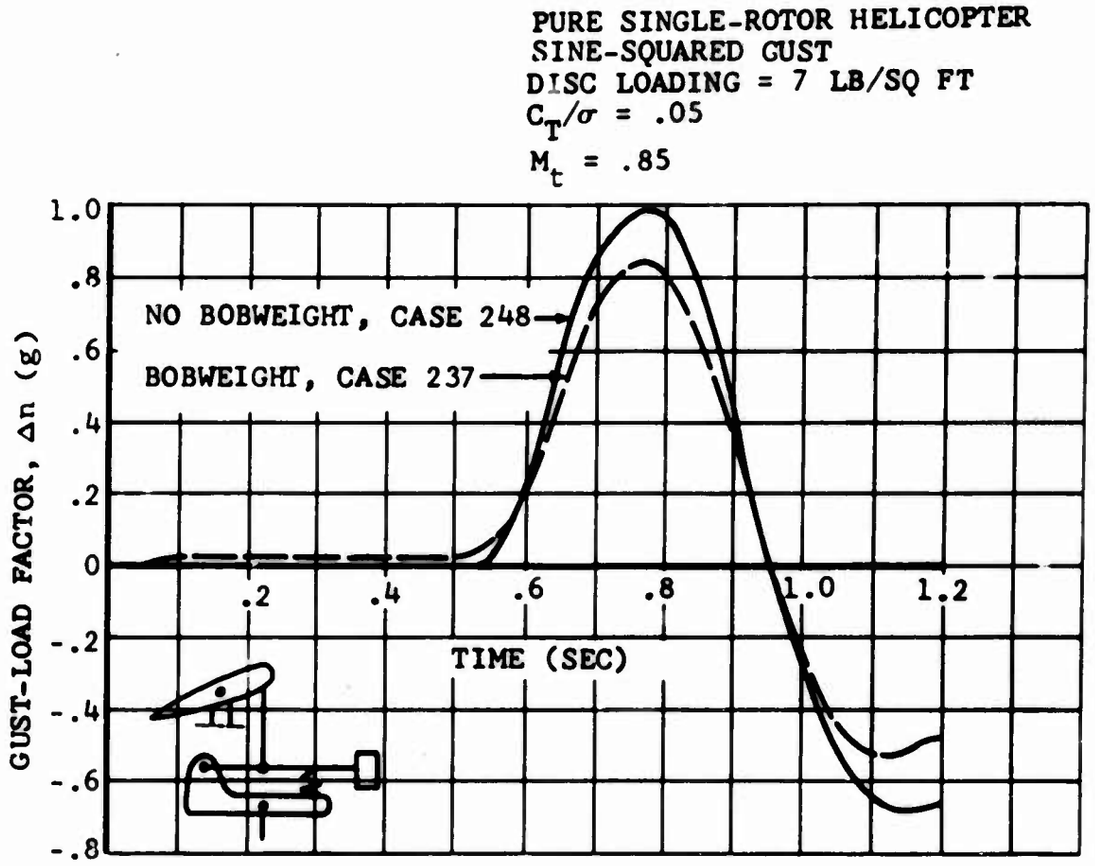

Figure 63. Gust Alleviation Due to a Bobweight ($\Delta\theta/\Delta n$ = -1 deg/g), Cases 237, 248.

EFFECT OF HORIZONTAL GUSTS

The effect of horizontal gusts has been investigated for a number of cases. The principal results are given in Figure 64 for the case of head-on horizontal gusts for forward speeds of 200 and 225 knots. Sudden-gust cases for the simplified analysis and sine-squared-gust cases for the detailed analysis are calculated for the horizontal gusts. The gradual penetration of the rotor disc into a horizontal sine-squared gust is represented in a manner similar to the vertical-gust case. The gust is assumed to consist of a sine-squared type of variation of the horizontal component of the wind velocity over a specified segment of the fixed x-axis. A ramp length, Hg, of 90 feet was used for these cases. The additional horizontal

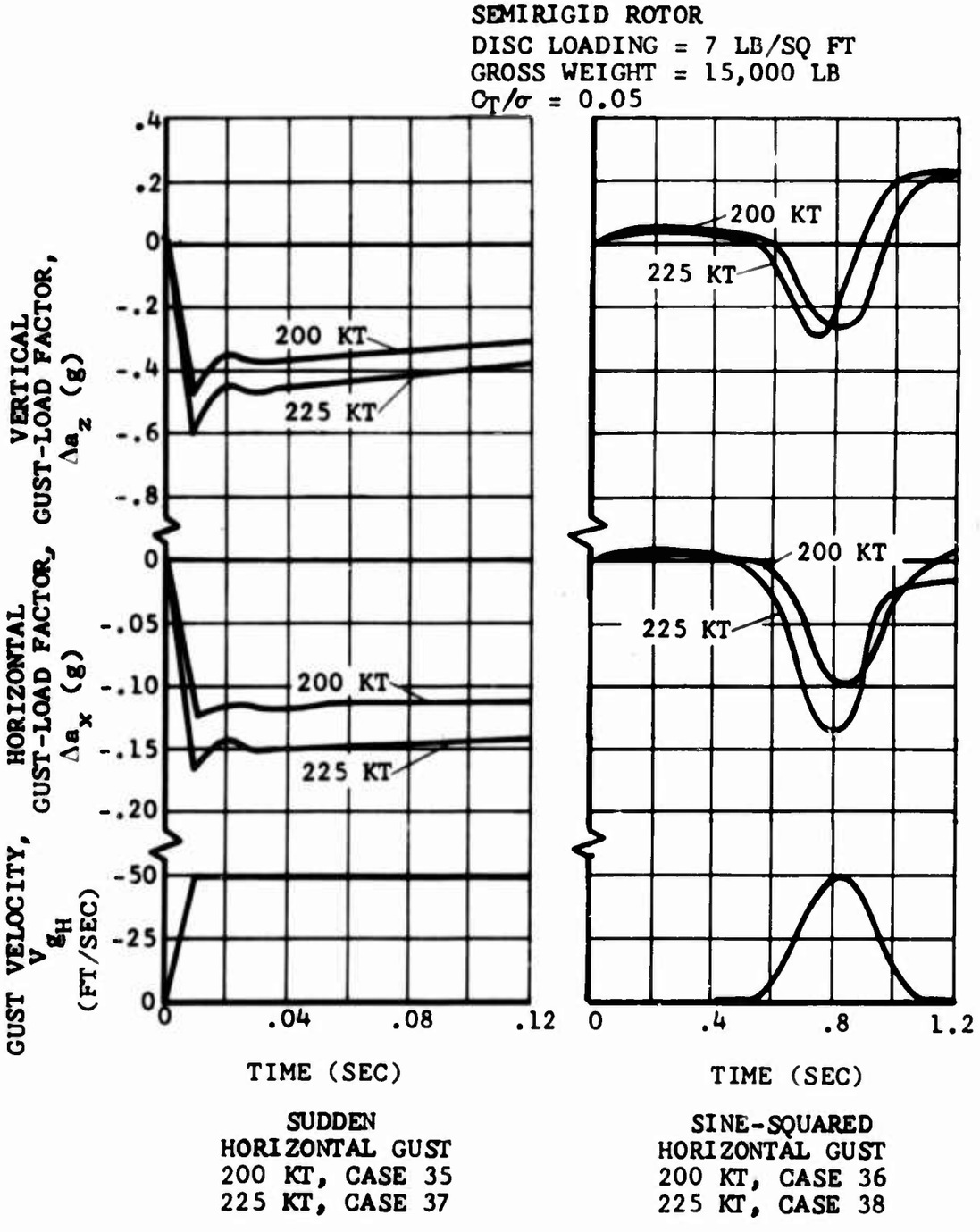

Figure 64. Effects of Horizontal Gusts, Pure Single-Rotor Helicopter.

velocity due to the gust is computed for each evaluated point on the rotor disc as a function of the x-coordinate (fixed reference) of that point.

The load factors involved are not of great consequence: less than .6g for the vertical load factor and less than .15g for the horizontal load factor. The effect on the rotor loads is equally small except for Case 38, where a blade-resonance condition results due to the gust. Table XII gives the computed values for the maximum oscillatory in-plane bending moments at the center of the rotor, normalized to the corresponding trim values.

TABLE XII. PRINCIPAL RESULTS OF HORIZONTAL GUST CASES

Disc Loading = 7; C_T/σ = .05; $M_{adv\ tip}$ = .9

Case No.	Forward Speed (Kt)	Horizontal Gust Type	Bending-Moment Factor Due to Gust
35	200	sudden	1.15
36	200	sine-squared	1.71
37	225	sudden	.78
38	225	sine-squared	2.02

A horizontal gust applied to a tilt-rotor aircraft in the airplane mode does not yield a large effect either. Figure 38 gives an example case, showing that a horizontal delta acceleration of -.38g is caused by a sine-squared horizontal gust of 50 ft/sec.

The effect of a lateral horizontal gust on a single-rotor helicopter is shown in Figure 65. It is seen that little effect results in the way of load factors on the airplane.

The use of a 50-ft/sec horizontal gust velocity with a ramp length of 90 feet is reasonably well established (Reference 36, Figures 20 and 21).

EFFECT OF ROTOR DYNAMICS

A major task of the gust-response study was the design of rotor dynamic characteristics for each combination of diameter, chord, number of blades, and rotor-hub type. If structural parameters for the rotor result in a natural frequency very near an excitation frequency of the forcing airloads, a numerical oscillation prevents proper operation of the program when aeroelastic feedback is included. The weight and stiffness distributions for the rotors used in this study are listed in

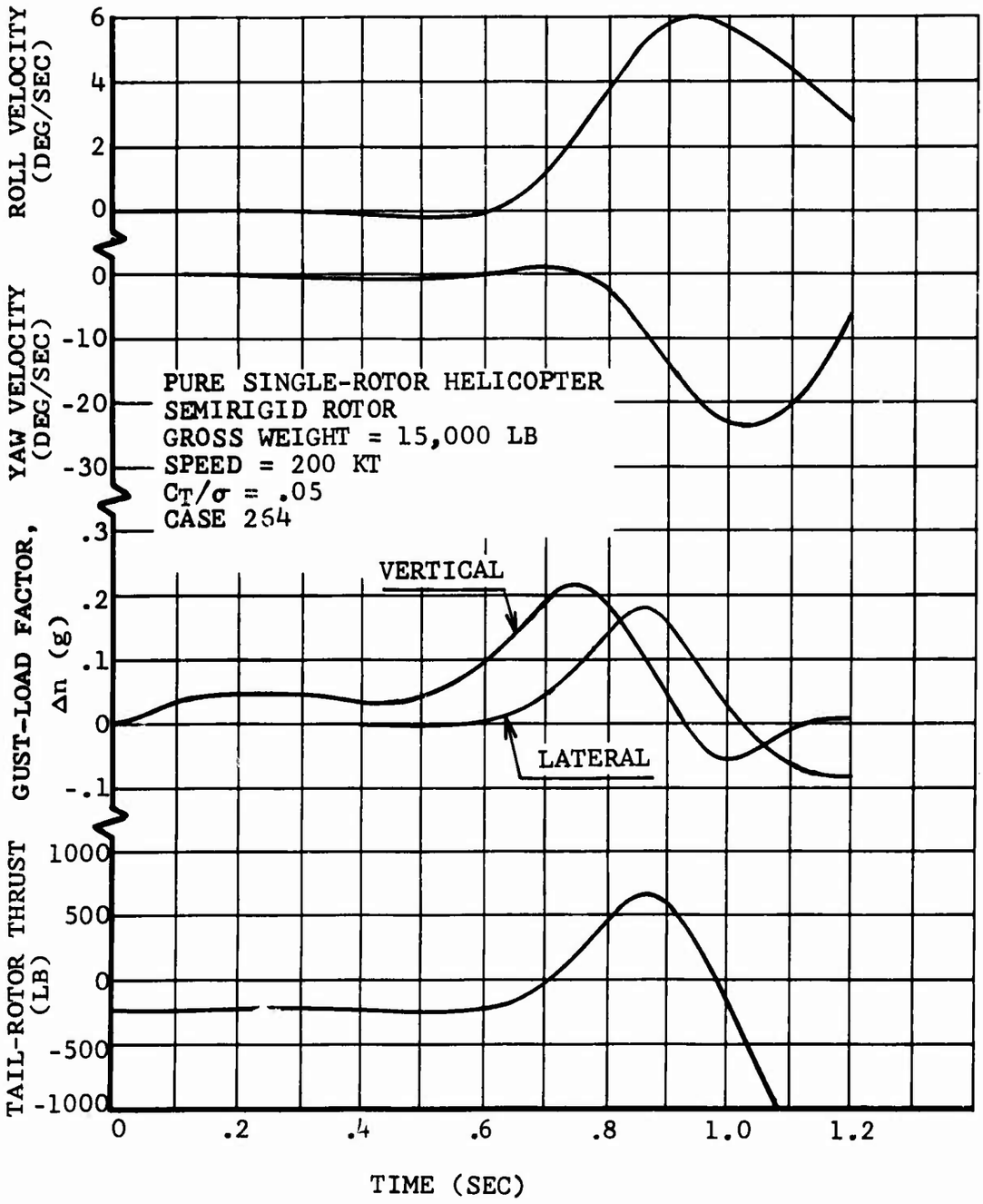

Figure 65. Time History of Response to a Lateral, Sine-Squared, 50-Ft/Sec Gust.

Appendix IV. Considerable effort was made to obtain realistic blade weight and stiffness distributions while controlling the dynamic characteristics to avoid resonances.

The rotor analysis considers three basic types of forced response, characterized by beam restraints at the hub centerline. Two of these are referred to as collective modes and cyclic modes. The collective modes describe the type of response to be expected from a sudden change in collective pitch. The cyclic modes describe the type of response to be expected from a sudden change in cyclic pitch. For simplicity, rigid mode refers to the response in the case of cantilevered boundary condition.

For a semirigid rotor, the collective mode is cantilevered beamwise (flatwise) and pinned chordwise (edgewise), the cyclic mode is pinned beamwise and cantilevered chordwise, and the rigid mode is cantilevered both beamwise and chordwise. The same centerline restraints apply to rigid and articulated rotors except that the cyclic mode is cantilevered beamwise. Hinges for the articulated rotor are simulated by extremely soft flexures located an appropriate distance from the axis of rotation. Lead-lag damper forces are applied based on the in-plane slope-change rate at 5% radius.

Collective pitch, built-in twist, and cyclic feathering are all included in the rotor dynamic analysis. Therefore, each of the three basic modes includes coupling effects among in-plane bending, out-of-plane bending, and blade-pitch displacements. In addition to the forced cyclic-feathering motions, the blade-pitching mode includes a torsionally rigid blade restrained by a single spring representing the control system.

The rotor dynamic response is calculated by harmonics of the rotor speed, with airloads components exciting modes as given in Table XIII.

TABLE XIII. COUPLED MODES EXCITED BY AIRLOAD HARMONICS

Airload Harmonic	Number of Blades		
	2	3	4
Steady	Rigid	Rigid	Rigid
1/Rev	Cyclic	Cyclic	Cyclic
2/Rev	Collective	Cyclic	Rigid
3/Rev	Cyclic	Collective	Cyclic
4/Rev	Collective	Cyclic	Collective

A special path is available in the rotor dynamic analysis to study both coupled and uncoupled bending natural frequencies versus rotor speed and airload-excitation frequencies. Figure 24 shows the fan plots for a typical four-bladed

rigid rotor used in the gust-response study. The lowest three uncoupled collective modes, Figure 24a, are cantilevered beamwise (flatwise), and the highest uncoupled collective mode is pinned chordwise (edgewise). In Figure 24b, the lowest and highest uncoupled cyclic modes are cantilevered chordwise, and the middle two uncoupled cyclic modes are pinned beamwise. Note that the uncoupled rigid modes, Figure 24c, match the uncoupled cantilevered modes of either the collective or the cyclic fan plot.

Coupled natural frequencies, including the effects of collective pitch and built-in blade twist, are also shown in the figure. The special path in the rotor-dynamics analysis will compute and plot the coupled frequencies for combinations of up to three values each of collective pitch and rotor rpm. For rotor designs used in this study, however, coupled frequencies were calculated only for the selected rpm and two collective-pitch values near the extremes of the anticipated range.

Figures 66 and 67 show oscillatory bending-moment ratios at the blade root for a series of pure single-rotor helicopter cases with a semirigid rotor. Figure 66 shows the ratios of maximum amplitude of oscillatory bending moment due to a sine-squared gust to that due to a sudden gust. The ratios in Figure 67 are maximum oscillatory bending moment due to a sine-squared gust to the oscillatory bending moment at the trim point. In both figures the ratios are shown as functions of advancing blade-tip Mach number for 200 krots and 225 knots. The oscillatory moments in a sine-squared gust are considerably higher than for a sudden gust (Figure 66), partly because of a smaller increase in rotor thrust. The sudden gust tends to stall a large amount of the rotor disc, leading to higher steady loads but lower oscillatory loads. The effect of rotor-thrust limit is also indicated in Figure 67, a comparison of maximum oscillatory loads in a sine-squared gust with those at the trim condition.

Part of the oscillatory-load level in a sine-squared gust is attributable to aeroelastic-feedback effects interacting between various harmonic airload components and the coupled rotor modes that are affected. Figure 68 is a typical time history of the maximum amplitude of oscillatory root bending moments, and illustrates the change in load level that occurs before the gust is reached. This change is due to the operation of the aeroelastic-feedback mechanism. The difference in the trim value and the steady-state value just before the gust excitation (at about .5 second, Figure 68) is a measure of the effect of including blade flexibility in the analysis.

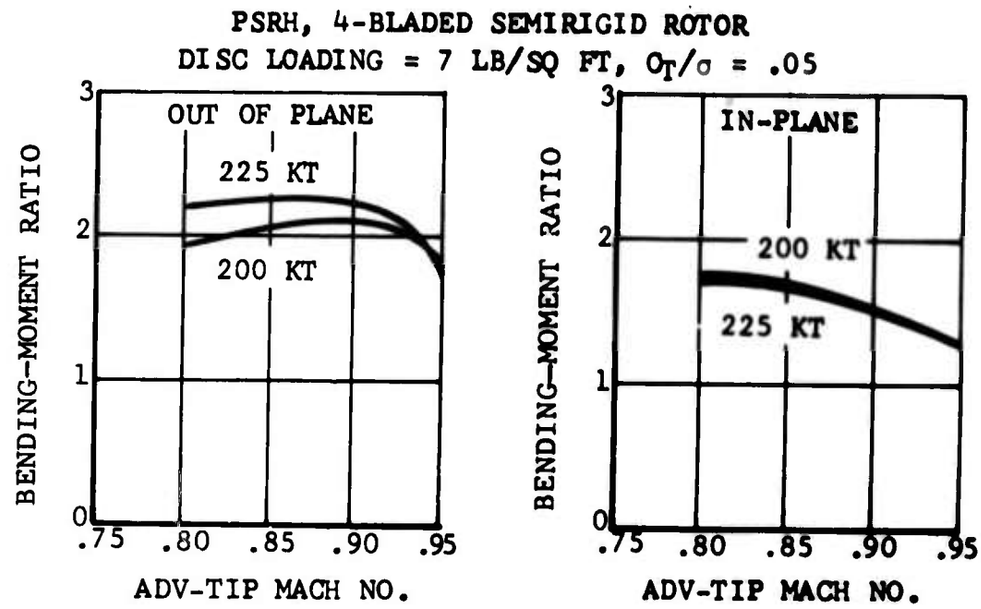

Figure 66. Ratio of Oscillatory Root Bending Moments, Sine-Squared/Sudden, Cases 1-16.

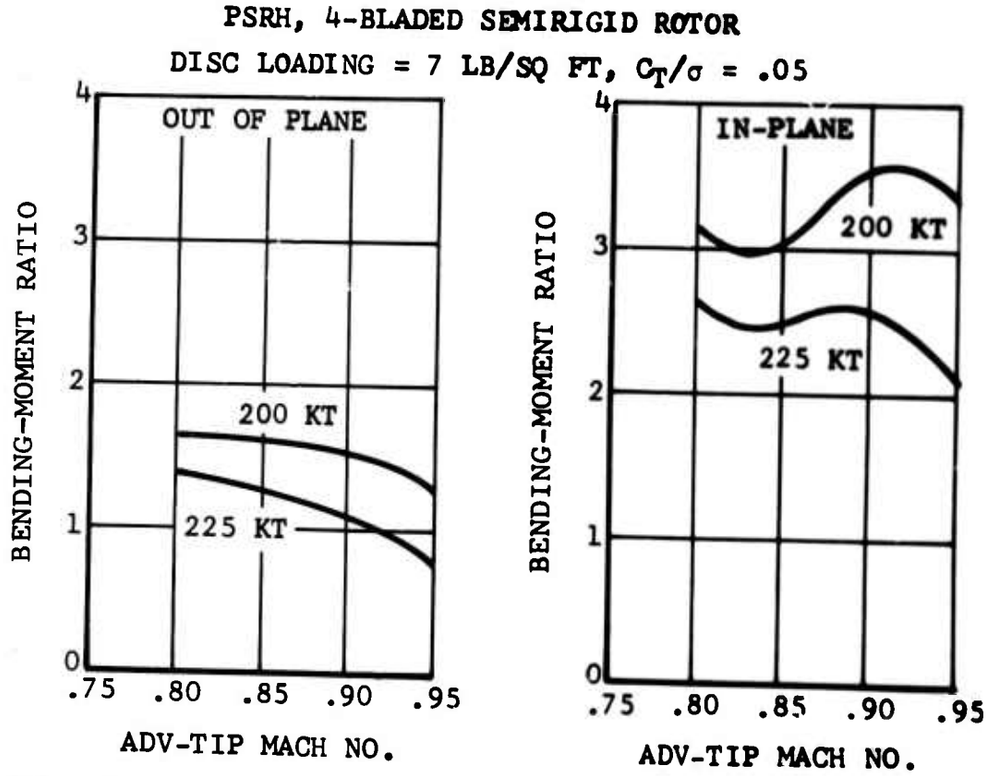

Figure 67. Ratio of Oscillatory Root Bending Moments, Sine-Squared/Trim, Cases 1-16.

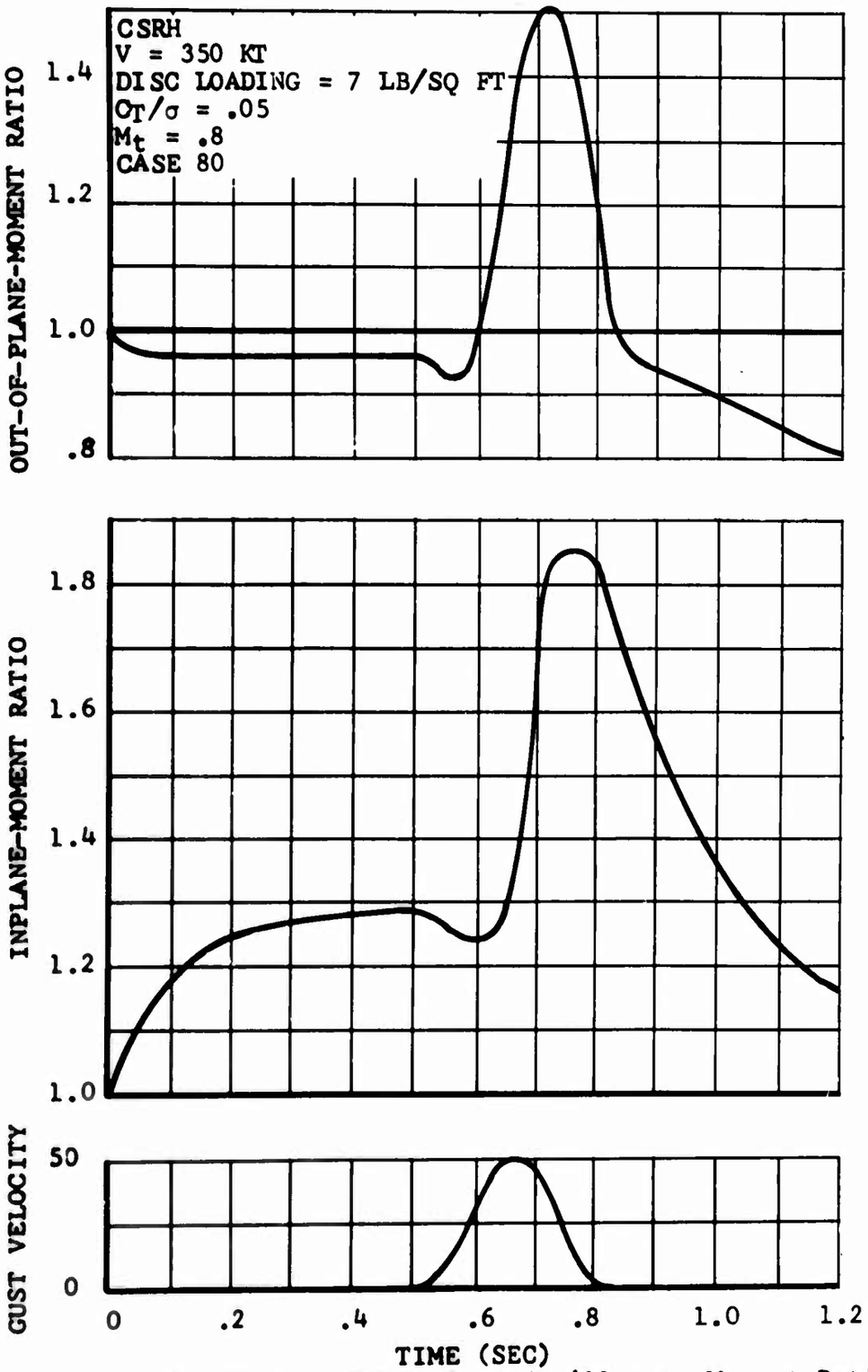

Figure 68. Maximum Blade Root Oscillatory Moment Ratio With Aeroelastic Feedback and Sine-Squared Gust

EFFECT OF BLADE TORSIONAL RESTRAINT

A limited consideration of blade torsion is included in the rotor dynamic analysis. Although the blade is considered to be torsionally rigid, blade-pitching moments act against a spring representing the blade-pitch control mechanism. The angular blade-pitch deflections are transmitted to the rotor aerodynamic analysis through the provisions for aeroelastic coupling.

The relative importance of blade torsional restraint on rotor loads was investigated by a series of three cases (275-277), in which only the torsional elasticity of the blade-pitch control system was varied. The cases are for a two-bladed single-rotor compound helicopter flying at a speed of 150 knots. As shown in Figure 69, the rotor loads increase only moderately as the oscillatory control displacement increases from zero to 1.5 degrees. It is to be noted that the rotor structural parameters used in this investigation have nearly optimum dynamic characteristics. For rotors with less well-behaved dynamics, blade-pitch control elasticity could be a primary variable in determining rotor loads.

MISCELLANEOUS EFFECTS

The computing program automatically accounts for the influence that elevator gust loads have on fuselage forces and moments. For this reason, the gust load on the entire aircraft, Δn, is found to differ slightly from the rotor thrust-weight ratio, $\Delta T/GW$.

Cases 1 and 2 (Table XXI) serve as examples. These are pure single-rotor helicopter cases with semirigid rotors. The forward speed is 200 knots in both cases. Case 1 is a sudden gust case, while Case 2 is a sine-squared gust case. The values of Δn and $\Delta T/GW$ for these two cases are as follows:

Case 1. $\Delta n = 1.81$ g; $\frac{\Delta T}{GW} = 1.70$ g

$$\text{Elevator Gust Load} = \Delta n - \frac{\Delta T}{GW} = 0.11 \text{ g}$$

Case 2. $\Delta n = 0.98$ g; $\frac{\Delta T}{GW} = 0.93$ g

$$\text{Elevator Gust Load} = 0.05 \text{ g}$$

Rotors with 2, 3, and 4 blades were investigated (Appendix IV). Beyond the differing dynamic design requirements, however, the number of rotor blades has little effect.

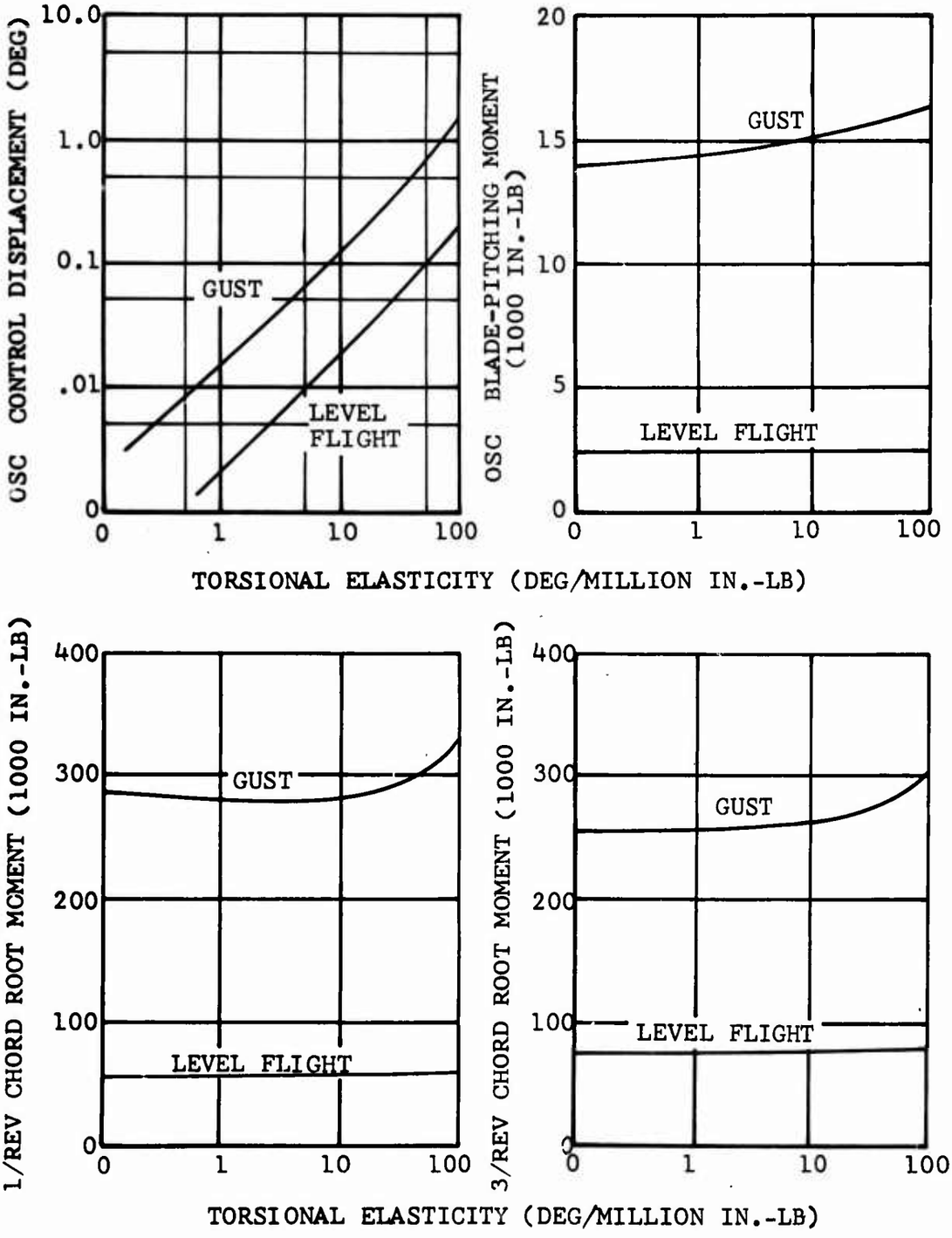

Figure 69. Effect of Control-System Flexibility on Oscillatory Rotor Loads for Level Flight and for 50-Ft/Sec Sine-Squared Vertical Gust.

A number of influences, such as the effect on tail-rotor behavior and the rolling and yawing that result from a gust, have not been investigated in detail. In general, however, these effects were found to play an insignificant role in the gust design-load problem. The effect of rpm changes was not investigated either, since it was assumed that a governor would hold the rpm within 2%. In governor open-loop mode, significant effects due to rpm variations may be expected.

SYNTHESIS OF RESULTS

In the previous section, Discussion of Results, the effects of various parameters on gust response were briefly evaluated. For a more complete presentation of the results, the reader is referred to Appendixes II and III, which give a listing of the most important parameters and findings of this study.

As previously discussed (see Introduction), the present military requirements for gust-load evaluation (MIL-S-8698) are inadequate. One of the principal objectives of this study was to derive new and relatively simple design rules which would enable the designer to determine gust loads for the aircraft without the benefit of an elaborate computing process. In order to accomplish this objective, it was originally planned to investigate the importance of certain parameters in the evaluation of the gust-alleviation factor K_g. This plan produced results from a large number (303) of cases. However, the attempt to determine K_g as a function of a particular parameter left many exceptions to be explained. Eventually, the idea of a gust factor was dropped in favor of a formula which would give directly the rotor-thrust increment due to a gust. The problems associated with attempting to determine gust-load functions are discussed below for each of the three rotorcraft configurations considered in this study. Finally, the development of the empirical formula is given.

GUST-ALLEVIATION FACTORS FOR THE PURE SINGLE-ROTOR HELICOPTER

The gust factor for the pure single-rotor helicopter seems to be affected very little by variation of rotor parameters. This is probably best illustrated by the histogram in Figure 28 (page 71). A K_g value of .6 would cover 95% of all pure single-rotor helicopter cases, while the majority of the cases have a K_g between .50 and .55. Figure 41 (page 89) shows that disc loading has only a small effect on K_g as determined by results of this study. Values of K_g are slightly lower for the higher disc loadings in some cases. The curve of Figure 2 (page 2) (from MIL-S-8698) shows an entirely different trend. The suggestion (8) to base K_g on a rotor-mass ratio in analogy with fixed-wing practice was also mentioned in the Introduction (see Figure 4, page 3). For the pure single-rotor helicopter cases, this approach resulted in Figure 70, in which the gust-factor function of Reference 8 is compared with the results of this study and the current criterion, MIL-S-8698. Obviously, no correlation is obtained; the gust-alleviation factor, K_g, of this study seems to be independent of the rotor-mass ratio. Variation of K_g with Lock number showed lowest K_g for highest Lock number for all rotor types and advance ratios calculated. However, the range of variation in K_g (about .15) is small compared with the change in Lock number (3.88). (See Table XI page 98).

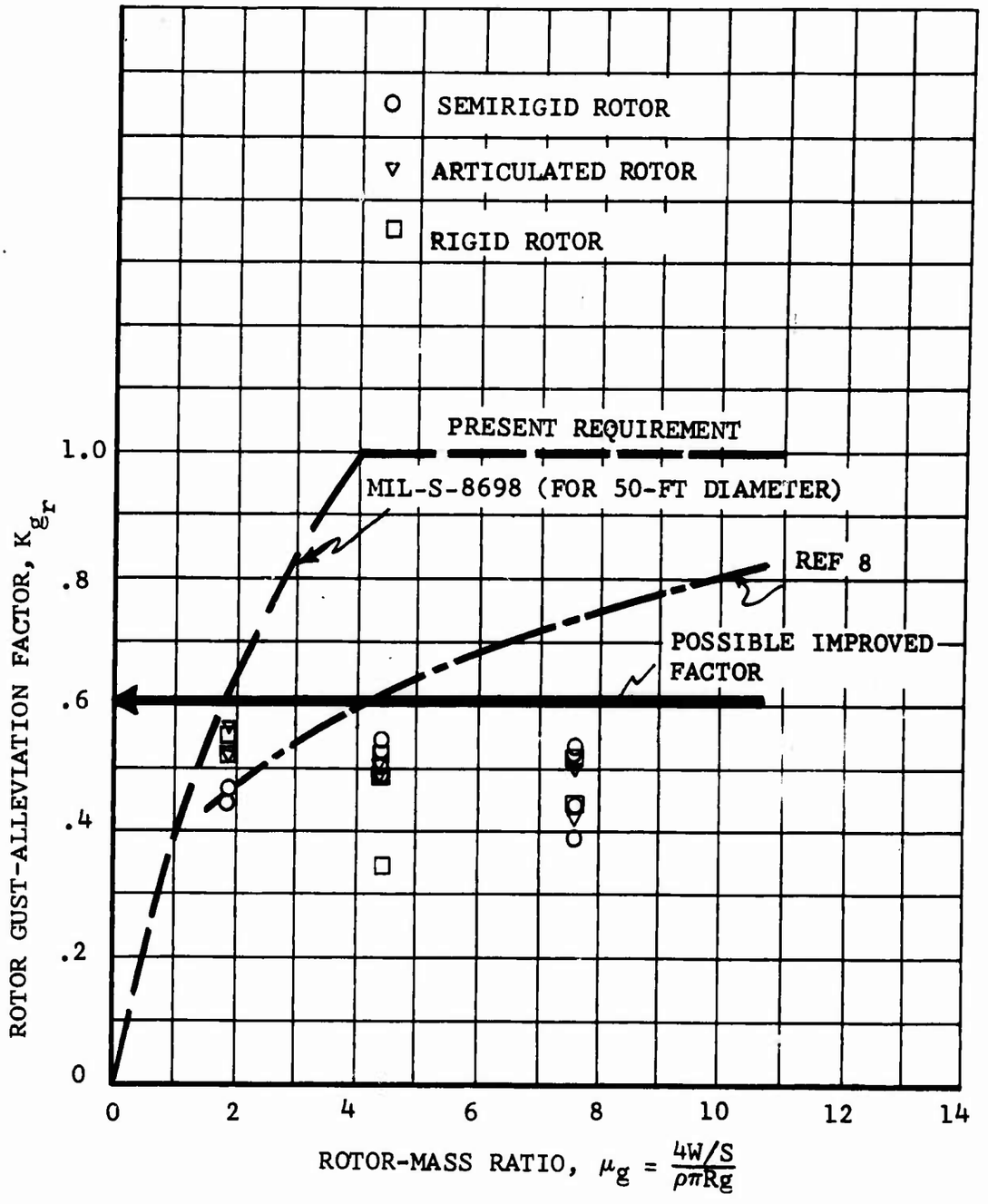

Figure 70. Rotor Gust-Alleviation Factor Versus Mass Ratio for Single-Rotor Helicopters - A Comparison With MIL-S-8698 and Reference 8.

Although several attempts were made to relate the gust factors to disc loading, Lock number, rotor-thrust coefficient, etc., no satisfactory solution was obtained. It is believed that effects such as in-plane rotor forces, elevator loads, control positions, and rotor-plane attitude at the initial trim position, as well as rotor-blade dynamic forces and deflections, are all influential factors.

The results for the pure single-rotor helicopter, regardless of the type of rotor, suggest a simple design rule which appears to be superior to the old requirements, yet conservative for all cases investigated. Such a rule could be formulated as follows:

> Gust loads on pure single-rotor helicopters due to a 50-ft/sec sine-squared gust can be determined by applying a gust-alleviation factor of $K_g = .6$ to the gust load computed due to a 50-ft/sec sudden gust.

GUST-ALLEVIATION FACTORS FOR THE PURE TANDEM HELICOPTER

The tandem helicopter's inherent capacity of a large cg range is directly associated with the gust-response factors which can be expected. During the penetration of a sine-squared gust, the thrust buildup on the forward rotor precedes that of the aft rotor, thereby furnishing a nose-up pitching moment proportional to the distance aft to the cg. Thus for an aft-cg condition, the pitch displacement from trim attitude adds a significant component of the forward speed to the maximum gust velocity. For the forward-cg cases, the pitch displacement is slight, and gust response fits the pattern established for the other configurations. An examination of the results showed that the maximum gust factor would be approximately .58 if the effect of pitch displacement is removed. This factor is compatible with the simple design rule for the pure single-rotor helicopter. A comparable design rule for the tandem helicopter, however, should include the effect of pitch displacement as related to distance between rotors, fuselage pitching inertia, and amount of rotor overlap. Variations of these parameters were not investigated by this study.

GUST-ALLEVIATION FACTORS FOR THE COMPOUND HELICOPTER

The compound helicopter presents a more complex situation than does the pure helicopter because of the load sharing between the rotor and the wing. It can be seen in Figures 29 and 30 that the gust factors, K_{g_r}, on the rotor are smaller than 0.7. Most of the gust factors for the wing, K_{g_w}, are found between 0.8 and 0.9, suggesting that the usual fixed-wing methods are a close approximation (a factor of 0.8 to 0.85 is found for the airplane mode of the tilt-rotor configurations, where the wing carries the major part of the load).

Although the results shown in Figures 35, 49, and 58 (pages 78, 95 and 106) indicate that forward speed does have some effect, the variation in K_g is small (about .10) over a speed range from 200 to 350 knots. Available data have been plotted in Figure 71 for both the rotor- and wing-gust factors. In Figure 71(a), K_{gr} for pure helicopters, based on data from this study and from Figure 16 of Reference 8, is included for comparison with the compound helicopter cases. Some pure fixed-wing airplane cases are included in the wing-gust factor plot (Figure 71(b)). It can be seen that considerable spread of the results, which does not appear to be a simple function of major parameters such as disc loading or rotor thrust coefficient, is possible. The highest values of K_{gr} occur at a disc loading of 7 lb/sq ft, with C_T/σ = .05. The lower values of rotor gust-load factor are from cases with both lower and higher disc loadings, and with C_T/σ values of both .02 and .05.

For design purposes, it appears that K_{gr} = 0.7 is a conservative factor for the compound configuration. This value is slightly higher than that suggested for the pure helicopter, because the rotor of a compound helicopter is usually unloaded, entirely or partly by the wing, in steady, level flight. The rotor's capability to assume a share of the gust load is, therefore, usually greater.

The wing-gust factor, K_{gw}, shows a clearer trend than does the rotor-gust factor. Increased gust-load capability of the rotor (Δn) is primarily a function of C_T/σ (see Figure 43, page 91). If the rotor takes a major share of the total load (see Figure 58, page 106), the upward acceleration of the wing is larger for a compound than for a fixed-wing aircraft. One must therefore expect to see a considerable upward velocity of the aircraft at the time the maximum wing load develops. This upward motion reduces the wing's angle of attack and reduces its gust factor. The bar graph in Figure 72 illustrates this effect by sampling K_{gw} for the two values of C_T/σ; for comparison the case of a fixed-wing airplane is also shown.

It thus appears that a reduction of the fixed-wing-gust factor K_{gw} is justified for rotors with low thrust coefficients. The exact determination of this reduction, however, remains a subject for further study.

EMPIRICAL FORMULA FOR ROTOR-GUST LOAD

In general, the use of an alleviation factor for the rotor is not altogether satisfactory. As an alternative to determining the actual gust load by applying a gust factor to the calculation for a sudden gust, gust loads on the rotor may be considered directly for the sine-squared gust cases. If in this way a reasonably simple rule can be found, the complex

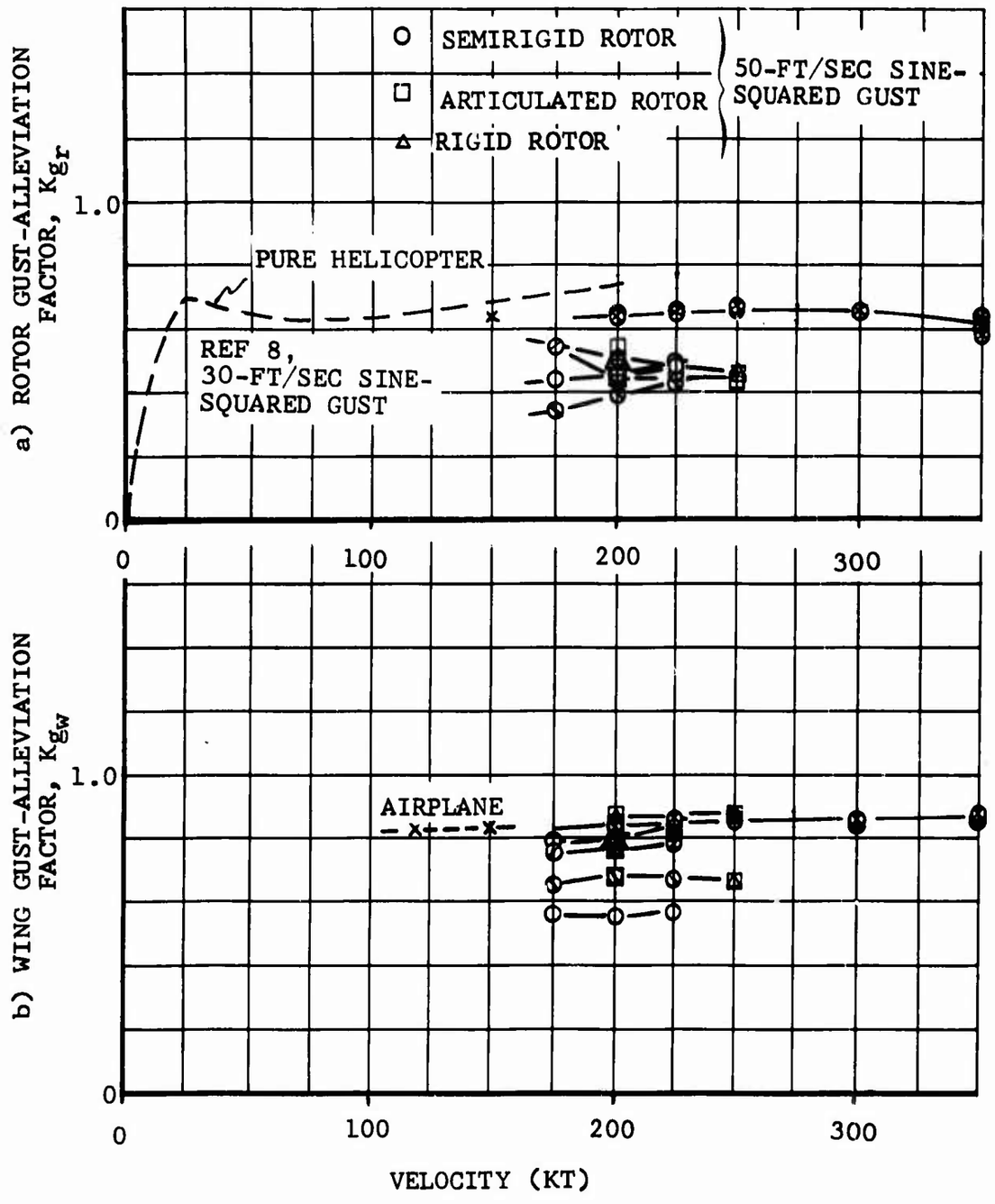

Figure 71. Rotor Gust- and Wing Gust-Alleviation Factors Versus Forward Speed for Compound Helicopters at High Speed and for Pure Helicopters and Airplanes at Low Speed.

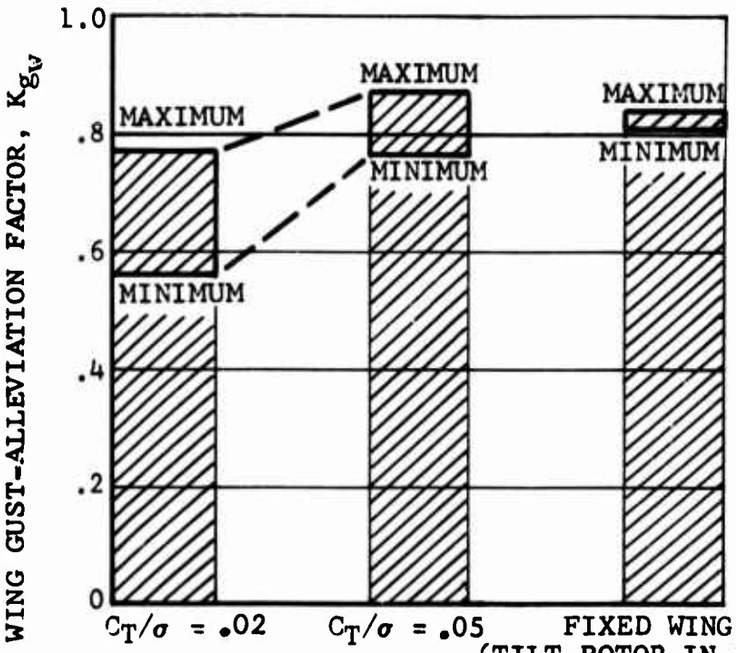

Figure 72. Effect of Rotor Thrust Coefficient-Solidity Ratio on Wing Gust-Alleviation Factor.

calculation of the sudden-gust case will be eliminated, as will the uncertainties in the actual values for the rotor-gust factor.

Inspection of the results for pure helicopters (Appendix III) shows that the disc loading has only a minor effect on the value of Δn, but that the rotor thrust coefficient-solidity ratio, C_T/σ, has considerable influence. This trend is verified in Figure 73, where the rotor gust-load ratio, $\Delta T/T_{hover}$, is plotted versus C_T/σ for all cases of this study. For the winged helicopter (tilt-rotor cases with the rotors lifting), only the thrust increase of the rotor is included.

Figure 73 presents some interesting facts:

- At high values of C_T/σ the capability of the rotor to carry additional thrust disappears. The maximum value of C_T/σ for the pure helicopter seems to be close to .15, which is in agreement with data presented in References 6 and 8, where a limit value of about .16 is indicated.

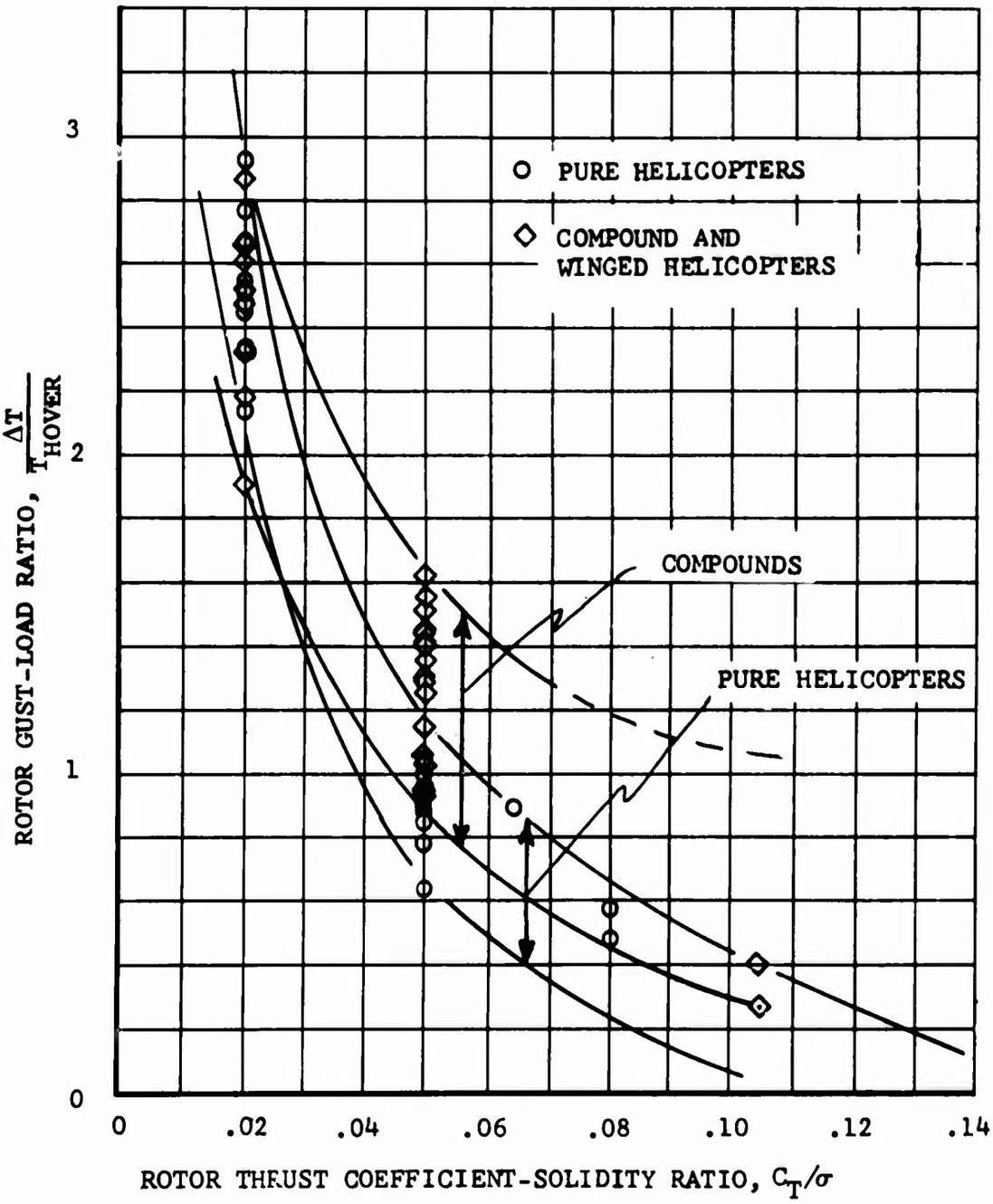

Figure 73. Rotor Gust-Load Ratio Versus Rotor Thrust Coefficient-Solidity Ratio.

- For compound-helicopter rotors, $\Delta T/T_{hover}$ approaches unity for high values of C_T/σ. This condition is possible if the wing unloads the rotor completely in trimmed flight prior to the gust.

This discussion suggests that $\Delta T/T_{hover}$ probably can be approximated by a simple function of C_T/σ and L_w (wing lift prior to the gust). Figure 74 shows $\Delta T/T_{hover}$ versus $\Delta T/T_{hover}$, where

$$\frac{\Delta T}{T_{hover}}_{empirical} = \frac{0.057}{(C_T/\sigma)_{hover}} + 0.85 \frac{L_w}{T_{hover}} - 0.3 \quad (19)$$

The correlation is surprisingly good, considering the wide variation of disc loading, tip speed, forward speed, and configuration, and the fact that details such as gradual penetration, sine-squared gusts, and nonsteady aerodynamics are included. Only at the high values of $\Delta T/T_{hover}$ do the data points show significant scatter. Attempts to explain and further reduce the scatter have not yet been successful. If the constant -0.3 were changed to -0.2 for semirigid rotors and to -0.1 for rigid and articulated rotors, all cases would be calculated conservatively.

The expression can be readily understood to be related to the mean-blade-lift coefficient and the maximum-lift coefficient. Approximately, $C_T/\sigma = .1C_L$ and ΔC_L due to a gust equals

$(dC_L/d\alpha) \cdot (V_g/\frac{3}{4}\Omega R)$. Assume $dC_L/d\alpha = 6$, $V_g = 50$ ft/sec, $\Omega R = 667$ ft/sec, then $\Delta C_L \approx 6\ (50/500) = .6$

The first term can be approximated as follows:

$$\frac{(C_T/\sigma) \text{ due to gust}}{(C_T/\sigma)_{hover}} = \frac{.1\Delta C_L}{(C_T/\sigma)_{hover}} = \frac{.06}{(C_T/\sigma)_{hover}} \quad (20)$$

The second term includes the unloading of the rotor by wing lift, L_W. The factor 0.85 is possibly an efficiency factor.

The constant determines the maximum C_T/σ that is available for additional rotor lift.

The fact that the rigid and articulated rotors show a higher value for $\Delta T/T_{hover}$ is probably due to the hub moment causing some nose-up fuselage motion that causes additional lift increase. This is similar to the effect described in connection with tandem-rotor helicopters.

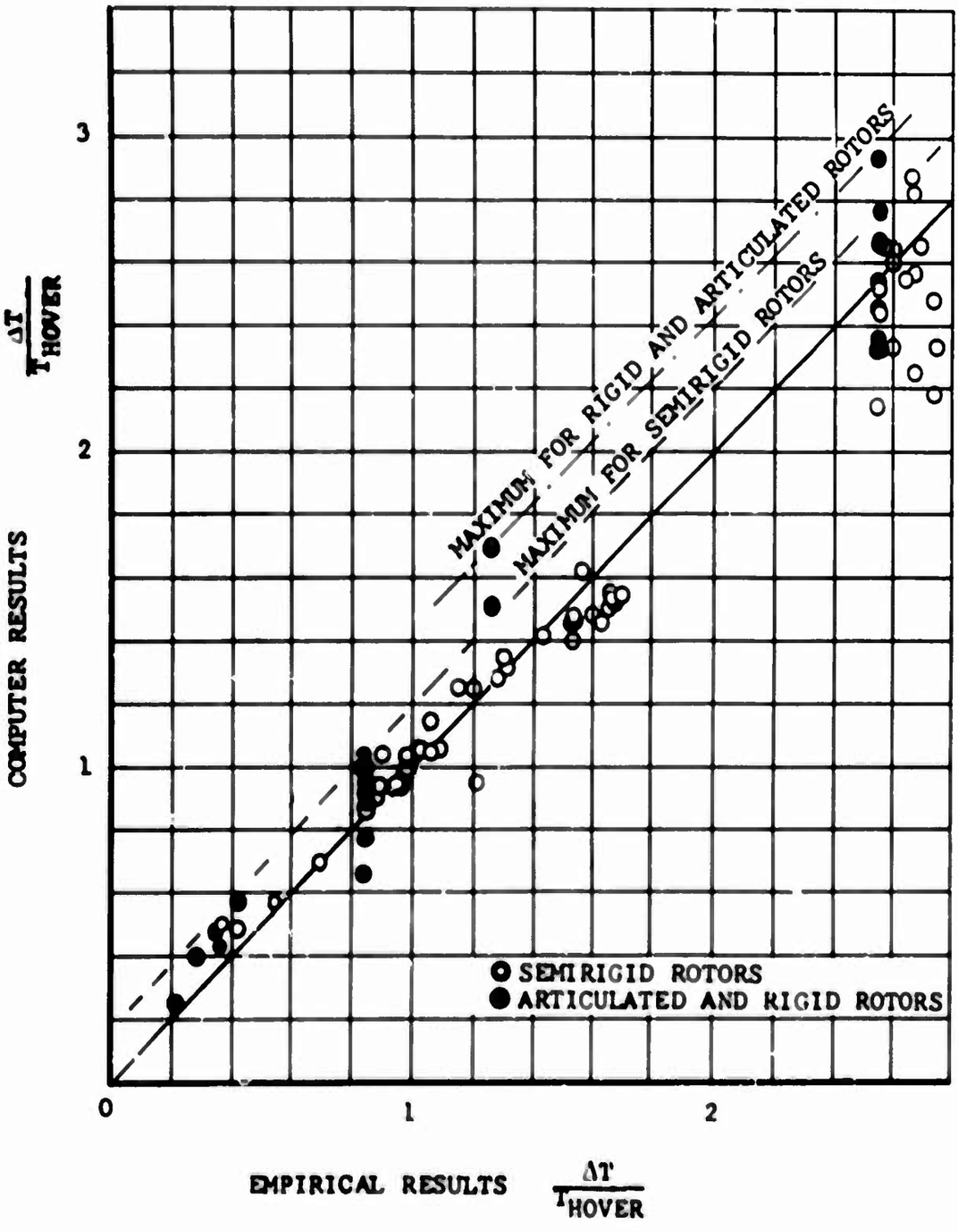

Figure 74. Correlation Between Computer Results and Empirical Equation for Rotor Gust-Load Ratio (Sine-Squared 50-Ft/Sec Gust).

From the standpoint of rotor design, the above expression can be most convenient to the designer. By simply determining the hovering C_T/σ and the minimum wing lift in steady flight, the rotor-gust load can readily be calculated. The wing- and elevator-gust loads can be found by conventional means and then reduced by a small amount (see Figure 72). The total gust load, then, is determined by summing the rotor-, wing-, and elevator-gust loads.

It is recommended that this approach, which is suitable for all the VTOL concepts and rotor types investigated in this study, be further developed and be given serious consideration for use in rotary-wing design requirements.

Several attempts were made to find a meaningful relationship for the computed rotor bending moments. Figure 75 shows the oscillatory beamwise moments at the blade root, in the form of a ratio of maximum values during the gust to the trim values, plotted against the ratio of thrust increase to hover thrust. No particular trend is discernible. During the selection of the rotor structural parameters, it was recognized that each rotor would have to be "designed" free of resonant conditions over an appreciable range of both rpm and collective pitch, as specified by the parameter variations in each group of cases. The possible variation in dynamic characteristics of a rotor, even for a specific aircraft configuration, cannot be represented by a simple rule that would relieve the designers of any of their present functions.

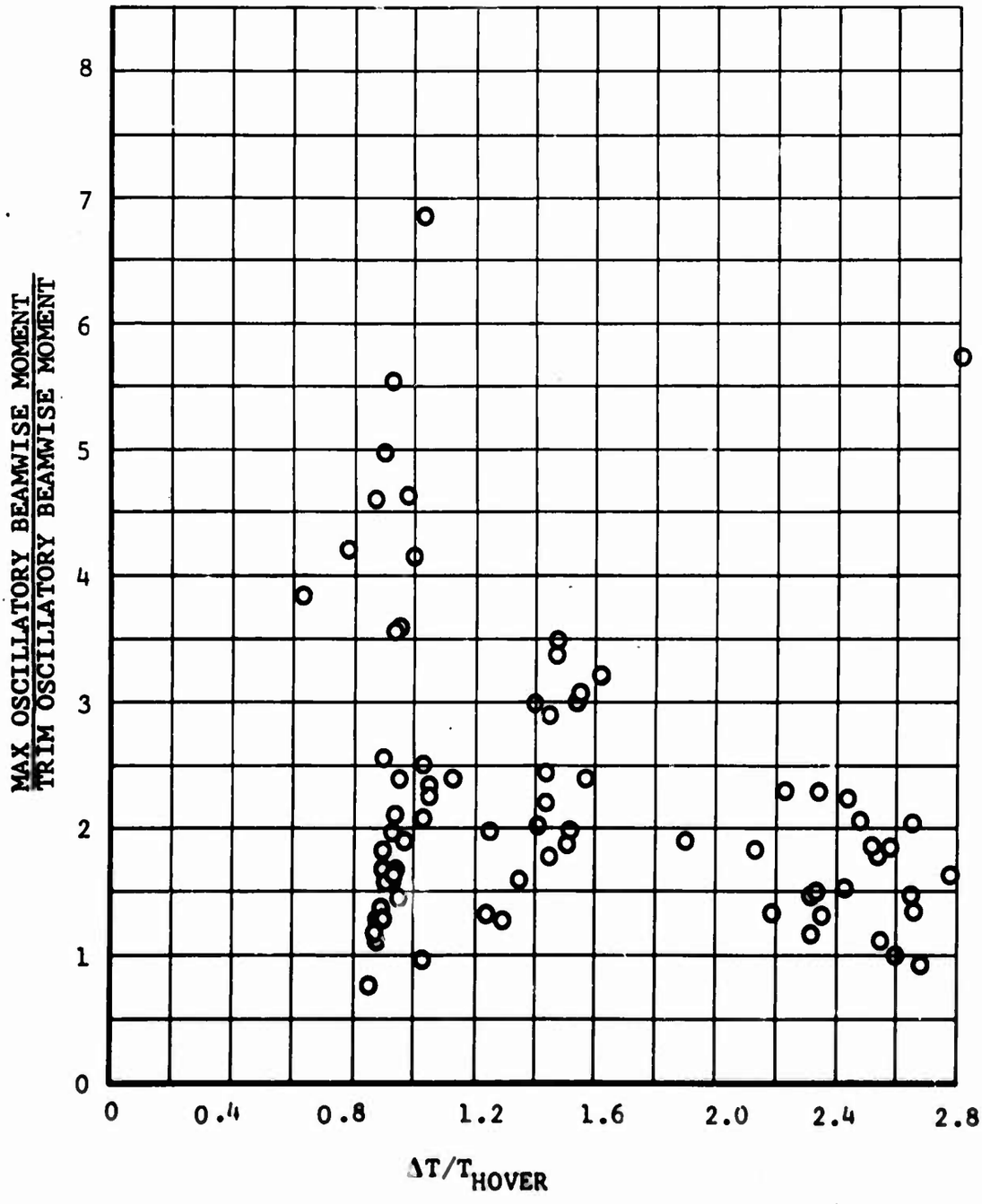

Figure 75. Beamwise Oscillatory Hub Bending Moment Ratio Versus Normalized Thrust Increment During Gust.

LITERATURE CITED

1. Focke, Henrich, DAS TRAG- UND HUBSCHRAUBERPROBLEM, Schriften der Duetschen Akademie der Luftfahrtforschung, Heft 22, 1937.

2. Crim, Almer D., GUST EXPERIENCE OF A HELICOPTER AND AN AIRPLANE IN FORMATION FLIGHT, NACA Technical Note 3354, National Advisory Committee for Aeronautics, 1954.

3. Amer, K.B., and Gustafson, F.B., CHARTS FOR ESTIMATION OF LONGITUDINAL STABILITY DERIVATIVES FOR A HELICOPTER ROTOR IN FORWARD FLIGHT, NACA Technical Note 2309, National Advisory Committee for Aeronautics, March 1951.

4. DESIGN REQUIREMENTS, HELICOPTER, MIL-S-8698 (ASG), February 1958.

5. GESSOW, A., EQUATIONS AND PROCEDURES FOR NUMERICALLY CALCULATING THE AERODYNAMIC CHARACTERISTICS OF LIFTING ROTORS, NACA Technical Note 3747, National Advisory Committee for Aeronautics, October 1956.

6. Livingston, C.L., and Murphy, M.R., FLYING QUALITIES CONSIDERATIONS IN THE DESIGN AND DEVELOPMENT OF THE HUEYCOBRA, Twenty-Fourth Annual National Forum Proceedings, American Helicopter Society, New York, N. Y., May 1968.

7. Ham, N.D., and Young, M.I., TORSIONAL OSCILLATION OF HELICOPTER BLADES DUE TO STALL, Journal of Aircraft, Vol. 3, No. 3, 1966, p. 218.

8. Drees, J.M., and McGuigan, M.J., HIGH-SPEED HELICOPTERS AND COMPOUNDS IN MANEUVERS AND GUSTS, Twenty-First Annual National Forum of the American Helicopter Society, Washington, D.C., 1965.

9. Blankenship, B.L., and Bird, B.J., PROGRAM C81-11 ROTORCRAFT FLIGHT SIMULATION (three volumes), BHC Report No. 599-068-900, Bell Helicopter Company, Hurst, Texas, January 1967.

10. Donely, P., SUMMARY OF INFORMATION RELATING TO GUST LOADS ON AIRPLANES, NACA Report 997, National Advisory Committee for Aeronautics, 1950.

11. Pratt, K.G., A REVISED FORMULA FOR THE CALCULATING OF GUST LOADS, NACA Technical Note 2964, National Advisory Committee for Aeronautics.

12. Etkin, B., DYNAMICS OF FLIGHT, New York, N.Y., John Wiley and Sons, Inc., 1959

LITERATURE CITED - Continued

13. Lucassen, L.R., and Drees, J.M., HELICOPTERS IN GUSTS (HEFSCHROEFVLIEGTUIGEN IN REMOUS), NLL Report Vol. 1562, National Aeronautical Research Institute, Amsterdam, The Netherlands, 1950.

14. Segel, L., AIR LOADINGS ON A ROTOR BLADE AS CAUSED BY TRANSIENT INPUTS OF COLLECTIVE PITCH, USAAVLABS Technical Report 65-65, U.S. Army Aviation Materiel Laboratories, Fort Eustis, Virginia, October 1965, AD624860.

15. Blankenship, B.L., and Harvey, K.W., A DIGITAL ANALYSIS FOR HELICOPTER PERFORMANCE AND ROTOR BLADE BENDING MOMENTS, Journal of the American Helicopter Society, Vol. 7, No. 4, October 1962.

16. Duhon, J.M., Harvey, K.W., and Blankenship, B.L., COMPUTER FLIGHT TESTING OF ROTORCRAFT, Journal of the American Helicopter Society, Vol. 10, No. 4, October 1965.

17. Weber, G.E., Jr., GUST RESPONSE OF STOPPED AND TRAILING ROTORS, BHC Report No. 599-068-901, Bell Helicopter Company, Hurst, Texas, April 1967.

18. Craig, H.V., VECTOR AND TENSOR ANALYSIS, New York, N.Y., McGraw-Hill Book Company, Inc., 1943, Chapter XII.

19. Drees, J.M., A THEORY OF AIRFLOW THROUGH ROTORS AND ITS APPLICATION TO SOME HELICOPTER PROBLEMS, The Journal of the Helicopter Society of Great Britian, Vol. 3, No. 2, 1949.

20. Myklestad, N.O., FUNDAMENTALS OF VIBRATION ANALYSIS, New York, N.Y., McGraw-Hill Book Company, Inc., 1956.

21. McDonald, M.D., MODIFICATION OF CLCD SUBROUTINE, BHC IOM 81:MM:sf-377, Bell Helicopter Company, Hurst, Texas, (Ref. 9, Vol. III, App. A), April 11, 1966, p. A-8.

22. Jenkins, J.L., Jr., CALCULATED BLADE RESPONSE AT HIGH TIP SPEED RATIO, Conference on V/STOL and STOL Aircraft, Ames Research Center, Moffett Field, California, April 1966.

23. Weber, G.E., Jr., ON TIME-DEPENDENT LIFT BUILDUP, BHC Report No. 299-099-308, Bell Helicopter Company, Hurst, Texas, March 1967.

24. Hochstrasser, U., SURVEY OF NUMERICAL ANALYSIS, edited by John Todd, New York., N.Y., McGraw-Hill Book Company, Inc., 1962.

LITERATURE CITED - Continued

25. Nielsen, K.L., METHODS IN NUMERICAL ANALYSIS, New York, N.Y., The Macmillan Company, 1957, pp. 232-242.

26. Hildebrand, F.B., INTRODUCTION TO NUMERICAL ANALYSIS, New York, N.Y., McGraw-Hill Book Company, Inc., 1956, p. 188.

27. Blankenship, B.L., A METHOD FOR THE NUMERICAL SOLUTION OF A SYSTEM OF SECOND ORDER DIFFERENTIAL EQUATIONS, BHC IOM 81:BLB:oah-1297, Bell Helicopter Company, Hurst, Texas, (Ref. 9, Vol. III, App. A), April 12, 1962, p. A-39.

28. Küssner, H.G., ZUSAMMENFASSENDER BERICHT ÜBER DEN INSTATIONÄREN AUFTRIEF VON FLÜGELN, Luftfahrtforschung, Band 13, Nr. 12, 1936.

29. Wagner, H., ÜBER DIE ENTSTEHUNG DES DYNAMISCHEN AUFTIEBES VON TRAGFLÜGELN, Ztschr f. Augew. Math. und Mech., Band 5, Heft 1, February 1925.

30. Miller, R.H., UNSTEADY AIRLOADS ON HELICOPTER ROTOR BLADES, Royal Aeronautical Society, October 25, 1963.

31. Davenport, F.J., ROTOR PERFORMANCE IN THE LIGHT OF RECENT ADVANCEMENTS IN AERODYNAMIC METHODOLOGY, presented at the Twenty-First Annual National Forum of the American Helicopter Society, Washington, D. C., 1965.

32. Buettiker, P., ON THE VELOCITIES INDUCED BY THE SUDDEN IMMERSION OF A FORWARD MOVING ROTOR INTO A VERTICAL GUST, BHC IOM 81:PB:oah-2250, Bell Helicopter Company, Hurst, Texas, (Ref. 9, Vol. III, App. A, p. A-21), August 26, 1965.

33. Carpenter, R.J., and Fridovich, B., EFFECT OF A RAPID BLADE PITCH INCREASE ON THE THRUST AND INDUCED-VELOCITY RESPONSE OF A FULL-SCALE HELICOPTER ROTOR, NACA Technical Note 3044, National Advisory Committee for Aeronautics, November 1953.

34. Rebont, Jean; Valensi, Jacques; and Soulez-Laviviere, Jean, WIND TUNNEL STUDY OF THE RESPONSE IN LIFT OF A ROTOR TO AN INCREASE IN COLLECTIVE PITCH IN THE CASE OF VERTICAL FLIGHT NEAR THE AUTOROTATIVE REGIME, NASA TTF-17, National Aeronautics and Space Administration, April 1960.

35. Bisplinghoff, R.L., Ashley, H., and Halfman, R.L., AEROELASTICITY, Reading, Mass., Addison-Wesley Publishing Company, Inc., 1957, p. 814.

36. AIRPLANE AIRWORTHINESS, TRANSPORT CATEGORIES, Federal Aviation Agency, Civil Aeronautics Regulations, Part 4b, September 1962.

37. Kordes, E. E., and Houbolt, J. C., EVALUATION OF GUST RESPONSE CHARACTERISTICS OF SOME EXISTING AIRCRAFT WITH WING BENDING FLEXIBILITY INCLUDED, NACA Technical Note 2897, National Advisory Committee for Aeronautics, February 1953.

APPENDIX I. SAMPLE OUTPUT FROM FLIGHT-SIMULATION PROGRAM

BELL HELICOPTER IBM 360/ PROGRAM C81-11
HELICOPTER RIGID BODY DYNAMICS ANALYSIS
COMPILED 1-21-67

AEROELASTIC FEEDBACK LOOP ACTIVE WITH FEEDBACK FACTOR = 0.100
WAGNER AND BUETTIKER FUNCTIONS ACTIVE ON TIME STEP 1

2 1090313 SINE-SQUARED GUST NON-STEADY DELTA 3 = -30
GW. = 8500. V = 150.
MODEL GUST STUDY

INPUT DATA

FUSELAGE GROUP

GROSS WEIGHT	[8500.000]	0.0	0.0	0.0	0.0	0.0	0.0	MASS MOMENTS OF INERTIA
C.G. LOCATION	[193.850	0.0	61.610]	[2530.000	11716.000	10164.000]	-671.000	
	-0.500	0.134	17.500	2.000	0.0	16.400	0.0	
	4.000	0.0	0.007	0.0	7.000	0.0	0.0	
	0.0	0.0	0.0	0.0	0.0	0.0	0.0	

WING GROUP

AREA	[27.900]	0.500	14.000	0.0	0.0	0.0	1000.000	
	1.000	1.000	1.200	0.0	1.100	0.0	0.0	
	0.0	0.0	0.0	0.010	0.0	0.000	0.0	
	0.200	0.061	20.000	20.000	[192.000	62.000	59.000]	C.P. LOCATION
	9.200	0.0	2.420	0.0	0.0	0.0	0.0	
	0.0	0.0	0.0	0.0	0.0	0.0	0.0	
	0.0	0.0	0.0	0.0	0.0	0.0	0.0	
	0.0	0.0	0.0	0.0	0.0	0.0	0.0	

MAIN ROTOR GROUP, WITH WEIGHT DISTRIBUTION

NUMBER OF BLADES	[2.000]	20.000	12.000	[22.000	27.000]	200.000	0.049	RADIUS (FT), CHORD (IN)
TWIST	[-10.000]	7.750	1.250	2.000	0.0	0.008	0.0	
	0.800	1.270	1.300	0.700	0.700	0.400	0.0	
	3.917	-7.442	3.625	0.008	0.0	0.000	0.040	
	0.340	0.107	0.0	0.0	0.0	0.0	[-30.000]	DELTA-3
	0.0	152.620	0.0	0.0	0.0	0.0	0.0	
WEIGHT DISTRIBUTION (LB/IN)	[3.237	5.860	6.040	2.120	0.941	0.759	0.661	
	0.624	0.593	0.557	0.516	0.617	1.116	1.116	
	0.649]	0.505	0.505	0.505	1.660	2.486	0.0	

PROP GROUP

0.0	0.0	0.0	0.0	0.0	0.0	0.0
0.0	0.0	0.0	0.0	0.0	0.0	0.0
0.0	0.0	0.0	0.0	0.0	0.0	0.0
0.0	0.0	0.0	0.0	0.0	0.0	0.0
0.0	0.0	0.0	0.0	0.0	0.0	0.0
0.0	0.0	0.0	0.0	0.0	0.0	0.0
0.0	0.0	0.0	0.0	0.0	0.0	0.0
0.0	0.0	0.0	0.0	0.0	0.0	0.0

TAIL ROTOR GROUP, WITH WEIGHT DISTRIBUTION

	2.000	20.000	12.000	4.250	8.410	520.700	0.251
PRECONE	0.0	[1.500]	1.062	0.500	0.0	0.0	0.0
	0.800	1.270	1.300	0.700	0.700	0.400	0.0
	3.917	-7.442	3.625	0.010	0.0	0.000	0.040
SLOPE OF LIFT CURVE AT LOW MACH NO.	0.340	[0.107]	0.0	0.0	0.0	0.0	45.000
	-14.850	118.270	0.0	0.0	0.0	0.200	0.0
	1.610	1.476	0.594	0.220	0.149	0.122	0.107
	0.103	0.110	0.098	0.098	0.098	0.098	0.098
	0.098	0.098	0.098	0.098	0.172	0.238	0.500

ELEVATOR GROUP

AREA [15.000] 1000.000 6.214 0.927 0.134 2.000 0.0
1.000 1.000 1.200 0.0 1.200 0.0 0.0
0.0 0.0 0.0 0.008 0.0 0.000 0.0
0.200 0.052 23.000 23.000 [398.500 56.000] 0.0 C.P. LOCATION
0.0 0.0 0.0 0.0 1.500 0.0 10.000

FIN GROUP

25.000 [501.000] 4.500 0.400 [84.000 0.0] 1000.000 C.P. LOCATION
1.000 1.000 1.200 0.0 1.200 0.0 0.0
0.0 0.0 0.0 0.008 0.0 0.000 0.0
0.200 0.040 0.0 0.0 0.0 0.0 0.200
50.000 50.000 0.0 0.0 0.0 0.0 0.0

COLLECTIVE AND CYCLIC CONTROLS GROUP

COLLECTIVE STICK [2.000 0.0 0.0 8.500 12.240 0.0 0.0
LATERAL CYCLIC [1.483 0.0 0.0 -10.800 17.800 0.0 0.0] F AND A CYCLIC
2.250 0.0 0.0 -13.200 27.000 0.0 0.0

PEDAL AND CONTROL LINKAGE GROUP

4.990 0.0 0.0 -7.000 29.950 0.0 0.0
0.0 0.0 0.0 0.0 0.0 0.0 0.0
0.0 0.0 0.0 0.0 0.0 0.0 0.0] PEDAL

FLIGHT CONSTANTS GROUP

FORWARD VELOCITY [150.000] 0.0 6600.000 [1157.000] 1.000 1000.000 [1100.000] ENGINE RPM
0.0 66.000 44.000 55.000 0.0 -6.900 -1.500
0.0 3.000 -1.000 2.000 1.000 18.000 1.400
31.800 2.000 0.0 8100.000 289.300 0.0 0.0
75.500 0.0 29.000 0.0 0.0 0.0 0.0

ALLOWABLE ERROR GROUP

50.000 50.000 50.000 100.000 50.000 50.000 10.000

ITERATION LIMITS GROUP, PLUS TCO2

40.000 0.0 0.0 40.000 9.000 0.0 1.000
9999.000 0.0 0.0 0.0 0.0 0.0 0.0
0.0 0.0 0.0 0.0 0.0 0.0 0.0

***** START OF ITERATION 4 *****

	L.WING	R.WING	ELEVATOR	FIN
AERODYNAMIC ANGLE	-0.132926	-0.132926	-0.151113	-0.010967
ANGLE OF ATTACK	0.111420	0.111420	0.011822	0.068173

VAR(I) 75.02977 50.39841 63.37225 30.99059 -0.12387 -0.03440 0.10182 0.01417 0.02484 0.01017

AUX.TM.	0.	AUX.TM.	0.	FUS.DRAG	332.	CLIMB ANG.	0.0			
PROP COLL	0.0	MR THRUST	7733.	MR H-FORCE	689.	MR Y-FORCE	-103.	MR VIND	4.663	
		TR THRUST	264.	TR H-FORCE	10.	TR Y-FORCE	2.	TR VIND	4.360	

FORCES AND MOMENTS

	TOTALS	R.WING	L.WING	FLE	FUS	R.PROP	L.PROP	M.R.	T.R.	GUN	FIN	W/OMR	STR
X-FORCE	-0.4	-80.5	-80.5	-15.6	-311.7	0.0	0.0	-523.7	-16.5	0.0	-22.0	1050.2	
Y-FORCE	0.4				-36.6	0.0	0.0	-236.6	263.9	0.0	300.0	-290.1	
Z-FORCE	5.0	-413.5	-413.5	-40.0	179.6	0.0	0.0	-7742.6	5.0	0.0		8429.9	
ROLL	4.9	-1343.8	1343.8	0.0		0.0	0.0	-1794.6	1239.8	0.0	559.8	0.0	0.0
PITCH	13.6	66.4	66.4	-649.9	252.5	0.0	0.0	4.0	214.9	0.0	41.1	0.0	57.2
YAW	20.9	261.6	-261.6	0.0	-302.0	0.0	0.0	121.3	-7208.1	0.0	-7679.0	15088.8	-0.0

PARTIAL DERIVATIVE MATRIX

	X-FORCE	Y-FORCE	Z-FORCE	YAW MOM.	PITCH MOM.	ROLL MOM.	MR MOM.F/A	MR MOM.LAT	TR MOM.F/A	TR MOM.LAT
F-A CYCLIC	5310.	-720.	77008.	14341.	-67130.	-5481.	785650.	-435777.	0.	0.0
LAT CYCLIC	756.	9006.	57210.	3772.	23599.	68291.	-68616.	-1016409.	0.	0.0
COLLECTIVE	3314.	-5908.	-191647.	123791.	-123243.	-44890.	-12785.	1539913.	0.	0.0
PEDAL	-528.	10681.	598.	-291366.	8361.	50246.	0.	0.	1780.	-15875.
PITCH (EULER)	-7698.	-2224.	-90619.	-678.	-95713.	-20348.	-17627.	424422.	-356.	-259.
ROLL (EULER)	5.	10409.	948.	-15531.	654.	3044.	-16542.	-5605.	46.	-422.
MR F/A FLAPPING	-4655.	2765.	16831.	6412.	43932.	20970.	-776780.	-1313259.	0.	0.0
MR LAT FLAPPING	9.	2644.	57133.	47207.	29211.	20054.	1275544.	-1022990.	0.	0.0
TR F-A FLAPPING	-286.	-745.	-1.	19927.	1042.	-3512.	0.	0.	14712.	15869.
TR LAT FLAPPING	434.	-5458.	225.	149212.	2545.	-26054.	0.	0.	-16987.	19120.
-ERROR	0.	-0.	-5.	-21.	-14.	-5.	55.	13.	1.	-0.

AEROELASTIC FEEDBACK LOOP ACTIVE WITH FEEDBACK FACTOR = 0.100
WAGNER AND BUETTIKER FUNCTIONS ACTIVE ON TIME STEP 1

2 1090313 SINE-SQUARED GUST NON-STEADY DELTA 3 = -30
GW. = 8500. V = 150.
MODEL GUST STUDY

HELICOPTER IS IN STABLE CONDITION.

MAIN ROTOR COLLECTIVE PITCH	(DEGREES)	16.260	TAIL ROTOR COLLECTIVE PITCH	(DEGREES)	2.289
F+A CYC PITCH	(DEGREES)	7.068	F+A CYC PITCH	(DEGREES)	0.0
LAT CYCLIC PITCH	(DEGREES)	-1.836	LAT CYCLIC PITCH	(DEGREES)	0.0
F+A FLAPPING	(DEGREES)	5.840	F+A FLAPPING	(DEGREES)	1.427
LAT FLAPPING	(DEGREES)	0.812	LAT FLAPPING	(DEGREES)	0.585
THRUST	(LBS)	7739.707	THRUST	(LBS)	265.991
H-FORCE	(LBS)	688.573	H-FORCE	(LBS)	9.965
Y-FORCE	(LBS)	-103.235	Y-FORCE	(LBS)	2.350
HORSEPOWER		931.625	HORSEPOWER		18.045
RPM		324.060	RPM		1656.598
MAST TILT ANGLE	(DEGREES)	0.0	MAST TILT ANGLE	(DEGREES)	0.0
ELEVATOR ANGLE OF ATTACK	(DEGREES)	0.688	FIN ANGLE OF ATTACK	(DEGREES)	3.909
BODY Z-FORCE (+DOWN)	(LBS)	-40.612	BODY Y-FORCE (+RIGHT)	(LBS)	300.254
BODY X-FORCE (+FWD)	(LBS)	-15.683	BODY X-FORCE (+FWD)	(LBS)	-22.031
FUSELAGE EULER ANGLE YAW	(DEGREES)	0.0	WING ANGLE OF ATTACK	(DEGREES)	6.385
PITCH	(DEGREES)	-7.097	BODY Z-FORCE (+DOWN)	(LBS)	-827.160
ROLL	(DEGREES)	-1.972	BODY X-FORCE (+FWD)	(LBS)	-161.030
HELICOPTER GROSS WEIGHT	(LBS)	8500.000	AUXILIARY PROPULSION,LEFT SIDE	(LBS)	0.0
FORWARD SPEED	(KNOTS)	150.000	RIGHT SIDE	(LBS)	0.0
RATE OF CLIMB	(FT/SEC)	0.0			
ENGINE RPM		6600.000			

PART 1 5 ITERATIONS 0.992 MINUTES ELAPSED COMPUTING TIME

STABILITY PARTIAL DERIVATIVE MATRIX

		X-FORCE	Y-FORCE	Z-FORCE	YAW MOM.	PITCH MOM.	ROLL MOM.	MR MOM.F/A	MR MOM.LAT	TR MOM.F/A	TR MOM.LAT
P	32.10	-93.33	-1387.50	435.16	-659.62	-913.89	1971.00	41916.14	92.82	104.47	
Q	29.42	2.59	-438.67	-28C.47	-4667.80	-148.68	36888.90	-19C2.41	4.56	1C.43	
R	-1.49	819.43	-42.9?	-21669.92	257.21	2799.61	-644.43	955.06	-1.09	-385.48	
U	-13.36	3.92	-12.39	-71.13	38.03	1?.66	-72.52	382.11	C.53	-2.39	
V	0.56	-61.6C	-13.05	318.6E	-13.43	109.16	460.87	20C.60	4.86	9.69	
W	3.84	-9.34	-30C.71	46.44	-283.1?	-68.16	-409.99	1339.92	-2.44	1.56	

INPUT DATA FOR MANEUVER

START (SEC)	DELT1 (SEC)	MAX1 (SEC)	DELT2 (SEC)	MAX2 (SEC)	MAX3 (SEC)	PLOT (MIN)
0.0	0.025	1.200	0.0	0.0	0.0	2.000

J	XCIT(J,1)	(J,2)	(J,3)	(J,4)	(J,5)	(J,6)
10	148.000	-50.000	180.000	0.0	0.0	0.0

0.675 SECONDS MANEUVER TIME 15.347 MINUTES ELAPSED COMPUTING TIME

LB,FT,DEG,SEC UNITS

MAIN ROTOR TIP PATH PLANE REFERENCE

	P	Q	OMEGA
ACCEL	64.545	9.128	0.0
VELOCITY	8.163	3.282	1944.359

EULER ANGLES FROM SWASH PLATE REFERENCE

	PSI	THETA	PHI
VELOCITY	0.0	[illegible]	9.012
LOCATION	0.0	5.984	1.436

M.TILT 0.0 CYC(F+A) 7.068 A1 5.984 A1S -1.387 THRUST 9759.33 HF [illegible] TORQ 14250.5 [illegible] [illegible]
COLLEC 16.260 CYC(LAT) -1.836 B1 1.436 B1S -0.387 RPM 324.05 YF -222.2 HP 879.9 [illegible] [illegible]

TAIL ROTOR TIP PATH PLANE REFERENCE

	P	Q	OMEGA
ACCEL	-4.672	-3.330	0.0
VELOCITY	-0.150	-0.373	9939.550

EULER ANGLES FROM SWASH PLATE REFERENCE

	PSI	THETA	PHI
VELOCITY	0.0	[illegible]	[illegible]
LOCATION	0.0	1.419	0.591

M.TILT 0.0 CYC(F+A) 0.0 A1 1.418 A1S 1.419 THRUST 260.76 HF 9.9 TORQ 57.5 VI [illegible]
COLLEC 2.239 CYC(LAT) 0.0 B1 0.591 B1S 0.591 RPM 1650.00 YF 2.2 HP 18.1 IP [illegible]

BODY REFERENCE

	U	V	W	P	Q	R
ACCEL	0.007	1.168	-10.544	-3.187	-3.610	-2.491
VELOCITY	251.235	1.371	-31.872	-0.275	-0.497	-0.275

EULER ANGLES FROM FIXED REFERENCE

	PSI	THETA	PHI	[illegible]
VELOCITY	-0.261	[illegible]	[illegible]	[illegible]
LOCATION	-0.071	-7.203	[illegible]	[illegible]

FIXED REFERENCE

	X	Y	Z
VELOCITY	253.252	-0.014	-0.148
LOCATION	170.498	0.002	-999.947

DISTANCE 170.9 VEL 150.05 HEADING ANGLE -0.001
ALTITUDE 999.9 GND VEL 150.05 CLIMB ANGLE 0.011

FIN/RUD ATK 3.338 YF 294.7 DRAG 22.2
ELEVATOR ATK 0.131 LIFT 9.6 DRAG 10.9
LEFT WING ATK 7.889 LIFT 513.9 DRAG 87.8
RIGHT WING ATK 7.393 LIFT 513.6 DRAG 87.8
FUSELAGE ATKY -0.313 ATKP -7.210 LIFT -147.1 DRAG 308.6 YF -38.4 YAWM -315.2 PCHM 496.2
CONTROL STCK(%) COLSTK [illegible] F/CYCSTK [illegible] L/CYCSTK [illegible] PEDAL [illegible]

PROPELLER/JET
COLL.L. 0.0 TORQ 0.0 VI 0.0 THRUST(L/C) 0.0 ENGINE TORQUE 14552.4 TOTAL HPREQ 897.9 GUST (CG) [illegible] -7.5
COLL.R. 0.0 HP 0.0 IP 0.0 THRUST(R) 0.0 SHAFT HP 897.9 [illegible] 1.0

FORCES AND MOMENTS

	TOTALS	R.WING	L.WING	ELE	FUS	R.PROP	L.PROP	M.R.	T.R.	GUN	FIN	[illegible]	[illegible]
X-FORCE	75.1	-87.8	-97.8	-10.9	-308.6	0.0	0.0	-457.0	-16.4	0.0	-22.2	1065.7	
Y-FORCE	-50.6				-38.4	0.0	0.0	-286.6	260.4	0.0	294.7	-200.7	
Z-FORCE	-2223.6	-513.6	-513.9	-9.6	147.3	0.0	0.0	-9767.0	4.9	0.0		8478.2	
ROLL	-399.4	-1669.1	1670.0	0.0		0.0	0.0	-2173.6	1223.3	0.0	549.9	0.0	0.0
PITCH	-738.3	82.0	82.1	-169.5	496.2	0.0	0.0	-1539.6	211.6	0.0	41.6	0.0	57.5
YAW	-566.1	285.4	-285.4	0.0	-315.2	0.0	0.0	146.9	-7112.3	0.0	-7544.0	14258.5	-0.0

INSTANTANEOUS BLADE VELOCITIES W.R.T. CONTROL PLANE

1090313 = IPSN -27540121 =KWH 16 =LOOP 16 =NPATH 81 =NPROG

STA	BEAM 0			90			180			270		
1	-0.	-1.	-1.	0.	1.	0.	0.	0.	0.	-0.	0.	0.
2	-0.	-2.	-2.	0.	1.	1.	1.	1.	-0.	-1.	0.	1.
3	-1.	-3.	-3.	0.	2.	2.	1.	1.	-1.	-1.	1.	2.
4	-1.	-4.	-4.	0.	3.	2.	2.	1.	-1.	-1.	1.	2.
5	-1.	-5.	-5.	0.	3.	3.	2.	1.	-1.	-1.	1.	3.
6	-1.	-6.	-5.	0.	4.	4.	2.	1.	-1.	-2.	2.	3.
7	-1.	-7.	-6.	0.	4.	4.	3.	1.	-2.	-2.	2.	4.
8	-1.	-8.	-6.	0.	5.	4.	3.	1.	-2.	-2.	2.	4.
9	-1.	-8.	-7.	1.	5.	5.	3.	0.	-2.	-2.	3.	5.
10	-1.	-8.	-7.	1.	5.	5.	2.	-0.	-3.	-2.	3.	5.
11	-1.	-9.	-7.	1.	6.	5.	2.	-1.	-3.	-2.	3.	5.
12	-1.	-9.	-7.	1.	6.	5.	2.	-1.	-4.	-2.	4.	6.
13	-1.	-8.	-7.	1.	6.	5.	1.	-2.	-4.	-2.	4.	6.
14	-0.	-8.	-7.	1.	7.	5.	-0.	-4.	-4.	-1.	5.	6.
15	-0.	-7.	-6.	2.	7.	5.	-1.	-5.	-5.	-1.	6.	7.
16	0.	-7.	-6.	2.	7.	5.	-3.	-7.	-6.	0.	6.	7.
17	1.	-6.	-6.	2.	8.	5.	-4.	-9.	-6.	1.	7.	7.
18	1.	-6.	-6.	2.	9.	5.	-6.	-11.	-7.	2.	8.	8.
19	2.	-6.	-6.	3.	11.	6.	-7.	-14.	-8.	3.	9.	8.
20	2.	-6.	-7.	3.	12.	7.	-9.	-17.	-9.	3.	10.	9.

CHORD STA	0			90			180			270		
1	0.	-0.	-0.	0.	0.	0.	0.	0.	0.	0.	-0.	-0.
2	0.	-0.	-0.	0.	0.	0.	0.	0.	0.	-0.	-0.	-0.
3	0.	-0.	-0.	0.	0.	0.	0.	0.	0.	-0.	-0.	-0.
4	0.	-0.	-0.	0.	0.	0.	0.	0.	0.	-0.	-0.	-0.
5	0.	-0.	-0.	0.	0.	0.	0.	0.	-0.	-0.	-0.	-0.
6	0.	-0.	-0.	0.	0.	-0.	0.	0.	-0.	-0.	-0.	-0.
7	0.	-0.	-0.	0.	0.	-0.	0.	0.	-0.	-0.	-0.	-0.
8	0.	-0.	0.	1.	0.	-0.	0.	0.	-0.	-1.	-0.	-0.
9	0.	0.	0.	1.	0.	-1.	-0.	0.	-0.	-1.	-1.	0.
10	0.	0.	1.	1.	0.	-1.	-0.	0.	-0.	-1.	-1.	0.
11	0.	0.	1.	1.	0.	-1.	-0.	0.	-0.	-1.	-1.	0.
12	1.	0.	1.	1.	-0.	-1.	-0.	0.	-0.	-1.	-1.	0.
13	1.	1.	1.	2.	-0.	-2.	-1.	0.	-1.	-1.	-1.	0.
14	1.	1.	2.	2.	-0.	-2.	-1.	0.	-1.	-2.	-1.	0.
15	1.	1.	2.	2.	-0.	-2.	-1.	-0.	-1.	-2.	-1.	0.
16	1.	1.	3.	3.	-0.	-2.	-2.	-0.	-1.	-2.	-1.	1.
17	1.	2.	3.	3.	-0.	-3.	-2.	-0.	-1.	-2.	-1.	1.
18	1.	2.	3.	3.	-0.	-3.	-2.	-1.	-1.	-2.	-1.	1.
19	1.	2.	3.	3.	-0.	-3.	-3.	-1.	-1.	-2.	-1.	1.
20	2.	2.	4.	4.	1.	-3.	-3.	-1.	-1.	-3.	-1.	1.

CONTROL DEFLECTIONS, DEGREES

0.0015 0.0009 -0.0007 0.0011 0.0037 0.0024 -0.0007 -0.0014 -0.0013 -0.0022 -0.0026 -0.0004

GUST VELOCITIES ON ROTOR DISC

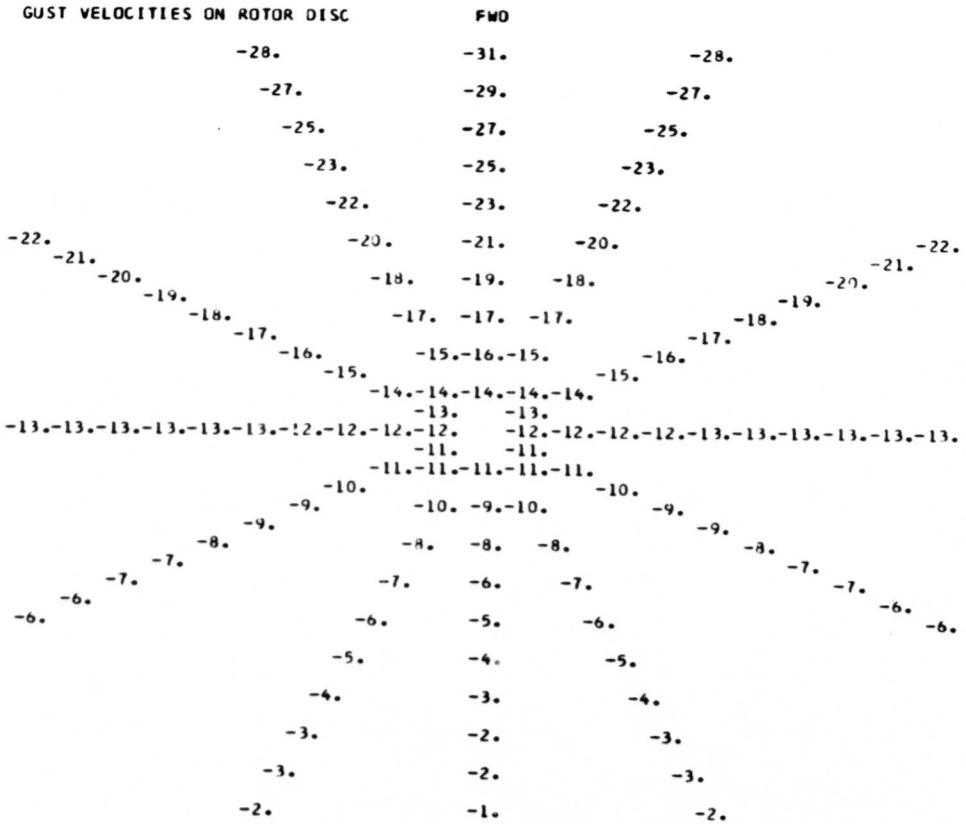

VGUSTW	VGUSTE	HGUSTW	HGUSTE	HGUSTF	YGUSTF
-11.922	-2.232	-1.510	-0.283	-0.032	0.008

BHC SYS/360-50 PROGRAM C02, MOMENT SYNTHESIS IPSN = 1090313
KWH = -27540121
PROD.540 ROTOR, 20 LB MID WT. 35 LB TIP LOOP = 16
C81 MANEUVER TIME = 0.675 SEC.

FUDGE	PEAK	DAMP	FABLE	DECAY	PLSOFT
0.0	0.0	0.0	0.0	0.01	1.00

STA	BEAMWISE MOMENT MEAN MXX	BEAMWISE MOMENT OSC MXX	AZIMUTH MAX	AZIMUTH MIN	CHORDWISE MOMENT MEAN MYY	CHORDWISE MOMENT OSC MYY	AZIMUTH MAX	AZIMUTH MIN
0	-8370.	14320.	280	190	85773.	121440.	300	120
1	1421.	5956.	250	180	79219.	109642.	300	120
2	3632.	11579.	240	70	73026.	98408.	300	120
2	20906.	23141.	290	120	70043.	95743.	300	120
3	15970.	18874.	290	110	65223.	85621.	300	120
4	9352.	15202.	280	110	60788.	75964.	300	130
5	4373.	12321.	0	110	56414.	66537.	300	130
6	866.	10185.	350	100	52109.	57678.	300	130
7	-1200.	8996.	240	100	46621.	50611.	300	230
8	-2103.	8602.	240	100	40431.	44911.	300	230
9	-2665.	8214.	240	100	34727.	39384.	300	230
10	-3002.	7842.	240	90	29495.	34043.	300	230
11	-3090.	7722.	240	90	24707.	28920.	300	230
12	-2889.	7955.	240	90	20361.	24054.	300	230
13	-3403.	8110.	240	150	16594.	19490.	300	230
14	-5828.	8085.	250	160	13509.	15294.	300	230
15	-9265.	8082.	250	160	10987.	11568.	70	230
16	-11226.	7701.	250	170	8430.	8183.	70	230
17	-10800.	8675.	80	170	5857.	5079.	70	230
18	-7848.	9132.	90	170	3386.	2993.	170	230
19	-3746.	7096.	90	180	845.	1139.	180	240
20	460.	1853.	290	10	-302.	137.	190	320

(COMPILED)
(10-20-66)

PARAMETER SUMMARY

RADIUS	264. IN.	GROSS WT.	8500. LBS.
DIAMETER	44. FT.	FWD.SPEED	150. KNOTS
CHORD	27.00 IN.	DRAG AREA	0.0 SQ.FT.
NO.BLADES	2.	DOWNLOAD	147. LBS.
ROTOR RPM	324.	ROTOR HP	879.
PRECONE	2.751 DEG.	A1 FLAPPING	5.98 DEG.
ROOT COLL.	16.263 DEG.	B1 FLAPPING	1.44 DEG.
TWIST	-10.002 DEG.	INFLOW	-0.0910
NO.HUB SEG.	2.	H FORCE	642. LBS.
TEETERING HUB GEOMETRY		TPP ATTITUDE	-8.3 DEG.

WING DATA LIFT -1027. LBS. CHORD 0.17 FT.
CL 0.4892 DRAG -176. LBS. SPAN166.73 FT.

VERTICAL HUB SHEAR = 1656. LBS.(TOTAL)

HUB VIBRATION		
(NON-ROTATING COORDINATES)	0.0	F/A
(INCHES, SINGLE AMPLITUDE)	0.0	LAT.
	0.0	VERT.

RESULTANT ROOT MOMENTS

	BEAM	CHORD
1/REV	0.	84557.
2/REV	14469.	0.0
3/REV	0.	53002.
4/REV	577.	0.0

BELL HELICOPTER IBM 360/ PROGRAM C01-11
HELICOPTER RIGID BODY DYNAMICS ANALYSIS
COMPILED 1-21-67

1 1090313 SINE-SQUARED GUST NON-STEADY DELTA 3 = -30
Go. = 0500. V = 150.
MODEL GUST STUDY

SYMBOL 1 = VERT. ACCEL. WRT. BODY, G-S
SYMBOL 2 = FWD. ACCEL. WRT. BODY, G-S
SYMBOL 4 = VOID

SCALE	1	FROM	-5.000	TO	5.000,	1 INCH =	1.000	3 FOR 1 + 2 ON SAME PRINT POS.
SCALE	2	FROM	-5.000	TO	5.000,	1 INCH =	1.000	5 FOR 1 + 4 ON SAME PRINT POS.
SCALE	4	FROM	-2000.000	TO	-1000.000,	1 INCH =	100.000	6 FOR 2 + 4 ON SAME PRINT POS.
								7 FOR 1 + 2 + 4 ON SAME PRINT POS.

INCHES

```
          0         1         2         3         4         5         6         7         8         9        10
          .         .         .         .         .         .         .         .         .         .         .
 0.0                                                 2         1
 0.02                                                2         1
 0.05                                                2         1
 0.07                                                2         1
 0.10                                                2         1
 0.12                                                2         1
 0.15                                                2         1
 0.17                                                2         1
 0.20                                                2         1
 0.22                                                2         1
 0.25                                                2         1
 0.27                                                2         1
 0.30                                                2         1
 0.32                                                2         1
 0.35                                                2         1
 0.38                                                2         1
 0.40                                                2         1
 0.42                                                2         1
 0.45                                                2         1
 0.47                                                2         1
 0.50                                                2         1
 0.52                                                2         1
 0.55                                                2         1
 0.57                                                2         1
 0.60                                                2         1
 0.63                                                2          1
 0.65                                                2           1
 0.67                                                2            1
 0.70                                                2             1
 0.72                                                2              1
 0.75                                                2               1
 0.77                                                2                1
 0.80                                                2                 1
 0.82                                                2                 1
 0.85                                                2                 1
 0.88                                                2                 1
 0.90                                                2                 1
 0.92                                                2                1
 0.95                                                2               1
 0.97                                                2             1
 1.00                                                2           1
 1.02                                                2         1
 1.05                                                2       1
 1.07                                                2     1
 1.10                                                2   1
 1.12                                                2 1
 1.15                                                2 1
 1.17                                                2   1
 1.20                                                2     1

0.10053
```

APPENDIX II. CASE DESCRIPTIVE INFORMATION AND TRIM DATA

TABLE XIV. CASE DESCRIPTIVE INFORMATION AND TRIM DATA, PURE SINGLE-ROTOR HELICOPTER

Case No.	Vel (Kt)	Gust Type	Main Rotor Data: Disc Ldg	C_T/σ	M_{tip}	Rad (Ft)	Chord (In.)	RPM	Mass Ratio	Lock No.
			Semirigid Rotor (4 Blades)							
1	200	SUDV	7.0	.05	.80	26.1	35.6	234.	4.47	8.31
2	200	SSQV	↓	↓	↓	↓	↓	↓	↓	↓
3	225	SUDV	↓	↓	↓	↓	↓	↓	↓	↓
4	225	SSQV	↓	↓	↓	↓	↓	↓	↓	↓
5	200	SUDV	↓	↓	.85	↓	↓	↓	↓	↓
6	200	SSQV	↓	↓	↓	↓	↓	↓	↓	↓
7	225	SUDV	↓	↓	↓	↓	↓	↓	↓	↓
8	225	SSQV	↓	↓	↓	↓	↓	↓	↓	↓
9	200	SUDV	↓	↓	.90	↓	↓	↓	↓	↓
10	200	SSQV	↓	↓	↓	↓	↓	↓	↓	↓
11	225	SUDV	↓	↓	↓	↓	↓	↓	↓	↓
12	225	SSQV	↓	↓	↓	↓	↓	↓	↓	↓
13	200	SUDV	↓	↓	.95	↓	↓	↓	↓	↓
14	200	SSQV	↓	↓	↓	↓	↓	↓	↓	↓
15	225	SUDV	↓	↓	↓	↓	↓	↓	↓	↓
16	225	SSQV	↓	↓	↓	↓	↓	↓	↓	↓
17	200	SUDV	4.0	.02	.90	34.5	67.1	177.	1.93	8.42
18	200	SSQV	↓	↓	↓	↓	↓	↓	↓	↓
19	175	SUDV	↓	↓	↓	↓	↓	↓	↓	↓
20	175	SSQV	↓	↓	↓	↓	↓	↓	↓	↓
21	200	SUDV	↓	.05	↓	↓	26.9	↓	↓	10.27
22	200	SSQV	↓	↓	↓	↓	↓	↓	↓	↓
23	225	SUDV	↓	↓	↓	↓	↓	↓	↓	↓
24	225	SSQV	↓	↓	↓	↓	↓	↓	↓	↓

Case No.	Trim Data						
	Coll (Deg)	F&A Cyc (Deg)	TPP Attack (Deg)	Thrust (Lb)	HPR (Hp)	Eff Drag Area (Ft^2)	Fuse Pitch (Deg)
1	19.7	12.8	- 7.8	15400.	2120.	10.4	- 4.4
2	19.7	12.8	- 7.8	15400.	2120.	10.4	- 4.4
3	24.1	16.8	-10.0	15500.	2990.	10.4	- 6.6
4	24.1	16.8	-10.0	15500.	2990.	10.4	- 6.6
5	19.9	13.0	- 8.1	15400.	2240.	10.5	- 4.5
6	19.9	13.0	- 8.1	15400.	2240.	10.5	- 4.5
7	24.5	17.2	-11.1	15500.	3180.	10.5	- 6.8
8	24.5	17.2	-11.1	15500.	3180.	10.5	- 6.8
9	20.5	13.7	- 8.8	15400.	2590.	10.6	- 4.8
10	20.5	13.7	- 8.8	15400.	2590.	10.6	- 4.8
11	25.4	18.2	-12.0	15500.	3730.	10.6	- 7.2
12	25.4	18.2	-12.0	15500.	3730.	10.6	- 7.2
13	21.6	15.1	-10.2	15300.	3310.	11.4	- 5.3
14	21.6	15.1	-10.2	15300.	3310.	11.4	- 5.3
15	27.6	20.5	-13.8	15400.	4940.	10.9	-8.1
16	27.6	20.5	-13.8	15400.	4940.	10.9	- 8.1
17	24.3	19.0	-18.2	14900.	5590.	12.0	- 7.3
18	24.3	19.0	-18.2	14900.	5590.	12.0	- 7.3
19	19.0	14.0	-13.1	15000.	3703.	12.1	- 4.5
20	19.0	14.0	-13.1	15000.	3703.	12.1	- 4.5
21	20.7	13.8	- 9.3	15300.	2600.	10.6	- 5.1
22	20.7	13.8	- 9.3	15300.	2600.	10.6	- 5.1
23	27.8	20.1	-12.9	15400.	4440.	10.6	- 8.0
24	27.8	20.1	-12.9	15400.	4440.	10.6	- 8.0

TABLE XIV - Continued

(PURE SINGLE-ROTOR HELICOPTER)

Case No.	Vel (Kt)	Gust Type	Main Rotor Data: Disc Ldg	C_T/σ	M tip	Rad (Ft)	Chord (In.)	RPM	Mass Ratio	Lock No.
			Semirigid Rotor (4 Blades)							
25	200	SUDV	10.0	.02	.90	21.8	106.2	280	7.64	5.05
26	200	SSQV								
27	175	SUDV								
28	175	SSQV								
29	200	SUDV		.05			42.5			7.10
30	200	SSQV								
31	225	SUDV								
32	225	SSQV								
33	200	RMPV	7.0			26.1	35.6	234	4.47	8.31
34	225	RMPV								
35	200	SUDH								
36	200	SSQH								
37	225	SUDH								
38	225	SSQH								
			Articulated Rotor (4 Blades)							
39	200	SUDV	4.0	.02	.90	34.5	67.1	177	1.93	8.42
40		SSQV		.02			67.1			8.42
41		SUDV		.05			26.9			10.27
42		SSQV		.05			26.9			10.27
43		SUDV	7.0	.02		26.1	89.0	234	4.47	6.58
44		SSQV		.02			89.0			6.58
45		SUDV		.05			35.6			8.31
46		SSQV		.05			35.6			8.31

Case No.	Trim Data						
	Coll (Deg)	F&A Cyc (Deg)	TPP Attack (Deg)	Thrust (Lb)	HPR (Hp)	Eff Drag Area (Ft^2)	Fuse Pitch (Deg)
25	23.0	18.1	-16.2	15100.	4720.	11.1	- 6.3
26	23.0	18.1	-16.2	15100.	4720.	11.1	- 6.3
27	18.5	17.5	-12.0	15300.	3570.	10.2	- .2
28	18.5	17.5	-12.0	15300.	3570.	10.2	- .2
29	20.5	13.9	- 8.4	15400.	2620.	10.6	- 4.5
30	20.5	13.9	- 8.4	15400.	2620.	10.6	- 4.5
31	24.9	17.8	-11.3	15500.	3580.	10.1	- 6.8
32	24.9	17.8	-11.3	15500.	3580.	10.1	- 6.8
33	20.5	13.7	- 8.8	15400.	2590.	10.6	- 4.8
34	25.4	18.2	-12.0	15500	3730.	10.6	- 7.2
35	20.5	13.7	- 8.8	15400.	2590.	10.0	- 4.8
36	20.5	13.7	- 8.8	15400.	2590.	10.0	- 4.8
37	25.4	18.2	-12.0	15500.	3730.	10.7	- 7.2
38	25.4	18.2	-12.0	15500.	3730.	10.7	- 7.2
39	24.1	13.6	-17.1	16500.	5640.	11.9	-13.6
40	24.1	13.6	-17.1	16500.	5640.	11.9	-13.6
41	20.6	12.5	- 9.1	15700.	2620.	10.8	- 6.6
42	20.6	12.5	- 9.1	15700.	2620.	10.8	- 6.6
43	23.1	13.2	-15.7	16600.	5200.	11.1	-12.2
44	23.1	13.2	-15.7	16600.	5200.	11.1	-12.2
45	20.4	12.4	-16.7	15800.	2620.	10.6	- 6.2
46	20.4	12.4	-16.7	15800.	2620.	10.6	- 6.2

TABLE XIV - Continued

(FURE SINGLE-ROTOR HELICOPTER)

Case No.	Vel (Kt)	Gust Type	Main Rotor Data: Disc Ldg	$\frac{C_T}{\sigma}$	M tip	Rad (Ft)	Chord (In.)	RPM	Mass Ratio	Lock No.
			Articulated Rotor (4 Blades)							
47	200	SUDV	10.0	.02	.90	21.8	106.2	280	7.64	11.4
48	↓	SSQV	↓	.02	↓	↓	106.2	↓	↓	11.4
49		SUDV		.05			42.5			10.6
50		SSQV		.05			42.5			10.6
			Rigid Rotor (4 Blades)							
51	200	SUDV	4.0	.02	.90	34.5	67.1	177	1.93	8.4
52	↓	SSQV	↓	.02	↓	↓	67.1	↓	↓	8.4
53		SUDV		.05			26.9			10.3
54		SSQV		.05			26.9			10.3
55		SUDV	7.0	.02		26.1	89.0	234	4.47	6.6
56		SSQV	↓	.02		↓	89.0	↓	↓	6.6
57		SUDV		.05			35.6			8.3
58		SSQV		.05			35.6			8.3
59		SUDV	10.0	.02		21.8	106.2	280	7.64	5.0
60		SSQV	↓	.02		↓	106.2	↓	↓	5.0
61		SUDV		.05			42.5			7.1
62	↓	SSQV	↓	.05	↓	↓	42.5	↓	↓	7.1
			Articulated Rotor (4 Blades)							
63	225	SUDV	7.0	.02	.90	26.1	89.0	234	4.47	6.6
64	↓	SSQV	↓	.02	↓	↓	89.0	↓	↓	6.6
65		SUDV		.05			35.6			8.3
66	↓	SSQV	↓	.05	↓	↓	35.6	↓	↓	8.3

Case No.	Trim Data						
	Coll (Deg)	F&A Cyc (Deg)	TPP Attack (Deg)	Thrust (Lb)	HPR (Hp)	Eff Drag Area (Ft^2)	Fuse Pitch (Deg)
47	22.6	12.7	-15.2	16700.	4960.	11.4	-11.9
48	22.6	12.7	-15.2	16700.	4960.	11.4	-11.9
49	20.5	12.5	- 8.2	15800.	2670.	10.6	- 5.8
50	20.5	12.5	- 8.2	15800.	2670.	10.6	- 5.8
51	24.1	13.6	-17.1	16500.	5640.	11.2	-13.6
52	24.1	13.6	-17.1	16500.	5640.	11.2	-13.6
53	20.6	12.5	- 8.1	15700.	2620.	10.7	- 6.6
54	20.6	12.5	- 8.1	15700.	2620.	10.7	- 6.6
55	23.1	13.2	-15.7	16600.	5200.	11.2	-12.2
56	23.1	13.2	-15.7	16600.	5200.	11.2	-12.2
57	20.4	12.4	- 8.6	15800.	2620.	10.6	- 6.2
58	20.4	12.4	- 8.6	15800.	2620.	10.6	- 6.2
59	22.6	12.7	-15.2	16600.	4960.	11.4	-11.9
60	22.6	12.7	-15.2	16600.	4960.	11.4	-11.9
61	20.5	12.5	- 8.2	15800.	2670.	10.6	- 5.8
62	20.5	12.5	- 8.2	15800.	2670.	10.6	- 5.8
63	30.3	19.0	-20.4	17100.	8420.	9.4	-15.5
64	30.3	19.0	-20.4	17100.	8420.	9.4	-15.5
65	25.3	16.9	-20.1	16000.	3780.	10.6	- 8.7
66	25.3	16.9	-20.1	16000.	3780.	10.6	- 8.7

TABLE XIV - Continued

(PURE SINGLE-ROTOR HELICOPTER)

Case No.	Vel (Kt)	Gust Type	Main Rotor Data: Disc Ldg	C_T/σ	M tip	Rad (Ft)	Chord (In.)	RPM	Mass Ratio	Lock No.
			Rigid Rotor (4 Blades)							
67	225	SUDV	7.0	.02	.90	26.1	89.0	234	4.47	6.6
68	↓	SSQV	↓	.02	↓	↓	89.0	↓	↓	6.6
69	↓	SUDV	↓	.05	↓	↓	35.6	↓	↓	8.3
70	↓	SSQV	↓	.05	↓	↓	35.6	↓	↓	8.3
			Semirigid Rotor (2 Blades)							
217	200	SUDV	7.0	.08	.9	26.1	43.8	234	4.47	10.3
218	200	SSQV	7.0	.08	.9	26.1	43.8	234	4.47	10.3
			Rigid Rotor (2 Blades)							
219	200	SUDV	7.0	.08	.9	26.1	43.8	234	4.47	10.3
220	200	SSQV	7.0	.08	.9	26.1	43.8	234	4.47	10.3
			Articulated Rotor (3 Blades)							
221	200	SUDV	7.0	.08	.9	26.1	28.1	234	4.47	10.3
222	200	SSQV	7.0	.08	.9	26.1	28.1	234	4.47	10.3
			Semirigid Rotor (4 Blades)							
235	200	SSQV	7.0	.05	.85	26.1	35.6	234	4.47	8.3
236	↓	↓	↓	↓	↓	↓	↓	↓	↓	↓
237	↓	↓	↓	↓	↓	↓	↓	↓	↓	↓
243	150	SUDV	↓	↓	↓	↓	↓	↓	↓	8.3
244	150	SSQV	↓	↓	↓	↓	↓	↓	↓	↓
245	100	SUDV	↓	↓	↓	↓	↓	↓	↓	↓
246	100	SSQV	↓	↓	↓	↓	↓	↓	↓	↓
247	200	SSQV	↓	↓	↓	↓	↓	↓	↓	↓

	Trim Data						
Case No.	Coll (Deg)	F&A Cyc (Deg)	TPP Attack (Deg)	Thrust (Lb)	HPR (Hp)	Eff Drag Area (Ft^2)	Fuse Pitch (Deg)
67	30.3	19.0	-20.5	17100.	8440.	9.6	-15.5
68	30.3	19.0	-20.5	17100.	8440.	9.6	-15.5
69	25.3	17.0	-11.7	16000.	3820.	10.6	- 8.7
70	25.3	17.0	-11.7	16000.	3820.	10.6	- 8.7
217	22.4	16.0	- 6.4	15400.	2240.	10.0	- 3.5
218	22.4	16.0	- 6.4	15400.	2240.	10.0	- 3.5
219	23.9	16.9	- 6.1	15500.	2670.	10.0	- 4.4
220	23.9	16.9	- 6.1	15500.	2670.	10.0	- 4.4
221	24.4	17.2	- 6.1	15600.	2760.	10.0	- 4.7
222	24.4	17.2	- 6.1	15600.	2760.	10.0	- 4.7
235	19.9	13.0	- 8.0	15400.	2260.	10.6	- 4.8
236	20.5	6.2	- 9.2	14700.	2700.	10.4	- 7.9
237	19.9	13.0	- 8.0	15400.	2260.	10.5	- 4.5
243	14.9	8.2	- 4.3	15200.	1300.	10.7	- 1.6
244	14.9	8.2	- 4.3	15200.	1300	10.7	- 1.6
245	12.9	5.6	- 2.1	15100.	970.	11.9	.2
246	12.9	5.6	- 2.1	15100.	970.	11.9	.2
247	19.9	13.1	- 8.1	15400.	2260.	10.5	- 4.5

TABLE XIV - Continued

(PURE SINGLE-ROTOR HELICOPTER)

Case No.	Vel (Kt)	Gust Type	Main Rotor Data: Disc Ldg	C_T/σ	M tip	Rad (Ft)	Chord (In.)	RPM	Mass Ratio	Lock No.
			Semirigid Rotor (4 Blades)							
248	200	SSQV	7.0	.05	.85	26.1	35.6	234	4.47	8.31
249	↓	SUDV	↓	↓	.85	↓	↓	↓	↓	↓
263	↓	SUDL	↓	↓	.90	↓	↓	↓	↓	↓
264	↓	SSQL	↓	↓	.90	↓	↓	↓	↓	↓
			Rigid Rotor (4 Blades)							
265	120	SUDV	4.69	.037	.857	24.	21.	300	3.25	7.3
266	↓	SSQV	↓	↓	↓	↓	↓	↓	↓	↓
267	↓	SUDV	↓	↓	↓	↓	↓	↓	↓	↓
268	↓	SSQV	↓	↓	↓	↓	↓	↓	↓	↓
			Semirigid Rotor (4 Blades)							
270	120	SSQV	4.69	.037	.857	24	21.	300.	3.25	7.3
			Articulated Rotor (4 Blades)							
278	150	SUDV	7.0	.05	.90	26.1	35.6	234	4.47	8.3
279	↓	SSQV	↓	↓	↓	↓	↓	↓	↓	8.3
280	↓	↓	↓	↓	↓	↓	↓	↓	↓	5.6
281	↓	↓	↓	↓	↓	↓	↓	↓	↓	4.4
282	175	SUDV	↓	↓	↓	↓	↓	↓	↓	8.3
283	↓	SSQV	↓	↓	↓	↓	↓	↓	↓	8.3
284	↓	↓	↓	↓	↓	↓	↓	↓	↓	5.6
285	↓	↓	↓	↓	↓	↓	↓	↓	↓	4.4
286	200	SUDV	↓	↓	↓	↓	↓	↓	↓	8.3
287	↓	SSQV	↓	↓	↓	↓	↓	↓	↓	8.3
288	↓	↓	↓	↓	↓	↓	↓	↓	↓	5.6
289	↓	↓	↓	↓	↓	↓	↓	↓	↓	4.4

Case No.	Trim Data						
	Coll (Deg)	F&A Cyc (Deg)	TPP Attack (Deg)	Thrust (Lb)	HPR (Hp)	Eff Drag Area (Ft^2)	Fuse Pitch (Deg)
248	19.9	13.1	- 8.1	15400.	2260.	10.5	- 4.5
249	20.4	6.1	-10.0	14700.	2370.	10.5	- 7.7
263	20.3	14.6	- 8.6	15300.	2590.	10.5	- 4.7
264	20.3	14.6	- 8.6	15300.	2590.	10.5	- 4.7
265	11.0	2.6	- 6.9	9090.	940.	20.6	- 4.3
266	↓	2.6	↓	9090.	↓	20.6	- 4.3
267		2.8		9070.		20.5	- 4.1
268		2.8		9070.		20.5	- 4.1
270	11.0	1.9	- 6.9	9040.	940.	20.6	- 4.9
278	14.9	6.8	- 4.1	15400.	1310.	8.4	- 2.7
279	↓	↓	↓	↓	↓	↓	↓
280							
281			- 4.2				
282	16.9	9.0	- 5.8	15600.	1740.		- 4.0
283	↓	9.0	- 5.8	↓	↓		- 4.0
284		8.9	- 5.9				- 4.1
285		8.9	- 5.9				- 4.1
286	20.3	12.3	- 8.4	15800.	2630.	8.3	- 6.0
287	↓	↓	- 8.4	↓	2630.	↓	- 6.0
288			- 8.5		2640.		- 6.1
289			- 8.6		2640.		- 6.1

TABLE XIV - Continued

(PURE SINGLE-ROTOR HELICOPTER)

Case No.	Vel (Kt)	Gust Type	Main Rotor Data: Disc Ldg	$\frac{C_T}{\sigma}$	M_{tip}	Rad (Ft)	Chord (In.)	RPM	Mass Ratio	Lock No.
			Semirigid Rotor (4 Blades)							
290	150	SUDV	7.0	.05	.90	26.1	35.6	234	4.47	8.3
291	↓	SSQV	↓	↓	↓	↓	↓	↓	↓	8.3
292		↓								5.6
293	↓									4.4
294	175	SUDV								8.3
295	↓	SSQV								8.3
296		↓								5.6
297	↓									4.4
298	200	SUDV								8.3
299	↓	SSQV								8.3
300		↓								5.6
301	↓									4.4
			Rigid Rotor (4 Blades)							
302	150	SUDV	7.0	.05	.90	26.1	35.6	234	4.47	8.3
303	↓	SSQV	↓	↓	↓	↓	↓	↓	↓	8.3
304		↓								5.6
305	↓									4.4
306	175	SUDV								8.3
307	↓	SSQV								8.3
308		↓								5.6
309	↓									4.4
310	200	SUDV								8.3
311	↓	SSQV								8.3
312		↓								5.6
313	↓		↓	↓	↓	↓	↓	↓	↓	4.4

Trim Data							
Case	Coll (Deg)	F&A Cyc (Deg)	TPP Attack (Deg)	Thrust (Lb)	HPR (Hp)	Eff Drag Area (Ft^2)	Fuse Pitch (Deg)
290	15.0	8.3	- 4.2	15200.	1320.	8.5	- 1.4
291	↓	↓	↓	↓	1320.	↓	↓
292					1310.		
293					1310.		
294	16.9	10.3	- 5.9	15300.	1720.	8.4	- 2.8
295	↓	↓	- 5.9	↓	↓	↓	↓
296			- 6.0				
297			- 6.0				
298	20.4	13.7	- 8.7		2610.		- 4.7
299	↓	↓	- 8.7		2610.		↓
300			- 8.8		2620.		
301			- 8.8		2620.	8.3	
302	14.9	6.8	- 4.1	15400.	1310.	8.4	- 2.7
303	↓	↓	↓	↓	↓	↓	↓
304							
305			- 4.2				
306	16.9	9.0	- 5.8	15600.	1740.		- 4.0
307	↓	9.0	- 5.8	↓	↓		- 4.0
308		8.9	- 5.9				- 4.1
309	17.0	8.9	- 5.9				- 4.1
310	20.3	12.3	- 8.4	15800.	2640.	8.3	- 6.0
311	↓	↓	- 8.4	↓	↓	↓	- 6.0
312			- 8.5				- 6.1
313	20.4		- 8.6				- 6.1

TABLE XV. CASE DESCRIPTIVE INFORMATION AND TRIM DATA, COMPOUND SINGLE-ROTOR HELICOPTER, No. 1

Wing: Area, 225 ft^2; Chord, 80.5 in.; Mass Ratio, 67.2

Case No.	Vel (Kt)	Gust Type	Main Rotor Data: Disc Ldg	$\frac{C_T}{\sigma}$	M_{tip}	Rad (Ft)	Chord (In.)	RPM	Mass Ratio	Lock No.
			Semirigid Rotor (4 Blades)							
71	200	SUDV	7.0	.05	.80	26.1	35.6	234.	4.47	8.31
72	200	SSQV	↓	↓	↓	↓	↓	↓	↓	↓
73	225	SUDV								
74	225	SSQV								
75	250	SUDV								
76	250	SSQV								
77	300	SUDV								
78	300	SSQV								
79	350	SUDV								
80	350	SSQV			↓					
81	200	SUDV			.85					
82	200	SSQV			↓					
83	225	SUDV								
84	225	SSQV								
85	250	SUDV								
86	250	SSQV								
87	300	SUDV								
88	300	SSQV								
89	350	SUDV								
90	350	SSQV			↓					
91	200	SUDV			.90					
92	200	SSQV			↓					
93	225	SUDV	↓	↓	↓	↓	↓	↓	↓	↓

Trim Data							
Case No.	Coll (Deg)	F&A Cyc (Deg)	TPP Attack (Deg)	Thrust (Lb)	Wing Lift (Lb)	HPR (Hp)	Fuse Pitch (Deg)
71	9.44	-2.54	-1.83	3126.	12159.	649.	- .64
72	9.44	-2.54	-1.83	3126.	12159.	649.	- .64
73	8.56	-3.26	-1.12	2662.	12694.	669.	- .09
74	8.56	-3.26	-1.12	2662.	12694.	669.	- .09
75	7.95	-3.46	-1.71	111.	15367.	605.	0.01
76	7.95	-3.46	-1.71	111.	15367.	605.	0.01
77	13.4	1.60	-2.94	5540.	10270.	734.	-1.48
78	13.4	1.60	-2.94	5540.	10270.	734.	-1.48
79	17.3	3.44	-1.44	10749.	5825.	1115.	-3.16
80	17.3	3.44	-1.44	10749.	5825.	1115.	-3.16
81	9.67	9.67	-4.25	1311.	13833.	862.	0.03
82	9.67	9.67	-4.25	1311.	13833.	862.	0.03
83	6.88	-2.99	-0.07	1671.	13335.	1038.	2.38
84	6.88	-2.99	-0.07	1671.	13335.	1038.	2.38
85	7.15	-2.68	-1.10	168.	14961.	1006.	1.80
86	7.15	-2.68	-1.10	168.	14961.	1006.	1.80
87	10.0	- .96	-2.36	1750.	13814.	1031.	-0.15
88	10.0	- .96	-2.36	1750.	13814.	1031.	-0.15
89	14.3	1.29	-1.37	7997.	8068.	1464.	-2.08
90	14.3	1.29	-1.37	7997.	8068.	1464.	-2.08
91	6.26	-3.10	-2.10	1251.	12510.	1601.	-3.50
92	6.22	-3.10	-2.10	1251.	12510.	1601.	-3.50
93	15.9	3.08	-5.29	8845.	6431.	2190.	-4.18

TABLE XV - Continued

(COMPOUND SINGLE-ROTOR HELICOPTER, No. 1)

Wing: Area, 225 ft^2; Chord, 80.5 in.; Mass Ratio, 67.2

Case No.	Vel (Kt)	Gust Type	Main Rotor Data: Disc Ldg	$\frac{C_T}{\sigma}$	M_{tip}	Rad (Ft)	Chord (In.)	RPM	Mass Ratio	Lock No.
			Semirigid Rotor (4 Blades)							
94	225	SSQV	7.0	.05	.90	26.1	35.6	234.	4.47	8.31
95	250	SUDV	↓	↓	↓	↓	↓	↓	↓	↓
96	250	SSQV								
97	300	SUDV								
98	300	SSQV								
99	350	SUDV								
100	350	SSQV			↓					
101	200	SUDV			.95					
102	200	SSQV			↓					
103	225	SUDV								
104	225	SSQV								
105	250	SUDV								
106	250	SSQV								
107	300	SUDV								
108	300	SSQV								
109	350	SUDV								
110	350	SSQV	↓	↓	↓	↓	↓	↓	↓	↓
111	200	SUDV	4.0	.02	.90	34.5	67.1	177.	1.93	8.42
112	200	SSQV	↓	↓	↓	↓	↓	↓	↓	↓
113	225	SUDV								
114	225	SSQV								
115	175	SUDV								
116	175	SSQV	↓	↓	↓	↓	↓	↓	↓	↓

Case No.	Trim Data						
	Coll (Deg)	Cyc (Deg)	TPP Attack (Deg)	Thrust (Lb)	Wing Lift (Lb)	HPR (Hp)	Fuse Pitch (Deg)
94	15.9	3.08	-5.29	8845.	6431.	2190.	-4.18
95	14.4	2.00	-3.23	8699.	6573.	2113.	-2.59
96	14.4	2.00	-3.23	8699.	6573.	2113.	-2.59
97	13.7	2.31	-3.89	3041.	12407.	1830.	-1.82
98	13.7	2.31	-3.89	3041.	12407.	1830.	-1.82
99	17.1	3.81	-1.95	8221.	7521.	2752.	-3.01
100	17.1	3.81	-1.95	8221.	7521.	2752.	-3.01
101	13.4	3.62	-6.32	2611.	12214.	2105.	-2.06
102	13.4	3.62	-6.32	2611.	12214.	2105.	-2.06
103	13.9	3.58	-5.87	2793.	12090.	2305.	-2.21
104	13.9	3.58	-5.87	2793.	12090.	2305.	-2.21
105	12.5	2.42	-5.21	-8.	14873.	2222.	-1.39
106	12.5	2.42	-5.21	-8.	14873	2222.	-1.35
107	12.5	1.69	-4.14	792.	14233.	2612.	-1.38
108	12.5	1.69	-4.14	792.	14233.	2612.	-1.38
109	17.5	4.00	-2.22	7156.	8266.	3925.	-3.74
110	17.5	4.00	-2.22	7156.	8266.	3925.	-3.74
111	19.9	15.3	-12.5	12662.	1841.	3655.	-2.98
112	19.9	15.3	-12.5	12662.	1841.	3655.	-2.98
113	23.6	19.1	-14.7	13489.	558.	4649.	-3.92
114	23.6	19.1	-14.7	13489.	558.	4649.	-3.92
115	16.6	12.3	-10.4	11776.	2943.	2781.	-1.83
116	16.6	12.3	-10.4	11776.	2943.	2781.	-1.83

TABLE XV - Continued

(COMPOUND SINGLE-ROTOR HELICOPTER, No. 1)

Wing: Area, 225 ft^2; Chord, 80.5 in.; Mass Ratio, 67.2

Case No.	Vel (Kt)	Gust Type	Main Rotor Data: Disc Ldg	$\frac{C_T}{\sigma}$	M_{tip}	Rad (Ft)	Chord (In.)	RPM	Mass Ratio	Lock No.
			Semirigid Rotor (4 Blades)							
117	200	SUDV	4.0	.05	.90	34.5	26.9	177.	1.93	10.3
118	200	SSQV	↓	↓	↓	↓	↓	↓	↓	↓
119	225	SUDV								
120	225	SSQV								
121	175	SUDV								
122	175	SSQV								
123	200	SUDV	10.0	.02		21.8	106.2	280.	7.64	5.04
124	200	SSQV	↓	↓		↓	↓	↓	↓	↓
125	225	SUDV								
126	225	SSQV								
127	175	SUDV								
128	175	SSQV								
129	200	SUDV		.05			42.5			7.10
130	200	SSQV		↓			↓			↓
131	225	SUDV								
132	225	SSQV								
133	175	SUDV								
134	175	SSQV	↓	↓	↓	↓	↓	↓	↓	↓
			Articulated Rotor (4 Blades)							
135	200	SUDV	4.0	.02	.90	34.5	67.1	177.	1.93	8.42
136	↓	SSQV	↓	.02	↓	↓	67.1	↓	↓	8.42
137		SUDV		.05			26.9			10.27
138		SSQV		.05			26.9			10.27

Case No.	Trim Data						
	Coll (Deg)	Cyc (Deg)	TPP Attack (Deg)	Thrust (Lb)	Wing Lift (Lb)	HPR (Hp)	Fuse Pitch (Deg)
117	17.1	10.9	-5.38	12334.	2709.	1754.	-2.60
118	17.1	10.9	-5.38	12334.	2709.	1754.	-2.60
119	20.3	13.6	-7.24	14561.	538.	2262.	-3.92
120	20.3	13.6	-7.24	14561.	538.	2262.	-3.92
121	14.2	8.39	-4.77	11062.	3926.	1290.	-1.19
122	14.2	8.39	-4.77	11062.	3926.	1290.	-1.19
123	20.4	17.4	-13.4	11406.	3255.	3450.	-2.43
124	20.4	17.4	-13.4	11406.	3255.	3450.	-2.43
125	22.5	19.4	-14.0	10670.	3599.	3475.	2.49
126	22.5	19.4	-14.0	10670.	3599.	3475.	2.49
127	19.3	21.0	-15.4	7628.	7037.	2744.	1.12
128	19.3	21.0	-15.4	7628.	7037.	2744.	1.12
129	17.1	11.9	-16.5	11047.	3949.	1728.	-1.87
130	17.1	11.9	-16.5	11047.	3949.	1728.	-1.87
131	20.7	15.0	-8.10	13216.	1723.	2888.	-3.38
132	20.7	15.0	-8.10	13216.	1723.	2888.	-3.38
133	14.7	9.27	-4.80	10656.	4333.	1358.	-0.87
134	14.7	9.27	-4.80	10656.	4333.	1358.	-0.87
135	13.9	6.72	-5.44	13797.	1921.	2688.	-2.94
136	13.9	6.72	-5.44	13797.	1921.	2688.	-2.94
137	16.9	9.52	-4.40	14271.	1135.	1798.	-3.50
138	16.9	9.52	-5.40	14271.	1135.	1798.	-3.50

TABLE XV - Continued

(COMPOUND SINGLE-ROTOR HELICOPTER, No. 1)

Wing: Area, 225 ft^2; Chord, 80.5 in.; Mass Ratio, 67.2

Case No.	Vel (Kt)	Gust Type	Main Rotor Data: Disc Ldg	$\frac{C_T}{\sigma}$	M_{tip}	Rad (Ft)	Chord (In.)	RPM	Mass Ratio	Lock No.
			Articulated Rotor (4 Blades)							
139	200	SUDV	7.0	.02	.90	26.1	89.0	234.	4.47	6.58
140	↓	SSQV	↓	.02	↓	↓	89.0	↓	↓	6.58
141	↓	SUDV	↓	.05	↓	↓	35.6	↓	↓	8.31
142	↓	SSQV	↓	.05	↓	↓	35.6	↓	↓	8.31
143	↓	SUDV	10.0	.02	↓	21.8	106.2	280.	7.64	5.04
144	↓	SSQV	↓	.02	↓	↓	106.2	↓	↓	5.04
145	↓	SUDV	↓	.05	↓	↓	42.5	↓	↓	7.10
146	↓	SSQV	↓	.05	↓	↓	42.5	↓	↓	7.10
			Rigid Rotor (4 Blades)							
147	200	SUDV	4.0	.02	.90	34.5	67.1	177.	1.93	8.42
148	↓	SSQV	↓	.02	↓	↓	67.1	↓	↓	8.42
149	↓	SUDV	↓	.05	↓	↓	26.9	↓	↓	10.27
150	↓	SSQV	↓	.05	↓	↓	26.9	↓	↓	10.27
151	↓	SUDV	7.0	.02	↓	26.1	89.0	234.	4.47	6.58
152	↓	SSQV	↓	.02	↓	↓	89.0	↓	↓	6.58
153	↓	SUDV	↓	.05	↓	↓	35.6	↓	↓	8.31
154	↓	SSQV	↓	.05	↓	↓	35.6	↓	↓	8.31
155	↓	SUDV	10.0	.02	↓	21.8	106.2	280.	7.64	5.04
156	↓	SSQV	↓	.02	↓	↓	106.2	↓	↓	5.04
157	↓	SUDV	↓	.05	↓	↓	42.5	↓	↓	7.10
158	↓	SSQV	↓	.05	↓	↓	42.5	↓	↓	7.10
			Articulated Rotor (4 Blades)							
159	250	SUDV	7.0	.02	.90	26.1	89.0	234.	4.47	6.54
160	↓	SSQV	↓	.02	↓	↓	89.0	↓	↓	6.54
161	↓	SUDV	↓	.05	↓	↓	35.6	↓	↓	8.31

Case No.	Trim Data						
	Coll (Deg)	Cyc (Deg)	TPP Attack (Deg)	Thrust (Lb)	Wing Lift (Lb)	HPR (Hp)	Fuse Pitch (Deg)
139	16.4	10.1	-8.92	13353.	2477.	3864.	-4.25
140	16.4	10.1	-8.92	13353.	2477.	3864.	-4.25
141	16.9	8.57	-4.54	15299.	373.	2413.	-3.79
142	16.9	8.57	-4.54	15299.	373.	2413.	-3.79
143	16.8	8.88	-7.05	15963.	266.	3280.	-3.94
144	16.8	8.88	-7.05	15963.	266.	3280.	-3.94
145	16.9	9.86	-5.13	13198.	2267.	1812.	-2.80
146	16.9	9.86	-5.13	13198.	2267.	1812.	-2.80
147	13.8	6.72	-5.44	13980.	1921.	2688.	-2.94
148	13.8	6.72	-5.44	13980.	1921.	2688.	-2.94
149	16.7	10.7	-6.17	11887.	3124.	1680.	-2.36
150	16.7	10.7	-6.17	11887.	3124.	1680.	-2.36
151	16.5	10.4	-9.13	13120.	2647.	3859.	-4.16
152	16.5	10.4	-9.13	13120.	2647.	3859.	-4.16
153	16.9	8.57	-4.54	15299.	373.	2413.	-3.79
154	16.9	8.57	-4.54	15299.	373.	2413.	-3.79
155	15.4	5.21	-6.21	15322.	840.	3060.	-3.61
156	15.4	5.21	-6.21	15322.	840.	3060.	-3.61
157	16.9	9.86	-5.12	13200.	2267.	1812.	-2.80
158	16.9	9.86	-5.12	13200.	2207.	1812.	-2.80
159	22.4	16.9	-12.2	14300.	840.	5700.	-5.4
160	22.4	16.9	-12.2	14300.	840.	5700.	-5.4
161	16.7	8.9	-3.4	13100.	2600.	2600.	-3.1

TABLE XV - Continued

(COMPOUND SINGLE-ROTOR HELICOPTER, No. 1)

Wing: Area, 225 ft^2; Chord, 80.5 in.; Mass Ratio, 67.2

Case No.	Vel (Kt)	Gust Type	Main Rotor Data: Disc Ldg	$\frac{C_T}{\sigma}$	M_{tip}	Rad (Ft)	Chord (In.)	RPM	Mass Ratio	Lock No.
			Articulated Rotor (4 Blades)							
162	250	SSQV	7.0	.05	.90	26.1	35.6	234.	4.47	8.31
163	240	SUDV	4.0	.02		34.5	67.1	177.	1.93	8.42
164	240	SSQV	↓	.02	↓	↓	67.1	↓	↓	8.42
165	250	SUDV	↓	.05	↓	↓	26.9	↓	↓	10.3
166	↓	SSQV	↓	.05	↓	↓	26.9	↓	↓	10.3
169	↓	SUDV	10.0	.05	↓	21.8	42.5	280.	7.64	7.1
170	↓	SSQV	10.0	.05	↓	21.8	42.5	280.	7.64	7.1
			Rigid Rotor (4 Blades)							
171	250	SUDV	7.0	.02	.90	26.1	89.0	234.	4.47	6.54
172	↓	SSQV	↓	.02	↓	↓	89.0	↓	↓	6.54
173	↓	SUDV	↓	.05	↓	↓	35.6	↓	↓	8.31
174	↓	SSQV	↓	.05	↓	↓	35.6	↓	↓	8.31
175	240	SUDV	4.0	.02	↓	34.5	67.1	177.	1.93	8.42
176	240	SSQV	↓	.02	↓	↓	67.1	↓	↓	8.42
177	250	SUDV	↓	.05	↓	↓	26.9	↓	↓	10.3
178	↓	SSQV	↓	.05	↓	↓	26.9	↓	↓	10.3
181	↓	SUDV	10.0	.05	↓	21.8	42.5	280.	7.64	7.1
182	↓	SSQV	10.0	.05	↓	21.8	42.5	280.	7.64	7.1
			Semirigid Rotor (4 Blades)							
223	200	SUDV	7.0	.10	.90	26.1	17.8	234.	4.47	4.14
224	200	SSQV	↓	↓	↓	↓	↓	↓	↓	↓
225	250	SUDV	↓	↓	↓	↓	↓	↓	↓	↓
226	250	SSQV	↓	↓	↓	↓	↓	↓	↓	↓

Case No.	Trim Data						
	Coll (Deg)	Cyc (Deg)	TPP Attack (Deg)	Thrust (Lb)	Wing Lift (Lb)	HPR (Hp)	Fuse Pitch (Deg)
162	16.7	8.9	-3.4	13100.	2600.	2600.	-3.1
163	12.4	6.6	-4.3	7500.	8200.	2400.	-1.0
164	12.4	6.6	-4.3	7500.	8200.	2400.	-1.0
165	16.0	9.5	-4.3	9800.	5600.	1500.	-2.1
166	16.0	9.5	-4.3	9800.	5600.	1500.	-2.1
169	17.8	10.8	-4.7	11800.	3500.	1900.	-2.8
170	17.8	10.8	-4.7	11800.	3500.	1900.	-2.8
171	22.7	17.6	-12.6	14100.	870.	5800.	-5.4
172	22.7	17.6	-12.6	14100.	870.	5800.	-5.4
173	16.7	8.9	-3.4	13100.	2600.	2600.	-3.1
174	16.7	8.9	-3.4	13100.	2600.	2600.	-3.1
175	12.4	6.6	-4.3	7500.	8200.	2400.	-1.0
176	12.4	6.6	-4.3	7500.	8200.	2400.	-1.0
177	16.0	9.5	-4.3	9600.	5600.	1500.	-2.1
178	16.0	9.5	-4.3	9600.	5600.	1500.	-2.1
181	17.8	10.8	-4.7	11800.	3500.	1900.	-2.8
182	17.8	10.8	-4.7	11800.	3500.	1900.	-2.8
223	18.0	12.5	-4.3	10000.	5200.	1100.	-1.2
224	18.0	12.5	-4.3	10000.	5200.	1100.	-1.2
225	28.7	20.3	1.5	13500.	1500.	3900.	-3.6
226	28.7	20.3	1.5	13500.	1500.	3900.	-3.6

TABLE XV - Continued

(COMPOUND SINGLE-ROTOR HELICOPTER, No. 1)

Wing: Area, 225 ft^2; Chord, 80.5 in.; Mass Ratio, 67.2

Case No.	Vel (Kt)	Gust Type	Main Rotor Data: Disc Ldg	$\frac{C_T}{\sigma}$	M_{tip}	Rad (Ft)	Chord (In.)	RPM	Mass Ratio	Lock No.
			Rigid Rotor (4 Blades)							
227	200	SUDV	7.0	.10	.90	26.1	17.8	234.	4.47	4.14
228	200	SSQV	↓	↓	↓	↓	↓	↓	↓	↓
229	250	SUDV	↓	↓	↓	↓	↓	↓	↓	↓
230	250	SSQV	↓	↓	↓	↓	↓	↓	↓	↓
			Articulated Rotor (3 Blades)							
231	200	SUDV	7.0	.10	.90	26.1	23.7	234.	4.47	4.14
232	200	SSQV	↓	↓	↓	↓	↓	↓	↓	↓
233	250	SUDV	↓	↓	↓	↓	↓	↓	↓	↓
234	250	SSQV	↓	↓	↓	↓	↓	↓	↓	↓

Case No.	Trim Data						
	Coll (Deg)	Cyc (Deg)	TPP Attack (Deg)	Thrust (Lb)	Wing Lift (Lb)	HPR (Hp)	Fuse Pitch (Deg)
227	20.2	12.2	-2.6	13600.	2100.	1500.	-2.9
228	20.2	12.2	-2.6	13600.	2100.	1500.	-2.9
229	27.6	20.3	- .4	12300.	2400.	3200.	-3.3
230	27.6	20.3	- .4	12300.	2400.	3200.	-3.3
231	20.6	12.6	-2.1	13600.	2000.	1500.	-2.9
232	20.6	12.6	-2.1	13600.	2000.	1500.	-2.9
233	26.7	19.3	- .3	12300.	2500.	3000.	-3.2
234	26.7	19.3	- .3	12300.	2500.	3000.	-3.2

TABLE XVI. CASE DESCRIPTIVE INFORMATION AND TRIM DATA, COMPOUND SINGLE-ROTOR HELICOPTER, NO. 2

Wing: Area, 27.8 ft^2; Chord, 45.0 in.; Mass Ratio, 81.5

Case No.	Vel (Kt)	Gust Type	Main Rotor Data: Disc Ldg	$\frac{C_T}{\sigma}$	M_{tip}	Rad (Ft)	Chord (In.)	RPM	Mass Ratio	Lock No.
			Semirigid Rotor (2 Blades)							
238	150	SSQV	5.6	.064	.86	22.	27.	324.	4.24	5.03
239	↓	↓	↓	↓	↓	↓	↓	↓	↓	↓
240										
250		SUDV								
251		SEDV								
252		SUDV								
253		SEDV								
254		SSQV								
255		RMPV								
256		RMPV								
257		SSQV								
258		RFTP								
259		SSQV								
260		↓								
261										
262		SUDV								
269		SEDV								
275		SSQV								
276		↓								
277	↓		↓	↓	↓	↓	↓	↓	↓	↓

Case No.	Trim Data						
	Coll (Deg)	F&A Cyc (Deg)	TPP Attack (Deg)	Thrust (Lb)	Wing Lift (Lb)	HPR (Hp)	Fuse Pitch (Deg)
238	16.3	6.7	-8.3	7700.	850.	950.	-6.9
239	↓	↓	↓	↓	↓	↓	↓
240	↓	↓	↓	↓	↓	↓	↓
250	↓	↓	↓	↓	↓	↓	↓
251	↓	↓	↓	↓	↓	↓	↓
252	↓	↓	↓	↓	↓	↓	↓
253	↓	↓	↓	↓	↓	↓	↓
254	↓	↓	↓	↓	↓	↓	↓
255	↓	↓	↓	↓	↓	↓	↓
256	↓	↓	↓	↓	↓	↓	↓
257	↓	↓	↓	↓	↓	↓	↓
258	↓	↓	↓	↓	↓	↓	↓
259	↓	↓	↓	↓	↓	↓	↓
260	↓	↓	↓	↓	↓	↓	↓
261	↓	↓	↓	↓	↓	↓	↓
262	↓	↓	↓	↓	↓	↓	↓
269	↓	↓	↓	↓	↓	↓	↓
275	↓	↓	↓	↓	↓	↓	↓
276	↓	↓	↓	↓	↓	↓	↓
277	↓	↓	↓	↓	↓	↓	↓

TABLE XVII. CASE DESCRIPTIVE INFORMATION AND TRIM DATA, TANDEM-ROTOR HELICOPTER

Case No.	Vel (Kt)	Gust Type	Main Rotor Data: Disc Ldg	$\frac{C_T}{\sigma}$	M_{tip}	Rad (Ft)	Chord (In.)	RPM	Mass Ratio	Lock No.
			Aft CG (4 Blades)							
183	200.	SUDV	7.	.02	.90	18.35	57.6	348.	6.43	5.61
184	↓	SSQV	↓	.02	↓	↓	57.6	↓	↓	↓
185	↓	SUDV	↓	.05	↓	↓	23.0	↓	↓	↓
186	↓	SSQV	↓	.05	↓	↓	23.0	↓	↓	↓
187	225.	SUDV	↓	.02	↓	↓	57.6	↓	↓	↓
188	↓	SSQV	↓	.02	↓	↓	57.6	↓	↓	↓
189	↓	SUDV	↓	.05	↓	↓	23.0	↓	↓	↓
190	↓	SSQV	↓	.05	↓	↓	23.0	↓	↓	↓
			Neutral CG (4 Blades)							
272	200.	SSQV	7.	.05	.90	18.35	23.0	348.	6.43	5.61
			Forward CG (4 Blades)							
274	200.	SSQV	7.	.05	.90	18.35	23.0	348.	6.43	5.61

Trim Data								
	Forward Rotor			Aft Rotor				
Case No.	Coll (Deg)	Thrust (Lb)	TPP Attack (Deg)	Coll (Deg)	Thrust (Lb)	TPP Attack (Deg)	F&A Cyc (Deg)	Fuse Pitch (Deg)
183	22.4	7700.	-15.7	22.4	7300.	-14.2	18.0	- 8.2
184	22.4	7700.	-15.7	22.4	7300.	-14.2	18.0	- 8.2
185	20.7	7100.	- 9.8	20.7	7900.	- 7.0	19.7	- 0.7
186	20.7	7100.	- 9.8	20.7	7900.	- 7.0	19.7	- 0.7
187	27.0	7600.	-19.2	27.0	7600.	-17.8	20.6	-12.2
188	27.0	7600.	-19.2	27.0	7600.	-17.8	20.6	-12.2
189	25.3	7400.	-12.3	25.3	7700.	- 8.9	26.8	- 1.0
190	25.3	7400.	-12.3	25.3	7700.	- 8.9	26.8	- 1.0
272	20.3	7800.	- 8.57	20.3	7400.	- 7.6	1.2	- 6.1
274	20.1	8650.	- 7.6	20.1	6700.	- 8.4	6.6	-11.1

TABLE XVIII. CASE DESCRIPTIVE INFORMATION AND TRIM DATA, SIDE-BY-SIDE HELICOPTER

Wing: Area, 330.5 ft^2; Chord, 80 in.; Mass Ratio, 67.6

Case No.	Vel (Kt)	Gust Type	Main Rotor Data: Disc Ldg	$\frac{C_T}{\sigma}$	M_{tip}	Rad (Ft)	Chord (In.)	RPM	Mass Ratio	Lock No.
			Helicopter Mode (3 Blades)							
199	120.	SSQV	9.87	.105	.9	19.25	20.	408.	67.6	5.39
200	150.	SSQV	9.87	.105	.9	19.25	20.	408.	67.6	5.39
			Transition Mode (3 Blades)							
201	120.	SSQV	9.87	.105	.9	19.25	20.	408.	67.6	5.39
202	120.	SSQV	↓	↓	↓	↓	↓	↓	↓	↓
203	150.	SSQV	↓	↓	↓	↓	↓	↓	↓	↓
204	150.	SSQV	↓	↓	↓	↓	↓	↓	↓	↓
			Airplane Mode (3 Blades)							
205	120.	SUDV	9.87	.105	.9	19.25	20.	408.	67.6	5.39
206	120.	SSQV	↓	↓	↓	↓	↓	↓	↓	↓
207	150.	SUDV	↓	↓	↓	↓	↓	↓	↓	↓
208	150.	SSQV	↓	↓	↓	↓	↓	↓	↓	↓
209	200.	SUDV	↓	↓	↓	↓	↓	↓	↓	↓
210	200.	SSQV	↓	↓	↓	↓	↓	↓	↓	↓
211	300.	SUDV	↓	↓	↓	↓	↓	↓	↓	↓
212	300.	SSQV	↓	↓	↓	↓	↓	↓	↓	↓
213	400.	SUDV	↓	↓	↓	↓	↓	↓	↓	↓
214	400.	SSQV	↓	↓	↓	↓	↓	↓	↓	↓

Trim Data							
Case No.	Coll (Deg)	F&A Cyc (Deg)	TPP Attack (Deg)	Thrust Per Rotor (Lb)	Wing Lift (Lb)	HPR (Hp)	Fuse Pitch (Deg)
199	30.3	7.3	- 6.8	11600.	440.	3330.	-5.1
200	33.0	8.4	- 8.3	13900.	-316.	5000.	-7.8
201	32.2	3.6	-20.1	4600.	13000.	1760.	4.3
202	37.1	.9	-45.6	2000.	17900.	1740.	7.9
203	35.3	5.3	-24.4	5340.	11800.	3860.	- .8
204	42.0	2.1	-51.0	1240.	18400.	1490.	2.4
205	60.2	0.	-71.1	1990.	20300.	1940.	14.4
206	60.2		-71.1	1990.	20300.	1940.	14.4
207	65.4		-84.5	850.	22300.	1460.	4.4
208	65.4		-84.5	850.	22300.	1460.	4.4
209	73.4		-90.8	980.	24100.	2080.	- .6
210	73.4		-90.8	980.	24100.	2080.	- .6
211	83.6		-93.3	1790.	29900.	4370.	-4.2
212	83.6		-93.3	1790.	29900.	4370.	-4.2
213	89.7		-94.3	2880.	34600.	8920.	-5.7
214	89.7		-94.3	2880.	34600.	8920.	-5.7

TABLE XIX. PARAMETERS FOR STOPPED-ROTOR ANALYSIS

R O T O R

Number of Blades 2 Radius 33.2 ft
Chord 15 in.

Blade Segment (% R)	Beamwise Stiffness (10^6 lb-in^2)	Weight/in. (lb/in.)
0-16.7	14000	15
16.7-33.3	2000	2.4
33.3-50.0	600	1.6
50.0-66.7	600	1.5
66.7-83.3	600	1.5
83.3-100.	600	1.5

M A S T

Mast Segment (% Length from Base)	Bending Stiffness (10^6 lb-in^2)	Length 8.3 ft Weight/ft (lb/ft)
0-33.3	80000	3
33.3-66.7	150	150
66.7-100.	100	3

TABLE XX. PARAMETERS FOR TRAILED-ROTOR ANALYSIS

ROTOR

Number of Blades 3

Radius 230 in.
Chord 21 in.

Blade Segment (% R)	Beamwise Stiffness (10^6 lb-in^2)	Weight/in. (lb/in.)
0-25	4500	4.07
25-50	1700	2.0
50-75	250	2.28
75-100	90	1.72

WING

Span 240 in.
Chord 85.3 73.3 in.

Wing Segment (% Semi-span)	Beamwise Stiffness (10^9 lb-in^2)	Torsional Stiffness (10^9 lb-in^2)	Weight/in. (lb/in.)	Inertia (lb-in-sec^2)
0-16.7	13	9.8	13.7	122,000
16.7-33.3	11.3	8.6	12.5	106,000
33.3-50.0	8	6.8	11.5	91.000
50.0-66.7	5	5.1	10.4	76,000
66.7-83.3	3	4.0	9.8	68,000
83.3-100.	Rigid	Rigid	1576	4,990,000

APPENDIX III. GUST RESPONSE CASE RESULTS

TABLE XXI. GUST-RESPONSE CASE RESULTS, PURE SINGLE-ROTOR HELICOPTER

Case No.	Gust Type: Shape	Gust Type: Length (Ft)	Gust Type: Max Vel (Ft/Sec)	Max Blade Root Osc Moment Ratio M_{gust}/M_{steady}: Beam	Max Blade Root Osc Moment Ratio M_{gust}/M_{steady}: Chord	Max Flap Velocity (Deg/Sec)
	Semirigid Rotor					
1	SUDV	0.	50.	0.86	1.80	58.1
2	SSQV	90.		1.67	3.15	25.6
3	SUDV	0.		0.63	1.54	60.1
4	SSQV	90.		1.38	2.64	27.7
5	SUDV	0.		0.79	1.79	59.5
6	SSQV	90.		1.64	3.05	25.8
7	SUDV	0.		0.57	1.46	61.3
8	SSQV	90.		1.28	2.50	27.7
9	SUDV	0.		0.74	2.40	61.0
10	SSQV	90.		1.58	3.57	26.3
11	SUDV	0.		0.50	1.73	63.0
12	SSQV	90.		1.11	2.57	27.9
13	SUDV	0.		0.71	2.57	62.5
14	SSQV	90.		1.29	3.34	27.3
15	SUDV	0.		0.44	1.61	65.7
16	SSQV	90.		0.76	2.10	28.9
17	SUDV	0.		0.91	1.27	32.4
18	SSQV	90.		1.54	4.10	12.3
19	SUDV	0.		0.99	1.04	28.8
20	SSQV	90.		1.87	2.83	10.8
21	SUDV	0.		0.85	3.40	55.8
22	SSQV	90.		1.90	8.00	25.4
23	SUDV	0.		0.63	1.45	57.9
24	SSQV	90.		1.44	4.28	27.1

Case No.	Max Rotor Thrust (Lb)	Max Δn (g)	Gust-Allev Factor (K_g)	Comments
1	40500.	1.81		
2	29000.	0.98	.543	
3	39900.	1.77		
4	28300.	0.93	.524	
5	41000.	1.84		
6	28900.	0.96	.529	
7	40400.	1.81		
8	28100.	0.92	.506	
9	41200.	1.87		
10	28700.	0.97	.516	
11	40500.	1.81		
12	28100.	0.92	.490	
13	40600	1.82		
14	28500.	0.94	.522	
15	39100.	1.73		
16	27700.	0.89	.519	
17	92700.	5.19		
18	51400.	2.39	.471	
19	98600.	5.61		
20	52700.	2.51	.447	
21	42100.	1.91		
22	30000.	1.03	.547	
23	40400.	1.79		
24	29200.	0.98	.555	

TABLE XXI - Continued
(PURE SINGLE-ROTOR HELICOPTER)

Case No.	Gust Type Shape	Length (Ft)	Max Vel (Ft/Sec)	Max Blade Root Osc Moment Ratio M_{gust}/M_{steady} Beam	Chord	Max Flap Velocity (Deg/Sec)
	Semirigid Rotor (Cont'd)					
25	SUDV	0.	50.	0.83	1.10	35.4
26	SSQV	90.		1.50	3.53	12.0
27	SUDV	0.		0.90	1.10	35.0
28	SSQV	90.		1.84	3.56	9.8
29	SUDV	0.		0.88	3.92	60.9
30	SSQV	90.		1.67	7.08	27.1
31	SUDV	0.		0.80	2.10	63.7
32	SSQV	90.		1.17	2.46	29.7
33	RMPV	90.		1.62	3.64	21.0
34	RMPV	90.		1.16	2.45	22.1
35	SUDH	0.		0.90	1.15	2.46
36	SSQH	90.		1.11	1.70	2.87
37	SUDH	0.		0.90	0.78	1.84
38	SSQH	90.		0.98	2.02	7.25
	Articulated Rotor					
39	SUDV	0.	50.	1.81	1.27	35.2
40	SSQV	90.		1.64	1.35	15.6
41	SUDV	0.		24.1	2.43	55.0
42	SSQV	90.		2.33	3.18	28.3
43	SUDV	0.		16.1	2.08	35.5
44	SSQV	90.		0.93	1.93	14.9
45	SUDV	0.		22.3	1.62	16.0
46	SSQV	90.		3.59	2.38	26.7
47	SUDV	0.		13.2	2.28	34.6

Case No.	Max Rotor Thrust (Lb)	Max Δn (g)	Gust-Allev Factor (K_g)	Comments
25	94100.	5.32		
26	50200.	2.33	.445	
27	96700.	5.43		
28	47200.	2.12	.393	
29	40300.	1.79		
30	28600	0.94	.531	
31	39800.	1.76		
32	28200.	0.91	.523	
33	27300.	0.90	.483	K_g obtained based on Case 9
34	26700.	0.80	.441	K_g obtained based on Case 10
35	10700.	-0.30		
36	18200.	0.20	.609	
37	9900.	-0.40		
38	18600.	0.22	.550	
39	93800.	5.22		
40	56700.	2.65	.521	
41	42400.	1.90		
42	30800.	1.07	.565	
43	94700.	5.30		
44	55100.	2.56	.492	
45	41500.	1.84		
46	29300.	0.96	.522	
47	95000.	5.31		

TABLE XXI - Continued
(PURE SINGLE-ROTOR HELICOPTER)

Case No.	Gust Type Shape	Length (Ft)	Max Vel (Ft/Sec)	Max Blade Root Osc Moment Ratio M_{gust}/M_{steady} Beam	Chord	Max Flap Velocity (Deg/Sec)
	Articulated Rotor (Cont'd)					
48	SSQV	90.	50.	1.17	3.12	12.6
49	SUDV	0.	↓	20.9	1.82	59.6
50	SSQV	90.	↓	4.61	2.60	25.9
	Rigid Rotor					
51	SUDV	0.	50.	6.45	4.85	35.2
52	SSQV	90.	↓	3.01	2.90	16.2
53	SUDV	0.	↓	6.72	1.28	55.0
54	SSQV	90.	↓	4.16	9.32	25.9
55	SUDV	0.	↓	4.74	2.69	35.5
56	SSQV	90.	↓	1.36	2.47	14.3
57	SUDV	0.	↓	6.56	7.06	60.0
58	SSQV	90.	↓	4.21	4.28	19.8
59	SUDV	0.	↓	66.2	5.24	34.6
60	SSQV	90.	↓	2.24	2.09	13.1
61	SUDV	0.	↓	7.20	6.92	59.6
62	SSQV	90.	↓	1.83	5.25	26.8
	Articulated Rotor					
63	SUDV	0.	50.	12.3	1.52	40.3
64	SSQV	90.	↓	1.12	1.79	18.1
65	SUDV	0.	↓	17.2	1.22	60.6
66	SSQV	90.	↓	3.51	1.64	28.4
	Rigid Rotor					
67	SUDV	0.	50.	3.97	3.96	40.3
68	SSQV	90.	↓	1.31	2.55	15.3

Case No.	Max Rotor Thrust (Lb)	Max Δn (g)	Gust-Allev Factor (K_g)	Comments
48	50000.	2.21	.425	
49	40400.	1.77		
50	28100.	0.88	.500	
51	93800.	5.22		
52	59000.	2.81	.551	
53	42400.	1.90		
54	30000.	1.02	.537	
55	94700.	5.30		
56	55000.	2.55	.491	
57	41500.	1.84		
58	26700.	0.81	.440	
59	94900.	5.31		
60	51600.	2.32	.447	
61	40400.	1.77		
62	28500.	0.91	.518	
63	86100.	4.67		
64	53400.	2.37	.525	
65	40800.	1.79		
66	29000.	0.93	.526	
67	86100.	4.67		
68	50400.	2.18	.483	

TABLE XXI - Continued
(PURE SINGLE-ROTOR HELICOPTER)

Case No.	Gust Type			Max Blade Root Osc Moment Ratio M_{gust}/M_{steady}		Max Flap Velocity (Deg/Sec)
	Shape	Length (Ft)	Max Vel (Ft/Sec)	Beam	Chord	
	Rigid Rotor (Cont'd)					
69	SUDV	0.	50.	3.70	2.33	62.1
70	SSQV	90.	↓	3.84	6.35	17.3
	Semirigid Rotor					
217	SUDV	0.	50.	1.05	2.75	108.
218	SSQV	90.	50.	1.40	6.11	40.
	Rigid Rotor					
219	SUDV	0.	50.	3.96	2.35	101.
220	SSQV	90.	50.	4.99	7.15	12.
	Articulated Rotor					
221	SUDV	0.	50.	17.73	1.56	82.
222	SSQV	90.	50.	8.57	1.91	34.
	Semirigid Rotor					
235	SSQV	90.	50.	1.85	3.28	24.6
236	↓	↓	↓	2.40	2.85	17.7
237	↓	↓	↓	1.75	2.62	18.8
243	SUDV	0.	↓	1.34	2.67	47.5
244	SSQV	90.	↓	2.61	4.35	16.9
245	SUDV	0.	↓	1.79	2.95	31.2
246	SSQV	90.	↓	1.95	4.35	6.2
247	↓	↓	↓	1.55	4.25	48.0
248	↓	↓	↓	1.77	2.99	27.5
249	SUDV	0.	↓	.82	2.33	94.8

Case No.	Max Rotor Thrust (Lb)	Max Δn (g)	Gust-Allev Factor (K_g)	Comments
69	40800.	1.79		
70	24400.	0.64	.36	
217	30300.	1.13		
218	22200.	0.54	.48	
219	29300.	1.05		
220	18200.	0.28	.27	
221	29100.	1.04		
222	23600.	0.62	.60	
235	28500.	0.95	*.51	$\delta_3 = 30^o$
236	26100.	0.83	*.45	Pitch Cone Coupling Ratio= -.5
237	26800.	0.84	*.45	Bob Weight =1 Deg/g
243	40300.	1.78		
244	29600.	1.01	.57	
245	40000.	1.72		
246	30400.	1.05	.61	
247	34800.	1.34	*.73	Pitch-Cone Coupling Ratio= .5
248	29100.	0.99	*.53	$\delta_3 = 0.$
249	40200.	1.85		$\delta_3 = 0.$, No Pitch-Cone Coupling

*Based on case number 249.

TABLE XXI - Continued

(PURE SINGLE-ROTOR HELICOPTER)

Case No.	Gust Type			Max Blade Root Osc Moment Ratio M_{gust}/M_{steady}		Max Flap Velocity (Deg/Sec)
	Shape	Length (Ft)	Max Vel (Ft/Sec)	Beam	Chord	
	Semirigid Rotor (Cont'd)					
263	SUDL	0.	50.	1.04	.94	18.0
264	SSQL	90.	↓	1.08	1.88	4.7
	Rigid Rotor					
265	SUDV	0.	50.	29.4	2.46	39.3
266	SSQV	90.		10.3	2.23	18.8
267	SUDV	0.		27.6	2.45	37.6
268	SSQV	90.	↓	16.2	2.44	26.7
	Semirigid Rotor					
270	SUDV	90.	50.	1.48	1.83	15.4
	Articulated Rotor					
278	SUDV	0.	-50.			66.0
279	SSQV	90.				17.1
280	↓	↓				14.5
281						12.5
282	SUDV	0.				75.9
283	SSQV	90.				22.8
284	↓	↓				19.6
285						17.1
286	SUDV	0.				83.2
287	SSQV	90.				27.9
288	↓	↓				24.7
289			↓			21.6

No.	Max Rotor Thrust (Lb)	Max Δn (g)	Gust-Allev Factor (K_g)	Comments
263	18900.	0.22		Horizontal Side Gust
264	18700.	0.21	.95	Horizontal Side Gust
265	29500.	2.58		Low Hub Spring, 1260 Ft-Lb/Deg
266	24300.	1.95	.76	Low Hub Spring, 1260 Ft-Lb/Deg
267	29400.	2.58		High Hub Spring, 3625 Ft-Lb/Deg
268	26400.	2.21	.85	High Hub Spring, 3625 Ft-Lb/Deg
270	23500.	1.84		
278	40500	1.78	-	Blade loads data not valid
279	30200	1.03	.58	for Cases 278-313 because of
280	31400	1.11	.62	resonance conditions.
281	32300	1.17	.66	
282	41000	1.81	-	
283	30100	1.02	.56	
284	31500	1.12	.62	
285	32600	1.19	.66	
286	41300	1.83	-	
287	29800	1.00	.55	
288	31500	1.11	.61	
289	32700	1.19	.65	

TABLE XXI - Continued

(PURE SINGLE-ROTOR HELICOPTER)

Case No.	Gust Type			Max Blade Root Osc Moment Ratio M_{gust}/M_{steady}		Max Flap Velocity (Deg/Sec)
	Shape	Length (Ft)	Max Vel (Ft/Sec)	Beam	Chord	
	Semirigid Rotor					
290	SUDV	0.	-50.			65.3
291	SSQV	90.				18.4
292	↓	↓				15.5
293	↓	↓				13.4
294	SUDV	0.				77.2
295	SSQV	90.				24.1
296	↓	↓				20.7
297	↓	↓				18.3
298	SUDV	0.				84.7
299	SSQV	90.				29.2
300	↓	↓				25.6
301	↓	↓	↓			22.6
	Rigid Rotor					
302	SUDV	0.	-50.			66.0
303	SSQV	90.				17.1
304	↓	↓				14.4
305	↓	↓				12.5
306	SUDV	0.				75.9
307	SSQV	90.				22.8
308	↓	↓				19.6
309	↓	↓				17.1
310	SUDV	0.				83.2
311	SSQV	90.				27.9
312	↓	↓				24.7
313	↓	↓	↓			21.6

Case No.	Max Rotor Thrust (Lb)	Max Δn (g)	Gust-Allev Factor (K_g)	Comments
290	40000	1.75	-	
291	29900	1.02	.58	
292	31000	1.10	.63	
293	31900	1.16	.66	
294	41000	1.83	-	
295	29700	1.02	.56	
296	31200	1.11	.61	
297	32300	1.19	.65	
298	41200	1.85	-	
299	29400	0.99	.54	
300	31000	1.10	.60	
301	32200	1.19	.64	
302	40500	1.78	-	
303	30200	1.03	.58	
304	31400	1.11	.62	
305	32300	1.17	.66	
306	41000	1.81	-	
307	30100	1.03	.57	
308	31500	1.12	.62	
309	32600	1.19	.66	
310	41300	1.83	-	
311	29800	1.00	.55	
312	31500	1.11	.61	
313	32700	1.19	.65	

TABLE XXII. GUST-RESPONSE CASE RESULTS, COMPOUND SINGLE-ROTOR HELICOPTER, NO. 1

Case No.	Gust Type			Max Blade Root Osc Moment Ratio M_{gust}/M_{steady}		Max Flap Velocity (Deg/Sec)
	Shape	Length (Ft)	Max Vel (Ft/Sec)	Beam	Chord	
	Semirigid Rotor					
71	SUDV	0.	50.	1.25	0.79	40.9
72	SSQV	90.		2.99	2.81	16.3
73	SUDV	0.		1.29	.74	42.9
74	SSQV	90.		3.22	3.00	19.0
75	SUDV	0.		1.23	0.72	44.8
76	SSQV	90.		3.08	2.58	22.3
77	SUDV	0.		1.03	1.06	51.0
78	SSQV	90.		2.03	2.44	28.5
79	SUDV	0.		0.89	0.93	48.8
80	SSQV	90.		1.32	1.87	31.9
81	SUDV	0.		1.25	0.53	40.6
82	SSQV	90.		2.90	1.96	16.5
83	SUDV	0.		1.31	0.38	43.0
84	SSQV	90.		3.37	2.24	19.6
85	SUDV	0.		1.25	0.43	45.3
86	SSQV	90.		3.00	2.13	22.1
87	SUDV	0.		2.14	0.59	50.2
88	SSQV	90.		2.39	1.92	28.5
89	SUDV	0.		0.98	0.71	50.6
90	SSQV	90.		1.60	2.04	31.9
91	SUDV	0.		1.54	0.54	40.3
92	SSQV	90.		3.49	1.69	16.8
93	SUDV	0.		1.24	1.05	51.1
94	SSQV	90.		1.98	2.06	24.0

Case No.	Max Rotor Thrust (Lb)	Max Wing Lift (Lb)	Max Δn		Gust-Alleviation Factor		Aux Prop (Lb)
			Rotor (g)	Wing (g)	Rotor (K_{g_r})	Wing (K_{g_w})	
71	35800.	27400.	2.17	1.01			2480.
72	24400.	24700.	1.42	0.83	.65	.82	2480.
73	35900.	29800.	2.21	1.14			2970.
74	24700.	27000.	1.47	0.95	.66	.84	2970.
75	34600.	34400.	2.30	1.27			3650.
76	23400.	31300.	1.55	1.06	.68	.84	3650.
77	38200.	33200.	2.18	1.53			4950.
78	26700.	30000.	1.41	1.31	.65	.86	4950.
79	41900.	32800.	2.09	1.79			7440.
80	29100.	29300.	1.24	1.55	.59	.87	7440.
81	35000.	29100.	2.25	1.02			2910.
82	23000.	26300.	1.44	0.83	.64	.81	2910.
83	35200.	30400.	2.24	1.13			3300.
84	23700.	27400.	1.47	0.94	.66	.83	3300.
85	35000.	34000.	2.32	1.27			3930.
86	23200.	30700.	1.54	1.05	.66	.82	3930.
87	37000.	36900.	2.35	1.54			5290.
88	25300.	33400.	1.57	1.3	.67	.85	5290.
89	41100.	35200.	2.20	1.81			7480.
90	28200.	31500.	1.35	1.56	.61	.86	7480.
91	34500.	27600.	2.22	1.01			3330.
92	23400.	24800.	1.46	0.82	.66	.82	3330.
93	39400.	23600.	2.04	1.15			3100.
94	27600.	20900.	1.25	0.96	.62	.84	3100.

TABLE XXII - Continued

(COMPOUND SINGLE-ROTOR HELICOPTER, No. 1)

Case No.	Gust Type Shape	Length (Ft)	Max Vel (Ft/Sec)	Max Blade Root Osc Moment Ratio M_{gust}/M_{steady} Beam	Chord	Max Flap Velocity (Deg/Sec)
	Semirigid Rotor (Cont'd)					
95	SUDV	0.	50.	1.26	0.72	51.4
96	SSQV	90.		2.11	2.03	25.9
97	SUDV	0.		1.11	0.77	51.5
98	SSQV	90.		1.77	1.74	27.9
99	SUDV	0.		0.94	0.73	49.2
100	SSQV	90.		1.28	1.67	29.8
101	SUDV	0.		1.76	1.00	41.3
102	SSQV	90.		2.44	1.35	16.7
103	SUDV	0.		1.56	0.96	44.9
104	SSQV	90.		2.22	1.38	20.0
105	SUDV	0.		1.43	0.85	47.5
106	SSQV	90.		1.99	1.34	23.3
107	SUDV	0.		1.22	0.83	53.2
108	SSQV	90.		1.88	1.45	29.4
109	SUDV	0.		1.02	0.81	48.7
110	SSQV	90.		1.33	1.55	30.2
111	SUDV	0.		1.01	1.22	28.8
112	SSQV	90.		1.80	2.44	12.2
113	SUDV	0.		0.98	1.36	30.0
114	SSQV	90.		1.49	2.69	12.7
115	SUDV	0.		1.05	0.83	26.7
116	SSQV	90.		2.07	3.53	10.28
117	SUDV	0.		1.01	3.14	49.8
118	SSQV	90.		2.50	5.74	15.2
119	SUDV	0.		0.77	1.61	52.9

Case No.	Max Rotor Thrust (Lb)	Max Wing Lift (Lb)	Max Δn Rotor (g)	Max Δn Wing (g)	Gust-Alleviation Factor Rotor (K_{g_r})	Gust-Alleviation Factor Wing (K_{g_w})	Aux Prop (Lb)
95	39600.	25700.	2.06	1.28			4170.
96	28000.	22700.	1.28	1.08	.62	.84	4170.
97	36300.	35600.	2.22	1.55			6320.
98	24700.	31900.	1.44	1.30	.65	.84	6320.
99	39900.	34800.	2.11	1.82			9110.
100	27500.	30600.	1.29	1.54	.61	.85	9110.
101	35700	27600	2.21	1.03			3800.
102	24200.	24600.	1.44	0.82	.65	.80	3800.
103	35800.	29400.	2.20	1.15			4500.
104	24600.	26200.	1.45	0.94	.66	.82	4500.
105	33800.	34200.	2.25	1.29			5620.
106	22800.	31600.	1.52	1.12	.67	.87	5620.
107	34500.	37500.	2.24	1.55			7230.
108	23600.	33600.	1.52	1.29	.67	.83	7230.
109	37800.	35500.	2.05	1.82			10400.
110	26800.	31400.	1.31	1.54	.64	.85	10400.
111	96900	16600.	5.62	0.99			2000.
112	51300.	10300.	2.57	0.56	.46	.57	2000.
113	93500.	17200.	5.33	1.11			3000.
114	52300.	10100.	2.59	0.64	.48	.58	3000.
115	97600.	15900.	5.72	0.86			1400.
116	48900.	10300.	2.47	0.49	.43	.57	1400.
117	41700.	17900.	1.95	1.01			1400.
118	27800.	15600.	1.03	0.79	.53	.78	1400.
119	46200	17600.	2.11	1.14			1700.

TABLE XXII - Continued
(COMPOUND SINGLE-ROTOR HELICOPTER, No. 1)

Case No.	Gust Type Shape	Length (Ft)	Max Vel (Ft/Sec)	Max Blade Root Osc Moment Ratio M_{gust}/M_{steady} Beam	Chord	Max Flap Velocity (Deg/Sec)
	Semirigid Rotor (Cont'd)					
120	SSQV	90.	50.	1.96	3.27	24.8
121	SUDV	0.		1.16	2.39	44.6
122	SSQV	90.		2.39	0.90	14.1
123	SUDV	0.		0.09	1.22	32.6
124	SSQV	90.		1.34	2.97	10.7
125	SUDV	0.		0.92	1.21	31.7
126	SSQV	90.		1.49	2.38	12.4
127	SUDV	0.		0.88	1.21	26.6
128	SSQV	90.		1.90	2.00	9.22
129	SUDV	0.		1.08	3.30	51.0
130	SSQV	90.		2.07	7.93	18.7
131	SUDV	0.		0.98	3.27	58.8
132	SSQV	90.		1.61	6.08	26.8
133	SUDV	0.		1.24	2.80	46.5
134	SSQV	90.		2.27	7.51	46.5
	Articulated Rotor					
135	SUDV	0.	50.	23.5	0.84	28.2
136	SSQV	90.		5.76	1.63	13.9
137	SUDV	0.		30.2	1.69	50.1
138	SSQV	90.		6.87	3.14	24.4
139	SUDV	0.		10.8	1.52	32.1
140	SSQV	90.		1.86	1.84	12.5
141	SUDV	0.		32.7	1.54	56.3
142	SSQV	90.		2.55	1.07	28.4
143	SUDV	0.		10.2	4.00	31.1

Case No.	Max Rotor Thrust (Lb)	Max Wing Lift (Lb)	Max Δn		Gust-Alleviation Factor		Aux Prop (Lb)
			Rotor (g)	Wing (g)	Rotor (K_{g_r})	Wing (K_{g_w})	
120	28600.	14000.	0.93	0.9	.44	.79	1700.
121	40900.	17200.	1.99	0.88			1200.
122	28000.	14000.	1.13	0.67	.57	.76	1200.
123	93600.	18100.	5.48	0.99			1800.
124	44200.	13500.	2.19	0.68	.40	.69	1800.
125	91500.	20400.	5.39	1.12			3000.
126	45400.	14900.	2.21	0.75	.43	.67	3000.
127	89900.	20100.	5.49	0.87			1500.
128	36100.	15500.	1.90	0.57	.35	.65	1500.
129	39400.	19200.	1.89	1.01			1500.
130	26500.	16200.	1.03	0.81	.54	.80	1500.
131	39700.	19000.	1.77	1.15			2000.
132	27200.	16800.	0.90	1.00	.53	.87	2000.
133	39200.	17600.	1.90	0.88			1200.
134	26400.	14900.	1.05	0.70	.55	.79	1200.
135	98600.	16700.	5.63	0.98			3000.
136	56200.	12000.	2.81	0.67	.50	.68	3000.
137	42200.	16300.	1.86	1.01			1400.
138	29700.	14000.	1.02	0.85	.55	.85	1400.
139	102600.	17400.	5.95	0.99			3000.
140	52100.	12800.	2.58	0.68	.43	.69	3000.
141	40900.	15500.	1.70	1.01			1800.
142	29800.	13400.	0.79	0.98	.48	.86	1800.
143	97200.	15100.	5.42	0.99			2500.

TABLE XXII - Continued)

(COMPOUND SINGLE-ROTOR HELICOPTER, No. 1)

Case No.	Gust Type Shape	Length (Ft)	Max Vel (Ft/Sec)	Max Blade Root Osc Moment Ratio M_{gust}/M_{steady} Beam	Chord	Max Flap Velocity (Deg/Sec)
	Articulated Rotor (Cont'd)					
144	SSQV	90.	50.	2.31	2.59	12.1
145	SUDV	0.	↓	23.4	1.72	52.5
146	SSQV	90.	↓	5.54	2.60	22.1
	Rigid Rotor					
147	SUDV	0.	50.	11.6	2.07	28.2
148	SSQV	90.	↓	4.06	4.35	14.2
149	SUDV	0.	↓	1.04	3.14	49.1
150	SSQV	90.	↓	0.97	5.40	19.9
151	SUDV	0.	↓	5.40	1.53	32.2
152	SSQV	90.	↓	2.05	2.42	12.5
153	SUDV	0.	↓	8.51	5.58	56.3
154	SSQV	90.	↓	4.98	5.07	25.4
155	SUDV	0.	↓	10.8	3.53	30.8
156	SSQV	90.	↓	2.30	2.58	12.1
157	SUDV	0.	↓	8.34	3.02	53.3
158	SSQV	90.	↓	2.39	4.55	22.4
	Articulated Rotor					
159	SUDV	0.	50.	8.6	2.2	35.8
160	SSQV	90.	↓	1.0	3.0	16.3
161	SUDV	0.	↓	7.5	3.1	54.6
162	SSQV	90.	↓	4.6	2.9	26.2
163	SUDV	0.	↓	20.3	.8	38.9
164	SSQV	90.	↓	7.1	1.7	15.4
165	SUDV	0.	↓	22.7	1.1	59.0
166	SSQV	90.	↓	1.9	2.6	24.6
169	SUDV	0.	↓	20.8	1.3	78.2
170	SSQV	90.	↓	5.1	2.2	28.4

Case No.	Max Rotor Thrust (Lb)	Max Wing Lift (Lb)	Max Δn		Gust-Alleviation Factor		Aux Prop (Lb)
			Rotor (g)	Wing (g)	Rotor (K_{g_r})	Wing (K_{g_w})	
144	50400.	11800.	2.29	0.77	.42	.78	2500.
145	39900.	17500.	1.78	1.01			1500.
146	27100.	15200.	0.93	0.86	.52	.85	1500.
147	98500.	16700.	5.63	0.99			3000.
148	57300.	12200.	2.89	0.68	.51	.69	3000.
149	41600.	18300.	1.98	1.01			1500.
150	27600.	15000.	1.04	0.79	.53	.78	1500.
151	102400.	17600.	5.95	0.99			3000.
152	52600.	13100.	2.64	0.69	.44	.79	3000.
153	40900.	15600.	1.7	1.01			1800.
154	28800.	13600.	0.9	0.88	.53	.87	1800.
155	96600.	15700.	5.42	0.99			2500.
156	50400.	12000.	2.34	0.74	.43	.75	2500.
157	39900.	17500.	1.78	1.01			1500.
158	27500.	15200.	0.95	0.86	.53	.85	1500.
159	99900.	19400.	5.71	1.23			5500.
160	53400.	13100.	2.60	0.82	.46	.66	5500.
161	40900.	21700.	1.85	1.28			4000.
162	27700.	19300.	0.97	1.12	.52	.87	4000.
163	95200.	26100.	5.85	1.19			5500.
164	51400.	20100.	2.92	0.79	.50	.66	5500.
165	41900.	24800.	2.14	1.28			3500.
166	28800.	21400.	1.27	1.05	.59	.82	3500.
169	39900.	22700.	1.87	1.28			3000.
170	27000.	19800.	1.01	1.02	.54	.80	3000.

TABLE XXII - Continued

(COMPOUND SINGLE-ROTOR HELICOPTER, No. 1)

Case No.	Gust Type Shape	Length (Ft)	Max Vel (Ft/Sec)	Max Blade Root Osc Moment Ratio M_{gust}/M_{steady} Beam	Chord	Max Flap Velocity (Deg/Sec)
	Rigid Rotor					
171	SUDV	0.	50.	3.9	1.8	35.9
172	SSQV	90.		1.7	2.6	15.4
173	SUDV	0.		7.8	3.1	54.6
174	SSQV	90.		4.6	3.5	26.3
175	SUDV	0.		10.4	1.3	38.9
176	SSQV	90.		4.7	5.7	15.8
177	SUDV	0.		6.1	2.7	59.0
178	SSQV	90.		4.2	6.3	19.6
181	SUDV	0.		6.9	4.2	78.1
182	SSQV	90.		2.8	3.5	28.5
	Semirigid Rotor					
223	SUDV	0.	50.	1.1	2.0	58.5
224	SSQV	90.		1.6	2.8	24.1
225	SUDV	0.		.5	2.0	60.5
226	SSQV	90.		.89	2.0	26.6
	Rigid Rotor					
227	SUDV	0.	50.	7.6	16.8	46.4
228	SSQV	90.		7.1	18.8	18.7
229	SUDV	0.		2.8	1.5	57.5
230	SSQV	90.		3.0	4.3	26.3
	Articulated Rotor					
231	SUDV	0.	50.	22.2	2.2	55.8
232	SSQV	90.		9.6	2.5	28.0
233	SUDV	0.		11.6	1.4	69.3
234	SSQV	90.		5.6	1.8	28.8

Case No.	Max Rotor Thrust (Lb)	Max Wing Lift (Lb)	Max Δn		Gust-Alleviation Factor		Aux Prop (Lb)
			Rotor (g)	Wing (g)	Rotor (K_{g_r})	Wing (K_{g_w})	
171	99400.	19400.	5.68	1.23			5500.
172	53700.	13500.	2.64	0.84	.46	.68	5500.
173	40900.	21800.	1.85	1.28			4000.
174	27700.	19400.	0.98	1.12	.53	.87	4000.
175	95200.	26100.	4.85	1.28			5500
176	53000.	20400.	3.03	0.81	.52	.68	5500.
177	41900.	24800.	2.15	1.28			3500.
178	28200.	11200.	1.24	1.03	.58	.81	3500.
181	39900.	22800.	1.87	1.28			3000.
182	27400.	19800.	1.0	1.02	.56	.79	3000.
223	25400.	20700.	1.03	1.03			1400.
224	20100.	18400.	0.67	0.88	.66	.85	1400.
225	26700.	21000.	0.88	1.30			3500.
226	23200.	18600.	0.65	1.14	.73	.88	3500.
227	26400.	17500.	0.86	1.10			1400.
228	19800.	16600.	0.41	0.97	.49	.94	1400.
229	26200.	21900.	0.93	1.30			3200.
230	22500.	22100.	0.68	1.31	.73	1.01	3200.
231	25800.	17500.	0.82	1.03			1400.
232	20600.	17200.	0.47	1.02	.57	.98	1400.
233	25600.	22000.	0.89	1.30			3200.
234	22100.	22400.	0.65	1.33	.74	1.02	3200.

TABLE XXIII. GUST-RESPONSE CASE RESULTS, COMPOUND SINGLE-ROTOR HELICOPTER, NO. 2

Case No.	Gust Type			Max Blade Root Osc Moment Ratio M_{gust}/M_{steady}		Max Flap Velocity (Deg/Sec)
	Shape	Length (Ft)	Max Vel (Ft/Sec)	Beam	Chord	
	Semirigid Rotor					
238	SSQV	60.	40.	1.87	9.10	13.5
239	↓	40.	30.	1.31	5.54	8.8
240	↓	27.	20.	.97	2.43	6.8
250	SUDV	0.	50.	1.21	3.00	54.7
251	SEDV	0.	↓	.98	1.02	21.5
252	SUDV	0.	↓	2.71	1.78	55.6
253	SEDV	0.	↓	2.42	1.53	21.7
254	SSQV	90.	↓	2.50	59.0	17.1
255	RMPV	27.	20.	1.29	2.56	6.2
256	RMPV	90.	50.	2.34	21.0	12.9
257	SSQV	120.	↓	1.71	64.0	13.2
258	RFTP	90.	↓	.92	114.	12.8
259	SSQV	90.	↓	2.14	11.7	13.7
260	↓	90.	↓	1.92	10.5	16.5
261	↓	90.	↓	1.92	8.72	16.5
262	SUDV	0.	↓	1.22	2.78	55.5
269	SEDV	0.	↓	2.25	7.75	23.7
275	SSQV	90.	↓	2.33	7.42	17.6
276	↓	↓	↓	2.00	7.50	17.9
277	↓	↓	↓	2.29	8.75	20.9

Case No.	Max Rotor Thrust (Lb)	Max Wing Lift (Lb)	Max Δn (g)	Gust-Allev Factor (K_g)	Comments
238	13700.	1800.	0.84		
239	12700.	1600.	0.69		
240	11000.	1400.	0.44		
250	18500.	2400.	1.54		Steady, no aeroelastic feedback
251	15000.	2300.	1.02		250 with penetration
252	15900.	2400.	1.24		Nonsteady, aeroelastic feedback
253	14400.	2200.	1.02		252 with penetration
254	13800.	1900.	0.88	.57	
255	11700.	1300.	0.54		
256	13300.	1800.	0.80		
257	13500.	1800.	0.81	.65	
258	13300.	1800.	0.80		Ramp up and down
259	13400.	1800.	0.83	.64	$\delta_3 = -30^o$
260	14000.	1900.	0.89	.72	No aeroelastic feedback
261	14000.	1900.	0.89	.58	Steady, no aeroelastic feedback
262	15900.	2400.	1.24		
269	12950.	2291.	.86		
275	14000.	2100.	0.88		Pitch-link softness 0. deg/(10^6 in.-lb)
276	14000.	2100.	0.89		Pitch-link softness 10. deg/(10^6 in.-lb)
277	14200.	2100.	0.91		Pitch-link softness 100. deg/(10^6 in.-lb)

TABLE XXIV. GUST-RESPONSE CASE RESULTS, TANDEM-ROTOR HELICOPTER

Case No.	Gust Type Shape	Length (Ft)	Max Vel (Ft/Sec)	Fwd Rotor Max Flap Velocity (Deg/Sec)	Fwd Rotor Max Rotor Thrust (Lb)	Aft Rotor Max Flap Velocity (Deg/Sec)	Aft Rotor Max Rotor Thrust (Lb/Sec)
	Aft CG						
183	SUDV	0.	50.	57.	39900.	42.	40600.
184	SSQV	90.		105.	51800.	122.	57600.
185	SUDV	0.		105.	17600.	96.	17400.
186	SSQV	90.		56.	16800.	60.	19100.
187	SUDV	0.		61.	37700.	45.	38700.
188	SSQV	90.		127.	51600.	138.	60500.
189	SUDV	0.		108.	16600.	94.	16500.
190	SSQV	90.		48.	15700.	57.	18000.
	Neutral CG						
272	SSQV	90.	50.	36.3	16894.	54.	17400.
	Forward CG						
274	SSQV	90.	50.	37.0	14700.	42.6	14300.

Case No.	Max Δn (g)	Gust-Alleviation Factor (Kg)	Comments
183	4.37		
184	4.97	1.14	Adverse fuselage pitching
185	1.35		
186	1.04	.77	
187	4.09		
188	4.56	1.12	Adverse fuselage pitching
189	1.22		
190	0.91	.74	
272	0.96	-	
274	0.89	-	

TABLE XXV. GUST-RESPONSE CASE RESULTS, SIDE-BY-SIDE HELICOPTER

Case No.	Gust Type: Shape	Gust Type: Length (Ft)	Gust Type: Max Vel (Ft/Sec)	Mast Tilt At Gust (Deg)	Max Flap Velocity (Deg/Sec)
	Helicopter Mode				
199	SSQV	90.	50.	0.	11.8
200	SSQV	↓	↓	↓	19.2
	Transition Mode				
201	SSQV	90.	50.	30.	- 13.7
202	SSQV			60.	- 31.3
203	SSQV			30.	- 27.6
204	SSQV	↓	↓	60.	- 36.2
	Airplane Mode				
205	SUDV	0.	50.	90.	41.1
206	SSQV	90.			15.8
207	SUDV	0.			40.9
208	SSQV	90.			18.1
209	SUDV	0.			61.6
210	SSQV	90.			- 28.4
211	SUDV	0.			109.0
212	SSQV	90.			- 125.1
213	SUDV	0.			142.0
214	SSQV	90.	↓	↓	1741.0

Case No.	Max Thrust Per Rotor (Lb)	Max Wing Lift (lb)	Max Δn (g)	Gust-Allev Factor (Kg)	Comments
199	16300.	15100.	1.16		
200	16500.	16900.	1.24		
201	9700.	23200.	0.90		
202	6102.	26200.	0.54		
203	10800.	31600.	1.37		
204	5000.	37300.	1.02		
205	4000.	32500.	0.79		
206	3400.	30300.	0.64	.81	
207	1900.	35000.	0.90		
208	1600.	37200.	0.80	.89	
209	1500.	52800.	1.69		
210	1400.	51400.	1.42	.84	
211	2100.	75000.	2.60		
212	2000.	74100.	2.14	.82	
213	2800.	10100.	3.55		
214	366000.	-53400.	16.44	3.83	Flapping instability at high speed

APPENDIX IV. ROTOR DESCRIPTIVE INFORMATION

TABLE XXVI. ROTOR STIFFNESS AND WEIGHT PARAMETERS

Pure and Compound Single-Rotor Helicopter

Rotor Number	6017	Number of Blades	4
Disc Loading	7.0	Radius	26.1 Ft
C_T/σ	.05	Chord	35.6 In.

Blade Segment (% R)	Beamwise EI/10^6 (Lb-In.^{2})	Chordwise EI/10^6 (Lb-In.^{2})	Weight/Inch (Lb/In.)
0-5	77.	1022.	4.890
5-10	3065.	1022.	8.290
10-15	4645.	15138.	8.080
15-20	1460.	16306.	3.570
20-25	470.	11107.	1.560
25-30	329.	9346.	1.280
30-35	252.	8067.	1.110
35-40	231.	7334.	1.050
40-45	208.	6550.	0.990
45-50	181.	6058.	4.134
50-55	159.	5553.	0.870
55-60	154.	5304.	0.850
60-65	154.	5042.	0.850
65-70	154.	5042.	0.850
70-75	154.	5042.	0.850
75-80	154.	5042.	0.850
80-85	154.	5042.	0.850
85-90	154.	5042.	0.850
90-95	154.	5042.	0.850
95-100	154.	5042.	0.850

TABLE XXVI - Continued

Pure and Compound Single-Rotor Helicopter

Rotor Number	6057	Number of Blades	4
Disc Loading	7.0	Radius	26.1 Ft
C_T/σ	.02	Chord	89.0 In.

Blade Segment (% R)	Beamwise EI/10^6 (Lb-In.^{2})	Chordwise EI/10^6 (Lb-In.^{2})	Weight/Inch (Lb/In.)
0-5	1453.	27248.	8.417
5-10	5402.	27248.	12.857
10-15	8285.	29834.	12.587
15-20	3784.	17392.	6.697
20-25	2376.	27804.	4.011
25-30	2174.	40335.	3.705
30-35	2064.	39554.	3.484
35-40	1628.	39050.	3.405
40-45	1603.	38318.	3.328
45-50	1572.	37845.	3.264
50-55	1931.	75226.	3.172
55-60	1922.	74767.	3.145
60-65	1922.	74314.	3.145
65-70	1922.	74314.	3.145
70-75	1922.	74314.	3.145
75-80	1922.	74314.	3.145
80-85	1922.	74314.	3.145
85-90	1922.	74314.	3.145
90-95	1922.	74314.	3.145
95-100	1922.	74314.	3.145

TABLE XXVI - Continued

Pure and Compound Single-Rotor Helicopter

Rotor Number	6033	Number of Blades	4
Disc Loading	4.0	Radius	34.5 Ft
C_T/σ	.05	Chord	26.9 In.

Blade Segment (% R)	Beamwise EI/10^6 (Lb-In.^{2})	Chordwise EI/10^6 (Lb-In.^{2})	Weight/Inch (Lb/In.)
0-5	27.	4096.	3.290
5-10	1093.	4096.	5.570
10-15	1648.	6156.	5.430
15-20	518.	6633.	2.400
20-25	167.	4501.	1.050
25-30	117.	3585.	0.861
30-35	89.	3281.	0.747
35-40	82.	2967.	0.707
40-45	74.	2661.	0.666
45-50	64.	2449.	0.632
50-55	55.	2255.	0.586
55-60	55.	2142.	2.504
60-65	55.	2040.	2.504
65-70	55.	2040.	0.572
70-75	55.	2040.	0.572
75-80	55.	2040.	0.572
80-85	55.	2040.	0.572
85-90	55.	2040.	0.572
90-95	55.	2040.	0.572
95-100	55.	2040.	0.572

TABLE XXVI - Continued

Pure and Compound Single-Rotor Helicopter

Rotor Number	6042	Number of Blades	4
Disc Loading	4.0	Radius	34.5 Ft
C_T/σ	.02	Chord	67.1 In.

Blade Segment (% R)	Beamwise EI/10^6 (Lb-In.^{2})	Chordwise EI/10^6 (Lb-In.^{2})	Weight/Inch (Lb/In.)
0-5	436.	57900.	12.240
5-10	17420.	57900.	20.750
10-15	26130.	87090.	20.220
15-20	8272.	94380.	8.933
20-25	2668.	63950.	3.903
25-30	1863.	53690.	3.203
30-35	1428.	46470.	2.778
35-40	1306.	42090.	2.627
40-45	1177.	37720.	2.477
45-50	1030.	34840.	2.352
50-55	900.	31930.	2.177
55-60	874.	30480.	2.127
60-65	874.	29030.	2.127
65-70	874.	29030.	2.127
70-75	874.	29030.	2.127
75-80	874.	29030.	2.127
80-85	874.	29030.	2.127
85-90	874.	29030.	2.127
90-95	874.	29030.	2.127
95-100	874.	29030.	2.127
Tip Weight			32.200 Lb

TABLE XXVI - Continued

Pure and Compound Single-Rotor Helicopter

Rotor Number	6022	Number of Blades	4
Disc Loading	10.0	Radius	21.8 Ft
C_T/σ	.05	Chord	42.5 In.

Blade Segment (% R)	Beamwise EI/10^6 (Lb-In.^{2})	Chordwise EI/10^6 (Lb-In.^{2})	Weight/Inch (Lb/In.)
0-5	88.	11560.	6.380
5-10	4016.	11560.	10.820
10-15	5248.	17460.	10.550
15-20	1658.	19010.	4.660
20-25	535.	12960.	2.034
25-30	374.	10700.	1.670
30-35	288.	9400.	1.450
35-40	262.	8470.	1.370
40-45	237.	7638.	1.290
45-50	206.	6955.	1.230
50-55	181.	6384.	1.140
55-60	175.	6110.	1.110
60-65	175.	5780.	1.110
65-70	175.	5780.	1.110
70-75	175.	5780.	1.110
75-80	175.	5780.	1.110
80-85	175.	5780.	1.110
85-90	175.	5780.	1.110
90-95	175.	5780.	1.110
95-100	175.	5780.	1.110

TABLE XXVI - Continued

Pure and Compound Single-Rotor Helicopter

Rotor Number	6069	Number of Blades	4
Disc Loading	10.0	Radius	21.8 Ft
C_T/σ	.02	Chord	106.2 In.

Blade Segment (% R)	Beamwise EI/10^6 (Lb-In.^{2})	Chordwise EI/10^6 (Lb-In.^{2})	Weight/Inch (Lb/In.)
0-5	369.	36090.	9.382
5-10	570.	36090.	13.822
10-15	1944.	26400.	13.552
15-20	2097.	28510.	7.662
20-25	1541.	41130.	5.036
25-30	1455.	35940.	4.690
30-35	1405.	32400.	4.449
35-40	1123.	30120.	4.370
40-45	1114.	28050.	4.293
45-50	1098.	26570.	4.229
50-55	909.	12540.	4.137
55-60	904.	12220.	4.110
60-65	777.	11820.	4.110
65-70	777.	11820.	4.110
70-75	777.	11820.	4.110
75-80	777.	11820.	4.110
80-85	777.	11820.	4.110
85-90	777.	11820.	4.110
90-95	777.	11820.	4.110
95-100	777.	11820.	4.110

TABLE XXVI - Continued

Pure Single-Rotor Helicopter

Rotor Number	8065	Number of Blades	4
Disc Loading	4.69	Radius	24.0 Ft
C_T/σ	.037	Chord	21.0 In.

Blade Segment (% R)	Beamwise EI/10^6 (Lb-In.^{2})	Chordwise EI/10^6 (Lb-In.^{2})	Weight/Inch (Lb/In.)
0-5	24.	6663.	2.700
5-10	399.	3260.	3.500
10-15	480.	1203.	4.350
15-20	823.	1103.	4.800
20-25	332.	2498.	3.120
25-30	75.	3049.	0.980
30-35	32.	2523.	0.725
35-40	30.	2259.	0.630
40-45	28.	2001.	0.617
45-50	28.	1751.	0.591
50-55	28.	1522.	0.581
55-60	28.	1289.	0.570
60-65	28.	1099.	0.562
65-70	28.	950.	0.558
70-75	28.	940.	0.557
75-80	28.	940.	0.557
80-85	25.	1020.	0.560
85-90	19.	1000.	0.525
90-95	13.	950.	0.494
95-100	9.	910.	0.463
Tip Weight			2.750 Lb

TABLE XXVI - Continued

Compound Single-Rotor Helicopter

Rotor Number	0166	Number of Blades	2
Disc Loading	5.6	Radius	22.0 Ft
C_T/σ	.064	Chord	27.0 In.

Blade Segment (% R)	Beamwise EI/10^6 (Lb-In.^{2})	Chordwise EI/10^6 (Lb-In.^{2})	Weight/Inch (Lb/In.)
0-5	14.	4287.	3.326
5-10	507.	5804.	6.900
10-15	694.	6088.	6.875
15-20	261.	6144.	2.432
20-25	95.	4117.	0.941
25-30	66.	3695.	0.759
30-35	50.	3270.	0.661
35-40	46.	2922.	0.624
40-45	42.	2638.	0.593
45-50	37.	2380.	0.557
50-55	33.	2172.	0.516
55-60	33.	2026.	0.617
60-65	36.	2028.	1.116
65-70	36.	2028.	1.116
70-75	33.	2010.	0.649
75-80	32.	2005.	0.505
80-85	32.	2005.	0.505
85-90	32.	2005.	0.505
90-95	32.	2005.	1.659
95-100	32.	2005.	2.240

TABLE XXVI - Continued

Tandem Helicopter

Rotor Number	6081	Number of Blades	4
Disc Loading	7.0	Radius	18.35 Ft
C_T/σ	.05	Chord	23.0 In.

Blade Segment (% R)	Beamwise EI/10^6 (Lb-In.^{2})	Chordwise EI/10^6 (Lb-In.^{2})	Weight/Inch (Lb/In.)
0-5	31.	8303.	5.683
5-10	4849.	8303.	10.150
10-15	6448.	15950.	9.883
15-20	1894.	17320.	3.993
20-25	483.	9776.	1.366
25-30	282.	7215.	1.021
30-35	172.	5364.	0.780
35-40	141.	4268.	0.701
40-45	109.	3173.	0.624
45-50	71.	2434.	0.560
50-55	39.	1712.	0.468
55-60	31.	1350.	0.441
60-65	31.	973.	0.441
65-70	31.	973.	0.441
70-75	31.	973.	0.441
75-80	31.	973.	0.441
80-85	31.	973.	0.441
85-90	31.	973.	0.441
90-95	31.	973.	0.441
95-100	31.	973.	0.441

TABLE XXVI - Continued

Tandem Helicopter

Rotor Number	6071	Number of Blades	4
Disc Loading	7.0	Radius	18.35 Ft
C_T/σ	.02	Chord	57.6 In.

Blade Segment (% R)	Beamwise EI/10^6 (Lb-In.^{2})	Chordwise EI/10^6 (Lb-In.^{2})	Weight/Inch (Lb/In.)
0-5	374.	24240.	6.902
5-10	5317.	24240.	11.340
10-15	6888.	31900.	7.812
15-20	2349.	33670.	5.142
20-25	935.	25250.	2.556
25-30	734.	22450.	2.210
30-35	624.	20900.	1.969
35-40	594.	19550.	1.890
40-45	561.	18370.	1.813
45-50	523.	17830.	1.749
50-55	491.	16840.	1.657
55-60	483.	16840.	1.630
60-65	483.	16380.	1.630
65-70	483.	16380.	1.630
70-75	483.	16380.	1.630
75-80	483.	16380.	1.630
80-85	483.	16380.	1.630
85-90	483.	16380.	1.630
90-95	483.	16380.	1.630
95-100	483.	16380.	1.630

TABLE XXVI - Continued

Side-By-Side Helicopter

Rotor Number	D215	Number of Blades	3
Disc Loading	9.87	Radius	19.25 Ft
C_T/σ	.105	Chord	20.0 In.

Blade Segment (% R)	Beamwise EI/10^6 (Lb-In.^{2})	Chordwise EI/10^6 (Lb-In.^{2})	Weight/Inch (Lb/In.)
0-5	4222.	3510.	5.800
5-10	690.	690.	3.400
10-15	1321.	1741.	2.500
15-20	999.	2068.	1.850
20-25	439.	2616.	0.800
25-30	245.	2107.	0.760
30-35	158.	1887.	0.610
35-40	138.	1798.	0.600
40-45	127.	1708.	0,600
45-50	116.	1310.	0.600
50-55	104.	1588.	0.810
55-60	92.	1519.	0.780
60-65	81.	1467.	0.750
65-70	71.	1390.	0.720
70-75	60.	1339.	0.690
75-80	52.	1290.	0.660
80-85	44.	1249.	0.630
85-90	36.	1278.	0.600
90-95	29.	1178.	0.570
95-100	24.	1148.	1.405

BELL HELICOPTER IBM 360/ PROGRAM C91-11
HELICOPTER RIGID BODY DYNAMICS ANALYSIS
COMPILED 4-19-67

7 4150217 ANALYTICAL STUDY OF HELICOPTER GUST RESPONSE
PSRH SUDDEN VERTICAL GUST 2 BLADED
DL = 7 TC = 0.16 M = .9 **SEMIRIGID ROTOR** 200 KNOTS

STABILITY PARTIAL DERIVATIVE MATRIX

	X-FORCE	Y-FORCE	Z-FORCE	YAW MOM.	PITCH MOM.	ROLL MOM.	MR MOM.F/A	MR MOM.LAT	TR MOM.F/A	TR MOM.LAT
P	142.11	-429.93	-3816.60	10587.11	-22.66	-2013.43	15914.64	59327.50	16.54	181.37
Q	-42.80	-171.12	-772.31	7876.17	-15287.22	-717.97	73276.06	4538.65	-77.58	79.01
R	26.29	2225.37	-229.49	-83643.96	144.09	6755.52	184.40	3972.54	-272.41	-477.50
U	-19.57	10.01	12.30	-386.26	53.86	30.70	36.63	442.22	0.39	-1.59
V	-0.30	-72.18	-17.77	2161.91	-2.43	-264.54	1395.63	375.79	3.49	14.62
W	21.98	-17.00	-422.37	384.57	-631.81	-101.97	-829.64	4033.60	-3.49	4.14

7 4150219 ANALYTICAL STUDY OF HELICOPTER GUST RESPONSE
PSRH SUDDEN VERTICAL GUST 2 BLADED
DL = 7 TC = .16 M = .9 RIGID ROTOR 200 KNOTS

STABILITY PARTIAL DERIVATIVE MATRIX

	X-FORCE	Y-FORCE	Z-FORCE	YAW MOM.	PITCH MOM.	ROLL MOM.	MR MOM.F/A	MR MOM.LAT	TR MOM.F/A	TR MOM.LAT
P	139.21	-246.83	-4410.94	-2121.88	252.67	-1620.90	29140.63	54631.46	124.63	14.06
Q	-133.33	210.60	477.34	-5282.42	-14795.90	1007.20	65299.71	17999.47	1.52	-101.13
R	-5.74	2499.15	-87.11	-94000.37	1072.15	7846.56	544.31	1443.62	-151.37	-559.31
U	-24.91	10.56	-4.57	-393.05	99.44	21.23	264.20	278.56	1.82	-4.69
V	-1.23	-64.46	-7.54	1967.08	-10.75	-253.61	1311.92	591.78	10.27	11.70
W	11.86	-14.66	-343.27	147.77	-549.32	-124.09	-1708.58	5362.90	-3.46	2.49

7 4150221 ANALYTICAL STUDY OF HELICOPTER GUST RESPONSE
PSRH SUDDEN VERTICAL GUST 3 BLADED
DL = 7 TC = .16 M = .9 ARTICULATED ROTOR 200 KNOTS

STABILITY PARTIAL DERIVATIVE MATRIX

	X-FORCE	Y-FORCE	Z-FORCE	YAW MOM.	PITCH MOM.	ROLL MOM.	MR MOM.F/A	MR MOM.LAT	TR MOM.F/A	TR MOM.LAT
P	313.16	-130.94	-4490.47	-4984.37	-1166.83	-680.32	6259.96	+1166.46	75.21	94.67
Q	172.93	147.02	-685.16	-4563.75	-16957.80	1112.99	25826.54	-769.00	-70.95	-1.20
R	-6.42	2339.33	-75.03	-87967.54	1065.67	7132.96	-12.75	937.42	-214.05	-555.41
U	-20.01	11.41	-4.66	-434.93	61.69	33.29	72.30	206.56	1.17	-3.87
V	1.64	-70.01	-24.01	1990.21	-31.39	-259.70	790.13	197.37	9.65	12.62
W	5.96	-14.51	-343.14	199.20	-554.53	-96.96	-494.05	3337.16	-4.42	3.58

7 4150223 ANALYTICAL STUDY OF HELICOPTER GUST RESPONSE
CSRH SUDDEN VERTICAL GUST 4 BLADED
DL = 7 TC = 0.2 M = .9 SEMIRIGID ROTOR 200 KNOTS

STABILITY PARTIAL DERIVATIVE MATRIX

	X-FORCE	Y-FORCE	Z-FORCE	YAW MOM.	PITCH MOM.	ROLL MOM.	MR MOM.F/A	MR MOM.LAT	TR MOM.F/A	TR MOM.LAT
P	184.30	-282.81	-2548.83	8769.14	-261.76	-1035.06	2140.50	34336.21	24.79	164.26
Q	-4.98	-32.06	-872.66	5384.76	-14927.68	86.25	31358.57	-1655.97	53.67	21.28
R	50.95	2193.68	-40.63	-82198.00	-814.20	6733.18	-59.28	1388.76	-300.67	-457.04
U	-18.23	9.74	-19.99	-311.07	40.46	29.84	-31.01	145.30	0.39	0.65
V	-1.08	-64.16	-6.72	2056.99	37.14	-215.48	410.74	88.50	9.82	13.44
W	24.28	-10.03	-694.19	102.36	-570.81	-53.67	-149.86	1394.64	-0.11	3.51

7 4150227 ANALYTICAL STUDY OF HELICOPTER GUST RESPONSE
CSRH SUDDEN VERTICAL GUST 4 BLADED
DL = 7 TC = 0.2 M = .9 RIGID ROTOR

STABILITY PARTIAL DERIVATIVE MATRIX

	X-FORCE	Y-FORCE	Z-FORCE	YAW MOM.	PITCH MOM.	ROLL MOM.	MR MOM.F/A	MR MOM.LAT	TR MOM.F/A	TR MOM.LAT
P	90.80	-129.83	-3209.38	-2209.77	437.12	-522.00	653.25	28369.88	101.41	39.35
Q	153.69	203.13	-1023.44	1909.77	-16474.64	954.10	29872.86	-4099.34	119.50	-126.21
R	44.51	2458.81	26.17	-92103.50	-650.61	7663.32	28.37	-297.55	-195.36	-620.39
U	-19.69	11.65	-28.42	-422.53	71.80	33.75	-47.19	205.29	1.51	-1.70
V	-0.76	-62.89	-12.63	1976.46	26.54	-213.59	544.79	72.99	10.45	11.67
W	0.80	-6.54	-645.44	20.65	-573.00	-36.35	-301.76	1994.01	0.01	1.90

7 4150231 ANALYTICAL STUDY OF HELICOPTER GUST RESPONSE
CSRH SUDDEN VERTICAL GUST 3 BLADED
DL = 7 TC = 0.2 M = .9 ARTICULATED ROTOR

STABILITY PARTIAL DERIVATIVE MATRIX

	X-FORCE	Y-FORCE	Z-FORCE	YAW MOM.	PITCH MOM.	ROLL MOM.	MR MOM.F/A	MR MOM.LAT	TR MOM.F/A	TR MOM.LAT
P	-91.46	-364.70	-3538.28	-212.50	1607.69	-1603.30	5038.34	41407.06	36.85	150.28
Q	-64.33	-73.69	-1826.56	3334.38	-17996.66	-324.05	22117.79	-1266.09	-41.20	23.31
R	3.08	2800.98	264.06	-104257.00	358.77	8577.88	-166.08	-2995.39	-170.27	-685.84
U	-27.41	10.43	-46.39	-389.66	64.03	30.78	0.64	269.98	0.47	-2.20
V	-1.07	-83.72	-24.57	2547.86	2.96	-296.79	698.97	52.65	7.05	18.09
W	-11.84	-13.02	-634.90	-23.61	-696.31	-78.28	-543.64	2525.27	-2.42	3.47

7 4250225 ANALYTICAL STUDY OF HELICOPTER GUST RESPONSE

CSRH SUDDEN VERTICAL GUST 4 BLADED

DL = 7 TC = 0.2 M = .9 SEMIRIGID ROTOR 250 KNOTS

STABILITY PARTIAL DERIVATIVE MATRIX

	X-FORCE	Y-FORCE	Z-FORCE	YAW MOM.	PITCH MOM.	ROLL MOM.	MR MOM.F/A	MR MOM.LAT	TR MOM.F/A	TR MOM.LAT
P	-185.18	-407.01	-3700.00	-4056.25	2211.49	-2203.13	5778.80	32999.25	69.01	87.65
Q	50.20	-145.63	-897.27	425.00	-19735.44	-1105.08	20399.89	-894.07	-61.88	-26.82
R	4.52	2980.96	350.79	-110399.94	1056.94	9155.86	-549.33	-2861.47	-154.32	-761.40
U	-34.31	13.85	-53.95	-523.44	41.25	41.04	9.72	194.03	0.56	-3.96
V	-1.21	-91.10	-22.91	2564.75	-16.51	-345.87	727.29	144.32	7.85	17.22
W	-26.45	-19.07	-763.67	113.87	-614.76	-123.89	-195.59	1944.92	-3.51	3.39

7 5050229 ANALYTICAL STUDY OF HELICOPTER GUST RESPONSE

CSRH SUDDEN VERTICAL GUST 4 BLADED

DL = 7 TC =0.2 M = 0.9 RIGID ROTOR 250 KNOTS

STABILITY PARTIAL DERIVATIVE MATRIX

	X-FORCE	Y-FORCE	Z-FORCE	YAW MOM.	PITCH MOM.	ROLL MOM.	MR MOM.F/A	MR MOM.LAT	TR MOM.F/A	TR MOM.LAT
P	-43.94	-334.81	-3602.74	512.50	1518.95	-1730.27	4512.46	32287.89	34.50	149.26
Q	74.66	-82.76	-668.36	-100.00	-19894.62	-411.79	12435.99	-94.71	-30.54	13.77
R	14.87	2937.33	195.31	-109631.19	343.96	9001.90	-149.73	-1644.79	-163.80	-741.42
U	-31.30	12.68	-49.99	-471.37	11.13	38.13	25.95	156.21	0.50	-2.12
V	0.02	-87.89	-4.93	2558.31	-10.28	-315.46	487.07	98.49	7.14	18.95
W	-14.47	-8.72	-739.77	77.19	-669.63	-47.73	-349.96	1945.76	-2.09	3.31

7 5050233 ANALYTICAL STUDY OF HELICOPTER GUST RESPONSE

CSRH SUDDEN VERTICAL GUST 3 BLADED

DL = 7 TC =0.2 M = 0.9 ARTICULATED ROTOR 250 KNOTS

STABILITY PARTIAL DERIVATIVE MATRIX

	X-FORCE	Y-FORCE	Z-FORCE	YAW MOM.	PITCH MOM.	ROLL MOM.	MR MOM.F/A	MR MOM.LAT	TR MOM.F/A	TR MOM.LAT
P	-61.08	-330.47	-3600.78	-718.75	1439.66	-1438.06	4703.31	42839.39	46.29	128.35
Q	88.40	70.48	-287.39	-997.50	-20094.70	576.68	1818.35	515.34	2.42	-17.64
R	19.97	2933.77	189.45	-109518.69	139.47	9000.54	-117.13	-2215.02	-162.68	-745.89
U	-30.05	12.95	-49.81	-488.37	18.18	39.35	105.47	208.68	0.74	-2.00
V	0.71	-83.67	3.73	2527.17	-9.26	-288.62	308.68	140.13	7.42	18.36
W	-9.79	-18.19	-696.56	26.62	-711.19	-119.33	-801.30	2621.69	-1.42	3.04

Unclassified

Security Classification

DOCUMENT CONTROL DATA - R&D

(Security classification of title, body of abstract and indexing annotation must be entered when the overall report is classified)

1. ORIGINATING ACTIVITY (Corporate author) Bell Helicopter Company P.O. Box 482 Fort Worth, Texas 76101	2a. REPORT SECURITY CLASSIFICATION Unclassified 2b. GROUP N/A

3. REPORT TITLE

ANALYTICAL STUDY OF HELICOPTER GUST RESPONSE AT HIGH FORWARD SPEEDS

4. DESCRIPTIVE NOTES (Type of report and inclusive dates)

Final Report

5. AUTHOR(S) (Last name, first name, initial)

Keith W. Harvey, Barney L. Blankenship, Jan M. Drees

6. REPORT DATE	7a. TOTAL NO. OF PAGES	7b. NO. OF REFS
September 1969	247	37

8a. CONTRACT OR GRANT NO. DA 44-177-AMC-308(T) b. PROJECT NO. Task 1F162204A14608 c. d.	9a. ORIGINATOR'S REPORT NUMBER(S) USAAVLABS Technical Report 69-1 9b. OTHER REPORT NO(S) (Any other numbers that may be assigned this report) BHC Report 299-099-106

10. AVAILABILITY/LIMITATION NOTICES

This document is subject to special export controls and each transmittal to foreign governments or foreign nationals may be made only with prior approval of US Army Aviation Materiel Laboratories, Fort Eustis, Virginia 23604.

11. SUPPLEMENTARY NOTES	12. SPONSORING MILITARY ACTIVITY
	U.S. Army Aviation Materiel Laboratories Fort Eustis, Virginia

13. ABSTRACT

An analytical study of helicopter gust response at high forward speeds is presented. A digital-computer program is described that includes rigid-body aircraft motions in space and the aeroelastic representation of two rotors. The rotors can be positioned to describe all general configurations. Various rotor types are considered, as well as compounding by the use of wings and auxiliary propulsion. Various maneuvers may be simulated, including subjecting the aircraft to gust disturbances.

Results cover a wide range of forward speeds, disk loadings, blade loadings, and advancing blade-tip Mach numbers. The effect of Lock number on gust response is included. The relative importance of gust shape, gradual penetration, nonsteady aerodynamics, and gust-alleviation devices are discussed.

A simple empirical expression is given that will adequately predict the rotor gust-load increase for a wide range of helicopter and compound designs.

DD FORM 1 JAN 64 1473

Unclassified

Security Classification

Unclassified

Security Classification

14. KEY WORDS	LINK A		LINK B		LINK C	
	ROLE	WT	ROLE	WT	ROLE	WT
Aeroelasticity						
Analytical Study						
Compound Helicopter						
Disk Loading						
Empirical						
Gradual Penetration						
Gust Alleviation						
Gust Response						
Gust Shape						
Helicopter						
High Forward Speed						
Lock Number						
Mach Number						
Maneuver						
Nonsteady Aerodynamics						
Thrust Coefficient						

INSTRUCTIONS

1. ORIGINATING ACTIVITY: Enter the name and address of the contractor, subcontractor, grantee, Department of Defense activity or other organization *(corporate author)* issuing the report.

2a. REPORT SECURITY CLASSIFICATION: Enter the overall security classification of the report. Indicate whether "Restricted Data" is included. Marking is to be in accordance with appropriate security regulations.

2b. GROUP: Automatic downgrading is specified in DoD Directive 5200.10 and Armed Forces Industrial Manual. Enter the group number. Also, when applicable, show that optional markings have been used for Group 3 and Group 4 as authorized.

3. REPORT TITLE: Enter the complete report title in all capital letters. Titles in all cases should be unclassified. If a meaningful title cannot be selected without classification, show title classification in all capitals in parenthesis immediately following the title.

4. DESCRIPTIVE NOTES: If appropriate, enter the type of report, e.g., interim, progress, summary, annual, or final. Give the inclusive dates when a specific reporting period is covered.

5. AUTHOR(S): Enter the name(s) of author(s) as shown on or in the report. Enter last name, first name, middle initial. If military, show rank and branch of service. The name of the principal author is an absolute minimum requirement.

6. REPORT DATE: Enter the date of the report as day, month, year, or month, year. If more than one date appears on the report, use date of publication.

7a. TOTAL NUMBER OF PAGES: The total page count should follow normal pagination procedures, i.e., enter the number of pages containing information.

7b. NUMBER OF REFERENCES: Enter the total number of references cited in the report.

8a. CONTRACT OR GRANT NUMBER: If appropriate, enter the applicable number of the contract or grant under which the report was written.

8b, 8c, & 8d. PROJECT NUMBER: Enter the appropriate military department identification, such as project number, subproject number, system numbers, task number, etc.

9a. ORIGINATOR'S REPORT NUMBER(S): Enter the official report number by which the document will be identified and controlled by the originating activity. This number must be unique to this report.

9b. OTHER REPORT NUMBER(S): If the report has been assigned any other report numbers *(either by the originator or by the sponsor)*, also enter this number(s).

10. AVAILABILITY/LIMITATION NOTICES: Enter any limitations on further dissemination of the report, other than those imposed by security classification, using standard statements such as:

(1) "Qualified requesters may obtain copies of this report from DDC."

(2) "Foreign announcement and dissemination of this report by DDC is not authorized."

(3) "U. S. Government agencies may obtain copies of this report directly from DDC. Other qualified DDC users shall request through _____."

(4) "U. S. military agencies may obtain copies of this report directly from DDC. Other qualified users shall request through _____."

(5) "All distribution of this report is controlled. Qualified DDC users shall request through _____."

If the report has been furnished to the Office of Technical Services, Department of Commerce, for sale to the public, indicate this fact and enter the price, if known.

11. SUPPLEMENTARY NOTES: Use for additional explanatory notes.

12. SPONSORING MILITARY ACTIVITY: Enter the name of the departmental project office or laboratory sponsoring *(paying for)* the research and development. Include address.

13. ABSTRACT: Enter an abstract giving a brief and factual summary of the document indicative of the report, even though it may also appear elsewhere in the body of the technical report. If additional space is required, a continuation sheet shall be attached.

It is highly desirable that the abstract of classified reports be unclassified. Each paragraph of the abstract shall end with an indication of the military security classification of the information in the paragraph, represented as (TS), (S), (C), or (U).

There is no limitation on the length of the abstract. However, the suggested length is from 150 to 225 words.

14. KEY WORDS: Key words are technically meaningful terms or short phrases that characterize a report and may be used as index entries for cataloging the report. Key words must be selected so that no security classification is required. Identifiers, such as equipment model designation, trade name, military project code name, geographic location, may be used as key words but will be followed by an indication of technical context. The assignment of links, roles, and weights is optional.

DD FORM 1 JAN 64 1473 (BACK)

Unclassified

Security Classification